

THE UNIVERSITY OF CALGARY

**Equalization Techniques for TDMA Cellular  
Radio with Co-channel Interference**

by

**Shuwei Huang**

A THESIS

SUBMITTED TO THE FACULTY OF GRADUATE STUDIES  
IN PARTIAL FULFILLMENT OF THE REQUIREMENTS FOR THE  
DEGREE OF DOCTOR OF PHILOSOPHY

DEPARTMENT OF ELECTRICAL AND COMPUTER ENGINEERING

CALGARY, ALBERTA

JULY, 2002

© Shuwei Huang 2002

**THE UNIVERSITY OF CALGARY**  
**FACULTY OF GRADUATE STUDIES**

The undersigned certify that they have read, and recommend to the Faculty of Graduate Studies for acceptance, a thesis entitled “Equalization Techniques for TDMA Cellular Radio with Co-channel Interference” submitted by Shuwei Huang in partial fulfillment of the requirements for the degree of Doctor of Philosophy.

---

Supervisor, Dr. A. B. Sesay  
Department of Electrical and Computer Engineering  
University of Calgary

---

Co-supervisor, Dr. B. R. Petersen  
Department of Electrical and Computer Engineering  
University of New Brunswick

---

Dr. M. Fattouche  
Department of Electrical and Computer Engineering  
University of Calgary

---

Dr. J. A. R. Blais  
Department of Geometrics Engineering  
University of Calgary

---

External Examiner, Dr. R. H. M. Hafez  
Department of Systems and Computer Engineering  
Carleton University

---

Date

# Abstract

Techniques to reduce the effect of co-channel interference (CCI), intersymbol interference (ISI) and noise in a time-division multiple access (TDMA) radio cellular radio system will allow an increase in network capacity without a loss in quality of service.

Two new analytical results have been derived and presented. The first result is the probability of error of a method for blind maximum likelihood (ML) data and channel estimation in the presence of noise. The second result is the mean square error of a displaced linear equalizer with infinite length on a time-varying channel in the presence of additive white Gaussian noise. These results provide measures of effectiveness of the blind maximum likelihood data and channel estimation method and the displaced linear equalizer used in the receiver.

In order to achieve good system performance in a fast time-varying environment, a novel block adaptation with blind channel estimation strategy has been developed. It involves combinations of channel estimation and interpolation. With this strategy, in addition to the channel estimates obtained from known sequences in a TDMA time slot, channel estimates are obtained using small sequences of unknown data and the ML blind data and channel estimation method. The time-varying channel during

a time slot can then be reconstructed by interpolating these channel estimates. Subsequently, the equalizer coefficients can be determined by using the Wiener-Hopf equations. A similar strategy can be applied to deal with time variations in the CCI. The effectiveness of this novel block adaptation strategy has been proven in the IS-136 application.

# Acknowledgements

I would like to express my sincere appreciation to the following people who have contributed directly or indirectly to the development this thesis.

My supervisors, Dr. A. B. Sesay and Dr. B. R. Petersen, have provided me with their guidance, encouragement and support. Without their help, the completion of this thesis would not have been possible.

Sincere thanks are also owed to the faculty, alumni, students and staff of the University of Calgary who helped me in so many ways during this endeavor.

I am grateful for the funding provided to me by the Natural Sciences and Engineering Research Council (NSERC), the Telecommunication Research Laboratories (TRLabs) and the University of Calgary.

Finally, I would like to thank my family for providing me with constant support and the opportunity to pursue my education.

# Table of Contents

<b>Approval Page</b>	<b>ii</b>
<b>Abstract</b>	<b>iii</b>
<b>Acknowledgements</b>	<b>v</b>
<b>Table of Contents</b>	<b>vi</b>
<b>List of Tables</b>	<b>xiii</b>
<b>List of Figures</b>	<b>xiv</b>
<b>List of Abbreviations and Acronyms</b>	<b>xviii</b>
<b>1 Introduction</b>	<b>1</b>
1.1 Motivation . . . . .	1
1.2 Literature Survey . . . . .	3
1.2.1 Equalization Techniques . . . . .	4
1.2.1.1 Linear and Non-Linear Equalization . . . . .	4
1.2.1.2 Adaptive Equalization . . . . .	5
1.2.1.3 Fractionally Spaced Equalization . . . . .	6

1.2.2	CCI Suppression Techniques . . . . .	7
1.2.3	Channel Estimation Techniques . . . . .	8
1.2.4	Strategies Dealing with Time-Varying Channels . . . . .	11
1.3	Thesis Contributions . . . . .	13
1.4	Thesis Organization . . . . .	15
<b>2</b>	<b>System Descriptions</b>	<b>18</b>
2.1	Transmitter . . . . .	19
2.2	Channel . . . . .	20
2.2.1	Noise . . . . .	21
2.2.2	Interference . . . . .	23
2.2.3	Channel Impulse Response . . . . .	25
2.2.3.1	Discrete-time Multipath Channel Impulse Response	25
2.2.3.2	Statistical Models for Fading Channels . . . . .	26
2.2.3.3	Jakes' Model . . . . .	27
2.2.3.4	Gans' Model . . . . .	30
2.2.3.5	Two-Ray Rayleigh Fading Model . . . . .	33
2.3	Receiver . . . . .	34
2.3.1	Linear Equalizer . . . . .	35
2.3.2	Decision Feedback Equalizer . . . . .	37
<b>3</b>	<b>Equalization, Channel Estimation and Interpolation Techniques</b>	<b>39</b>
3.1	Channel Estimation Techniques . . . . .	39
3.1.1	LSSE Channel Estimation . . . . .	40
3.1.2	LSSE Channel and Co-channel Estimation . . . . .	42

3.1.3	ML Blind Data and Channel Estimation . . . . .	45
3.1.4	ML Blind Data, Channel and Co-channel Estimation . . . . .	48
3.1.5	Sign Ambiguity Problem of Blind Data and Channel Estimation	49
3.1.6	Probability of Error in ML Blind Data and Channel Estimation	50
3.1.6.1	Statistical Properties of Noise Component in the Channel Estimate . . . . .	51
3.1.6.2	Probability of Selecting the Right Channel Estimate	54
3.1.7	Channel Modeling with Frequency Estimation Using Cross Correlation . . . . .	57
3.2	Equalization Techniques Dealing with Time-Varying Channels . . . . .	62
3.2.1	Optimum MSE Equalizer . . . . .	63
3.2.2	Fixed Equalizer . . . . .	64
3.2.3	Displaced Equalizer . . . . .	65
3.2.4	Curve Fitting Equalizer . . . . .	67
3.2.4.1	Polynomial Exact Fit . . . . .	67
3.2.4.2	Polynomial LS Fit . . . . .	69
3.2.4.3	Cubic Spline Fit . . . . .	70
3.3	Block Adaptation Strategies in Time-Varying Environment . . . . .	72
3.3.1	Background in Block Adaptation . . . . .	73
3.3.2	Block Adaptation with Blind Data and Channel Estimation	74
3.4	Mean Square Error Analysis . . . . .	77
3.4.1	MSE Criterion . . . . .	77
3.4.2	MMSE of Infinite LE on Time-Invariant Channels . . . . .	78
3.4.3	Average MMSE of Infinite LE on Fading Channels . . . . .	80

3.4.3.1	Model and Statistics of the Channel Taps . . . . .	81
3.4.3.2	Transmit Filter . . . . .	83
3.4.3.3	PDF of Fourier Transform of the Channel Autocorrelation . . . . .	83
3.4.3.4	Average MMSE of Infinite LE on Time-Varying Channels . . . . .	86
3.4.4	MSE of Displaced LE on Fading Channels . . . . .	88
3.4.4.1	Perturbations in the Time-Varying Channels . . . . .	89
3.4.4.2	Estimated Information-Bearing Symbol at a Displaced Time . . . . .	93
3.4.4.3	Average MSE at a Displaced Time . . . . .	96
<b>4</b>	<b>Application to IS-136 800 MHz Operation</b>	<b>102</b>
4.1	Background . . . . .	102
4.2	System Descriptions . . . . .	104
4.2.1	Transmitter . . . . .	104
4.2.1.1	Encoder . . . . .	104
4.2.1.2	Up Sampler . . . . .	105
4.2.1.3	Transmit Filter and Receive Filter . . . . .	105
4.2.2	Channel . . . . .	109
4.2.3	Receiver . . . . .	110
4.2.3.1	Equalizer . . . . .	110
4.2.3.2	Decoder . . . . .	112
4.3	Performance of Receivers . . . . .	113
4.3.1	DFE Bounds . . . . .	113

4.3.2	Adaptive DFE . . . . .	115
4.3.2.1	RLS-DFE with no Tracking . . . . .	116
4.3.2.2	RLS-DFE with Tracking . . . . .	118
4.3.3	Calculated DFE Using Wiener-Hopf Equations . . . . .	122
4.3.3.1	MSE of Channel Estimation . . . . .	122
4.3.3.2	Calculation of Optimum DFE Coefficients . . . . .	124
4.3.3.3	Performance of Calculated DFE Using Wiener-Hopf Equations . . . . .	124
4.3.4	Displaced DFE . . . . .	125
4.4	Discussion . . . . .	126
4.4.1	Comparison of Performance . . . . .	126
4.4.2	Comparison of Complexity . . . . .	129
<b>5</b>	<b>Application to IS-136 1.9 GHz Operation</b>	<b>133</b>
5.1	Background . . . . .	133
5.2	Performance of Receivers . . . . .	134
5.2.1	DFE and LE Bounds . . . . .	135
5.2.2	DFE and LE Partial Bounds . . . . .	139
5.2.2.1	Channel Samples at SYNC and CDVCC only . . . . .	139
5.2.2.2	Insertion of the Channel Samples . . . . .	141
5.2.2.3	Partial Bounds with Channel Information . . . . .	142
5.2.2.4	Partial Bounds with Channel and Co-channel Infor- mation . . . . .	145
5.2.2.5	Comparison . . . . .	147
5.2.3	Performance with Blind ML Data and Channel Estimation . . . . .	150

5.2.4	MSE of Receivers with DLE . . . . .	153
5.2.4.1	Average MMSE . . . . .	154
5.2.4.2	Average MSE . . . . .	158
5.2.5	Probability of Error in ML Blind Data and Channel Estimation	163
5.3	Discussion . . . . .	164
5.3.1	Performance Issues . . . . .	165
5.3.1.1	DDFE, DLE and Curve Fitting DFE . . . . .	165
5.3.1.2	Lower Bounds, Partial Bounds and Blind Channel Estimation . . . . .	165
5.3.2	Complexity Issues . . . . .	169
5.3.2.1	Complexity Measure . . . . .	169
5.3.2.2	Blind Channel Estimation . . . . .	169
5.3.2.3	Blind Channel Estimation and Blind Channel and Co-channel Estimation . . . . .	173
5.3.2.4	DDFE, DLE and Curve Fitting DFE . . . . .	176
<b>6</b>	<b>Conclusions and Future Work</b>	<b>179</b>
6.1	Summary and Conclusions . . . . .	179
6.2	Future Work . . . . .	182
	<b>References</b>	<b>195</b>
	<b>A Evaluation of Instantaneous MMSE</b>	<b>196</b>
	<b>B Evaluation of Expectation by Four-Dimensional Numerical Integration</b>	<b>202</b>

B.1	Four-dimensional Simpson's Rule . . . . .	202
B.2	Evaluation of the Expectation . . . . .	207
<b>C</b>	<b>MMSE of an AWGN Channel</b>	<b>209</b>

# List of Tables

4.1	Mapping of the $\pi/4$ DQPSK symbol . . . . .	105
4.2	$\pi/4$ DQPSK decision rules . . . . .	112
4.3	Operation counts for different DFE methods . . . . .	131
5.1	Comparison in complexity and BER performance . . . . .	175
5.2	Operation counts three receiver types . . . . .	177

# List of Figures

2.1	Baseband model of a digital wireless communication system . . . . .	19
2.2	Model for co-channel interference . . . . .	23
2.3	Transmission in the multipath environment [1] . . . . .	25
2.4	Multipath channel at different snapshots [1] . . . . .	27
2.5	Theoretical and simulated Rayleigh PDF . . . . .	30
2.6	Simulation of Rayleigh fading channel tap using Gans' model . . . . .	32
2.7	Receiver with linear equalizer . . . . .	35
2.8	Receiver with DFE . . . . .	37
3.1	Transmission in the presence of CCI . . . . .	43
3.2	Exhaustive search algorithm . . . . .	47
3.3	Decision region of $\hat{r}_o$ . . . . .	56
3.4	Transmission over a time-varying channel . . . . .	59
3.5	Magnitude of the cross-power density . . . . .	61
3.6	Error at the output of an equalizer . . . . .	64
3.7	Interpolated channel in fixed equalizer method . . . . .	65
3.8	Interpolated channel in displaced equalizer method . . . . .	66
3.9	A TDMA time slot . . . . .	73

3.10	Interpolation in the conventional block adaptation method . . . . .	74
3.11	Interpolation in the proposed block adaptation method . . . . .	75
3.12	Baseband communication system . . . . .	77
3.13	MSE of DLE in a time slot . . . . .	89
3.14	The two components in $\hat{b}_1(t)$ . . . . .	95
4.1	Raised cosine pulses . . . . .	107
4.2	2-ray channel model . . . . .	109
4.3	Variation of one channel tap . . . . .	111
4.4	$T/2$ -spaced DFE and decoder . . . . .	111
4.5	BER lower bound for DFE (800 MHz operation, CIR = $\infty$ ) . . . . .	115
4.6	BER lower bound for DFE (800 MHz operation, SNR = 30 dB) . . . . .	116
4.7	BER lower bound for DFE at various path delay (800 MHz operation) . . . . .	117
4.8	BER performance of RLS-DFE without tracking . . . . .	118
4.9	BER performance of RLS-DFE, 14 symbols per block . . . . .	120
4.10	BER performance of RLS-DFE, 7 symbols per block . . . . .	121
4.11	Channel estimation MSE versus CIR . . . . .	123
4.12	Calculated DFE used in a time slot . . . . .	124
4.13	BER distribution of calculated DFE . . . . .	125
4.14	DDFE used in a time slot . . . . .	126
4.15	BER distribution of DDFE and standard calculated DFE . . . . .	127
4.16	Comparison of BER performance . . . . .	128
4.17	Comparison of computational complexity . . . . .	132
5.1	BER lower bound (1.9 GHz operation, CIR = $\infty$ ) . . . . .	136

5.2	BER lower bound (1900 MHz operation, SNR = 30 dB) . . . . .	138
5.3	Variation of one channel tap (1900 MHz operation) . . . . .	139
5.4	Performance of DFE receiver, Case <i>A0</i> . . . . .	140
5.5	Channel sample insertion schemes . . . . .	142
5.6	DDFE partial bounds . . . . .	143
5.7	Curve fitting DFE partial bounds . . . . .	144
5.8	DLE partial bounds . . . . .	145
5.9	DDFE partial bounds with co-channel information . . . . .	146
5.10	Curve fitting DFE partial bounds with co-channel information . . . . .	147
5.11	DLE partial bounds with co-channel information . . . . .	148
5.12	Partial bounds for scheme <i>B4</i> . . . . .	149
5.13	Histogram of the LSSE . . . . .	150
5.14	DDFE receiver with blind channel estimation . . . . .	152
5.15	Curve fitting DFE receiver with blind channel estimation . . . . .	153
5.16	DLE receiver with blind channel estimation . . . . .	154
5.17	Blind channel estimation receivers with scheme <i>B4</i> . . . . .	155
5.18	MMSE for infinite LE . . . . .	156
5.19	Average MSE at 100 km/hr, theoretical analysis . . . . .	159
5.20	Channel and receiver pairs at various SNR and $ \Delta t $ . . . . .	160
5.21	Average MSE at 100 km/hr, simulation result . . . . .	161
5.22	Average MSE at 100 km/hr, theoretical result . . . . .	162
5.23	Probability of error in blind channel estimation . . . . .	163
5.24	DLE receiver performance for scheme <i>B4</i> . . . . .	166
5.25	DDFE receiver performance for scheme <i>B4</i> . . . . .	167

5.26	Curve fitting DFE receiver performance for scheme $B4$ . . . . .	168
5.27	MSE of channel estimate vs. length of estimation sequence . . . . .	170
5.28	BER performance for scheme $A2$ . . . . .	171
5.29	Insertion scheme $B6$ . . . . .	172
5.30	BER performance for scheme $A2$ and $B6$ . . . . .	173
5.31	BER performance for scheme $B4$ and $B6$ . . . . .	174
5.32	BER performance for scheme $B2$ and $B4$ . . . . .	176
A.1	Function to be integrated, $h(y)$ . . . . .	199
A.2	Area under the curve $h(y)$ , using <i>Table of Integrals</i> . . . . .	200
A.3	Correct area under the curve $h(y)$ . . . . .	201
B.1	Comparison of numerical integration results . . . . .	208
C.1	Data communication in an AWGN channel . . . . .	209

# List of Abbreviations and Acronyms

<u>Symbol</u>	<u>Description</u>
ACI	Adjacent Channel Interference
AMPS	Advanced Mobile Phone Service
AWGN	Additive White Gaussian Noise
BER	Bit-Error-Rate
$\mathbf{c}$	Covariance matrix
CCI	Co-Channel Interference
CDVCC	Coded Digital Verification Color Code
CIR	Carrier-to-Interference Ratio
DDFE	Displaced Decision Feedback Equalizer
DFE	Decision Feedback Equalizer
DLE	Displaced Linear Equalizer
$E[\blacksquare]$	Mathematical expectation of $\blacksquare$
$E_0$	Amplitude of the electric field component of the received signal
$E_b$	Baseband equivalent of the electric field component of the received signal

EDGE	Enhanced Data Rate for Global Evolution
EIA	Electronic Industries Association
$Ei(x)$	Exponential integral function
$E_r$	Average power of the received signal
$E_z$	Electric field component of the received signal
EM	Expectation Maximization
FDMA	Frequency-Division Multiple Access
FIR	Finite Impulse Response
FM	Frequency Modulation
FSE	Fractionally Spaced Equalizer
GA	Genetic Algorithm
GHz	Gigahertz (one billion cycles per second)
GSM	Global System for Mobile communication
$\mathbf{\blacksquare}^H$	Hermitian transpose of $\mathbf{\blacksquare}$
$H_{ub}(f)$	Transfer function of the Gans' channel simulator
Hz	Hertz
$I$	In-phase component of the $\pi/4$ -DQPSK symbol
IS-136	EIA Interim Standard 136
IS-54	EIA Interim Standard 54
ISI	Intersymbol Interference
$J(\mathbf{\blacksquare})$	Cost function
$J_n(x)$	The $n$ th order Bessel function of the first kind
JDCE	Joint Data and Channel Estimation
JMLSE	Joint Maximum Likelihood Sequence Estimation

LE	Linear Equalizer
LMS	Least-Mean-Square
LSE	Least Square Estimation
LSSE	Least Sum of Squared Errors
MAP	Maximum A Posteriori estimation
MHz	Megahertz (one million cycles per second)
ML	Maximum Likelihood
MLE	Maximum Likelihood Estimation
MLSE	Maximum Likelihood Sequence Estimation
MMSE	Minimum Mean Square Error
MSE	Mean Square Error
MUSIC	Multiple Signal Classification
$N_b$	Equalizer coefficient update frequency
$N_c$	Length of channel
$N_{ff}$	Number of feed forward taps in a DFE
$N_h$	Length of the overall channel
$N_{iw}$	Number of incident waves
$N_m$	Number of resolvable multipaths
$N_o$	Power spectral density of noise
$N_s$	Number of channel samples in a time slot
$N_t$	Length of the training sequence
NTT	Nippon Telegraph and Telephone
$N_w$	Number of taps in the equalizer
$\mathcal{O}(\blacksquare)$	Order of $\blacksquare$

PDF	Probability Density Function
$P_r$	Mean received power
$Q$	Quadrature component of the $\pi/4$ -DQPSK symbol
RLS	Recursive Least-Squares
$S$	Auto correlation matrix of the transmitted sequence
SNR	Signal-to-Noise Ratio
SSE	Sum of Squared Errors
SYNC	Synchronization
$T$	Symbol period
$\mathbf{A}^T$	Transpose of $\mathbf{A}$
TACS	Total Access Communication System
TDMA	Time-Division Multiple Access
$\mathbf{A}_I$	Time-Invariant variable $\mathbf{A}$
$\mathbf{A}_V$	Time-Varying variable $\mathbf{A}$
USDC	United States Digital Cellular system
VA	Viterbi Algorithm
ZF	Zero-Forcing
$b_n$	Information symbol
$\hat{b}_n$	Estimated information symbol at the output of receiver
$c(t)$	Continuous-time channel impulse response
$dB$	Decibel
$\det(\mathbf{A})$	Determinant of $\mathbf{A}$
$f$	frequency
$h(t)$	Overall channel impulse response

iid	Independently Identically Distributed
kHz	Kilohertz (one thousand cycles per second)
km/hr	Kilometers per hour
$p(t)$	Continuous-time transmit filter impulse response
$r(t)$	Received signal
$s(t)$	Transmitted signal at the output of transmitter
$v$	Vehicle speed
$w(t)$	Equalizer impulse response
$\mathbf{z}$	Cross correlation vector of the input and output of the channel
$\Delta\theta$	Differential phase
$\Phi(f)$	Power spectral density
$\Xi(f)$	Fourier transform of the auto correlation function $\xi(t)$
$\alpha$	Envelope of the complex attenuation
$\beta$	Roll off factor of the raised cosine pulse
$\delta(t)$	Dirac delta function
$\eta(t)$	Baseband noise
$\gamma$	Signal-to-noise ratio
$\lambda$	Wavelengths
$\nu(t)$	Interfering signal
$\phi$	Random phase angle of the Doppler shift
$\pi/4$ -DQPSK	$\pi/4$ -shifted Differential Quadrature Phase Shift Keying
$\sigma^2$	Variance of a random variable
$\tau$	Time delay
$\varepsilon$	Mean square error

$\varepsilon_{min}$	Minimum mean square error
$\varphi(t)$	Characteristic function of the quadratic form
$\vartheta$	Phase of the complex attenuation
$\xi(t)$	Auto correlation function of the overall channel
$\zeta$	Incident angle

# Chapter 1

## Introduction

### 1.1 Motivation

The global demand for wireless communications has grown rapidly over the last decade and the growth is predicted to continue over the next decade [2–10]. The attraction of wireless networking is its ability to offer mobility and portability which conventional wired systems lack. In addition, wireless networking provides connectivity with minimal infrastructure requirements. With this advantage, it can support an initially sparse subscriber base with low penetration rate. Wireless technology also provides “instant networks” in countries which lack existing copper or fiber infrastructure, and makes telecommunication service possible for some remote areas [6], where both time and cost to deploy a wired network are prohibitive.

For cellular phone usage only, the annual increase in cellular subscribers world wide averaged about 40% over the past decade [8], leaping from four million in 1988 to 123 million in 1995 [2], with a projection of over 590 million by the end of year 2001 [8]. It is anticipated that, by 2010, more than half of all communications

will be carried by mobile cellular networks [5], and wireless technology will become the primary source for voice communication, with a total market penetration of 50-60% [8].

The potential market for wireless communications is enormous, especially in the developing countries. The land-line telephone densities in countries like China, India, Pakistan and the Phillipines, are 30 times lower than in some countries in North America and Europe. It is estimated that approximately three billion people have no phone at home [2] and they become a huge source for potential cellular subscribers.

As a mainstream communication medium with an enormous potential to grow, cellular technology is poised to take on new challenges, providing high-speed data transmission services as well as voice communication services to users on the move. This gives rise to the third generation cellular networks with the goal of providing personal communication services any time and anywhere. The major improvement of the third generation cellular networks is the provision of multiple-data-rate services. High data rate enables a broader range of services, including wireless Internet access, video conferencing, wireless e-mail and multimedia, beyond the traditional voice only services. According to analysts, by the year of 2003, there will be more than one billion wireless phones with Internet access capabilities [3]. These additional high-speed data services, in turn, are fueling the demand for wireless cellular communications.

The rapid growth of the wireless mobile community and its demand for high-speed communications stand in contrast to the rather scarce spectrum resource available. It is of growing interest to maximize the capacity of the network system in the most cost-efficient manner. Therefore, it is essential to employ some feasible

receiver schemes at the base station to achieve good system performance, and hence high system capacity.

This research thesis investigates various receiver schemes that can potentially provide good performance in time division multiple access (TDMA) cellular radio transmission. The major performance limiting factors in TDMA cellular communication are the interference and the multipath fading environment. Interference includes intersymbol interference (ISI) and co-channel interference (CCI); the effect of interference can be reduced by the use of equalization. The multipath fading environment where transmission is carried out causes the channel to vary with time in an unpredictable manner. It is essential to employ some advanced techniques to estimate the time-varying channel accurately so that the transmitted data signal can be retrieved at the receiver end with minimum error. Therefore, in this research thesis, equalization and channel estimation techniques are studied and discussed, and various combinations of equalization and channel estimation techniques are investigated in some practical applications. Evaluations of different techniques are based on the system performance they offer and the complexity for receiver implementation.

## **1.2 Literature Survey**

In this section, a summary of some of the previous work related to the four subject areas, namely, equalization techniques, CCI suppression techniques, channel estimation techniques and strategies dealing with time-varying channels, is presented. This is not meant to be a comprehensive literature survey. Its purpose is to provide the readers with the background references on some of the ongoing research

in the subject areas.

## 1.2.1 Equalization Techniques

### 1.2.1.1 Linear and Non-Linear Equalization

Depending on the linearity of the digital filter, an equalizer falls into two categories: linear equalizer (LE) and non-linear equalizer. The LE is well known for its simplicity in implementation and analysis. However, it causes noise enhancement at channel spectral nulls, and it is often not suitable for applications where frequency selective fading takes place [11].

Non-linear equalizers, such as maximum likelihood sequence estimation (MLSE) and decision feedback equalization, can more effectively deal with the frequency selective fading problem. In fact, MLSE is the optimum equalizer in the presence of ISI and white noise in the sense of minimizing the probability of sequence error [12, 13], given knowledge of the channel impulse response. Despite its optimality, MLSE has two inherent limitations: the memory and computational requirement for metric computations, and the decision delay, which makes it difficult to track the fast fading channels in high-speed mobile communications [11, 13–16]. It is suggested that the computational burden can be eased by reducing the number of states and sequences in the MLSE detector [17]. The decision delay problem can also be removed by using the zero-delay tentative decisions extracted from the surviving paths instead of the final decision at the output of the MLSE, and good tracking performance can be offered by the adaptive MLSE [14–16, 18, 19].

Decision feedback equalization is a suboptimum and less complex equalization technique, compared to MLSE. A decision feedback equalizer (DFE) consists of a

feed forward filter which is used to minimize the effects of noise and precursors caused by the future symbols, and a feedback filter whose task is to properly weight the decision of the previous symbol so that the postcursors caused by the previous symbol can be cancelled out. In this way, with the correct past decision, a DFE can completely eliminate the ISI introduced by the selective fading channel and it is widely used in mobile communication applications. Some of these DFEs are modified to meet the need of a specific application. Belfiore et al. proposed a distortion predictive DFE whose feedback filter is a predictor, driven by the difference between the outputs of the feed forward filter and the decision device [20]. As a result, the noise and the residual ISI at the output of the feed forward filter can be predicted by the feedback filter and subtracted from the feed forward filter output. In applications of fast fading channels, a bi-directional DFE is used to locate the deep fade and recover data after it occurs [21]. As implied by its name, a bi-directional DFE operates in both forward and reverse directions.

### 1.2.1.2 Adaptive Equalization

For the last few decades, adaptive signal processing theory has been well established. As suggested by the word *adaptive*, this type of equalization can self-adjust to the unknown environment to provide reliable performance. For more background information, the readers are referred to the textbook by Haykin [22] and papers by Qureshi [23] and Proakis [12].

Adaptive equalization techniques are widely used in many practical applications due to their robustness in the sense that they do not require any prior information of the channel and the transmitted data [11, 22]. In mobile radio communication applications, an adaptive equalizer can adjust not only to the unknown channel,

but also the time-varying characteristics of the channel [14, 16, 24, 25]. An array of adaptive equalizers can also be used in flat fading applications to perform diversity combining to cancel interference [25, 26].

In order to obtain the gain provided by diversity combining and compensate for ISI at the same time, Scott proposed a digital multichannel baseband filter as an appropriate structure for receivers with both antenna diversity and adaptive equalization capability [27]. This multichannel baseband filter can also be a DFE with fractionally-spaced Feedforward filter [27]. This filter structure will be used in the applications in this thesis.

### 1.2.1.3 Fractionally Spaced Equalization

In a fractionally spaced equalizer (FSE), the delay between taps is only a fraction of the symbol duration. An FSE is usually used so that the fractionally spaced sampling of the input signal to the FSE meets the Nyquist sampling criterion to avoid aliasing [12].

The use of an FSE has other advantages compared with a conventional  $T$ -spaced equalizer. Simulation results given in the paper by Gitlin et al. [28] have demonstrated its effectiveness over the  $T$ -spaced equalizer. This superior performance can be explained by the fact that it realizes the optimum linear receiver. In fact, an FSE combines the functions of a matched filter, which reduces the effect of the noise, and equalization, which compensates for the ISI, into one single filter structure [12, 23, 28]. Consequently, it can compensate for severe delay distortion more effectively with less noise enhancement and its performance is insensitive to the sampling phase [23, 28].

### 1.2.2 CCI Suppression Techniques

The first approach to CCI suppression is the use of diversity techniques. In this approach, several replicas of the same information signal are transmitted over statistically independent paths in space, time or frequency, depending on the type of diversity. Diversity techniques were originally used to combat fading in the multipath environment [11]. Since the same interfering signals are present in the received signal from each diversity path, these received signals can be combined to suppress the interfering signals. Winters first showed that the signals from  $L_d$  receiving antennas can be combined to suppress the interfering signals, by the use of an optimum combiner [26]. Due to its interference suppression capability, the system performance offered by the optimum combining technique is superior to the traditional maximal ratio combining technique where interference at each receiving antennas is assumed to be independent [26]. Calderbank et al. in a recent paper reported that time diversity provided by repetitive channel coding can also be used for interference cancellation [29]. Results from both space and time diversity combining techniques showed that receiver receiving signals from  $L_d$  different antennas or time slots can completely eliminate  $L_d - 1$  interfering signals and an  $L_d$ -fold increase in user capacity can be achieved [29, 30]. Based on these results, Winters et al. generalized that with  $L_d + N_d$  antennas in the receiver,  $N_d - 1$  interfering users can be nulled out, and each of the  $N_d$  users can also benefit from the  $L_d + 1$  path diversity improvement [31]. Space and time diversity can also be combined in applications of CCI cancellation [29, 32].

Instead of eliminating the interfering signals, the multi-user detection techniques in the second approach to CCI suppression, are used to demodulate all users jointly. Verdú showed that the optimum multi-user detector consists of a bank of single-user

matched filters followed by Viterbi algorithm (VA) for all users and its complexity increases exponentially with the number of users [33]. While the optimum solution may be prohibitively complex, designing and applying suboptimum solutions to practical problems is a more attractive research area [34–37]. Suboptimum receiver structures such as the truncated T-MLSE using only a portion of the path metric, and T/2-MLSE are reported to offer good interference rejection capability [36]. With only one T/2-spaced noise whitening filter for each receiving antenna, a T/2-MLSE receiver is more suitable for implementations [36]. While in these two MLSE based receivers, perfect channel estimates are assumed to be available for all users in the system, they can be estimated using the ML criterion with training sequences, as shown in the paper by Ranta et al., where a joint MLSE (JMLSE) detector is used with the Viterbi algorithm [37].

CCI cancellation can also be achieved by introducing interference cancellation into the channel estimation process. This is accomplished by estimating and incorporating the impairment correlation matrix, where non-zero off-diagonal elements allow interference to be cancelled, in channel estimation and tracking [38].

### 1.2.3 Channel Estimation Techniques

Depending on the availability of the training sequence, channel estimation techniques can be coarsely classified into two categories: non-blind and blind techniques.

When a training sequence is available, estimation of the channel is straight forward by using one of the criteria for optimization, such as least square estimation (LSE), maximum likelihood estimation (MLE) or maximum *a posteriori* estimation (MAP) [37, 39–42]. The LSE method requires no *a priori* statistical information of the noise and the channel, whereas the MLE method requires the statistics of the

noise and it is the best linear unbiased estimator for the estimation problem [42]. When the noise is uncorrelated, both the LSE and MLE yield the same solution. On the other hand, MAP requires both statistical information on the noise and the channel, and it is not as robust as the LSE and MLE. The channel can also be estimated using adaptive algorithms, such as recursive least-squares (RLS), least-mean-square (LMS) and the Kalman filter algorithm [13, 15, 16, 22, 38, 43, 44]. The Kalman filter algorithm is designed for applications of dynamic systems and it is robust in estimating and tracking the time-varying channels.

For blind channel estimation techniques, there are two well known approaches in the literature: second- and higher- order statistics-based methods and joint data and channel estimation (JDCE) methods.

Without a training sequence, the algorithms in the first approach use second-order cyclostationary statistics of the oversampled received signal [45, 46] or higher-order statistics of the  $T$ -spaced received signal [22, 47, 48] to identify the unknown channel. Since these statistics convey phase information, they allow recovery of the phase, as well as the magnitude response of the unknown, possibly non-minimum phase channel. However, this class of algorithms exhibits slow convergence due to the fact that large number of samples must be processed in order for the estimates of the statistics to be accurate. Especially in the case of digital mobile communications, these algorithms simply may not be able to track the variations of the environment. Therefore, these blind algorithms may not be suitable for applications where rapid acquisition is a necessary requirement.

The ML-based JDCE methods are proposed to improve the rate of convergence in blind system identification, at the expense of computational complexity. The straight forward, yet exhaustive solution described in the paper by Seshadri [17] in-

volves two steps: least square channel estimation for all the possible data sequences, and the selection of the data sequence and its corresponding channel estimate which maximize the likelihood of the received signal. This solution is optimum yet its complexity grows exponentially with the size of the data record. In his paper, Seshadri proposed an optimum blind trellis search algorithm in which complexity increases linearly with the size of the data record [17]. While these optimum solutions may be prohibitively complex to implement, except for small data alphabet size and small data record, designing for suboptimum algorithms is an active research area. The segmental K-means algorithm and the expectation maximization (EM) algorithm iterate between estimations of channel and data until convergence is achieved [49]. Since both algorithms rely on the quality of the initial guess of the channel, high error rate led by a bad initial channel estimate is inevitable and global convergence cannot be guaranteed. A suboptimum blind trellis search algorithm, in which more than one best estimate of the transmitted data sequence will be retained into each state, is reported to exhibit superior convergence property and offer excellent performance [17]. In fact, this algorithm can deal with channels with fast fading rate relative to the symbol rate, and provide reliable performance for the EIA Interim Standard (IS-54) mobile communication system [14]. The JDCE method proposed by Chen et al. uses a genetic algorithm (GA) to select populations for channel estimates for each of which a VA is employed to decode data [50]. On the other hand, the “quantized” channel approach to JDCE operates over a grid in the channel space that could be made finer by using the ML criterion to confine the channel estimate in the neighborhood of the unknown channel [51]. This algorithm enables efficient parallel implementation of VA which is employed to decode data [51]. Both JDCE methods with GA and with the quantized channel approach have demonstrated

good convergence properties.

### 1.2.4 Strategies Dealing with Time-Varying Channels

In mobile communications, the fact that the unknown communication channel also varies rapidly with time makes reliable transmission of data even more difficult to accomplish. In the past decades, various strategies have been proposed to deal with the fast time-varying environment. Some of these strategies are summarized in this section.

Tracking of the variations in the fast time-varying channel using various adaptive algorithms is an effective approach to combat fading. Since training is only available for a very short period during a TDMA time slot, update of the channel information, and hence the equalizer, relies on the decoded data. Therefore, tracking is usually decision directed and the performance of a receiver employing such a tracking scheme depends heavily on the accuracy of the past decisions. These adaptive algorithms include the well known LMS and RLS algorithms [13, 16, 24, 40, 52]. In general, the LMS algorithm displays better tracking behavior than the RLS algorithm since the RLS algorithm is model dependent [24]. Haykin et al. proposed extended forms of the RLS algorithm which demonstrate superior tracking behavior compared with the standard RLS and LMS algorithm [24]. This can be explained by the fact that the RLS algorithm is a special form of Kalman filter. By incorporating some good tracking properties of the Kalman filter into the standard RLS algorithm, the extended RLS should track better [24]. The Kalman filter is well known for its excellent tracking capability and it is in fact the optimum linear tracking device on the basis of second-order statistics [24]. It is also widely used in applications of tracking fast time-varying communication media and superior performance is

reported [15, 38, 44].

A simple way to deal with time-varying channel is the use of a bi-directional equalizer. It is an equalizer which operates in both forward and reverse directions to process signal before and after the training sequence. As simple as it is, results showed that it is an effective strategy [21, 53, 54], provided that the known training sequence occurs as often as deep fades [21].

At a moderate fading rate, both the decision-directed tracking strategies and bi-directional equalization have proven to be effective. However, at a high fading rate, such as 100 Hz for an application with symbol Rate of 24.3 kHz, these strategies are no longer feasible due to the error propagation problem in the decision directed strategies [55], and more than one deep fade may occur between two training sequences in bi-directional equalization. In this case, an increase in occurrence of known channel samples during a time slot is required. This can be achieved by either increasing the frequency of training at the expense of reduction in system throughput, or some other means. Lo et al. proposed a block adaptation strategy in which more interpolated channel estimates are used [55]. These channel estimates are obtained by interpolating those estimated from training sequences from several adjacent time slots by using a raised cosine lowpass interpolator [55]. Despite the inherent processing delay, which could be up to a few time slots, this method offers good immunity to fast fading and hence better system performance [41, 55, 56].

Another approach to the fast fading problem involves the subspace expansion of the time-varying parameters of the channel [57, 58]. By expanding the time-varying channel coefficients onto a set of basis sequences, from which time-invariant parameters are to be determined, the problem is transformed to a time-invariant one [57]. The performance offered by such an approach depends on the model of

the channel, as well as the choice of basis sequences.

## 1.3 Thesis Contributions

This research thesis mainly focuses on equalization and channel estimation techniques and the goal is to find some combination of these techniques that can provide good performance for TDMA systems. The contributions of this thesis consist of practical algorithms and methods developed to achieve this goal, as well as the theoretical analyses of some of the existing and new methods.

The first contribution is the development of an exhaustive ML blind data, channel and co-channel estimation method which is an extension of the exhaustive ML blind data and channel estimation method described by Seshadri [17]. This method allows the estimation of the co-channel and interfering signal, which could lead to CCI suppression.

The second contribution is the development of a Doppler frequency estimation technique using cross correlation of the transmitted and received signal, which allows successful modeling of the time-varying channel. In the work of Tsatsanis et al. [57], frequency estimation is accomplished by using the autocorrelation and the fourth-order statistics of the received signal. By using the cross correlation, accuracy of the frequency estimation can be improved.

The third and the fourth contributions are the two equalization techniques that deal with time-varying channels, the displaced equalizer and the curve fitting techniques. The displaced equalizer requires no interpolation like the fixed equalizer but its performance is better. This equalizer only operates in the forward direction, whereas the bi-directional equalizer [21] and the MLSE equalizer used in GSM op-

erate in both forward and reverse directions. The curve fitting technique is more complex but offers better performance. Both of these techniques are used to deal with time-varying channels.

The novelty of this thesis is also demonstrated by the formulation of the block adaption with blind channel estimation strategy to deal with the fast time-varying channel within a TDMA time slot. This strategy involves combinations of channel estimation and interpolation methods. In a TDMA time slot, there are usually one or two known sequences and with the channel estimates obtained from these sequences, it might be insufficient to predict the time variations between known sequences. In this strategy, more channel estimates can be obtained together with small sequences of unknown data by using the ML blind data and channel estimation method. The time-varying channel during a time slot can then be reconstructed by interpolating these channel estimates using one of the interpolation methods and the coefficients of the equalizer can be determined by using the Wiener-Hopf equations. A similar strategy can be applied to deal with the time variations in the co-channel as well in order to suppress the CCI.

In addition to the development of methods and algorithms, this thesis also makes theoretical contributions. The first theoretical contribution deals with the probability of error analysis of the effect of noise on the ML blind data and channel estimation method. The derivation of an upper bound for the probability of selecting a wrong channel estimate is also presented.

The second and the most important theoretical contribution is the MSE analysis of a displaced LE with infinite length on fading channels. An expression of the MSE of the displaced LE on noisy fading channels is also derived.

## 1.4 Thesis Organization

The outline of the thesis is given in the table of contents. In this section, the organization of the thesis is described in more detail.

In Chapter 1, the motivation contrasts the increasing demand for service with limited bandwidth resource in the existing cellular market, and suggests equalization and channel estimation techniques to improve the performance, and hence, the capacity of a TDMA system. The previous work related to the four subject areas – equalization techniques, channel estimation techniques, CCI suppression techniques and strategies dealing with time-varying channels – is summarized in the literature survey section. The thesis contributions section highlights some of the novel achievements of this thesis and this section describes how this thesis is organized to achieve the goal.

Chapter 2 describes a model of the digital wireless communication system which consists a transmitter, a channel and a receiver. With these models, the statistical properties of the transmitted data, the noise and the interference are discussed. Some commonly used models for the multipath fading channel and its variations are presented. Two receiver types, the continuous-time infinite-length LE and DFE are also considered.

In Chapter 3, the major contributions of this thesis, which involves algorithm development and theoretical analysis, are described in detail. In the channel estimation area, an exhaustive ML blind data, channel and co-channel estimation technique and a Doppler frequency estimation technique, both extended from the previous work, are proposed. The sign ambiguity problem and the probability of error associated with blind data and channel estimation are investigated. The two proposed equalization techniques dealing with time-varying channels are the dis-

placed equalizer and the curve fitting equalizer. In order to characterize and equalize the time-varying channel accurately and efficiently, a block adaptation technique with blind channel estimation is proposed, which involves combinations of different channel estimation and interpolation techniques. An expression for the MSE of a displaced LE with infinite duration under a time-varying channel is also derived at the end of the chapter, as the result of a novel theoretical analysis.

Chapter 4 shows the application of some of the above techniques in the 800 MHz operation of the EIA Interim Standard 136 (IS-136) TDMA cellular system. This chapter first shows some background information and a description of the IS-136 system. The performance of three receiver types, namely the adaptive DFE, the standard channel estimation based DFE and the DDFE are studied and compared. The complexity associated with each receiver type is also discussed.

Chapter 5 presents the application to the IS-136 system at a carrier frequency of 1.9 GHz. Compared to the 800 MHz case, the system in this application experiences a Doppler frequency twice as high, and the faster channel variations in this application makes predicting the time-varying channel more difficult. Performance of various LE and DFE receivers, including bounds and partial bounds, where perfect channel estimation is assumed, as well as the performance with ML blind data and channel estimation is presented and compared. In order to verify some of the theoretical analysis performed in Chapter 3, simulation results are also presented as a comparison, and the difference between theoretical and simulated results is explained. Complexity of receivers with different channel estimation and interpolation techniques and different equalizer types is also studied and compared at the end of the chapter.

Chapter 6 concludes the thesis with a summary of work accomplished in each

chapter, followed by suggestions for possible extensions of the research topics of this thesis.

# Chapter 2

## System Descriptions

The purpose of a communication system is to transmit an information-bearing signal from one location to another. In digital communications, the digital information is converted into analog waveforms that match the characteristics of the communication channel before it can be transmitted over the channel. This conversion is often performed at the transmitter. Due to its inherent limitations, the communication channel is usually corrupted by noise and interference. The goal of the receiver is to reproduce the original information-bearing signal which is distorted by the impaired communication channel.

Figure 2.1 shows a baseband model of the digital wireless communication system. The basic elements of the communication system are shown here: the transmitted information symbol  $b_n$ , the transmitter with a pulse shaping filter with impulse response  $p(t)$ , the channel with impulse response  $c(t)$ , the baseband noise  $\eta(t)$ , the interference  $\nu(t)$ , the receiver and the estimated symbol  $\hat{b}_n$  at its output. A number of basic assumptions are made in this model. It is assumed that the signal of interest and the signals of the interferers are modulated using a linear modulation

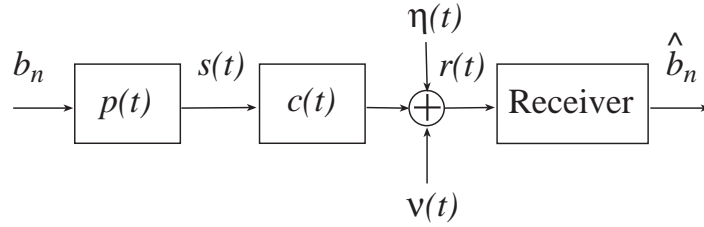


**Figure 2.1:** Baseband model of a digital wireless communication system

scheme and they are all transmitted at the same symbol rate  $1/T$  Hz. Furthermore, the discussions in this chapter are limited to baseband transmission only, and the conversion between baseband and passband representations is detailed in the work of Proakis [11].

## 2.1 Transmitter

The input to the transmitter  $\{b_n\}$  is an encoded information-bearing symbol which is obtained by mapping the binary bits using one of the encoding schemes. These transmitted symbols are complex valued, in general. They are mutually uncorrelated with unit variance and zero mean, that is,

$$E[b_n] = 0 \quad (2.1)$$

and

$$E[b_n b_m^*] = \sigma_b^2 \delta_{n-m}, \quad (2.2)$$

where  $\blacksquare^*$  denotes the complex conjugate of  $\blacksquare$ ,  $\sigma_b^2$  is the variance of the transmitted

data and it is unity, and  $\delta_n$  is the discrete-time impulse function defined as

$$\delta_n = \begin{cases} 0, & n \neq 0 \\ 1, & n = 0. \end{cases} \quad (2.3)$$

The notation  $E[\blacksquare]$  in Equations 2.1 and 2.2 denotes mathematical expectation.

The transmitter modulates the information-bearing symbol upon an analog real signal pulse waveform  $p(t)$ , which shapes the spectrum of the transmitted signal. For each symbol, a pulse is produced. The signal at the output of the transmitter is a sequence of pulses centered at  $nT$ , with amplitude  $b_n$ , assuming linear modulation schemes [11, 59]:

$$s(t) = \sum_{n=-\infty}^{\infty} b_n p(t - nT). \quad (2.4)$$

The pulse  $p(t)$  is band-limited to  $W$ ,  $|f| \leq W$ , where  $W$  is the channel bandwidth. Since the communication channel is also band-limited to  $W$ , the purpose of pulse shape is to band-limit the transmitted signal. Therefore, the transmitted signal has a band-limited frequency response characteristic  $S(f)$ .

## 2.2 Channel

As shown in Figure 2.1, the communication channel is modeled by a channel impulse response  $c(t)$ , additive noise  $\eta(t)$  and additive interference  $\nu(t)$ . It is a common practice, for convenience, to combine the pulse used in the transmitter

with the channel impulse response to obtain an overall channel, denoted by  $h(t)$ :

$$h(t) = p(t) \star c(t), \quad (2.5)$$

where symbol  $\star$  denotes the continuous-time convolution operation and it is defined as

$$\blacksquare(t) \star \blacklozenge(t) = \int_{-\infty}^{\infty} \blacksquare(\tau) \blacklozenge(t - \tau) d\tau. \quad (2.6)$$

The received signal  $r(t)$  consists of three components: the distorted signal at the output of  $c(t)$ , which conveys the information symbols, the noise and the interference. It is given by the following equation:

$$r(t) = \sum_{n=-\infty}^{\infty} b_n h(t - nT) + \eta(t) + \nu(t). \quad (2.7)$$

In the following sections, the models of the noise, interference and the channel impulse response are discussed in detail.

### 2.2.1 Noise

Noise in a communication system generally refers to the unwanted random process that introduce distortion to the transmission and processing of the signal of interest. Its presence is inevitable and it is a limiting factor on the power required in the transmission of the information-bearing signal over the channel. Noise is random in nature and it is usually independent of the signal of interest.

Noise may originate from the surrounding environment. Components in the communication system, such as nonlinear amplifiers and quantizers, and other electrical

devices at the receiver can also introduce noise. It is difficult to analyze, individually, these different types of noise. Therefore, the noise from different sources are lumped together, and the net effect is modeled as an additive component to the received signal. It is commonly referred to as channel noise or front-end receiver noise [60].

Noise introduced at the receiver input belongs to the class of thermal noise. It is often statistically characterized as a random Gaussian process with zero mean, and it is uncorrelated with the transmitted data:

$$E[\eta(t)] = 0 \quad (2.8)$$

$$E[b_n \eta^*(t)] = E[b_n^* \eta(t)] = 0 \quad (2.9)$$

Here  $\eta(t)$  is the baseband representation of the noise and it is complex-valued. In order to simplify the analysis of the system performance, the channel noise is assumed to be white. This assumption can be justified in practice. This implies that the channel noise is mutually uncorrelated in time and it has a constant power spectral density over the entire frequency range:

$$E[\eta(t_0)\eta^*(t_1)] = N_o\delta(t_0 - t_1), \quad (2.10)$$

where  $t_0$  and  $t_1$  two different points in the time axis. The parameter  $N_o$  is the noise power spectral density measured in Watts per Hertz and the power spectral density of the noise is given by:

$$\Phi_\eta(f) = N_o. \quad (2.11)$$

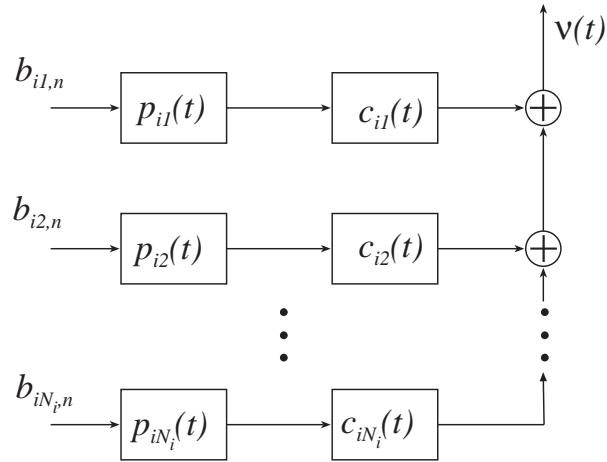


**Figure 2.2:** Model for co-channel interference

Due to the complex nature of the baseband noise, its real and imaginary parts each have a power spectral density of  $N_o/2$ .

### 2.2.2 Interference

In TDMA transmission, the most common system-generated cellular interference are CCI and adjacent channel interference (ACI). ACI results from the signals which are transmitted in the frequency channel adjacent to the signal of interest. Often, it can be minimized through proper receiver filter design and channel assignment [1] and it is not in the scope of this thesis. Here the main focus is on CCI.

In cellular systems, CCI originates from the frequency reuse plan which allows the frequency channel to be reused in another cell [61]. This results in signals from co-channel cells being received in the desired cell. Unlike channel noise, CCI cannot be overcome by raising the power level of the transmitted signal, since it would increase the level of CCI for the co-channel cells and ACI for the neighboring cells. One way to suppress CCI in a cellular system is to use equalization, which will be discussed in detail in later chapters.

Figure 2.2 shows a model of CCI [37,62].  $\{b_{ik,n}\}$  is the complex-valued transmitted data sequence of the  $k$ th interferer, for  $k = 1, 2, \dots, N_i$ , where  $N_i$  is the number of interferers. The subscript  $i$  denotes “interference”. The transmitted data of the interferers, the data of interest and the noise are assumed to be statistically independent, and the data of the interferers have zero mean with unit variance, that is,

$$E[b_{ik,n}] = 0 \quad (2.12)$$

$$E[b_{ik,n} b_{iq,m}^*] = \sigma_b^2 \delta_{n-m} \delta_{k-q} \quad (2.13)$$

$$\sigma_b^2 = 1 \quad (2.14)$$

$$E[b_n b_{ik,m}^*] = E[b_n^* b_{ik,m}] = 0 \quad (2.15)$$

$$E[b_{ik,n} \eta^*(t)] = E[b_{ik,n}^* \eta(t)] = 0. \quad (2.16)$$

$p_{ik}(t)$  is the pulse used in the transmitter and  $c_{ik}(t)$  is the co-channel of the  $k$ th interferer. The impulse response of the  $k$ th overall co-channel  $h_{ik}(t)$  is given by the convolution of the pulse and the co-channel:

$$h_{ik}(t) = p_{ik}(t) \star c_{ik}(t). \quad (2.17)$$

The interference at the input of the desired receiver is the sum of all the individual interference:

$$\nu(t) = \sum_{k=1}^{N_i} \sum_{n=-\infty}^{\infty} b_n h_{ik}(t - nT). \quad (2.18)$$

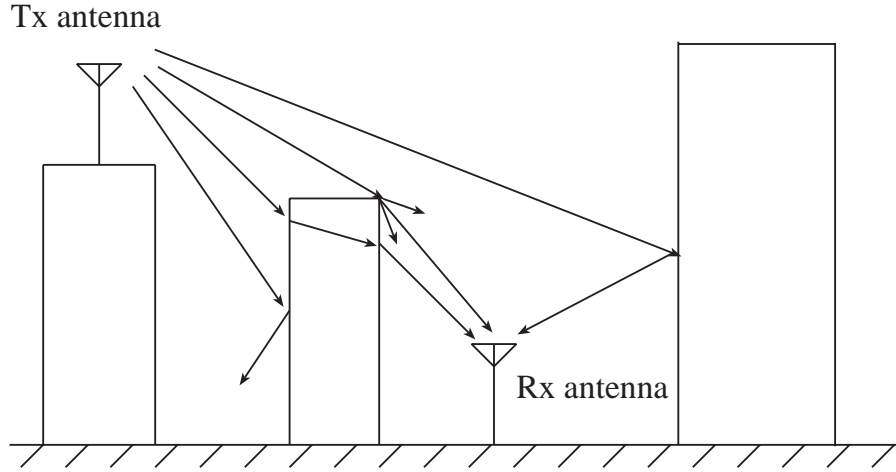


**Figure 2.3:** Transmission in the multipath environment [1]

### 2.2.3 Channel Impulse Response

In radio communication, the transmission media is considered to be linear, in terms of their influence on the signal of interest [63]. Therefore, a radio channel can be modeled as a linear filter [1] in which the impulse response is used to model the random attenuation and propagation delay introduced on the signal of interest by the physical channel.

#### 2.2.3.1 Discrete-time Multipath Channel Impulse Response

For most cellular radio transmission in urban areas with many high-rise buildings, there is no direct line-of-sight path between the transmitter and the receiver. As illustrated in Figure 2.3, due to multiple reflections, diffractions and scatterings from different objects and obstacles in the surroundings, the communication signal propagates along different paths at different directions and time, depending on the length of the path. The interaction between signals arriving from different paths gives rise to multipath fading.

There is an attenuation and propagation delay associated with each path. Both of these parameters are time-varying due to the changes in the structure of the transmission media and the time variations are random and often independent. Therefore, the impulse response of the multipath channel is also time-varying in a random manner and it can be characterized statistically.

The impulse response of the multipath channel can be described as a function of both time  $t$  and time delay  $\tau$ , and its discrete multipath continuous time model is given by [11]

$$c(t; \tau) = \sum_{n=0}^{N_m-1} \alpha_n(t) e^{-j\vartheta_n(t)} \delta(\tau - \tau_n(t)) \quad (2.19)$$

where  $\alpha_n(t) e^{-j\vartheta_n(t)}$  is the complex attenuation with envelope  $\alpha_n(t)$  and phase  $\vartheta_n(t)$ , and  $\tau_n(t)$  is the time delay occurring in the  $n$ th path. The complex attenuation and the time delay are all random processes that vary with time.

Equation 2.19 implies that at any time, the snapshot of the multipath channel is a function of  $\tau$  and the snapshot is different at different time instants. Figure 2.4 gives an example of the multipath channel impulse response at different snapshots.

### 2.2.3.2 Statistical Models for Fading Channels

The  $N_m$  replicas of transmitted signal received are from  $N_m$  *resolvable* paths. Here, *resolvable* is emphasized since the actual number of paths is much greater than  $N_m$ . Let  $\Delta\tau$  in Figure 2.4 be the resolvable delay interval. Within this interval, all the replicas of the transmitted signal received are summed and the sum of these replicas is assumed to arrive from one equivalent path which is also the resolvable path. Since the arrival of a large number of these replicas falls into one delay interval,

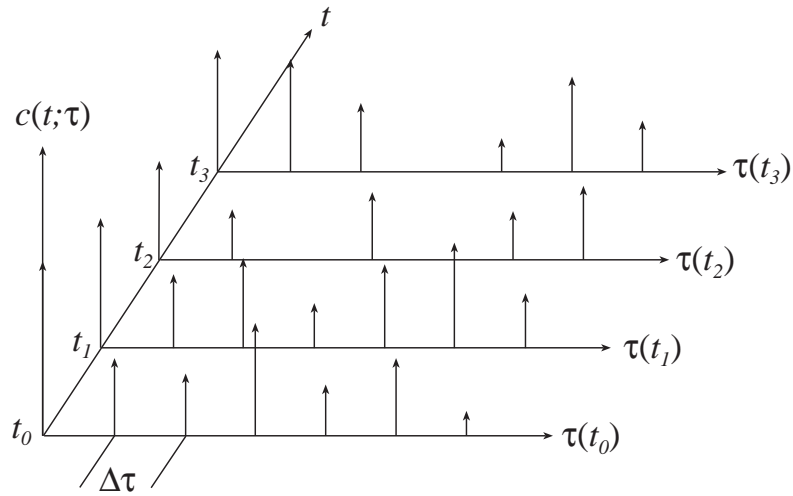


**Figure 2.4:** Multipath channel at different snapshots [1]

the central limit theorem can be applied. Therefore, the sum of the replicas and each resolvable channel path can be approximated as complex-valued Gaussian processes in time with zero mean.

If each resolvable path is modeled as a complex-valued Gaussian process, by changing the complex Gaussian random variables to polar coordinates, it is straight forward to conclude that the envelope of the attenuation is Rayleigh and the phase is uniformly distributed. This type of fading is referred to as Rayleigh fading.

### 2.2.3.3 Jakes' Model

Jakes [64] developed a model in which the statistical properties of electromagnetic fields of the signal received by a mobile are exploited. This model assumes a fixed transmitter with a vertically polarized antenna. Suppose there are  $N_{iw}$  component waves incident on the mobile traveling at a velocity of  $v$ . For the  $k$ th wave

incident at an angle  $\zeta_k$  with the direction of motion, the associated Doppler shift is

$$\begin{aligned} f_k &= \frac{v}{\lambda_w} \cos \zeta_k \\ &= f_m \cos \zeta_k \end{aligned} \quad (2.20)$$

where  $\lambda_w$  is the wavelength of the incident waves and  $f_m$  denotes maximum Doppler shift. The electric field component of the received signal is

$$E_z = E_0 \sum_{k=1}^{N_{iw}} \alpha_k \cos(2\pi f_c t + \vartheta_k), \quad (2.21)$$

where  $E_0 \alpha_k$  is the amplitude of the  $k$ th incident wave in the electric field,  $f_c$  is the carrier frequency,  $\vartheta_k$  is phase shift given by

$$\vartheta_k = 2\pi f_k t + \phi_{p,k} \quad (2.22)$$

and  $\phi_{p,k}$  is the random phase angle uniformly distributed from 0 to  $2\pi$ .

The baseband equivalent of  $E_z$  is given by

$$E_b = E_0 \sum_{k=1}^{N_{iw}} \alpha_k e^{j(2\pi f_m t \cos \zeta_k + \phi_{p,k})}. \quad (2.23)$$

Let  $p(\zeta)d\zeta$  denote the fraction of the total power of the incident waves within  $d\zeta$  of the angle  $\zeta$ , where  $p(\zeta)$  is the power per unit angle. Then the following relation holds:

$$\alpha_k^2 = p_\zeta(\zeta)d\zeta. \quad (2.24)$$

Assuming the distribution of power with the arrival angle  $\zeta$  is uniform:

$$p_{\zeta}(\zeta) = \frac{P_r}{2\pi}, \quad -\pi \leq \zeta \leq \pi \quad (2.25)$$

where  $P_r$  is the mean received power, and the  $N_{iw}$  incident waves are uniformly distributed over an interval of  $2\pi$ :

$$d\zeta = \frac{2\pi}{N_{iw}}, \quad (2.26)$$

then  $\alpha_k^2$  takes the value of  $P_r/N_{iw}$  and the  $k$ th arrival angle is

$$\zeta_k = \frac{2\pi k}{N_{iw}}. \quad (2.27)$$

In Equation 2.23, if  $N_{iw}$  is a large number, the central limit theorem can be applied and  $E_b$  is approximately complex Gaussian and its envelope  $|E_b|$  is Rayleigh distributed. In fact,  $|E_b|$  gives a good approximation to a Rayleigh random variable for  $N_{iw} \geq 7$  [65]. Figure 2.5 shows a comparison between theoretical and simulated Rayleigh probability density function using Jakes' model with  $N_{iw} = 9$ . In the work of Jakes [64],  $E_b$  is the baseband equivalent of the electric field component of the received signal. However, since the magnitude of Equation 2.23 gives a Rayleigh fading waveform, this model is usually used to simulate the Rayleigh fading channel paths [14,55,66]. As suggested in Equation 2.23, since the Rayleigh fading waveform can be approximated by the envelope of the sum of  $N_{iw}$  sinusoids, this model is also referred to as the "sum of sines" model. Consequently the frequency spectrum of  $E_b$  is discrete, with  $N_{iw}$  impulses at the Doppler frequency associated with each incident wave.

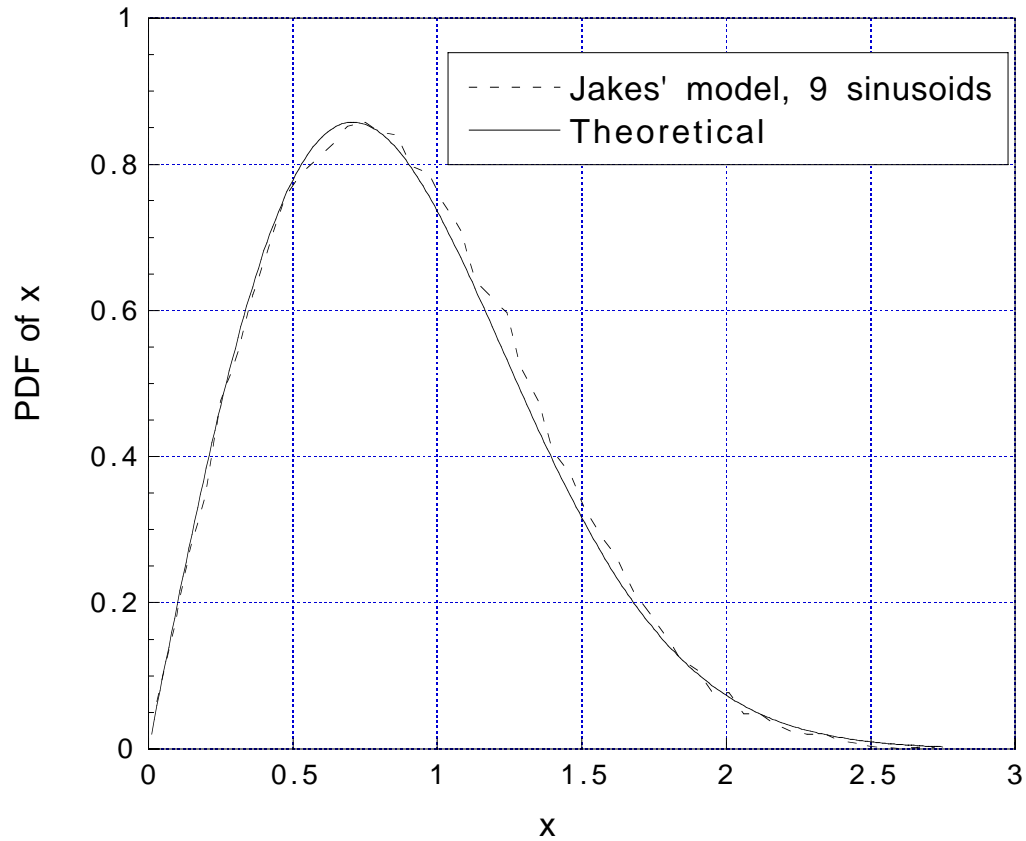


**Figure 2.5:** Theoretical and simulated Rayleigh PDF

#### 2.2.3.4 Gans' Model

Another model often used to simulate the Rayleigh fading channel path is Gans' model. Instead of the physical aspect of the fading mechanism, Gans focused on the relationship between the received power and the frequency and developed a spectrum analysis.

For a mobile moving at a velocity of  $v$ , this model assumes that the incident waves arrive from all directions with random phases, and the received power is uniformly distributed with respect to the angle of arrival, for any velocity. If the transmitted signal is narrowband with a carrier frequency of  $f_c$ , the instantaneous

frequency of the received signal component with an angle of arrival of  $\zeta$  is given by

$$f(\zeta) = f_c + f_m \cos \zeta. \quad (2.28)$$

For simplicity, only the one-sided power spectral density  $\Phi_{1u}(f)$  of the received signal is considered. From Equation 2.28, the instantaneous frequency changes from  $f_c + f_m$  to  $f_c - f_m$  as the angle of arrival increases from 0 to  $\pi$ .

For each  $\zeta$  and the corresponding  $f(\zeta)$ , the received power differentials must be the same [67]:

$$2p_\zeta(\zeta)d\zeta = \Phi_{1u}(f)(-df). \quad (2.29)$$

In the above equation, the factor 2 accounts for both the positive as well as the negative angles and the minus sign for  $df$  on the right hand side accounts for the fact that as  $\zeta$  increases,  $f(\zeta)$  decreases [67]. Rearranging Equation 2.29 gives

$$\Phi_{1u}(f) = -2p_\zeta(\zeta) \frac{d\zeta}{df} \quad (2.30)$$

By differentiating Equation 2.28,  $d\zeta/df$  can be obtained and the expression for  $\Phi_{1u}(f)$  is given by

$$\Phi_{1u}(f) = \frac{P_r}{\pi f_m \sqrt{1 - \left(\frac{f-f_c}{f_m}\right)^2}}. \quad (2.31)$$

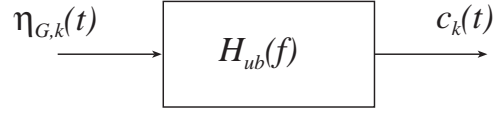


**Figure 2.6:** Simulation of Rayleigh fading channel tap using Gans' model

Therefore, the double-sided power spectral density of the received signal is [67]

$$\Phi_u(f) = \begin{cases} \frac{P_r}{2\pi f_m \sqrt{1 - \left(\frac{f+f_c}{f_m}\right)^2}}, & |f + f_c| \leq f_m \\ \frac{P_r}{2\pi f_m \sqrt{1 - \left(\frac{f-f_c}{f_m}\right)^2}}, & |f - f_c| \leq f_m \\ 0, & \text{otherwise.} \end{cases} \quad (2.32)$$

Note that Equation 2.32 produces an infinite power spectral density at  $f = \pm f_c \pm f_m$  which occurs when the angle of arrival is exactly 0 or  $\pi$ . The assumption that the incident waves arrive at the mobile from all directions implies a continuous distribution of the angle of arrival  $\zeta$ . Based on this assumption, the probability that the incident wave arrives at an angle of exactly 0 or  $\pi$  is zero. Therefore, the representation for the power spectral density is also valid for these boundary conditions.

The baseband spectrum is

$$\Phi_{ub}(f) = \begin{cases} \frac{P_r}{\pi f_m \sqrt{1 - \left(\frac{f}{f_m}\right)^2}}, & |f| \leq f_m \\ 0, & \text{otherwise.} \end{cases} \quad (2.33)$$

Unlike the frequency spectrum of  $E_b$ ,  $\Phi_{ub}(f)$  is continuous in frequency, except at  $|f| = f_m$ . Since the power spectral density given in Equation 2.33 take the shape of a ‘‘U’’, it is often referred to as the U-shaped Doppler spectrum.

Figure 2.6 shows a block diagram of a method of generating one tap of the

Rayleigh fading baseband channel. The  $k$ th tap of the Rayleigh fading channel is generated by applying a complex white Gaussian noise  $\eta_{G,k}(t)$ , with a power spectral density of  $N_{Go}$ , to the channel generator with transfer function of

$$H_{ub}(f) = \sqrt{\Phi_{ub}(f)}. \quad (2.34)$$

Therefore, the Rayleigh fading channel tap at the output of the generator is given by

$$c_k(t) = \int_{-\infty}^{\infty} h_{ub}(t - \tau)\eta_{G,k}(t)d\tau \quad (2.35)$$

where  $h_{ub}(t)$  is the time domain impulse response of the generator.

By applying the power spectral density relation of the input and output of a linear time-invariant system, the power spectral density of the time variations of the channel tap can be obtained:

$$\begin{aligned} \Phi_c(f) &= N_{Go}|H_{ub}(f)|^2 \\ &= N_{Go}\Phi_{ub}(f) \end{aligned} \quad (2.36)$$

which describes that the power spectral density of the variations in a Rayleigh fading channel tap at the output of the generator is also U-shaped.

### 2.2.3.5 Two-Ray Rayleigh Fading Model

In analyzing a communication system with a high data rate, it is important that the model for the multipath channel impulse response exhibit both fading, as well as the time delay properties of the physical channel. The two-ray Rayleigh fading

model, in which the channel impulse response consists of only two independent paths, can serve this purpose, for analyzing the performance aspect related to the IS-136 TDMA cellular standard [53]. The model can demonstrate these important characteristics of a mobile radio channel, yet its simplicity allows theoretical analysis and computer simulations [14, 53, 68, 69].

The impulse response of the two-ray model is given by

$$\begin{aligned} c(t; \tau) &= \alpha_0(t)e^{-j\vartheta_0(t)}\delta(\tau) + \alpha_1(t)e^{-j\vartheta_1(t)}\delta(\tau - \tau_1) \\ &= c_0(t)\delta(\tau) + c_1(t)\delta(\tau - \tau_1), \end{aligned} \quad (2.37)$$

where  $c_0(t)$  and  $c_1(t)$  are the independent complex gains or the tap coefficients of the two rays, whose envelope is Rayleigh and phase is uniformly distributed.

The term  $\tau_1$  is the time delay interval between path 0 and path 1. By varying  $\tau_1$ , different time delay effects can be provided and the degree of frequency selectivity of the channel can be varied. In one extreme case,  $\tau_1$  can be set to zero, and path 1 merges with path 0. As a result, a flat Rayleigh channel can be obtained.

## 2.3 Receiver

The input to the receiver is the information-bearing signal distorted by the channel, and the output is the estimated version of the transmitted data. Therefore, the task of the receiver is to retrieve the transmitted data faithfully so that the error rate can be as low as possible.

In high data rate transmission, ISI results from the multipath channel; if left uncompensated, could be severe enough to cause incorrect detection of the transmitted data. This makes it necessary to employ an equalizer in the receiver design

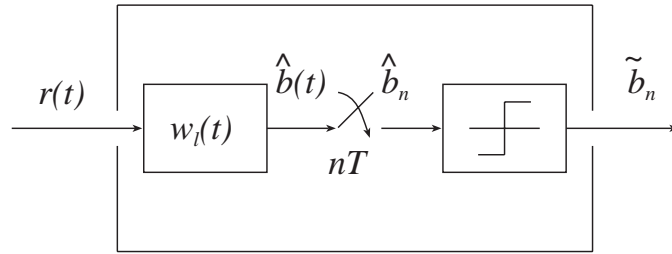


**Figure 2.7:** Receiver with linear equalizer

to compensate or reduce the ISI in the received signal. Equalization is usually accomplished by a filtering operation. In the presence of additive white Gaussian noise (AWGN) in the system, the equalizer also acts as a matched filter to reduce the effect of noise.

In this section, two types of receivers, namely a receiver with an LE and a receiver with a DFE are considered. Note that the impulse response in the equalizers are time-invariant. For a time-invariant channel, once this impulse response is determined, there is no need to update. For a time-varying channel, this impulse response can be adjusted, by means of adaptive algorithms [11, 22, 23] or other updating methods [55], to accommodate the changes taking place in the channel.

### 2.3.1 Linear Equalizer

Figure 2.7 shows a block diagram of the receiver with an LE. The receiver consists of an LE with an impulse response of  $w_l(t)$ , a symbol-spaced sampler and a decision device.

The input to the LE is the received signal  $r(t)$  and the output  $\hat{b}(t)$  is given by

$$\hat{b}(t) = r(t) \star w_l(t). \quad (2.38)$$

The signal  $\hat{b}(t)$  is sampled at the symbol rate to get

$$\begin{aligned}\hat{b}_n &= \hat{b}(t)\Big|_{t=nT} \\ &= \hat{b}(nT),\end{aligned}\tag{2.39}$$

which is the unquantized estimated version of the transmitted data. The LE can also be modeled as a tapped delay line or a linear transversal equalizer, which takes the sampled received signal as input and gives  $\hat{b}_n$  at the output if the delay between the taps is a symbol period. If the delay is a fraction of a symbol period, a fractionally spaced LE is used, which is studied in detail in the work by Gitlin and Weinstein [28].

The output of the sampler is then applied to a decision device. Following some non-linear decision rules, the decision device maps  $\hat{b}_n$  to the nearest level of the transmitted data and gives an estimated version of the transmitted data  $\tilde{b}_n$  at the output.

In the presence of ISI, an LE may not be an effective choice in receiver design. In order to minimize or completely eliminate ISI, an equalizer is usually implemented based on the zero-forcing(ZF) criterion, which is simply the inverse filter of the channel. In the case of selective fading channels, it enhances the noise at the frequencies where the channel exhibits spectral nulls [23]. The use of the mean square error criterion, on the other hand, results in incomplete elimination of the ISI, even though the effects of both noise and ISI can be reduced. Under this condition, a DFE is usually used to replace an LE.

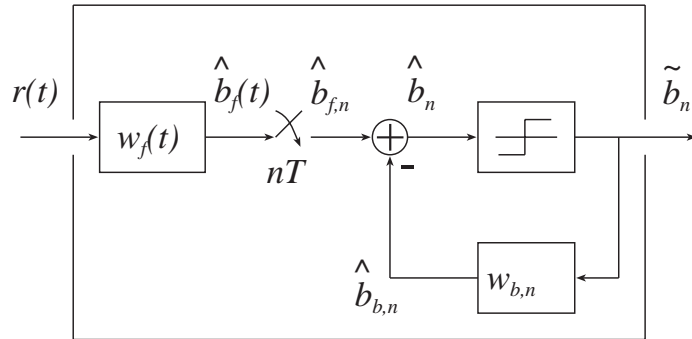


Figure 2.8: Receiver with DFE

### 2.3.2 Decision Feedback Equalizer

Figure 2.8 shows a block diagram of the receiver with a DFE. It consists of a feed forward filter with impulse response  $w_f(t)$ , a sample-rate sampler, a decision device, and a feedback filter  $w_{b,n}$ .

The input to the feed forward filter is the received signal, and the output is given by

$$\hat{b}_f(t) = r(t) \star w_f(t). \quad (2.40)$$

This output signal is sampled at the symbol rate to get

$$\begin{aligned} \hat{b}_{f,n} &= \hat{b}_f(t) \Big|_{t=nT} \\ &= \hat{b}_f(nT). \end{aligned} \quad (2.41)$$

As with the LE, the feed forward filter of the DFE can be modeled as a tapped delay line, with a delay of  $T$ , or fraction of  $T$  between taps.

The unquantized estimated version of the transmitted data is obtained by sub-

tracting the output of the feedback filter  $\hat{b}_{b,n}$  from  $\hat{b}_{f,n}$ :

$$\hat{b}_n = \hat{b}_{f,n} - \hat{b}_{b,n}. \quad (2.42)$$

This signal is then applied to the decision device to obtain an estimate of the transmitted data  $\tilde{b}_n$ . The output of the decision device is then fed back to the discrete-time filter  $w_{b,n}$  to get

$$\hat{b}_{b,n} = \tilde{b}_n \star w_{b,n}, \quad (2.43)$$

where the symbol  $\star$  denotes discrete-time convolution defined as

$$\blacksquare_n \star \blacklozenge_n = \sum_{m=-\infty}^{\infty} \blacksquare_{n-m} \blacklozenge_m. \quad (2.44)$$

Similar to the LE, the feed forward filter of a DFE minimizes the effects of noise and the precursors caused by the future symbols. The only difference between a DFE and an LE is the addition of the feedback filter in a DFE. A DFE feeds the estimated version of the transmitted symbol back, via the feedback filter. In this way, the post cursors caused by the previous symbols, assuming these symbols are estimated correctly, can be properly weighted by the feedback filter and subtracted from the estimate of the current symbol. Therefore, a DFE can completely eliminate the ISI induced by the channel, without noise enhancement.

# Chapter 3

## Equalization, Channel Estimation and Interpolation Techniques

### 3.1 Channel Estimation Techniques

In cellular radio transmission, data carrying signals are often transmitted to the receiver via a channel that introduces impairments. One effective way to recover the transmitted data is to first estimate the channel impulse response, then perform equalization on the received data. The performance of the receiver, calculated based on the estimated channel, depends on the accuracy of the channel estimate. Therefore, choosing an effective channel estimation algorithm is of great importance in receiver design.

In this section, previous work on channel estimation, such as the least sum of squared errors (LSSE) channel estimation algorithms for static channels in Sections 3.1.1 and 3.1.2, and ML blind data and channel estimation method in Section 3.1.3, is included to provide convenient reference to the readers. In Section 3.1.5,

the sign ambiguity problem associated with blind deconvolution is also addressed. An example is given to show that the sign ambiguity problem can be avoided by employing differential encoding. The rest of this section includes development of new algorithms and analysis, which forms part of the contributions of this research thesis. As an extension to these channel estimation methods, the proposed ML blind data, channel and co-channel estimation method is presented. Due to the channel noise, the ML blind estimation method may lead to incorrect selection of the data sequence and channel estimate. A theoretical analysis on the probability of error in the ML blind data and channel estimation is performed. Finally, a new frequency estimation method using cross correlation is also proposed to handle the situation where the channel is time-varying.

### 3.1.1 LSSE Channel Estimation

Given the input and the output of the channel, the channel impulse response can be identified using the LSSE criterion [39]. The channel estimate is determined such that the sum of the squared errors between the actual output of the channel and the output of the estimated channel is minimized.

Let  $\mathbf{c}$  and  $\hat{\mathbf{c}}$  be the actual channel and the channel estimate, respectively, and  $\mathbf{s}$  be the data sequence to be transmitted. The output of the actual channel and of the estimated channel are given by

$$r_n = \mathbf{c}^T \mathbf{s}_n + \eta_n \quad (3.1)$$

and

$$\hat{r}_n = \hat{\mathbf{c}}^T \mathbf{s}_n, \quad (3.2)$$

respectively, where the operation “ $T$ ” denotes transpose and  $\eta_n$  is the zero mean additive white Gaussian noise.

The sum of squared error (SSE) is a function of the channel estimate, and it is defined in Equation 3.3:

$$\text{sse}(\hat{\mathbf{c}}) = \sum_{n=0}^{K-1} |r_n - \hat{r}_n|^2 \quad (3.3)$$

where  $K$  is the length of the received sequence, and it is defined as

$$K = N_t - N_c + 1. \quad (3.4)$$

Here,  $N_t$  is the length of the training sequence and  $N_c$  is the number of taps in the channel. The channel estimate  $\hat{\mathbf{c}}$  is optimum when the SSE is minimized.

The minimization of SSE is given by Crozier et al. [39] and the optimum channel estimate, when the training sequence is available and  $s$  is known to the receiver, is given by Equation 3.5:

$$\hat{\mathbf{c}}_{opt} = (\mathbf{S}^T)^{-1} \mathbf{z} \quad (3.5)$$

where  $\mathbf{S}$  is the auto correlation matrix of the training sequence defined as

$$\mathbf{S} = \sum_{n=0}^{K-1} \mathbf{s}_n \mathbf{s}_n^H, \quad (3.6)$$

the symbol “ $H$ ” denotes Hermitian transpose,  $\mathbf{z}$  is the cross correlation vector of the channel output and the training sequence  $\mathbf{s}$  and is defined as

$$\mathbf{z} = \sum_{n=0}^{K-1} r_n \mathbf{s}_n^*, \quad (3.7)$$

and  $\mathbf{s}_n$  is the input vector to the channel given by

$$\mathbf{s}_n = \begin{bmatrix} s_n \\ s_{n-1} \\ \vdots \\ s_{n-N_c+1} \end{bmatrix}. \quad (3.8)$$

Finally, the LSSE is given by Equation 3.10:

$$\text{lsse} = \text{sse}(\hat{\mathbf{c}}_{opt}) \quad (3.9)$$

$$= E_r - \hat{\mathbf{c}}_{opt}^H \mathbf{z} \quad (3.10)$$

where  $E_r$  is the average power of the received signal, defined as

$$E_r = \sum_{n=0}^{K-1} |r_n|^2. \quad (3.11)$$

### 3.1.2 LSSE Channel and Co-channel Estimation

In TDMA cellular radio transmission, CCI is present in most cases, due to the frequency reuse plan. The LSSE channel estimation algorithm discussed in the previous section can be modified to estimate both channel and co-channel impulse responses.

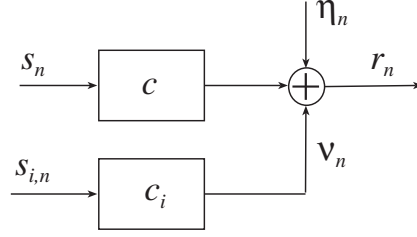


**Figure 3.1:** Transmission in the presence of CCI

Figure 3.1 shows a model for data transmission in the presence of CCI. Here,  $s_i$  is the interfering signal transmitted in the co-channel cell, and  $\mathbf{c}_i$  is the vector consisting of all the impulse responses of the co-channels. In the presence of CCI, the output of the channel  $r_n$  is given by the following equation:

$$r_n = \mathbf{c}^T \mathbf{s}_n + \nu_n + \eta_n, \quad (3.12)$$

where  $\nu_n$  is the CCI defined as

$$\nu_n = \mathbf{c}_i^T \mathbf{s}_{i,n}. \quad (3.13)$$

When training is available in both channel and co-channel transmissions, the estimate of the received signal can be expressed as

$$\hat{r}_n = \hat{\mathbf{c}}^T \mathbf{s}_n + \hat{\mathbf{c}}_i^T \mathbf{s}_{i,n}, \quad (3.14)$$

and the SSE is given by

$$\text{sse}(\hat{\mathbf{c}}_2) = E_r - \hat{\mathbf{c}}_2^H \mathbf{z}_2 - \hat{\mathbf{c}}_2^T \mathbf{z}_2^* + \hat{\mathbf{c}}_2^T \mathbf{S}_2 \hat{\mathbf{c}}_2^* \quad (3.15)$$

where

$$\hat{\mathbf{c}}_2 = \begin{bmatrix} \hat{\mathbf{c}} \\ \hat{\mathbf{c}}_i \end{bmatrix}, \quad (3.16)$$

$$\mathbf{z}_2 = \begin{bmatrix} \mathbf{z} \\ \mathbf{z}_i \end{bmatrix} \quad (3.17)$$

and

$$\mathbf{S}_2 = \begin{bmatrix} \mathbf{S} & \mathbf{S}_i \\ \mathbf{S}_i^H & \mathbf{S}_{ii} \end{bmatrix}. \quad (3.18)$$

In Equation 3.17,  $\mathbf{z}_i$  is the cross correlation vector of the channel and is defined as

$$\mathbf{z}_i = \sum_{n=0}^{K-1} r_n \mathbf{s}_{i,n}^*. \quad (3.19)$$

In Equation 3.18,  $\mathbf{S}_{ii}$  is the auto correlation of the data transmitted in the co-channel, defined as

$$\mathbf{S}_{ii} = \sum_{n=0}^{K-1} \mathbf{s}_{i,n} \mathbf{s}_{i,n}^H, \quad (3.20)$$

and  $\mathbf{S}_i$  is the correlation matrix between the training sequences of the desired and co-channel data transmission:

$$\mathbf{S}_i = \sum_{n=0}^{K-1} \mathbf{s}_n \mathbf{s}_{i,n}^H. \quad (3.21)$$

The optimum channel and co-channel estimates are determined by minimizing SSE. Taking the gradient of both sides of Equation 3.15, with respect to  $\hat{\mathbf{c}}_2$ , the following equation is obtained:

$$\hat{\mathbf{c}}_{2,opt} = (\mathbf{S}_2^T)^{-1} \mathbf{z}_2 \quad (3.22)$$

The LSSE occurs when the channel and co-channel estimates are optimum, and the LSSE is given by Equation 3.24:

$$\text{lsse} = \text{sse}(\hat{\mathbf{c}}_{2,opt}) \quad (3.23)$$

$$= E_r - \hat{\mathbf{c}}_{2,opt}^H \mathbf{z}_2. \quad (3.24)$$

### 3.1.3 ML Blind Data and Channel Estimation

In order to reduce transmission overhead in some data transmission applications, a training sequence is not available. In this case, the channel impulse response and the data sequence have to be identified using blind methods.

ML blind data and channel estimation method is based on the maximum likelihood criterion [11, 17, 50]. The noise samples  $\eta_n$  in the received data  $r_n$ , defined in Equation 3.12, are complex Gaussian random variables, assumed to be independent identically distributed (iid), with zero mean, variance  $\sigma_\eta^2$ , and with probability density function (PDF) given by

$$p_\eta(\eta_m) = \frac{1}{\sqrt{2\pi\sigma_\eta^2}} \exp\left(-\frac{|\eta_m|^2}{2\sigma_\eta^2}\right) \quad (3.25)$$

where  $|\blacksquare|$  is the magnitude of  $\blacksquare$ . For  $K$  independent noise samples, the joint PDF

is

$$p_{\eta}(\eta_0, \eta_1, \dots, \eta_{K-1}) = \frac{1}{(\pi\sigma_{\eta}^2)^{\frac{K}{2}}} \exp\left(-\frac{1}{\sigma_{\eta}^2} \sum_{n=0}^{K-1} |\eta_n|^2\right). \quad (3.26)$$

Therefore, the joint PDF of the received signal,  $\mathbf{r} = [r_0 \ r_1 \ \dots \ r_{K-1}]^T$ , conditioned on arbitrary channel and co-channel estimates, and an arbitrary data sequence is

$$p(\mathbf{r}|\hat{\mathbf{c}}, \hat{\mathbf{s}}_n, \hat{\mathbf{c}}_i, \hat{\mathbf{s}}_{i,n}) = \frac{1}{(2\pi\sigma_{\eta}^2)^{\frac{K}{2}}} \exp\left(-\frac{1}{2\sigma_{\eta}^2} \sum_{n=0}^{K-1} |r_n - \hat{\mathbf{c}}^T \hat{\mathbf{s}}_n - \hat{\mathbf{c}}_i^T \hat{\mathbf{s}}_{i,n}|^2\right). \quad (3.27)$$

This is also called the likelihood function. The ML estimates of the  $\mathbf{c}$  and  $\mathbf{s}_n$  are the vectors that maximize the likelihood function, or equivalently, minimize the cost function,

$$J(\mathbf{r}|\hat{\mathbf{c}}, \hat{\mathbf{s}}_n, \hat{\mathbf{c}}_i, \hat{\mathbf{s}}_{i,n}) = \sum_{n=0}^{K-1} |r_n - \hat{\mathbf{c}}^T \hat{\mathbf{s}}_n - \hat{\mathbf{c}}_i^T \hat{\mathbf{s}}_{i,n}|^2. \quad (3.28)$$

The joint ML estimates of the channel impulse response  $\hat{\mathbf{c}}_{ML}$  and the data  $\hat{\mathbf{s}}_{n,ML}$  are given by

$$(\hat{\mathbf{c}}_{ML}, \hat{\mathbf{s}}_{n,ML}) = \arg \left[ \min_{\hat{\mathbf{c}}, \hat{\mathbf{s}}_n} J(\mathbf{r}|\hat{\mathbf{c}}, \hat{\mathbf{s}}_n, \hat{\mathbf{c}}_i, \hat{\mathbf{s}}_{i,n}) \right], \quad (3.29)$$

where  $\arg$  denotes the arguments which satisfy the condition that follows. Here, the statistical information of the interfering signal is not known. In order to reduce the complexity of the estimation problem, the interference component is treated as a constant. Therefore, the receiver designed this way cannot suppress the CCI explicitly.

Following Equation 3.29, the receiver thus performs two tasks in order to determine the maximum likelihood estimates of the channel and the data. In the

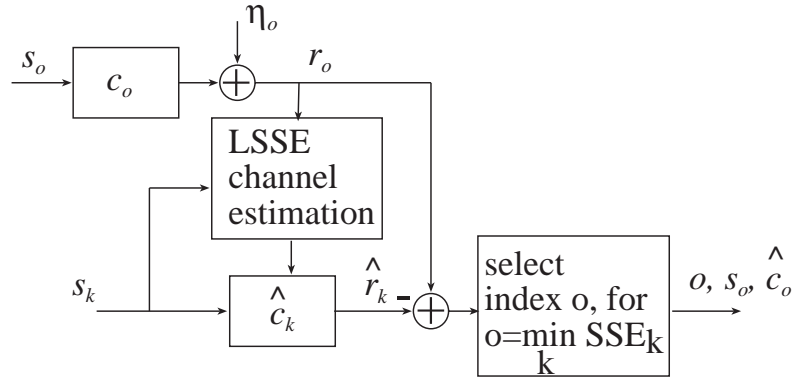


**Figure 3.2:** Exhaustive search algorithm

first step, LSSE channel estimation is performed, and an LS channel estimate and the LSSE of its output are determined for every possible input data sequence. In the second step, the LSSE of all the channel estimates are compared. The channel estimate with the lowest LSSE and its corresponding input sequence are chosen to be the maximum likelihood estimates of the channel and the data. This exhaustive search algorithm is illustrated in Figure 3.2.

The approach described above requires intensive computation, and its computational complexity grows exponentially with the length of the data sequence [11]. In fact, the number of possible input sequences is  $M^L$ , where  $M$  is the alphabet size and  $L$  is the length of the input sequence. For a long data sequence or a large data alphabet size, such a method is prohibitive in its computational intensity. Sub-optimum solutions are adopted for this purpose [17, 50, 51]. This intensive computational requirement can also be lowered by reducing the alphabet size [17]. For a small data record and a small data alphabet size, however, this method is feasible. In fact, it provides optimum solution and gives good performance.

### 3.1.4 ML Blind Data, Channel and Co-channel Estimation

In order to estimate the transmitted data more accurately in the presence of the CCI, the fact that the received signal consists of an interference component should be taken into account. Optimal detection requires that the co-channel be estimated and the CCI component in the received signal be taken into consideration when the DFE coefficients are calculated. The receiver designed in this way can suppress the CCI.

In this section, a new ML blind data, channel and co-channel estimation technique is presented. This technique is an extension to the existing ML blind data and channel estimation technique detailed in Section 3.1.3, in which the channel and co-channel estimates are chosen to minimize the likelihood function. With the co-channel information, CCI can be suppressed and better system performance can be achieved.

The likelihood function of the received data signal  $r_n$ , conditioned on the transmitted data, channel and co-channel is given in Equation 3.27. The maximum likelihood solutions of the data, channel and co-channel can be determined by maximizing the conditional likelihood function or, equivalently by minimizing the cost function given by Equation 3.28. The estimates of the data, channel and co-channel are given by

$$(\hat{\mathbf{c}}_{ML}, \hat{\mathbf{s}}_{n,ML}, \hat{\mathbf{c}}_{i,ML}, \hat{\mathbf{s}}_{i,n,ML}) = \arg \left[ \min_{\hat{\mathbf{c}}, \hat{\mathbf{s}}_n, \hat{\mathbf{c}}_i, \hat{\mathbf{s}}_{i,n}} J(\mathbf{r} | \hat{\mathbf{c}}, \hat{\mathbf{s}}_n, \hat{\mathbf{c}}_i, \hat{\mathbf{s}}_{i,n}) \right]. \quad (3.30)$$

To solve Equation 3.30 involves two steps. In the first step, LSSE channel and co-channel estimation is performed and the LSSE is determined for every possible combination of desired and interfering data sequences. In the second step, the LSSE

of all the channel and co-channel estimates are compared. The lowest LSSE and its corresponding data, channel and co-channel estimates are selected as the ML solution to Equation 3.30. The number of possible combinations of bits for both signals is  $M^{L+L_i}$ , where  $L_i$  is the length of the data sequence for the co-channel. As with the blind ML data and channel estimation method, the computational requirement of this method is the major drawback, despite its optimality.

### 3.1.5 Sign Ambiguity Problem of Blind Data and Channel Estimation

In the work of Seshadri [17], a brief suggestion was made that differential encoding can be employed to avoid the sign ambiguity problem associated with the blind data and channel estimation. In this section, an example is presented to demonstrate this important property of the differential encoding schemes.

In joint blind data and channel estimation, both the input data and the channel are unknown to the receiver. The only known information is the received signal and the possible bit combinations. By minimization of the likelihood function, the input data and the channel can be estimated jointly, as detailed in Sections 3.1.3 and 3.1.4. This gives rise to the sign ambiguity problem.

Let  $\mathbf{s}$  and  $\mathbf{c}$  be the input sequence and the channel, respectively and  $r$  be the received signal. Both data and channel pairs  $(\mathbf{s}, \mathbf{c})$  and  $(-\mathbf{s}, -\mathbf{c})$  give the same received signal  $r$ . With only the knowledge of  $r$ , it is impossible to determine the actual data and channel pair. This is called the sign ambiguity problem of blind deconvolution.

With differential encoding, this problem can be resolved. Suppose the two adjacent transmitted symbols are  $s_0$  and  $s_1$ , then the differential phase  $\Delta\theta_1$  is given

by

$$\Delta\theta_1 = \arg(s_0^* s_1). \quad (3.31)$$

If, due to the sign ambiguity problem, the two transmitted symbols are mistaken to be  $-s_0$  and  $-s_1$ , the result is the same differential phase. Since only the differential phase determines the original binary bits, no bit error will be caused due to this phase ambiguity problem.

### 3.1.6 Probability of Error in ML Blind Data and Channel Estimation

It is mentioned in the previous section that the ML method provides the optimum solution for the data and channel estimates. However, due to the impairments caused by the channel, the quality of the LSSE channel estimate is affected. As a result, the ML blind data and channel estimation method may select the channel estimate corresponding to a data sequence which differs from the input sequence. In this section, the probability of error in ML data and channel estimation is investigated. Since CCI and channel noise have different statistical characteristics, considering both effects on the channel estimation quality would complicate the analysis a great deal. In order to simplify the analysis, the CCI and the channel noise are both modeled as white Gaussian processes, and are lumped together into one noise source. Towards this goal, the statistical property of the noise component in the channel estimate is studied. A model is then developed and some assumptions are made to achieve this goal.

### 3.1.6.1 Statistical Properties of Noise Component in the Channel Estimate

When there is no interference in the system, the received signal is given by Equation 3.1. By substituting this expression for  $r_n$  into the cross correlation given in Equation 3.7, it is easy to find that the channel estimate obtained by solving Equation 3.5 consists of two components, the channel impulse response and an additive component due to the additive noise:

$$\hat{\mathbf{c}}_{opt} = \mathbf{c} + \mathbf{c}_\eta. \quad (3.32)$$

When there is no noise, this noise component in Equation 3.32 is zero and the optimum channel estimate given by the LSSE algorithm is the actual channel itself.

For a simple channel with two taps,  $\mathbf{c}_\eta$  is given by the following equation:

$$\mathbf{c}_\eta = \begin{bmatrix} c_{\eta,0} \\ c_{\eta,1} \end{bmatrix} \quad (3.33)$$

$$= \begin{bmatrix} \sum_{n=0}^{K-1} \lambda_{0,n} \\ \sum_{n=0}^{K-1} \lambda_{1,n} \end{bmatrix} \quad (3.34)$$

$$= \begin{bmatrix} \sum_{n=0}^{K-1} k_{0,n} \eta_n \\ \sum_{n=0}^{K-1} k_{1,n} \eta_n \end{bmatrix}, \quad (3.35)$$

where

$$k_{0,n} = \frac{N_1 s_{n+1}^* - N_2 s_n^*}{D}, \quad (3.36)$$

$$k_{1,n} = \frac{N_3 s_n^* - N_2^* s_{n+1}^*}{D}, \quad (3.37)$$

and the coefficients  $N_1$ ,  $N_2$ ,  $N_3$  and  $D$  are defined, respectively, as

$$N_1 = \sum_{n=0}^{K-1} |s_n|^2 \quad (3.38)$$

$$N_2 = \sum_{n=0}^{K-1} s_n s_{n+1}^* \quad (3.39)$$

$$N_3 = \sum_{n=0}^{K-1} |s_{n+1}|^2 \quad (3.40)$$

and

$$D = \sum_{n=0}^{K-1} |s_{n+1}|^2 \sum_{n=0}^{K-1} |s_n|^2 - \sum_{n=0}^{K-1} s_n^* s_{n+1} \sum_{n=0}^{K-1} s_n s_{n+1}^*. \quad (3.41)$$

Since the noise is a complex Gaussian variate, with PDF given in Equation 3.25, the  $n$ th term in the summation in Equation 3.35,  $\lambda_{i,n} = k_{i,n} \eta_n$ , for  $i = 0, 1$ , is zero mean, complex Gaussian, with a variance of  $k_{i,n}^2 \sigma_\eta^2$ . The noise component of the channel estimate is then multivariate complex Gaussian, with PDF given by the following equation:

$$p(c_{\eta,i}) = \frac{1}{\pi^K \det(\mathbf{C}_{\lambda,i})} \exp(-\boldsymbol{\lambda}_i^H \mathbf{C}_{\lambda,i}^{-1} \boldsymbol{\lambda}_i), \quad (3.42)$$

where

$$\boldsymbol{\lambda}_i = \begin{bmatrix} \lambda_{i,0} \\ \lambda_{i,1} \\ \vdots \\ \lambda_{i,K-1} \end{bmatrix}, \quad (3.43)$$

$\mathbf{C}_{\lambda,i}$  is the covariance matrix of  $\boldsymbol{\lambda}$ , and defined as

$$\mathbf{C}_{\lambda,i} = E[(\boldsymbol{\lambda}_i - E[\boldsymbol{\lambda}_i])(\boldsymbol{\lambda}_i - E[\boldsymbol{\lambda}_i])^H], \quad (3.44)$$

and  $\det(\blacksquare)$  is the determinant of the matrix  $\blacksquare$ . Since  $\boldsymbol{\lambda}_i$  has zero mean, the covariance matrix is diagonal, with  $k_{i,n}^2 \sigma_\eta^2$  on its main diagonal, and Equation 3.42 can be further simplified as

$$p(c_{\eta,i}) = \frac{1}{\pi^K \prod_{n=0}^{K-1} k_{i,n}^2 \sigma_\eta^2} \exp\left(-\sum_{n=0}^{K-1} \frac{|\lambda_{i,n}|^2}{k_{i,n}^2 \sigma_\eta^2}\right). \quad (3.45)$$

The variance of the noise component in the channel estimate is the sum of the variances for all the terms in the summation in Equation 3.35:

$$\sigma_{c_{\eta,i}}^2 = \sum_{n=0}^{K-1} k_{i,n}^2 \sigma_\eta^2. \quad (3.46)$$

For binary signaling, the input sequence only consists of  $\pm 1$  and the coefficients  $N_1$  and  $N_3$  have the value of  $K$ .  $N_2$  has a much smaller value compared with  $N_1$  and  $N_3$ , and it can be neglected. For the coefficient  $D$ , the first term has the value of  $K^2$  and the second is much smaller and hence can be ignored. Therefore, the variance

of  $c_{\eta,i}$  can be approximated by the following equation:

$$\sigma_{c_{\eta}}^2 = \frac{1}{K} \sigma_{\eta}^2. \quad (3.47)$$

Equation 3.47 shows that the variance of the noise component in the channel estimate is related to the variance of the channel noise by a simple factor.

### 3.1.6.2 Probability of Selecting the Right Channel Estimate

The block diagram in Figure 3.2 illustrates the process of ML blind data and channel estimation. Let  $\mathbf{s}_o$  and  $\mathbf{c}_o$  be the actual input sequence and the channel impulse response, and  $r_o$  be the received signal, given by Equation 3.48:

$$r_o = \mathbf{c}_o^T \mathbf{s}_o + \eta_o. \quad (3.48)$$

This received signal is used to estimate the channel impulse response  $\hat{\mathbf{c}}_k$  for every possible input sequence  $s_k$ , for  $k = 0, 1, \dots, 2^{N_s} - 1$ , where  $N_s$  is the length of the input sequence.

For the actual input sequence  $s_o$ , the estimated output is

$$\hat{r}_o = \mathbf{s}_o^T \hat{\mathbf{c}}_o, \quad (3.49)$$

and for the other potential input sequences, the estimated output is

$$\hat{r}_k = \mathbf{s}_k^T \hat{\mathbf{c}}_k, \quad k \neq o. \quad (3.50)$$

By substituting Equation 3.32 into Equation 3.49, the estimated received signal is

$$\hat{\mathbf{r}}_o = \mathbf{s}_o^T \mathbf{c}_o + \mathbf{s}_o^T \mathbf{c}_{\eta,o}. \quad (3.51)$$

Equation 3.51 can be rewritten in terms of  $r_o$ :

$$\hat{r}_o = r_o + r_o', \quad (3.52)$$

where  $r_o'$  is a perturbation on  $r_o$  and it is given as

$$r_o' = \mathbf{s}_o^T \mathbf{c}_{\eta,o} - \eta_o. \quad (3.53)$$

In order to simplify the analysis, it is assumed that the noise term in the channel estimate is independent of the channel noise. Then the perturbation  $r_o'$  is zero mean Gaussian, with variance given by

$$\sigma_{r_o'}^2 = \sigma_{c_\eta}^2 + \sigma_\eta^2. \quad (3.54)$$

For the ML blind data and channel estimation method, the decision rule for the channel estimate is  $\hat{c} = \hat{c}_i$  if and only if

$$\| \hat{\mathbf{r}}_o - \mathbf{r}_i \|^2 < \| \hat{\mathbf{r}}_k - \mathbf{r}_i \|^2, \quad k = 0, 1, \dots, 2^{N_s} - 1, \text{ and } k \neq i \quad (3.55)$$

in the  $N_s$  dimensional case, where  $\hat{\mathbf{r}}_o$ ,  $\mathbf{r}_i$  and  $\hat{\mathbf{r}}_k$  represent the  $N_s$ -dimensional vectors of the received signals, and  $\| \blacksquare \|$  denotes Euclidean distance. In order to make a correct decision,  $\hat{\mathbf{r}}_o$  has to be in the neighborhood of  $\mathbf{r}_o$ , so that the following

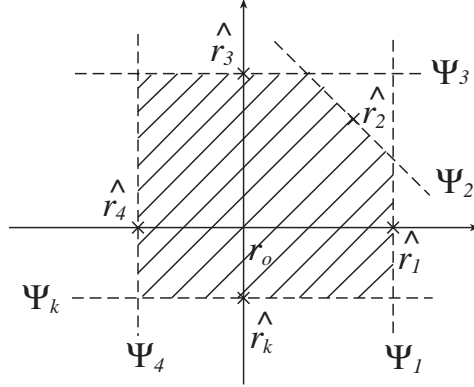


**Figure 3.3:** Decision region of  $\hat{r}_o$

condition is satisfied:

$$\|\hat{\mathbf{r}}_o - \mathbf{r}_o\|^2 < \|\hat{\mathbf{r}}_k - \mathbf{r}_o\|^2, \quad k = 0, 1, \dots, 2^{N_s} - 1, \text{ and } k \neq o. \quad (3.56)$$

Therefore, the decision region for selecting the correct data and channel pair in a two-dimensional case, is shown in Figure 3.3, and it is shaped by the surfaces  $\psi_k$  at  $\hat{r}_k$ . If  $\hat{\mathbf{r}}_o$  falls inside the shaded region, it has the smallest distance to  $\mathbf{r}_o$  and the correct channel estimate is selected. Otherwise, a channel estimate with the estimated output signal closest to  $r_o$  will be selected, and an error occurs. It is clear that the concept of decision regions, which for simplicity is illustrated for a two-dimensional plane in Figure 3.3, extends directly to the case of an arbitrary number of bits in the input sequence.

As mentioned before, the perturbation  $r_o'$  is Gaussian distributed with zero mean, and its PDF, in the one dimension case, is the bell-shaped curve centered around the origin. In the  $N_s$  dimension case, its PDF is an  $N_s$  dimensional surface, with a bell-shaped cross section, and the “volume” under the surface is unity. The probability of selecting the right channel estimate is part of this “volume” centered

at the origin, bounded by surfaces  $\psi_k$ . The mathematics involved in determining the exact probability is very complicated. In order to simplify the problem, only the lower and upper bounds are considered. In other words, only the minimum distance  $d_{min}$ , the distance between  $r_o$  and the closest plane, is required. The lower bound for the probability of selecting the right channel estimate is thus a symmetrical “volume” under the  $N_s$  dimensional surface, bounded by  $d_{min}$  and centered around the origin. Finally, the lower bound for the probability of selecting the right channel estimate is given by the following equation:

$$P_{lb}(\text{selecting the right channel estimate}) = \left( \text{erf} \left( \frac{d_{min}}{\sqrt{2}\sigma_{r_o'}} \right) \right)^{N_s}. \quad (3.57)$$

Therefore, the upper bound of the probability of selecting a wrong channel estimate, or the probability of error in the ML data and channel estimation method is

$$P_{e,ub} = 1 - P_{lb} \quad (3.58)$$

$$= 1 - \left( \text{erf} \left( \frac{d_{min}}{\sqrt{2}\sigma_{r_o'}} \right) \right)^{N_s}. \quad (3.59)$$

### 3.1.7 Channel Modeling with Frequency Estimation Using Cross Correlation

In wireless mobile communications, the multi-path channel is changing constantly as the vehicle traverses the environment. The rate of change in the channel depends on the speed of the vehicle. In order to estimate the time-varying channel during a TDMA time slot, a certain channel model is adopted, so that only a small set of parameters, which represents the characteristics of the channel variations, needs to be estimated.

A multi-path channel can be modeled as a combination of a number of complex exponentials [57, 64]. In the work of Tsatsanis et al. [57], the discrete-time fading channel model given by the following equation is used [57]:

$$c_{n;i} = \sum_{q=0}^{N_x-1} \gamma_{i,q} e^{j\omega_q n}. \quad (3.60)$$

In this model, each channel tap consists of  $N_x$  complex exponential components. There are two sets of parameters to be estimated: complex gain  $\gamma_{i,q}$  and real angular frequency  $\omega_q$ . These parameters,  $\gamma_{i,q}$  and  $\omega_q$  can be used to characterize the time-varying channel and they are time-invariant. Therefore, by modeling the time-varying channel this way, the time-varying problem is transformed into a time-invariant one.

Tsatsanis et al. also suggested that the angular frequency  $\omega_q$  can be estimated using both the autocorrelation and the fourth order statistics of the received signal and the complex gain  $\gamma_{i,q}$  can be determined by minimizing the least squares of the error of the output, or using adaptive algorithms [57]. In frequency estimation, the fourth-order statistics are involved since the autocorrelation only gives the differences between different angular frequencies. The fourth-order statistics are usually noisy and it is difficult to identify the peaks in the spectrum where the angular frequencies are located. Here, a frequency estimation method using the second order cross correlation between the transmitted and the received signals, is proposed. Since the Fourier transform of the cross correlation shows peaks where the angular frequencies are, the use of the higher order statistics can be avoided.

Figure 3.4 shows a block diagram of the transmission of a signal over a time-varying channel. With input signal  $s_n$ , the output of the time-varying channel is

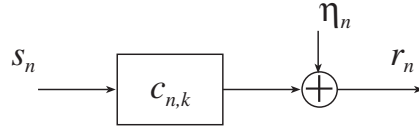


**Figure 3.4:** Transmission over a time-varying channel

given by the following equation:

$$r_n = \sum_{i=0}^{N_c-1} s_i c_{n;n-i} + \eta_n. \quad (3.61)$$

The cross correlation between the input and the output signals is defined as

$$\phi_{rs}(n, m) = E[r_n s_m^*]. \quad (3.62)$$

Since the output signal is not a stationary process, the cross correlation is a function of both  $n$  and  $m$ . By substituting Equations 3.61 and 3.60 into Equation 3.62, the cross correlation can be rewritten as

$$\phi_{rs}(n, m) = \begin{cases} \sigma_s^2 \sum_{q=0}^{N_x-1} \gamma_{n-m,q} e^{j\omega_q n}, & 0 \leq n - m \leq N_c - 1 \text{ and } 0 \leq n \leq N - 1 \\ 0, & \text{otherwise,} \end{cases} \quad (3.63)$$

assuming that

$$E[s_n s_m^*] = \sigma_s^2 \delta_{n-m} \quad (3.64)$$

and

$$E[\eta_n s_m^*] = 0. \quad (3.65)$$

From Equation 3.63, one can observe that by multiplying the received signal by the complex conjugate of the transmitted signal and taking the expectation, the transmitted signal component is essentially “removed” from the received signal. Only the time-varying channel remains in this expression.

The cross correlation is the sum of  $N_x$  complex exponentials. In order to identify the frequency components in the cross correlation, the Fourier transform of  $\phi_{rs}(n, m)$  is taken, with respect to time index  $n$ . The cross-power density spectrum is given by

$$\Phi_{rs}(\omega; m) = \sum_{n=-\infty}^{\infty} \phi_{rs}(n, m) e^{-j\omega n} \quad (3.66)$$

$$= \begin{cases} \sigma_s^2 \sum_{q=0}^{N_x-1} \sum_{i=0}^{N_c-1} \gamma_{n-m,q} e^{-j(\omega-\omega_q)n}, & 0 \leq n - m \leq N_c - 1 \\ 0, & \text{otherwise.} \end{cases} \quad (3.67)$$

By taking the derivative of the magnitude of  $\Phi_{rs}(\omega; m)$  with respect to  $\omega$  and setting it to zero, one can find that the magnitude of the spectrum reaches maximum at  $\omega_q$ . Therefore, the frequency components of the time-varying channel can be estimated by identifying the peaks in the magnitude of the cross-power density spectrum.

As an example, Figure 3.5 shows the magnitude of the cross-power density spectrum,  $|\text{Phi}_{rs}(\omega; m)|$  for a time-varying channel tap at maximum Doppler frequency  $f_m$  of 180 Hz. There are three replicas of the transmitted signal arriving at the receiver, and the channel model consists of three complex exponentials at frequencies of -180 Hz, -114 Hz and 173 Hz, as indicated by the solid vertical lines in Figure 3.5. With a data record of 500 symbols, this method provides peaks that are visually separable, which is not the case for a data record with 300 symbols.

In some TDMA transmissions, such as IS-136, the number of data symbols in a time slot is usually not more than 200, only a small fraction of which is known

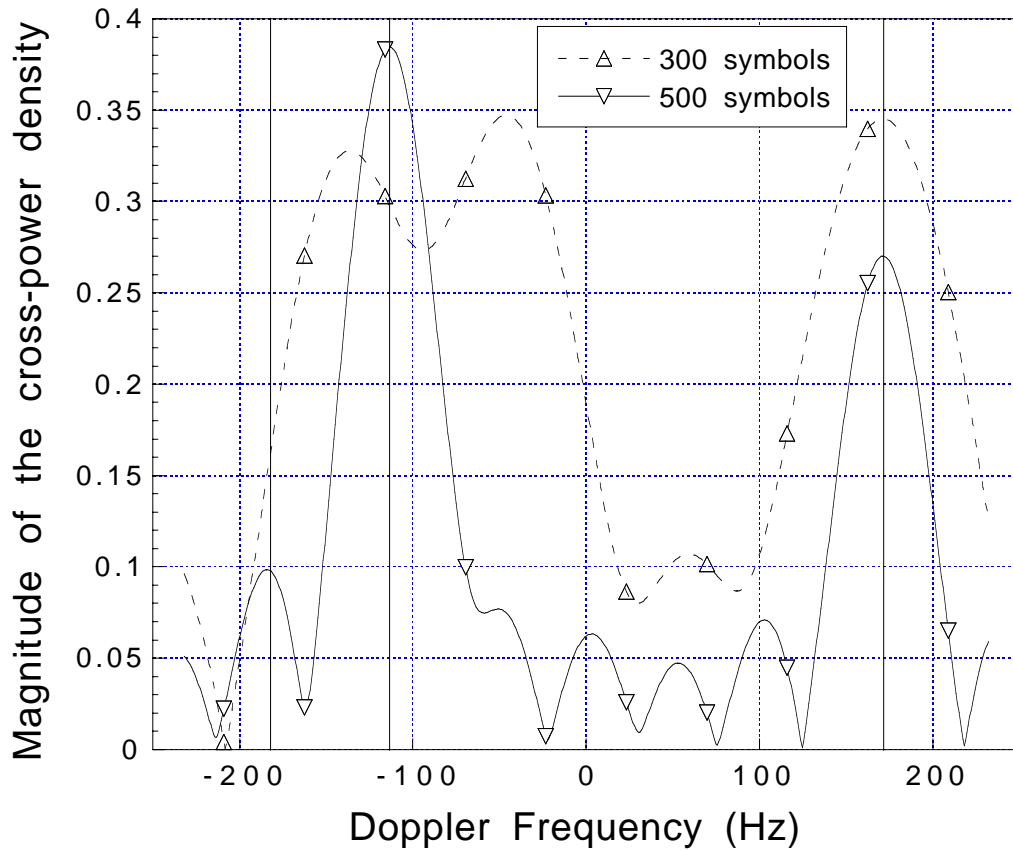


**Figure 3.5:** Magnitude of the cross-power density

to the receiver and can be used as training sequence. The size of the data record required to estimate the frequencies makes this method unattractive to apply to these TDMA transmissions.

Estimation of frequencies from the cross correlation is one of the spectral estimation problems. Spectral estimation methods fall into two categories: parametric and non-parametric methods. The conventional Fourier method used in the above example is periodogram-based and it belongs to the class of non-parametric methods. The resolution of these methods does not depend on the signal-to-noise ratio (SNR). It is related to the length of the data record: the longer the data record, the better the resolution [70]. Therefore, a large number of data is required to resolve

the peaks in the cross-power density spectrum in the above example.

## 3.2 Equalization Techniques Dealing with Time-Varying Channels

In TDMA cellular radio communications, transmission of data signals usually occurs over a fading multi-path channel. The channel impulse response varies constantly, depending on the speed of the mobile, due to the changes in the surroundings. When the mobile is traveling at highway speeds, the time-varying channel exhibits Doppler fading rates of up to about 180 Hz. Consequently, even for relatively low symbol rates in TDMA transmission, a transmitted signal experiences rapid variations during a long TDMA time slot, and an estimate of the channel at just the start of each time slot may not be sufficient. This gives rise to the need for increasing the frequency of equalizer updates and, consequently, for channel interpolation.

When there are some channel samples available during a TDMA time slot, by means of either LSSE channel estimation or blind ML data and channel estimation, the time-varying channel can be reconstructed by interpolation. Based on the interpolated channel, the equalizer coefficients can be updated. The accuracy of the interpolated channel, and hence the receiver performance, depend on the interpolation technique used and the number of channel samples available. An increase in channel estimation frequency can improve the accuracy of the interpolated channel, regardless of the interpolation technique.

In this section, derivation of the optimum equalizer in the mean square error (MSE) sense is first presented. Then, several equalization updating techniques for

time-varying channels and the their underlying channel interpolation techniques are proposed. For the purpose of comparison of the interpolation models, the conventional fixed equalizer is also included in this section.

### 3.2.1 Optimum MSE Equalizer

The purpose of an equalizer is to compensate for the undesired effect introduced by the communication channel, so that the transmitted signal can be retrieved at its output. Figure 3.6 shows an equalizer,  $\mathbf{w}$ , used in the receiver and its output error  $e_n$ . The equalizer is optimum in the MSE sense when the MSE of its output is minimized. The cost function is, therefore, the MSE of the equalizer output:

$$J = E [ |e_n|^2 ] . \quad (3.68)$$

The output error signal  $e_n$  is the difference between desired response or the transmitted signal  $b_n$ , that is,

$$e_n = b_n - \hat{b}_n, \quad (3.69)$$

where the equalizer output  $\hat{b}_n$  is simply the convolution between the received signal  $\mathbf{r}_n$  and the equalizer  $\mathbf{w}$ ,

$$\hat{b}_n = \mathbf{r}_n^H \mathbf{w}. \quad (3.70)$$

Applying the principle of orthogonality, the optimum equalizer,  $\mathbf{w}_{opt}$ , is given

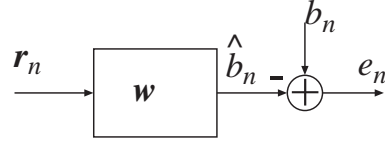


Figure 3.6: Error at the output of an equalizer

by the following equation [22]:

$$\mathbf{R}\mathbf{w}_{opt} = \mathbf{p}, \quad (3.71)$$

or

$$\mathbf{w}_{opt} = \mathbf{R}^{-1}\mathbf{p}, \quad (3.72)$$

where the autocorrelation matrix  $\mathbf{R}$  and the cross correlation vector  $\mathbf{p}$  are given by

$$\mathbf{R} = E[\mathbf{r}_n^H \mathbf{r}_n], \quad (3.73)$$

and

$$\mathbf{p} = E[\mathbf{r}_n b_n^*]. \quad (3.74)$$

Equation 3.71 is also referred to as the matrix form of the Wiener-Hopf equations.

With the estimated channel and the known transmitted sequence, both the auto correlation matrix and the cross correlation vector can be estimated and the optimum equalizer can be determined by using Equation 3.72.

### 3.2.2 Fixed Equalizer

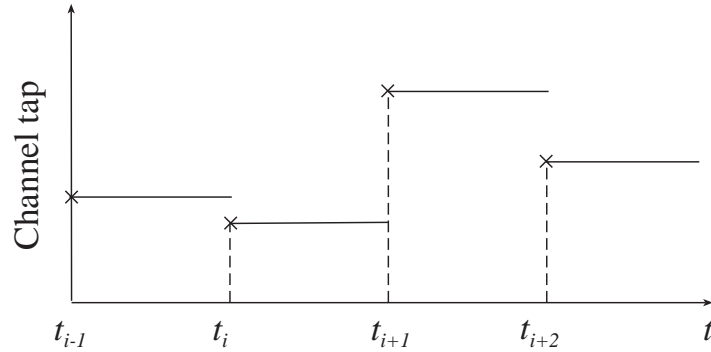


**Figure 3.7:** Interpolated channel in fixed equalizer method

The interpolation method used in a fixed equalizer is illustrated in Figure 3.7. A set of  $N_s$  channel samples  $\{c_i\}$  are available at time  $\{t_i\}$ . In the time interval  $[t_i, t_{i+1}]$ , the interpolated channel takes the value of the channel sample  $c_i$  at time  $t_i$ . Therefore, the channel is treated as if it were time invariant in the interval  $[t_i, t_{i+1}]$ , and this is the simplest interpolation method. The interpolated channel is given by the following equation:

$$c(t) = c_i, \quad t_i \leq t \leq t_{i+1}. \quad (3.75)$$

The equalizer coefficients  $\mathbf{w}_i$  are calculated at each available channel sample, and kept fixed until the next available channel sample where the update takes place.

### 3.2.3 Displaced Equalizer

Displaced equalizer is an equalizer updating technique, in which equalizer coefficients are computed in the middle of a received signal interval and applied to the entire interval. The interpolation technique used in the displaced equalizers is similar to that for the fixed equalizer method, requires no interpolation. Figure 3.8 shows the basic idea behind the interpolation method used in a displaced equalizer.

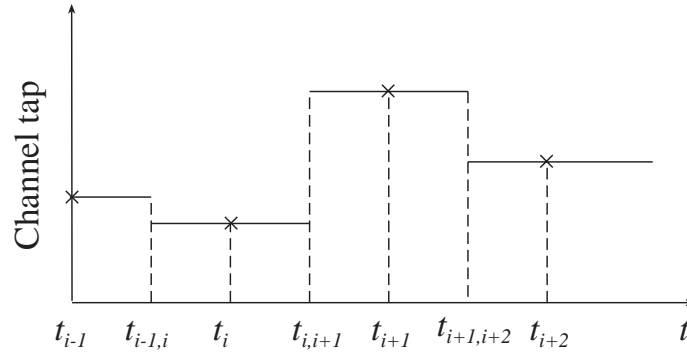


**Figure 3.8:** Interpolated channel in displaced equalizer method

As shown in the figure, time instants  $t_{i-1,i}$  and  $t_{i,i+1}$  are the midpoints between time  $t_{i-1}$  and  $t_i$ ,  $t_i$  and  $t_{i+1}$ , respectively. The channel coefficients in time interval  $[t_{i-1,i}, t_{i,i+1}]$ , are fixed at the values of  $c_i$ , which are determined at time  $t_i$ . Therefore, the interpolated channel in this interval can be described by the following equation:

$$c(t) = c_i, \quad t_{i-1,i} \leq t \leq t_{i,i+1}. \quad (3.76)$$

In general, this interpolation method gives a more accurate interpolated channel compared with the previous method. Since interval  $[t_{i-1,i}, t_{i,i+1}]$  is closer in time to  $t_i$  than  $t_{i-1}$ , it makes more sense for the interpolated channel to take the value of  $c_i$  instead of  $c_{i-1}$ .

The equalizer coefficients are updated based on the interpolated channel and should take the values of  $\mathbf{w}_i$ , which are calculated at  $t_i$  for the interval  $[t_{i-1,i}, t_{i,i+1}]$ . No update is required within this interval. Since,  $\mathbf{w}_i$  is applied to the interval  $[t_{i-1,i}, t_{i,i+1}]$  in this equalization method, compared to the fixed equalizer method where  $\mathbf{w}_i$  is applied to interval  $[t_i, t_{i+1}]$ , the equalizer  $\mathbf{w}_i$  seems to be displaced from interval  $[t_i, t_{i+1}]$  to  $[t_{i-1,i}, t_{i,i+1}]$ . Therefore, the equalizer using this updating method is called the displaced equalizer.

### 3.2.4 Curve Fitting Equalizer

The interpolation models adopted by both fixed equalizer and displaced equalizer techniques result in piecewise interpolated channels. These models work very well when the channel is stationary or slowly time-varying. However, as in most cases, the channel is fast time-varying. Despite their simplicity, these techniques cannot accurately characterize the variations in a channel tap, especially in the case of high mobile speed. In this case, a more accurate model for interpolation, for example, polynomials, splines, or piecewise linear model, can be used, in order to improve the performance. In this section, some curve fitting techniques which employ a polynomial or a cubic spline model are proposed. The equalizer coefficients are updated using the Wiener-Hopf equations based on the interpolated channel. The goal here is to incorporate a more accurate interpolated channel to achieve better performance in the fast time-varying environment.

#### 3.2.4.1 Polynomial Exact Fit

The curve fitting model adopted here is an  $(N_p - 1)$ th order polynomial. One tap of the time-varying channel can be modeled by

$$c(t) = a_0 + a_1t + a_2t^2 + \cdots + a_{N_p-1}t^{N_p-1}. \quad (3.77)$$

To completely model a tap coefficient of the time-varying channel, the polynomial coefficients must be determined. To determine  $N_p$  coefficients,  $N_s = N_p$  channel samples are required. Fitting this polynomial to the set of  $N_s$  channel samples  $\{c_i\}$ ,

the coefficients of the polynomial are determined by solving equation

$$\mathbf{a} = \mathbf{T}_1^{-1} \mathbf{c}, \quad (3.78)$$

where

$$\mathbf{a} = \begin{bmatrix} a_0 \\ a_1 \\ \vdots \\ a_{N_s-1} \end{bmatrix}, \quad (3.79)$$

$$\mathbf{c} = \begin{bmatrix} c_0 \\ c_1 \\ \vdots \\ c_{N_s-1} \end{bmatrix}, \quad (3.80)$$

and

$$\mathbf{T}_1 = \begin{bmatrix} 1 & t_0 & \cdots & t_0^{N_s-1} \\ 1 & t_1 & \cdots & t_1^{N_s-1} \\ \vdots & \vdots & \ddots & \vdots \\ 1 & t_{N_s-1} & \cdots & t_{N_s-1}^{N_s-1} \end{bmatrix}. \quad (3.81)$$

Using this curve fitting method, all the channel samples are on the resulting polynomial.

In general, within an observation interval, the accuracy of the interpolated channel improves as the number of available channel samples increases. However, the

duration of a time slot is usually in the order of  $10^{-3}$  seconds, and furthermore, for higher order polynomials, the matrix  $\mathbf{T}_1$  can be ill-conditioned. Therefore, this method can run into numerical problems in this particular application for higher order polynomials. This provides motivation for the proposal of the two curve fitting methods discussed in the following sections – polynomial LS fit and spline fit.

### 3.2.4.2 Polynomial LS Fit

In this curve fitting method, the goal is to fit a set of  $N_s$  channel sample points  $(t_i, c_i)$  to the model given in Equation 3.77, so that the squared error of the curve-fitted channel at time instants  $t_i$  is minimized. With this method, there is no restriction on the order of the polynomial  $N_p$ . When  $N_s \geq N_p$ , the problem is equivalent to solving an over determined system with  $N_s$  equations and  $N_p$  unknowns in the LS sense.

The coefficients of the polynomial are determined by solving the following equation:

$$\mathbf{a}_{LS} = \arg \left[ \min_{\mathbf{a}} \sum_{i=0}^{N_s-1} [c_i - c(t_i; a_0 \cdots a_{N_p-1})]^2 \right]. \quad (3.82)$$

Minimization of the sum of squared errors in Equation 3.82 yields

$$\mathbf{a} = \mathbf{T}_2^{-1} \mathbf{b}, \quad (3.83)$$

where

$$\mathbf{T}_2 = \begin{bmatrix} 1 & \bar{t} & \dots & \overline{t^{N_p-1}} \\ \bar{t} & \overline{t^2} & \dots & \overline{t^{N_p}} \\ \vdots & \vdots & \ddots & \vdots \\ \overline{t^{N_p-1}} & \overline{t^{N_p}} & \dots & \overline{t^{2(N_p-1)}} \end{bmatrix} \quad (3.84)$$

and

$$\mathbf{b} = \begin{bmatrix} \bar{c} \\ \overline{tc} \\ \vdots \\ \overline{t^{N_p-1}c} \end{bmatrix}. \quad (3.85)$$

Here,  $\overline{\blacksquare^m \blacklozenge^n}$  denotes average, and it is defined as

$$\overline{\blacksquare^m \blacklozenge^n} = \frac{1}{N_s} \sum_{i=0}^{N_s-1} \blacksquare_i^m \blacklozenge_i^n. \quad (3.86)$$

### 3.2.4.3 Cubic Spline Fit

The time-varying channel tap can also be interpolated using a spline function. A spline function is a function that consists of polynomial pieces joined together at the known data samples, called knots, with certain smoothness conditions, and it

is defined as

$$c(t) = \begin{cases} g_0(t), & t_0 \leq t \leq t_1 \\ g_1(t), & t_1 \leq t \leq t_2 \\ \vdots & \vdots \\ g_{N_s-2}(t) & t_{N_s-2} \leq t \leq t_{N_s-1} \end{cases}. \quad (3.87)$$

In the above equation,  $g_i(t)$  is a polynomial, and it takes the value of  $c_i$  and  $c_{i+1}$  at its end points.

Each segment of the polynomial in a cubic spline is a cubic polynomial. In addition, each segment is required to have the same first and second derivatives as the adjoining segment at the knot between them, so that the overall curve is smooth. The task here is to determine the coefficients of the cubic polynomials.

Let  $u_i = c''(t_i)$  for  $0 \leq i \leq N_s - 1$ , and  $\Delta t_i = t_{i+1} - t_i$  for  $0 \leq i \leq N_s - 2$ . Since the second derivative of a cubic spline is linear in interval  $[t_i, t_{i+1}]$  and it takes the value of  $u_i$  and  $u_{i+1}$  at the end points, it takes the form [71]

$$g_i''(t) = \frac{u_{i+1}}{\Delta t_i}(t - t_i) + \frac{u_i}{\Delta t_i}(t_{i+1} - t). \quad (3.88)$$

By integrating Equation 3.88 twice and evaluating the integration constants using the interpolation conditions of  $g_i(t_i) = c_i$  and  $g_i(t_{i+1}) = c_{i+1}$ , the  $i$ th segment of the spline can be obtained, in terms of  $u_i$  [71]:

$$g_i(t) = \frac{u_{i+1}}{6\Delta t_i}(t - t_i)^3 + \frac{u_i}{6\Delta t_i}(t_{i+1} - t)^3 + \left( \frac{c_{i+1}}{\Delta t_i} - \frac{\Delta t_i}{6}u_{i+1} \right) (t - t_i) \quad (3.89)$$

$$+ \left( \frac{c_i}{\Delta t_i} - \frac{\Delta t_i}{6}u_i \right) (t_{i+1} - t). \quad (3.90)$$

The second derivative  $u_i$  can be determined by using the condition on the first

derivative at the knots. By differentiating the  $i$ th and  $(i - 1)$ th segments of the cubic spline, and equating them,  $N_s - 2$  equations are obtained [71]:

$$\Delta t_{i-1}u_{i-1} + 2(\Delta t_{i-1} + \Delta t_i) + \Delta t_i u_{i+1} = \frac{c_{i+1} - c_i}{6\Delta t_i} - \frac{c_i - c_{i-1}}{6\Delta t_{i-1}}, 1 \leq i \leq N_s - 2. \quad (3.91)$$

In order to solve the  $N_s$  unknown second derivatives, two more equations are needed, in addition to the above  $N_s - 2$  equations. The remaining two equations are given by using the “not-a-knot” end condition, which requires that the third derivative of the spline be a single constant in the first two subintervals and another single constant in the last two subintervals. These two equations are

$$\Delta t_1 u_0 - u_1(\Delta t_0 + \Delta t_1) + \Delta t_0 u_2 = 0 \quad (3.92)$$

and

$$\Delta t_{N_s-2} u_{N_s-3} - u_{N_s-2}(\Delta t_{N_s-3} + \Delta t_{N_s-2}) + \Delta t_{N_s-3} u_{N_s-1} = 0. \quad (3.93)$$

Similar to the previous curve fitting method, the degree of the spline is not restricted by the number of channel samples.

### 3.3 Block Adaptation Strategies in Time-Varying Environment

Figure 3.9 shows a typical time slot in a TDMA transmission. There are usually one or two known training sequences within a time slot, and here two are shown in



**Figure 3.9:** A TDMA time slot

the diagram. The rest are transmitted data that are unknown to the receiver. In order to achieve good system performance in TDMA cellular radio, especially at high mobile speed, block adaptation strategy proposed by Lo et al. is proven to offer good immunity to fast fading [41, 55, 56]. In this section, the work on block adaptation done by Lo et al. is briefly described. Then a new block adaptation with blind data and channel estimation method is proposed to reduce the amount of processing delay and improve the system throughput associated with the conventional block adaptation method proposed by Lo et al. at the expense of complexity. This new method involves combinations of channel estimation and equalization techniques discussed in the previous sections.

### 3.3.1 Background in Block Adaptation

The conventional block adaptation method proposed by Lo et al. computes the time-varying channel during the unknown data period by interpolating a set of estimated channel samples obtained through periodic training at adjacent TDMA time slots. Figure 3.10 shows the interpolation of a time-varying channel within a TDMA time slot in the conventional block adaptation method. In this figure, the letter “T” denotes a training section and “D” denotes an unknown data section. With periodic training, a snap shot of the time-varying channel, denoted by  $\times$ , can be estimated by using one of the channel estimation algorithm such as LSSE. By interpolating  $Q$  consecutively estimated channel samples from periodic training, with generally  $Q/2$  from the past and  $Q/2$  from the future, channel samples denoted

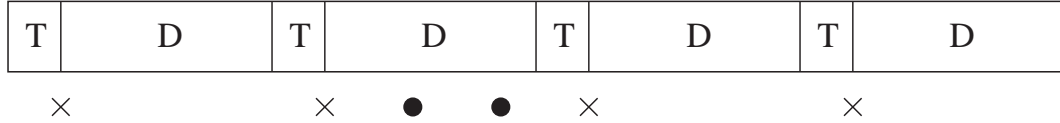


**Figure 3.10:** Interpolation in the conventional block adaptation method

by ● can be obtained during the unknown data section in the current time slot. The interpolation is carried out by a truncated raised cosine interpolator. By using the interpolated channel samples, together with the channel samples obtained from training, the equalizer coefficients are computed periodically to adapt to the fast time-varying channel.

While this method provides good immunity to decision errors caused by deep fades, it suffers from the inherent limitation of processing delay. In the worst case, except for the one from the current time slot, the other  $Q - 1$  estimated channel samples from training are from the future time slots, and the processing delay in this case is  $Q - 1$  time slots. Another limitation associated with this method is that the frequency of the periodic training sequences, and hence the length of the time slot, depends on the Doppler frequency. In order to provide reliable interpolation for all vehicle speeds, Nyquist's sampling criterion must be satisfied, which requires the frequency of the training sequences to be at least twice the maximum Doppler frequency in the worst case. This results in reduction in system throughput.

### 3.3.2 Block Adaptation with Blind Data and Channel Estimation

A new block adaptation method is proposed here to improve the processing delay and system throughput associated with the conventional method. Unlike the conventional block adaptation method, the new method interpolates the estimated

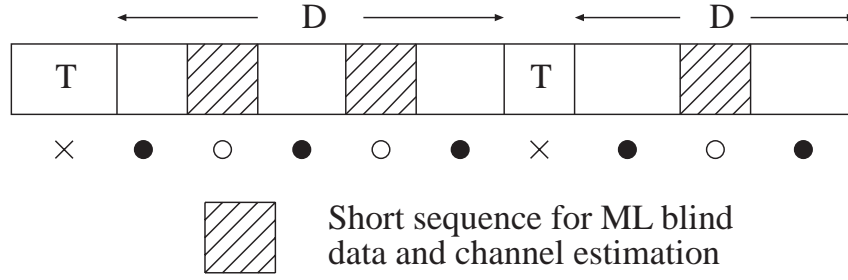


**Figure 3.11:** Interpolation in the proposed block adaptation method

channel obtained using the training sequence in the current time slot and using the ML blind data and channel estimation method.

Figure 3.11 shows interpolation in the new block adaptation method within a time slot. In this time slot, there are two training sequences from where estimated channel samples, denoted by  $\times$ , can be obtained by the LSSE channel estimation method. These channel samples are considered to be in the middle of the training sequences. However, with these two channel samples, it is not sufficient to predict the variations of the channel in the entire time slot, especially in the high mobile speed case. In the proposed method, more channel samples, and the corresponding short estimation sequences are made available in the unknown data section by using the ML blind data and channel estimation method, described in Section 3.1.3. As shown in Figure 3.11, short estimation sequences, represented by the shaded boxes, can be selected in the unknown data sections to perform ML blind data and channel estimation. The estimated channel samples obtained in this way, denoted by  $\circ$ , are also considered to be in the middle of the estimation sequence. The frequency of these channel samples depends on the maximum Doppler frequency.

The length of the estimation sequence has to be at least twice the memory of the channel, to provide a reliable channel estimate. There are two reasons to keep this sequence short. The LSSE channel estimation and ML blind channel estimation

used in the proposed block adaptation method are estimation algorithms for time-invariant channels. Therefore, the estimation sequences should be sufficiently short so that the time-varying channel during the estimation sequences is essentially time-invariant. Furthermore, the complexity of the blind channel estimation method grows exponentially with the length of the estimation sequence. Therefore, one should consider all these issues when implementing this algorithm.

With these channel samples available in a time slot, the time-varying channel can be interpolated and the equalizer coefficients can be updated to adapt to the fast time-varying channel between the training and the estimation sequences. This task is carried out by using one of the equalizer updating methods – the fixed equalizer, the displaced equalizer or the curve fitting equalizer. The interpolated channel samples, denoted by • in Figure 3.11, are obtained by interpolation using the model underlying the fixed equalizer, displaced equalizer or curve fitting equalizer updating methods.

In this way, the processing delay is eliminated since all the data can be recovered by the end of the current time slot. No additional training sequence is required and the system throughput is improved, compared to the conventional method. The trade-off is the intensive computational requirement.

This method can also be extended to suppress CCI. Snap shots of the co-channel impulse response can be obtained together with the desired channel impulse response using the ML blind data, channel and co-channel estimation method. Then the time-varying channel and co-channel can be interpolated using the interpolator in one of the three equalizer updating methods. The interpolated co-channel can be incorporated into the formulation of the Wiener-Hopf equations. The equalizer computed in this way is capable of suppressing CCI, as well as tracking the time-

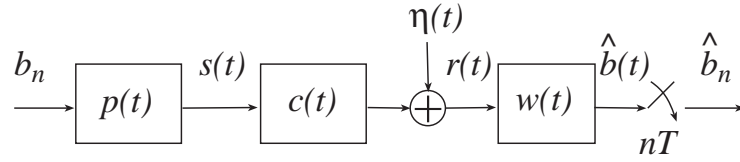


**Figure 3.12:** Baseband communication system

varying channel and co-channel.

## 3.4 Mean Square Error Analysis

Mean square error analyses of various equalizer types on a time-invariant channel have been presented in detail in the literature [11, 28, 72, 73]. Discussion in this section is intended to develop a new MSE expression for a displaced LE on time-varying channels.

### 3.4.1 MSE Criterion

A typical baseband communication system is shown in the block diagram in Figure 3.12. The discrete sequence  $\{b_n\}$  is a sequence of information-bearing symbols. This information-bearing sequence is pulse shaped by the transmit filter  $p(t)$  and transmitted through the frequency selective time-invariant channel  $c(t)$  with additive white Gaussian noise  $\eta(t)$ . The received signal  $r(t)$  is applied to a linear equalizer,  $w(t)$ , with infinite duration in time, which produces an output denoted by  $\hat{b}(t)$ . This continuous-time signal is then sampled at the symbol rate to produce  $\hat{b}_n$ .

The objective here is to design the equalizer  $w(t)$ , so that the information-bearing symbol  $b_n$  can be faithfully estimated at the receiver end, with the estimation error

minimized in some statistical sense.

Usually, mean square error (MSE) criterion is chosen for statistical optimization of the equalizer. The cost function or performance index for the MSE criterion is the mean-square value of the estimation error  $e_n$ , namely,

$$\varepsilon_I = E [ |e_n|^2 ] \quad (3.94)$$

$$= E \left[ \left| b_n - \hat{b}_n \right|^2 \right], \quad (3.95)$$

where  $\varepsilon_I$  denotes the MSE of the equalizer output on a time-invariant channel.

The choice of MSE criterion for statistical optimization of the equalizer is dictated by its mathematical tractability. In particular, MSE criterion leads to a second order dependence of the cost function on the unknown linear equalizer. This will become apparent in the following section. Furthermore, this second order dependence of the cost function on the linear equalizer results in a quadratic error surface, which gives a unique solution for the optimum equalizer at its minimum [22]. Another advantage associated with the MSE criterion is the useful relationship between the minimum MSE (MMSE) and the probability of error. In fact, the MSE criterion allows ISI and noise to be taken into account jointly, and in most practical applications, it leads to values of error probability very close to that minimizing the probability of error [72]. An upper bound on the probability of error can also be derived from the expression for the MMSE [74, 75].

### 3.4.2 MMSE of Infinite LE on Time-Invariant Channels

The MMSE of an infinite LE on a time-invariant channel is derived in the work of a few researchers [11, 28, 72]. Since the new MSE expression for the displaced

equalizer is developed based on the MMSE expression of an infinite LE on time-invariant channels, the expression for the time-invariant channels is presented in this section as a starting point of the development of the new MSE expression.

Let  $h(t)$  be the overall time-invariant channel, which includes the transmit filter and the physical channel. Its autocorrelation function  $\xi(t)$  is defined as

$$\xi(t) = h(t) \star h^*(-t), \quad (3.96)$$

with the associated Fourier transform given by the following equation:

$$\begin{aligned} \Xi(f) &= \mathcal{F}\{\xi(t)\} \\ &= \mathcal{F}\{h(t) \star h^*(-t)\} \\ &= H(f)H^*(f) \\ &= |H(f)|^2. \end{aligned} \quad (3.97)$$

$\xi(t)$  can be sampled to get

$$\xi[n] = \xi(t)|_{t=nT}. \quad (3.98)$$

The MMSE is given by the following expression:

$$\varepsilon_{I,\min} = \left\langle \frac{1}{1 + \frac{1}{N_o} \Xi_{\frac{1}{T}}(f)} \right\rangle, \quad (3.99)$$

where subscript “min” on  $\varepsilon_I$  denotes minimum. In Equation 3.99,  $\Xi_{\frac{1}{T}}(f)$  is the

discrete time continuous frequency Fourier transform:

$$\Xi_{\frac{1}{T}}(f) = \mathcal{F}\{\xi[n]\}, \quad (3.100)$$

and it is related to the continuous time continuous frequency Fourier transform  $\Xi(f)$  by the following equation:

$$\Xi_{\frac{1}{T}}(f) = \frac{1}{T} \sum_{k=-\infty}^{\infty} \Xi\left(f + \frac{k}{T}\right). \quad (3.101)$$

The optimum infinite LE which gives the MMSE can also be obtained [72, 76]:

$$W(f) = \frac{H^*(f)}{N_o + \Xi_{\frac{1}{T}}(f)}. \quad (3.102)$$

It is assumed that the channel estimate used to derive the optimum LE is perfect. This assumption will be effective for the rest of the MSE analysis.

### 3.4.3 Average MMSE of Infinite LE on Fading Channels

In the previous section, an MMSE expression was presented for the linear equalizer on a time-invariant channel. This section describes the development of a new expression for the average MMSE of an infinite-length linear equalizer on a fading time-varying channel in the presence of additive white Gaussian noise, based on the expression in Equation 3.99. Towards this goal, a model and its statistics for the time-varying channel is first investigated. A simple transmit filter is then chosen to simplify the analysis. The PDF of the overall channel and, finally, an expression of average MMSE and its relationship with the average SNR for LE on fading channel are also derived.

### 3.4.3.1 Model and Statistics of the Channel Taps

The channel model used here is a 2-ray model, with a delay interval of  $T/2$ :

$$c(\tau; t) = c_0(t)\delta(\tau) + c_1(t)\delta(\tau - \frac{T}{2}). \quad (3.103)$$

From the above equation, the channel is a function of both the time index  $t$  and the time delay  $\tau$ , and its time-varying Fourier transform, taken with respect to the time delay  $\tau$  is given by

$$C(f; t) = c_0(t) + c_1(t) \exp\left(-j2\pi f \frac{T}{2}\right). \quad (3.104)$$

The two taps  $c_0(t)$  and  $c_1(t)$ , given by the Equations 3.105 and 3.106, are complex and time-varying, that is,

$$c_0(t) = c_{0,R}(t) + jc_{0,I}(t) \quad (3.105)$$

and

$$c_1(t) = c_{1,R}(t) + jc_{1,I}(t). \quad (3.106)$$

The channel taps are independently generated by the Gans' channel generator described in Section 2.2.3.4. Input to the generator is a zero-mean white Gaussian noise sequence. Since the generator is linear, the output is also Gaussian. Therefore, the channel taps are complex Gaussian, with their magnitude Rayleigh distributed and phase uniformly distributed.

The autocorrelation functions of the channel taps are summarized in the follow-

ing equations:

$$\begin{aligned}
 \phi_{00}(\Delta t) &= E [c_0(t)c_0^*(t - \Delta t)] \\
 &= E [(c_{0,R}(t) + jc_{0,I}(t)) (c_{0,R}(t - \Delta t) - jc_{0,I}(t - \Delta t))] \\
 &= \phi_{0R}(\Delta t) + \phi_{0I}(\Delta t),
 \end{aligned} \tag{3.107}$$

and similarly,

$$\begin{aligned}
 \phi_{11}(\Delta t) &= E [c_1(t)c_1^*(t - \Delta t)] \\
 &= \phi_{1R}(\Delta t) + \phi_{1I}(\Delta t),
 \end{aligned} \tag{3.108}$$

where  $\phi_{iR}(\Delta t)$  and  $\phi_{iI}(\Delta t)$ , for  $i = 0, 1$ , are the autocorrelation function of the real and imaginary part of tap  $i$ , respectively, and defined as

$$\phi_{iR}(\Delta t) = E [c_{i,R}(t)c_{i,R}^*(t - \Delta t)] \tag{3.109}$$

and

$$\phi_{iI}(\Delta t) = E [c_{i,I}(t)c_{i,I}^*(t - \Delta t)]. \tag{3.110}$$

For the two channel taps with identical statistical properties, it follows that

$$\phi_{0R}(\Delta t) = \phi_{0I}(\Delta t) = \phi_{1R}(\Delta t) = \phi_{1I}(\Delta t) = \phi_{R,I}(\Delta t), \tag{3.111}$$

and

$$\phi_{00}(\Delta t) = \phi_{11}(\Delta t) = 2\phi_{R,I}(\Delta t). \quad (3.112)$$

Since the two taps are independent, the cross correlation functions are

$$\phi_{01}(\Delta t) = E [c_0(t)c_1^*(t - \Delta t)] \quad (3.113)$$

$$= 0, \quad (3.114)$$

and similarly,

$$\phi_{10}(\Delta t) = 0. \quad (3.115)$$

### 3.4.3.2 Transmit Filter

In order to simplify the mathematics in this analysis, a rectangular pulse with zero rolloff factor is used as the transmit filter:

$$|P(f)| = \begin{cases} \sqrt{T}, & |f| \leq \frac{1}{2T} \\ 0, & \text{otherwise,} \end{cases} \quad (3.116)$$

where  $T$  is the symbol period.

### 3.4.3.3 PDF of Fourier Transform of the Channel Autocorrelation

In this section, an expression for the PDF of  $\Xi_{\frac{1}{T}}(f; t)$  is derived. The term  $\Xi_{\frac{1}{T}}(f; t)$ , the discrete time continuous frequency Fourier transform of the autocor-

relation of the time-varying channel is given by

$$\Xi_{\frac{1}{T}}(f; t) = \frac{1}{T} \sum_{k=-\infty}^{\infty} \Xi \left( f + \frac{k}{T}; t \right) \quad (3.117)$$

where  $\Xi(f; t)$  is the Fourier transform of the autocorrelation of the time-varying channel. Since a transmit filter with zero rolloff is used, there is no aliasing due to sampling of the autocorrelation of the overall channel and there is only one term in the summation in the expression for  $\Xi_{\frac{1}{T}}(f; t)$ , namely,

$$\begin{aligned} \Xi_{\frac{1}{T}}(f; t) &= \frac{1}{T} \Xi(f; t) \\ &= \frac{1}{T} |H(f; t)|^2. \end{aligned} \quad (3.118)$$

In Equation 3.118,  $H(f; t)$  is the time-varying Fourier transform of the overall channel  $h(\tau; t)$ , and  $|H(f; t)|^2$  can be written as

$$\begin{aligned} |H(f; t)|^2 &= |P(f)|^2 |C(f; t)|^2 \\ &= T |C(f; t)|^2. \end{aligned} \quad (3.119)$$

Let  $x \equiv \Xi_{\frac{1}{T}}(f; t)$ . With the two tap channel given in Equation 3.104 and the transmit filter given by Equation 3.116,  $x$  can be written as

$$x = \mathbf{c} \mathbf{Q} \mathbf{c}^H, \quad (3.120)$$

where  $\mathbf{c}$  and  $\mathbf{Q}$  are defined as

$$\mathbf{c} = \begin{bmatrix} c_0(t) \\ c_1(t) \end{bmatrix} \quad (3.121)$$

and

$$\mathbf{Q} = \begin{bmatrix} 1 & \exp(-j2\pi f \frac{T}{2}) \\ \exp(j2\pi f \frac{T}{2}) & 1 \end{bmatrix}. \quad (3.122)$$

The right hand side of Equation 3.120 is a quadratic form in complex Gaussian variables  $c_0(t)$  and  $c_1(t)$ . Since  $\mathbf{Q}$  is a Hermitian matrix, and  $\mathbf{c}$  has zero mean, the characteristic function of the quadratic form is given by Turin [77],

$$\varphi(t) = \prod_{n=1}^{N_c} (1 - jt\lambda_n)^{-1}, \quad (3.123)$$

where  $t$  is an independent variable,  $\lambda_n$  are the eigenvalues of matrix  $\mathbf{LQ}$  and  $\mathbf{L}$  is the covariance matrix of  $\mathbf{c}$ , defined as

$$\mathbf{L} = E[(\mathbf{c} - E[\mathbf{c}])(\mathbf{c} - E[\mathbf{c}])^H]. \quad (3.124)$$

The two eigenvalues can be obtained by solving the characteristic equation for  $\mathbf{LQ}$ :

$$\lambda_1 = 4\phi_{R,I}(0) \quad (3.125)$$

$$\lambda_2 = 0. \quad (3.126)$$

Therefore, there is only one term in the product term in Equation 3.123.

Finally, the PDF of  $x$  can be derived by using the fact that the characteristic

function and the PDF are a Fourier transform pair [77]:

$$p_X(x) = \begin{cases} \frac{1}{\lambda_1} \exp(-\frac{x}{\lambda_1}), & x \geq 0 \\ 0, & \text{otherwise.} \end{cases} \quad (3.127)$$

#### 3.4.3.4 Average MMSE of Infinite LE on Time-Varying Channels

For time-varying channels, the instantaneous value of the MMSE of an infinite LE is also time-varying, given by

$$\varepsilon_{V,\min}(t) = \left\langle \frac{1}{1 + \frac{1}{N_o} \Xi_{\frac{1}{T}}(f; t)} \right\rangle, \quad (3.128)$$

where  $\varepsilon_{V,\min}$  denotes the MMSE of the equalizer output on a time-varying channel. In Equation 3.128, the operation  $\langle \blacksquare \rangle$  denotes the average of  $\blacksquare$  over frequency, defined as

$$\langle \blacksquare \rangle = T \int_{-\frac{1}{2T}}^{\frac{1}{2T}} \blacksquare df \quad (3.129)$$

The average MMSE of the LE on a time-varying channel can be derived by taking the expectation of the MMSE expression given in Equation 3.128 with respect to the time-varying channel:

$$\bar{\varepsilon}_{V,\min} = E[\varepsilon_{V,\min}(t)] \quad (3.130)$$

$$= \left\langle E\left[\frac{1}{1 + \frac{1}{N_o} x}\right] \right\rangle, \quad (3.131)$$

where  $\bar{\blacksquare}$  denotes the average of  $\blacksquare$ . With the PDF of  $x$  derived in the previous section, the expectation in Equation 3.131 can be evaluated using the following

definition [78]:

$$E[f(x)] = \int_{-\infty}^{\infty} f(x)p_X(x)dx, \quad (3.132)$$

with

$$f(x) = \frac{1}{1 + \frac{1}{N_o}x}. \quad (3.133)$$

By evaluating the integral in Equation 3.132 and the angle brackets in Equation 3.131, the final expression for the average MMSE of an infinite LE on a fading channel can be obtained:

$$\bar{\epsilon}_{v,\min} = \frac{N_o}{\lambda_1} \exp\left(\frac{N_o}{\lambda_1}\right) \text{Ei}\left(\frac{N_o}{\lambda_1}\right), \quad (3.134)$$

where  $\text{Ei}(x)$  is called the exponential integral function, and it is defined as

$$\text{Ei}(x) = \begin{cases} \int_x^{\infty} \frac{e^{-t}}{t} dt, & x > 0 \\ \text{not defined,} & x \leq 0 \end{cases}. \quad (3.135)$$

Note that the SNR at the input of the infinite LE is

$$\gamma_{\text{in}} = \frac{P_{\text{signal+ISI}}}{P_{\text{noise}}} \quad (3.136)$$

$$= \frac{\lambda_1}{N_o}, \quad (3.137)$$

where the subscript “in” on  $\gamma$  denotes the input of the LE, and  $P_{\text{signal+ISI}}$  and  $P_{\text{noise}}$  denote the power of the signal plus ISI and the power of noise, respectively.

Therefore, Equation 3.134 can be rewritten in terms of input SNR:

$$\bar{\varepsilon}_{V,\min} = \frac{1}{\gamma_{\text{in}}} \exp\left(\frac{1}{\gamma_{\text{in}}}\right) \text{Ei}\left(\frac{1}{\gamma_{\text{in}}}\right). \quad (3.138)$$

As expected, the limit of the right hand side of Equation 3.138 is 0 as  $\gamma \rightarrow \infty$ .

### 3.4.4 MSE of Displaced LE on Fading Channels

In the case of time-invariant channels, if the optimum LE given in Equation 3.102 is used in the receiver, the MSE remains constant at MMSE for the entire time slot. This is not true for a time-varying channel. The optimum LE derived for a snap shot of the time-varying channel is no longer optimum at another time instant, and the resulting MSE increases. The rate of increase in MSE depends on the rate of change in the channel.

The diagram in Figure 3.13 shows the MSE when a displaced LE (DLE) is used in the case of fading channel. In the time interval shown in the figure, the MSE reaches its minimum at the mid-point  $t_0$  where the channel estimate is available. The time instant  $t_1$ , at which the channel estimate is not available is termed a displaced time. At  $t_1$ , the LE, which is derived and being optimum at  $t_0$ , gives a higher MSE  $\varepsilon_1$ . The following theoretical development is intended to derive an expression for  $\varepsilon_1$ , in terms of  $\bar{\varepsilon}_{V,\min}$  and the time difference  $\Delta t$  between  $t_1$  and  $t_0$ .

The fading channel, due to its time-varying nature, involves two dimensions: the time and the time delay. Up to this point, time is represented by the symbol  $t$  and the time delay by the symbol  $\tau$ . In order to simplify the notation in the theoretical analysis, for the remainder of this chapter, all the time-varying filters and waveforms at time instances  $t_0$  and  $t_1$  will be represented by the subscripts

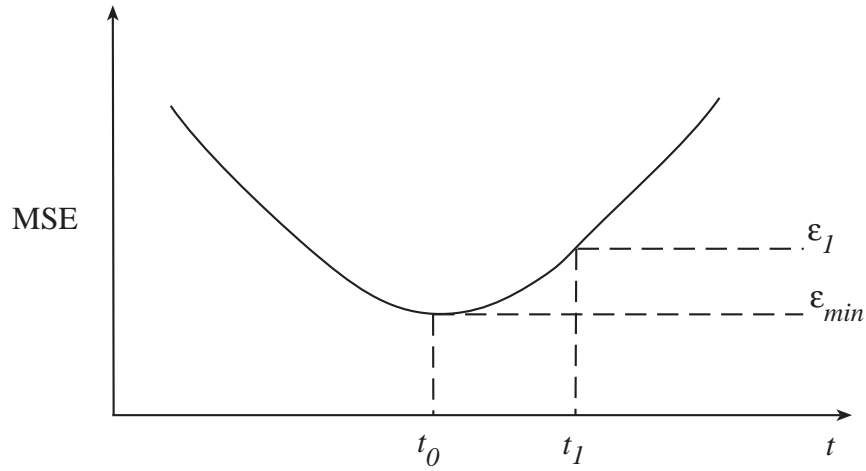


**Figure 3.13:** MSE of DLE in a time slot

0 and 1, respectively. The time delay will be represented by the symbol  $t$ . For example, for the time-varying channel at  $t_1$ , instead of  $c(t_1; \tau)$ ,  $c_1(t)$  will be used.

#### 3.4.4.1 Perturbations in the Time-Varying Channels

The theoretical development in this section leads to an expression of the variance of the perturbations in the time-varying channel. Since the MSE at  $t_1$  depends on the perturbation of the time-varying channel from  $t_0$  to  $t_1$ , the result developed here will be useful in deriving an expression for the MSE at  $t_1$ , as it will become apparent in the later section.

At time  $t_0$  and  $t_1$ , the time-varying channel are given by the following equations:

$$c_0(t) = c_{00}\delta(t) + c_{01}\delta\left(t - \frac{T}{2}\right) \quad (3.139)$$

$$c_1(t) = c_{10}\delta(t) + c_{11}\delta\left(t - \frac{T}{2}\right). \quad (3.140)$$

Define  $y_0 = c_{10} - c_{00}$  and  $y_1 = c_{11} - c_{01}$  to be the perturbations of tap 0 and tap 1, respectively, of the channel at  $t_1$  with respect to  $c_0(t)$ . Then the channel at  $t_1$  can

also be written in terms of the channel at  $t_0$  and the perturbations:

$$c_1(t) = c_0(t) + y_0\delta(t) + y_1\delta\left(t - \frac{T}{2}\right) \quad (3.141)$$

$$= c_0(t) + c_p(t), \quad (3.142)$$

where  $c_p(t)$  is the channel perturbation defined as

$$c_p(t) = y_0\delta(t) + y_1\delta\left(t - \frac{T}{2}\right), \quad (3.143)$$

and the Fourier transform of  $c_1(t)$  is given by

$$C_1(f) = C_0(f) + (y_0 + y_1e^{-j\pi fT}). \quad (3.144)$$

Since the channel taps are zero-mean complex Gaussian random processes, the perturbations in the channel taps  $y_i$ , for  $i = 0, 1$ , are zero-mean complex Gaussian i.i.d. random variables. The variance of the perturbation  $\sigma_y^2$  is defined as

$$\sigma_y^2 = E[|y_i|^2] \quad (3.145)$$

$$= E[|c_{1i} - c_{0i}|^2]. \quad (3.146)$$

Substituting Equation 2.35 into Equation 3.146 and simplifying, the following expression for  $\sigma_y^2$  can be obtained:

$$\sigma_y^2 = 2N_{Go} (E_{u,00} - \text{Re}\{E_{u,01}\}), \quad (3.147)$$

where  $E$  with subscript  $u$  denotes the energy of the Gans' channel generator and it

is defined as

$$E_{u,mk} = \int_{-\infty}^{\infty} h_{ub}(t_m - \tau)h_{ub}^*(t_k - \tau)d\tau. \quad (3.148)$$

Evaluation of  $E_{u,00}$  is straight forward by change of variable and by the use of Parseval's theorem:

$$\begin{aligned} E_{u,00} &= \int_{-\infty}^{\infty} |h_{ub}(t_0 - \tau)|^2 d\tau \\ &= \int_{-\infty}^{\infty} |h_{ub}(\tau)|^2 d\tau \\ &= \int_{-\infty}^{\infty} |H_{ub}(f)|^2 df \\ &= \int_{-\infty}^{\infty} \Phi_{ub}(f) df, \end{aligned} \quad (3.149)$$

where  $\Phi_{ub}(f)$  is the U-shaped Doppler spectrum defined in Equation 2.33. By evaluating the integral in Equation 3.149 [79], the following simple expression for  $E_{u,00}$  can be obtained:

$$E_{u,00} = P_r T_o, \quad (3.150)$$

where  $T_o$  is 1 s, and it appears in the above equation so that the units on the left and right hand sides of the equation are the same.

For  $E_{u,01}$ , the following relation is obtained by the change of variable:

$$\begin{aligned} E_{u,01} &= \int_{-\infty}^{\infty} h_{ub}(t_1 - \tau)h_{ub}^*(t_0 - \tau)d\tau \\ &= \int_{-\infty}^{\infty} h_{ub}(\tau + \Delta t)h_{ub}^*(\tau)d\tau. \end{aligned} \quad (3.151)$$

Taking the Fourier transform of Equation 3.151, with respect to  $\Delta t$ , the following relation is obtained:

$$\mathcal{F}\{E_{u,01}\} = |H_{ub}(f)|^2. \quad (3.152)$$

The inverse Fourier transform of  $|H_{ub}(f)|^2$ ,  $E_{u,01}$  is given by

$$\begin{aligned} E_{u,01} &= \mathcal{F}^{-1}\{|H_{ub}(f)|^2\} \\ &= \int_{-\infty}^{\infty} |H_{ub}(f)|^2 e^{j2\pi f \Delta t} df \end{aligned} \quad (3.153)$$

$$= \int_{-\infty}^{\infty} \Phi_{ub}(f) e^{j2\pi f \Delta t} df. \quad (3.154)$$

By evaluating the integral in Equation 3.154 [79], the following expression for  $Re\{E_{u,01}\}$  can be obtained:

$$Re\{E_{u,01}\} = P_r J_0(2\pi f_m \Delta t), \quad (3.155)$$

where  $J_n(x)$  is the  $n$ th order Bessel function of the first kind, and is defined as

$$J_n(x) = \frac{1}{2\pi} \int_{-\pi}^{\pi} \exp(jx \sin \theta - jn\theta) d\theta. \quad (3.156)$$

Finally, the expression for the variance of the perturbations in the time-varying channel is

$$\sigma_y^2 = 2P_r N_{Go} (1 - J_0(2\pi f_m \Delta t)). \quad (3.157)$$

Note that  $\sigma_y^2$  is a function of  $\Delta t$ . When  $\Delta t = 0$ ,  $t_1$  coincides with  $t_0$ , and the perturbation of the channel with respect to itself and its variance are zero. As

$\Delta t$  increases,  $\sigma_y^2$  oscillates as a damped sinusoid. This behavior can be accounted for by the multiple sinusoidal nature of the channel tap generated by using Gans' model. The U-shaped Doppler spectrum in Gans' channel model is band limited by  $-f_m$  and  $f_m$ . In the extreme case, there are only two frequency components  $-f_m$  and  $f_m$  in the U-shaped Doppler spectrum. The channel taps consist of one single sinusoid with a frequency of  $f_m$  and so is the variance of the channel perturbations. As  $\Delta t \rightarrow \infty$ ,  $c_1(t)$  and  $c_0(t)$  are so far apart that they are essentially uncorrelated, and  $\sigma_y^2$  takes the value of  $2P_r N_{G_o}$ .

#### 3.4.4.2 Estimated Information-Bearing Symbol at a Displaced Time

At time  $t_0$  and  $t_1$ , the output of the transmit filter  $p(t)$  and the received signals of the communication system in Figure 3.12 are

$$s_0(t) = \sum_{n=-\infty}^{\infty} b_0[n]p(t - nT) \quad (3.158)$$

$$s_1(t) = \sum_{n=-\infty}^{\infty} b_1[n]p(t - nT) \quad (3.159)$$

$$r_0(t) = s_0(t) \star c_0(t) + \eta_0(t) \quad (3.160)$$

$$r_1(t) = s_1(t) \star c_1(t) + \eta_1(t), \quad (3.161)$$

where the operation  $\star$  here denotes the continuous time convolution. When the DLE method is used, the channel estimate is available at  $t_0$  where the optimum LE coefficients are computed. This equalizer is used during the entire interval as described in Section 3.2.3. Therefore, at  $t_1$ , the transmitted signal retrieved at the output of the receiver is estimated from the received signal  $r_1(t)$  using the equalizer

computed at  $t_0$ :

$$\hat{b}_1(t) = r_1(t) \star w_0(t) \quad (3.162)$$

$$= [s_1(t) \star c_1(t) + \eta_1(t)] \star w_0(t). \quad (3.163)$$

Substituting Equations 3.159 and 3.141 into Equation 3.163, the following expression for  $\hat{b}_1(t)$  can be obtained:

$$\begin{aligned} \hat{b}_1(t) &= \left[ \sum_{n=-\infty}^{\infty} b_1[n]p(t - nT) \star \left( c_0(t) + y_0\delta(t) + y_1\delta\left(t - \frac{T}{2}\right) \right) + \eta_1(t) \right] \star w_0(t) \\ &= \hat{b}_{1o} + \hat{b}_{1p}, \end{aligned} \quad (3.164)$$

where

$$\hat{b}_{1o}(t) = \sum_{n=-\infty}^{\infty} b_1[n]p(t - nT) \star c_0(t) \star w_0(t) + \eta_1(t) \star w_0(t), \quad (3.165)$$

and

$$\hat{b}_{1p}(t) = y_0 \sum_{n=-\infty}^{\infty} b_1[n]p(t - nT) \star w_0(t) + y_1 \sum_{n=-\infty}^{\infty} b_1[n]p(t - nT) \star w_0\left(t - \frac{T}{2}\right). \quad (3.166)$$

Equation 3.164 suggests that the output of the receiver at  $t_1$  consists of two components:  $\hat{b}_{1o}(t)$  and  $\hat{b}_{1p}(t)$ . As the channel  $c_1(t)$  can be decomposed into two components  $c_0(t)$  and  $c_p(t)$ , the output of the receiver at  $t_1$  can also be separated into two components, with  $\hat{b}_{1o}(t)$  corresponding to  $c_0(t)$  and  $\hat{b}_{1p}(t)$  to  $c_p(t)$ . These two components, as shown in the diagram in Figure 3.14, can be described as follows:  $\hat{b}_{1o}$  is the desired output of the system, estimated from the received signal that was

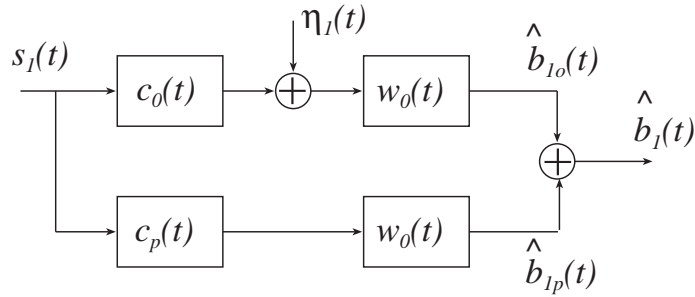


**Figure 3.14:** The two components in  $\hat{b}_1(t)$

transmitted through the channel  $c_0(t)$ , using the optimum receiver  $w_0(t)$ ;  $\hat{b}_{1p}$  is the excess component, resulting from the perturbations of the channel  $c_p(t)$ . The reason for separating these two components will become apparent when an expression for MSE at  $t_1$  is derived in the next section.

The term  $\hat{b}_{1p}(t)$  can be further simplified. Since  $p(t)$  is a sinc pulse,  $\hat{b}_{1p}(t)$  can be rewritten as

$$\hat{b}_{1p}(t) = y_0 \sum_{n=-\infty}^{\infty} b_1[n] w_{0,bl}(t - nT) + y_1 \sum_{n=-\infty}^{\infty} b_1[n] w_{0,bl} \left( t - nT - \frac{T}{2} \right), \quad (3.167)$$

where  $w_{0,bl}(t)$  is the band-limited receiver and it is defined as

$$w_{0,bl}(t) = p(t) \star w_0(t). \quad (3.168)$$

Finally, the estimated transmitted symbol at  $t_1$ ,  $\hat{b}_1[n]$ , can be obtained by sampling the output of the receiver at time  $t = nT$ ,

$$\begin{aligned} \hat{b}_1[n] &= \hat{b}_1(t) \Big|_{t=nT} \\ &= \hat{b}_{1o}[n] + \hat{b}_{1p}[n], \end{aligned} \quad (3.169)$$

where

$$\hat{b}_{1o}[n] = \sum_{m=-\infty}^{\infty} b_1[m]p(nT - mT) \star c_0(nT) \star w_0(nT) + \eta_1(nT) \star w_0(nT), \quad (3.170)$$

and

$$\hat{b}_{1p}[n] = y_0 \sum_{m=-\infty}^{\infty} b_1[m]w_{0,bl}(nT - mT) + y_1 \sum_{m=-\infty}^{\infty} b_1[m]w_{0,bl}\left(nT - mT - \frac{T}{2}\right). \quad (3.171)$$

Since the optimum receiver is a function of the channel at  $t_0$ ,  $\hat{b}_1[n]$  is a function of the channel at  $t_0$  and the channel perturbations.

#### 3.4.4.3 Average MSE at a Displaced Time

The MSE at a displaced time  $t_1$ ,  $\varepsilon_1$ , is defined as

$$\varepsilon_1 = E_B[|b_1[n] - \hat{b}_1[n]|^2]. \quad (3.172)$$

Substituting Equation 3.169 into the above equation, the following expression for  $\varepsilon_1$  is obtained:

$$\begin{aligned} \varepsilon_1 &= E_B[|b_1[n] - \hat{b}_{1o}[n] - \hat{b}_{1p}[n]|^2] \\ &= E_B[|b_1[n] - \hat{b}_{1o}[n]|^2] \\ &\quad - E_B[2\text{Re}\{(b_1[n] - \hat{b}_{1o}[n])\hat{b}_{1p}^*[n]\}] + E_B[|\hat{b}_{1p}[n]|^2]. \end{aligned} \quad (3.173)$$

The first term in Equation 3.173 effectively results in the MMSE of an infinite LE on a time-invariant channel. The symbol  $b_1[n]$  is transmitted through the overall

channel  $h_0(t)$ , and the receiver output  $\hat{b}_{1o}[n]$  is estimated by using the LE  $w_0(t)$ , which is optimum if the channel is  $h_0(t)$ . As in  $c_1(t)$  and  $\hat{b}_1[n]$ , the MSE at  $t_1$  also consists of two parts: the minimum MSE for time-invariant channel and an excess MSE. This justifies the need for separating  $\hat{b}_1[n]$  into two components in the previous section.

As in  $\hat{b}_1[n]$ ,  $\varepsilon_1$  is also a function of  $c_0(t)$ ,  $y_0$  and  $y_1$ . Since the samples of  $c_0(t)$ ,  $y_0$  and  $y_1$  are random variables, the average value for  $\varepsilon_1$  can be obtained by taking the expectations of  $\varepsilon_1$  with respect to these random variables. Due to the linearity and uniform convergence of the expectation operation, the order in which the expectations are taken is interchangeable.

For the first term in Equation 3.173, the expectation with respect to the channel at  $t_0$  is taken first. The result of taking the expectation is the average MSE for fading channel,  $\bar{\varepsilon}_{V,\min}$ , which is given in Equation 3.134. Since  $\bar{\varepsilon}_{V,\min}$  is a constant, its expected value over the channel perturbations remains constant:

$$\begin{aligned} E_Y[E_H[E_B[|b_1[n] - \hat{b}_{1o}[n]|^2]]] &= E_Y[E_H[\varepsilon_{I,\min}]] \\ &= E_Y[\bar{\varepsilon}_{V,\min}] \\ &= \bar{\varepsilon}_{V,\min}, \end{aligned} \tag{3.174}$$

which is also equal to  $\bar{\varepsilon}_0$ , the average MSE at  $t_0$ .

Taking the expectation of the second term in Equation 3.173 over the channel perturbations  $y_0$  and  $y_1$  and interchanging the order of linear operations, one can

write

$$E_Y[E_B[2Re\{(b_1[n] - \hat{b}_{1o}[n])\hat{b}_{1p}^*[n]\}]] = E_B[2Re\{E_Y[(b_1[n] - \hat{b}_{1o}[n])\hat{b}_{1p}^*[n]]\}]. \quad (3.175)$$

The result of evaluating the expectation over the channel perturbation in the above equation is zero, since the perturbations have zero mean.

Evaluating the expectation of the third term in Equation 3.173 over the transmitted symbol, it can be expressed as follows:

$$E_B \left[ \left| \hat{b}_{1p} \right|^2 \right] = \sigma_b^2 \sum_{m=-\infty}^{\infty} \left| y_0 w_{0,bl}(nT - mT) + y_1 w_{0,bl} \left( nT - mT - \frac{T}{2} \right) \right|^2. \quad (3.176)$$

Taking the expectation of the above equation with respect to the channel perturbations, the equations below can be obtained:

$$E_Y \left[ E_B \left[ \left| \hat{b}_{1p} \right|^2 \right] \right] = \sigma_b^2 \sigma_y^2 \sum_{m=-\infty}^{\infty} |w_{0,bl}(mT)|^2 + \left| w_{0,bl} \left( mT - \frac{T}{2} \right) \right|^2 \quad (3.177)$$

$$= 2\sigma_b^2 \sigma_y^2 \sum_{m=-\infty}^{\infty} |w_{0,bl}(mT)|^2 \quad (3.178)$$

The summation term in Equation 3.178 is the energy in the band limited optimum LE at  $t_0$  and can be expressed in the frequency domain by deploying Parseval's

theorem:

$$\begin{aligned} \sum_{m=-\infty}^{\infty} |w_{0,bl}(mT)|^2 &= T \int_{-\frac{1}{2T}}^{\frac{1}{2T}} |W_{0,bl,\frac{1}{T}}(f)|^2 df \\ &= \int_{-\frac{1}{2T}}^{\frac{1}{2T}} \left| \sum_{k=-\infty}^{\infty} W_{0,bl}\left(f + \frac{k}{T}\right) \right|^2 df \\ &= \int_{-\frac{1}{2T}}^{\frac{1}{2T}} |W_0(f)|^2 df \end{aligned} \quad (3.179)$$

$$(3.180)$$

where the subscript “ $\frac{1}{T}$ ” denotes discrete-time continuous-frequency Fourier transform. Therefore, the expected value of the third term in Equation 3.173, with respect to the channel perturbation is

$$E_Y \left[ E_B \left[ \left| \hat{b}_{1p} \right|^2 \right] \right] = 2\sigma_b^2 \sigma_y^2 \int_{-\frac{1}{2T}}^{\frac{1}{2T}} |W_0(f)|^2 df. \quad (3.181)$$

Taking the expectation of both sides in Equation 3.181 over the channel at  $t_0$ , and evaluating the integral on the right hand side, one can write

$$E_H \left[ E_Y \left[ E_B \left[ \left| \hat{b}_{1p} \right|^2 \right] \right] \right] = 2A\sigma_b^2 \sigma_y^2, \quad (3.182)$$

where A is defined as

$$A = \frac{1}{\lambda_1} \left[ e^{\frac{N_o}{\lambda_1}} \text{Ei} \left( \frac{N_o}{\lambda_1} \right) \left( 1 + \frac{N_o}{\lambda_1} \right) - 1 \right], \quad (3.183)$$

and could be written in terms of  $\gamma_{\text{in}}$ , the input SNR:

$$A = \frac{1}{\lambda_1} \left[ e^{\frac{1}{\gamma_{\text{in}}}} \text{Ei} \left( \frac{1}{\gamma_{\text{in}}} \right) \left( 1 + \frac{1}{\gamma_{\text{in}}} \right) - 1 \right]. \quad (3.184)$$

The expression for the average MSE at  $t_1$  is given by the following equation:

$$\begin{aligned}
\bar{\varepsilon}_1 &= E_H [E_Y [\varepsilon_1]] \\
&= \bar{\varepsilon}_0 + 2A\sigma_b^2\sigma_y^2 \\
&= \bar{\varepsilon}_{V,\min} + 4AP_r N_{Go}\sigma_b^2(1 - J_0(2\pi f_m \Delta t)) \\
&= \bar{\varepsilon}_{V,\min} + \Delta\varepsilon(\gamma_{\text{in}}, f_m, \Delta t),
\end{aligned} \tag{3.185}$$

where  $\Delta\varepsilon(\gamma_{\text{in}}, f_m, \Delta t)$  is the excess MSE, defined as

$$\Delta\varepsilon(\gamma_{\text{in}}, f_m, \Delta t) = 4AP_r N_{Go}\sigma_b^2(1 - J_0(2\pi f_m \Delta t)). \tag{3.186}$$

Observe that the average MSE at  $t_1$  consists of two terms: the average MMSE and the excess MSE. The expression in Equation 3.185 is in fact the general average MSE expression for any arbitrary time  $t_k$ . At time  $t_k$ , if the time-varying channel is available, and is used to derive an optimum LE receiver, the average MSE can achieve its minimum at  $\bar{\varepsilon}_{V,\min}$ , which is constant. However, if no channel information is available at this time and the optimum LE derived at  $t_0$  is used, the excess MSE is added to the average MSE to adjust change in the time-varying channel from  $t_0$  to  $t_k$ . The excess MSE depends on the amount of change in the channel, and is a function of the rate of change in the channel and the time interval in which this change takes place. Therefore, it is a function of  $f_m$  and  $\Delta t$ .

For  $\Delta t \geq 0$ , Equation 3.185 gives an expression for the average MSE when a fixed LE is used in a receiver. The fact that  $\bar{\varepsilon}_1$  is an even function of  $\Delta t$  suggests that the MSE curve is symmetrical with respect to the axis  $\Delta t = 0$ , and the MSE value approaches minimum as  $\Delta t$  approaches 0 from both positive and negative sides. This mathematically verifies the possibility of the use of a displaced LE and

---

its performance advantage over a fixed LE.

# Chapter 4

## Application to IS-136 800 MHz Operation

### 4.1 Background

The commercial development of cellular systems has evolved remarkably since the World Allocation Radio Conference approved frequency allocations for cellular telephone in the 800-900 MHz band [1]. In the late 70's and early 80's, the first generation cellular systems were established in different countries, based on FDMA and analog FM technology. Total Access Communication System (TACS) in Europe and Nippon Telephone (NTT) in Japan are some typical examples of the first generation analog cellular systems. In North America, the Advanced Mobile Phone Service, also known as AMPS or IS-21, was developed and is widely used.

As cellular phones became more popular, the analog systems cannot support the increasing demand for capacity in large cities. The second generation digital cellular systems, such as the United States Digital Cellular system (USDC) and

Global System for Mobile Communications (GSM) in Europe, emerge to improve both the capacity and the system performance. The USDC system using TDMA method is standardized as Interim Standard 136 (IS-136) [80].

The IS-136 system was designed to share the same channel frequencies, frequency reuse plan and base stations as AMPS. Frequency reuse gives rise to co-channel interference (CCI) which cannot be overcome by raising the power of the transmitted signal since it would increase the level of CCI for the co-channel cells and adjacent channel interference (ACI) for the neighboring cells. Additionally, transmission in most cellular radio applications is accomplished in a time-varying multipath environment. This causes frequency selective fading in the transmitted signal.

Emerged in the early 90's, IS-136 TDMA system was designed mainly for voice traffic and a data rate of 48.6 kb/s was sufficient. At the end of the 90's, wireless network operators face explosion of data traffic due to the general use of wireless Internet, strong demand from users for new mobile multimedia services, and increasing demand from users for general mobility [81]. It is predicted that, by the end of 2002, packet-based multimedia services, including IP telephony, will account for over 50 percent of all wireless traffic [82]. There is a need in the wireless industry to evolve the current infrastructure and network services to meet the demand for high speed data services. As an interim solution for the evolution from the second to the third generation wireless network, TDMA operators are planning for Enhanced Data Rate for Global Evolution (EDGE) to deliver 384 kb/s with full mobility [82]. Although IS-136 TDMA standard is not adopted by the TDMA operators, it is a good example to demonstrate the effectiveness of the methods and algorithms developed in this thesis. Furthermore, the methods and algorithms developed in this thesis are general and they can be used in other practical applications and standards

such as GSM. Therefore, IS-136 TDMA system is used in this thesis as an example.

In this chapter, some of the equalization and interpolation techniques discussed in Chapter 3 will be deployed to achieve a 5% BER performance in the IS-136 mobile to base station transmission for the 800 MHz operation, in the presence of CCI. To achieve this goal, the BER of a Displaced DFE (DDFE) is tested. For comparison, the DFE bound for such a system is obtained through simulation. The performance of conventional adaptive DFE and calculated DFE using Wiener-Hopf equations is also presented for this purpose.

## 4.2 System Descriptions

### 4.2.1 Transmitter

The transmitter in IS-136 consists of a  $\pi/4$  DQPSK encoder, an up sampler and a transmit filter. Specified in IS-136 standard, the input bits to the transmitter are first converted to a sequence of  $\pi/4$  DQPSK symbols. Then the sequence is sent to an up sampler to double the sampling frequency. These  $T/2$ -spaced symbols are further pulse shaped by a square root raised cosine pulse with a roll off factor of 35%, and finally, transmitted through a time varying Rayleigh fading channel.

#### 4.2.1.1 Encoder

The  $\pi/4$  DQPSK encoder maps a pair of input bits into one of the four possible differential phases. The relationship of the input bits and the differential phase is outlined in Table 4.1 [83].

Depending on the differential phase and the previous  $\pi/4$  DQPSK symbol, the

Input Bits	Differential Phase ( $\Delta\theta_k$ )
00	$\pi/4$
01	$3\pi/4$
11	$-3\pi/4$
10	$-\pi/4$

**Table 4.1:** Mapping of the  $\pi/4$  DQPSK symbol

current  $k$ th transmitted symbol can be generated using Equation 4.1,

$$\begin{bmatrix} I_k \\ Q_k \end{bmatrix} = \begin{bmatrix} \cos(\Delta\theta_k) & -\sin(\Delta\theta_k) \\ \sin(\Delta\theta_k) & \cos(\Delta\theta_k) \end{bmatrix} \begin{bmatrix} I_{k-1} \\ Q_{k-1} \end{bmatrix} \quad (4.1)$$

where  $(I_k, Q_k)$  and  $(I_{k-1}, Q_{k-1})$  are the in-phase and quadrature components of the  $k$ th and  $(k-1)$ th  $\pi/4$  DQPSK symbols, respectively. It can also be interpreted that the  $k$ th symbol is generated by rotating the previous symbol by an angle of  $\Delta\theta_k$ .

#### 4.2.1.2 Up Sampler

The up sampler in the transmitter is used to double the symbol rate, since the a square root raised cosine pulse with 35% roll-off is used in the transmit filter. It places one zero between two consecutive  $\pi/4$  DQPSK symbols and its output  $x_k$  is given by the following equation [84]:

$$x_k = \begin{cases} b\left(\frac{k}{2}\right), & k = 0, 2, 4, \dots, \\ 0, & \text{otherwise} \end{cases} \quad (4.2)$$

#### 4.2.1.3 Transmit Filter and Receive Filter

The purpose of the transmit filter, also known as the pulse shaping filter, is to

band-limit the input signal and perform a digital-to-analog conversion, so that the input signal can fit in the analog band limited channel.

One basic requirement of the transmit filter is to have zero ISI at the pulse sampling time. The transmit filter used here is a square root raised cosine pulse, which exhibits this important property.

In order to reduce the noise power outside of signal bandwidth, an identical square root raised cosine pulse is used as the receive filter at the receiver front end. Since the combination of the transmit and the receive filters gives a raised cosine pulse, for simulation purpose, these two filters are combined and only one single raised cosine filter is used in place of the transmit filter.

The time domain and frequency domain representations of the raised cosine pulse are given in Equations 4.3 and 4.4 [60]:

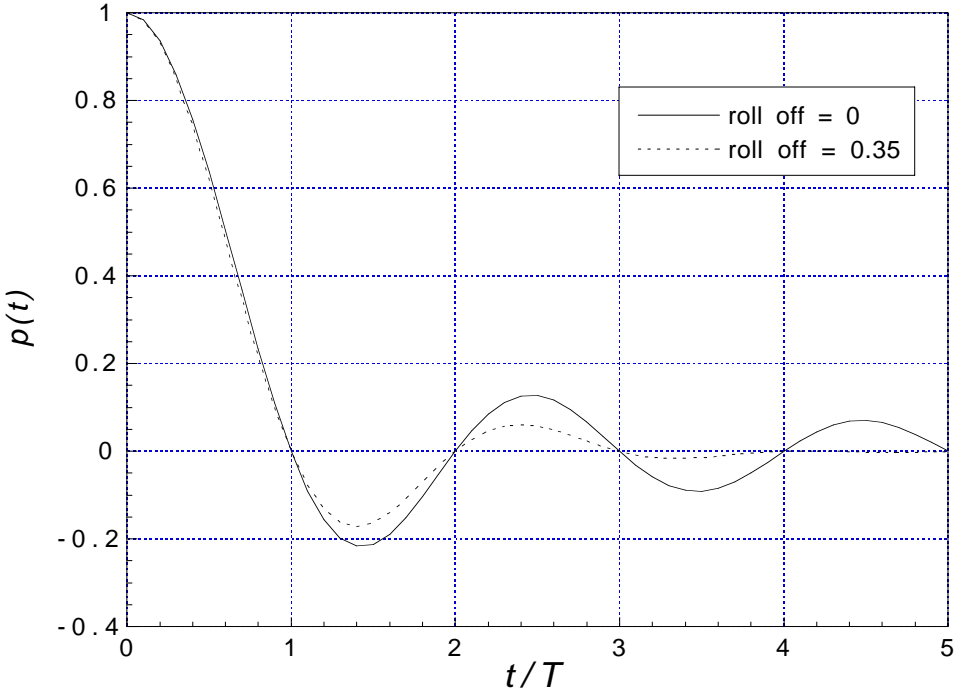
$$p(t) = \text{sinc}\left(\frac{t}{T}\right) \frac{\cos\left(\frac{\pi\beta t}{T}\right)}{1 - \frac{4\beta^2 t^2}{T^2}} \quad (4.3)$$

$$P(f) = \begin{cases} T, & 0 \leq |f| \leq \frac{1-\beta}{2T} \\ \frac{T}{2} \left[1 + \cos\left(\frac{T\pi}{\beta} \left(|f| - \frac{1-\beta}{2T}\right)\right)\right], & \frac{1-\beta}{2T} \leq |f| \leq \frac{1+\beta}{2T} \\ 0, & |f| > \frac{1+\beta}{2T} \end{cases} \quad (4.4)$$

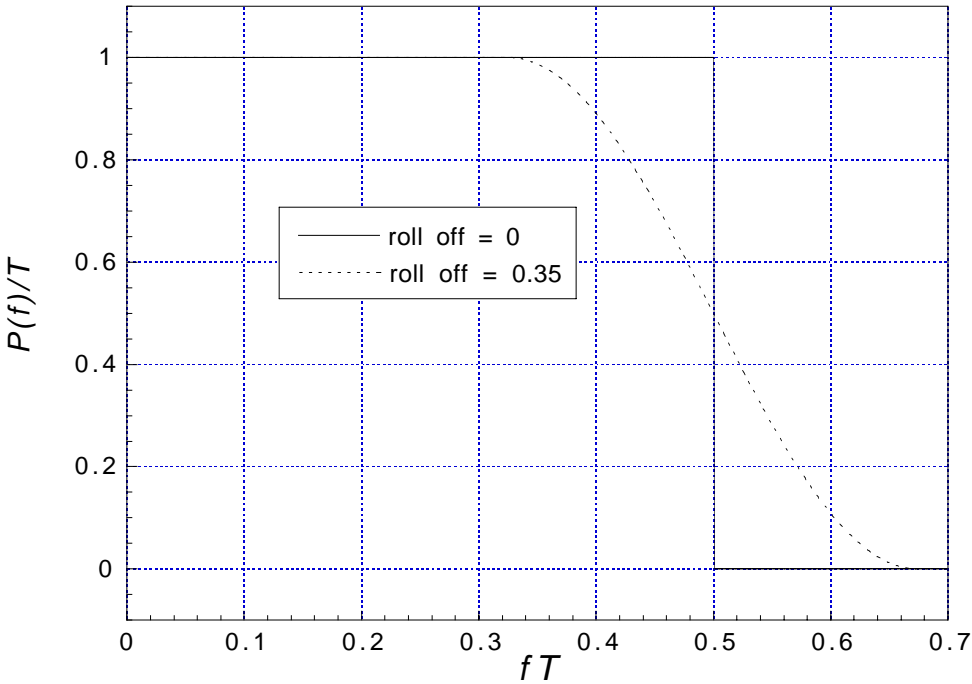
where  $\beta$  is the roll off factor,  $0 \leq \beta \leq 1$ , and  $T$  is the symbol duration.

Figure 4.1 shows the time domain and frequency domain characteristics of the raised cosine pulses with roll off factors of 0 and 35%. One can observe that the pulse decays more rapidly with a higher roll off factor.

As shown in Figure 4.1, the highest frequency component in the frequency response of the pulse shaping filter is  $1.35/(2T)$ . According to the Nyquist sampling



(a) Time domain



(b) Frequency domain

Figure 4.1: Raised cosine pulses

criterion, the condition for anti-aliasing is

$$f_s \geq \frac{1.35}{T}, \quad (4.5)$$

where  $f_s$  is the sampling frequency.

Here, a sampling frequency of  $\frac{2}{T}$  is used. The reason for this is three fold. Firstly, raising the sampling frequency twice, instead of 1.35 times, simplifies the computation. Secondly, as shown in the next section, the resolution of the channel model IS-136 is  $T/2$ , and the input to the channel should also be  $T/2$ -spaced, in order to maintain the resolution. Finally, a fractionally spaced equalizer can also be used in the receiver to achieve better BER performance, as mentioned in Section 1.2.

In digital signal processing, the transmit filter is usually implemented as an FIR filter, which means sampling and truncation are involved. In order to achieve a close approximation, the number of taps in the FIR filter should be sufficiently large, so that it contains at least 98% of energy of the continuous time raised cosine pulse.

The energy of a continuous time signal and a discrete time signal are given by

$$E = \int_{-\infty}^{\infty} |p(t)|^2 dt = \int_{-\infty}^{\infty} |P(f)|^2 df \quad (4.6)$$

and

$$E = T \sum_{n=0}^{N-1} |p[n]|^2, \quad (4.7)$$

respectively.  $N$  is the length of the FIR filter. For  $\beta = 0.35$ , the energy of the raised cosine pulse is  $7.3T/8$ .  $N$  should be chosen such that the energy of the FIR filter is at least 98% of the continuous time pulse.

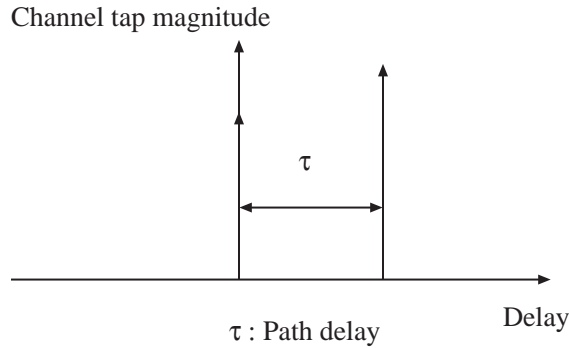


**Figure 4.2:** 2-ray channel model

Truncation in the time domain involved in the approximation process results in side lobes with infinite duration in the frequency spectrum. The two adjacent samples should be sufficiently far apart, so that the sum of the side lobes is not as significant. This is another benefit of using a sampling frequency of  $2/T$ , instead of  $1.35/T$ .

### 4.2.2 Channel

In wireless communications, a signal usually propagates in a multipath environment, due to reflections of the signal from buildings, mountains and other obstacles. A multipath channel model has been developed in 2.2. Here, a 2-ray channel model is adopted. This model consists of two significant multipath components, one arriving after another with a path delay interval of  $T/2$ . Figure 4.2 shows a 2-ray channel at a time instant.

The two components, with equal average power, are varying independently, with Rayleigh distributions. The 2-ray channel can be represented by Equation 4.8:

$$c[n] = c_0[n]\delta[n] + c_1[n]\delta\left[n - \frac{1}{2}\right] \quad (4.8)$$

where

$$c_0[n] = |c_0[n]| e^{j \arg(c_0[n])} \quad (4.9)$$

$$c_1[n] = |c_1[n]| e^{j \arg(c_1[n])} \quad (4.10)$$

and

$$E\{|c_0[n]|^2\} = E\{|c_1[n]|^2\}. \quad (4.11)$$

Figure 4.3 shows variation of the magnitude of one channel tap, for both 100 km/hr and 8 km/hr. In the case of 800 MHz operation, the Doppler frequency for 100 km/hr is 77.5 Hz. At a mobile speed of 100 km/hr, with a symbol rate of 24.3 kHz and 162 symbols per time slot, the transmitted signal experiences 3 deep fades in 6 time slots. On average, there will be one deep fade in every two time slots.

### 4.2.3 Receiver

There are two receive antennas, followed by the equalizer and the decoder. Here the decoder is integrated into the equalizer and a block diagram of the arrangement is shown in Figure 4.4.

#### 4.2.3.1 Equalizer

In a digital communication system, the system performance is mainly degraded by fading, ISI, CCI and noise. Both fading and ISI occur when the signal propagates in the multipath environment in which there are propagation delay and attenuation associated with each path. CCI originates from the frequency reuse plan of the

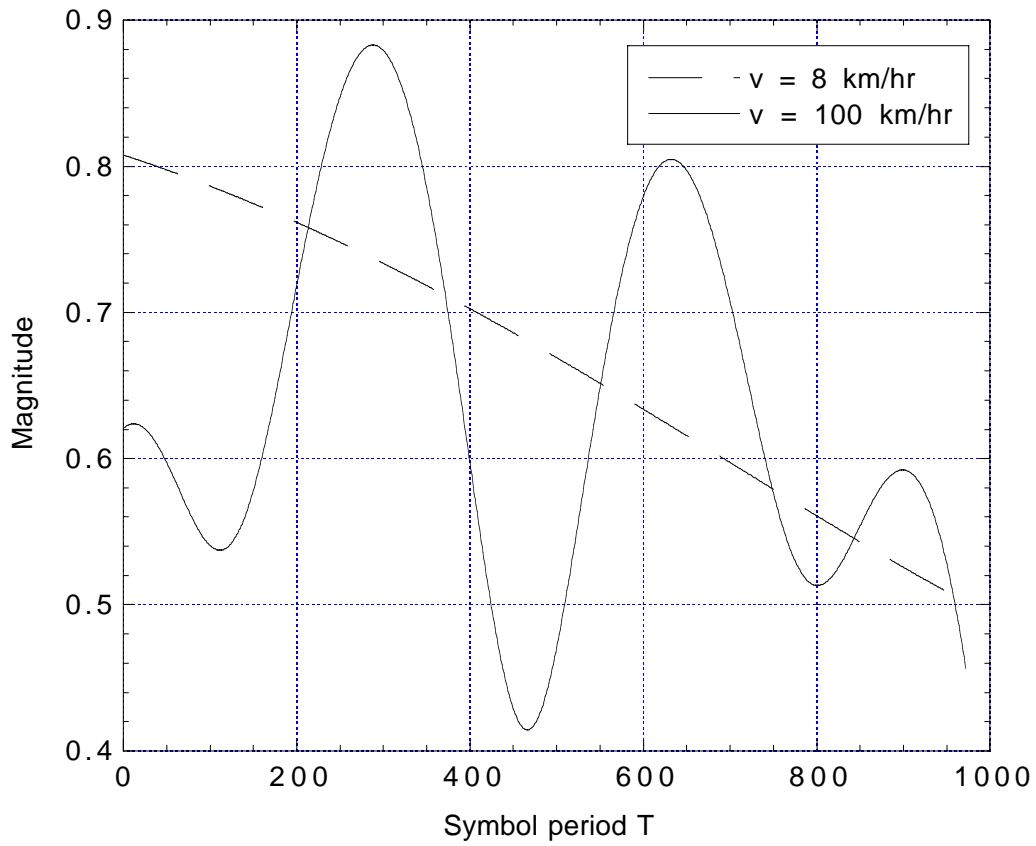


Figure 4.3: Variation of one channel tap

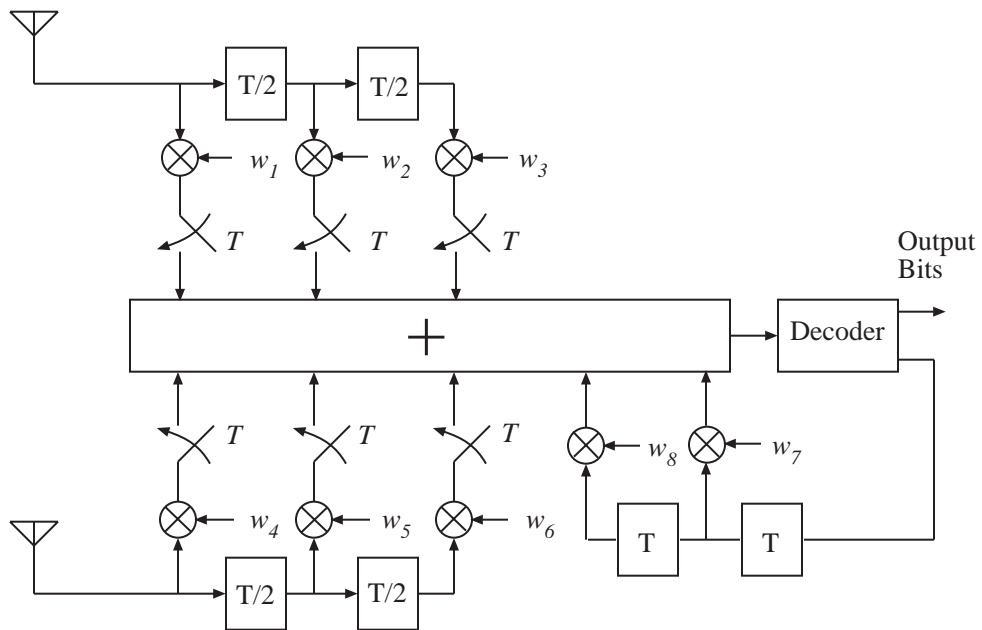


Figure 4.4:  $T/2$ -spaced DFE and decoder

$Re[e^{j\Delta\theta_k}]$	$Im[e^{j\Delta\theta_k}]$	Estimated bits
$\geq 0$	$\geq 0$	00
$\geq 0$	$< 0$	10
$< 0$	$\geq 0$	01
$< 0$	$< 0$	11

**Table 4.2:**  $\pi/4$  DQPSK decision rules

TDMA system. It comes from cells sharing the same frequency channel. Noise is the most common problem in any given kind of communication system. It includes the noise from surrounding environment, noise from the non-linear devices and thermal noise from the components of the communication system.

Equalization, in this case, has several tasks: to compensate the fading channel, to cancel the interferences and to serve as a matched filter to reduce the effect of the noise in the system. For the IS-136 800 MHz operation, a T/2-spaced DFE is used in order to provide remedies for all the above problems.

#### 4.2.3.2 Decoder

The task of a decoder is to apply a specific decision rule, depending on the application, to the input symbols to estimate the original input data sequence to the transmitter.

In this case, the decoder first determines the  $k$ th differential phase  $\Delta\tilde{\theta}_k$  by subtracting the phase of the  $(k-1)$ th symbol from the  $k$ th symbol. Then it follows the decision rules outlined in Table 4.2 to estimate the input bits to the transmitter.

The decoder is integrated into the DFE. Since the system performance will improve by feeding the clean symbols, as opposed to the noisy symbols, back to the DFE, this task is also accomplished by the decoder. It retrieves the clean differential phases from the output bits, following the conversion rules tabulated in Table 4.1,

and reconstructs the current symbol by adding the differential phase to the previous symbol phase.

## 4.3 Performance of Receivers

In this section, BER performance of different DFE schemes is presented. The DFE used in the receiver has five  $T/2$ -spaced taps in the two feed forward filters, and three  $T$ -spaced taps in the feedback filter (5-5-3 DFE). The choice of the number of taps in the DFE is the result of considering the trade-off between complexity and performance. First, a receiver with a known channel impulse response is tested in such system. This is the ideal case, and it sets the lower BER bound of the system performance for DFE receivers. Then the performance of an adaptive DFE, calculated DFE using Wiener-Hopf equations and displaced DFE (DDFE) are evaluated and compared against the lower bound.

### 4.3.1 DFE Bounds

Here, the receiver is assumed to have perfect knowledge of the time-varying channel for each symbol in the time slot. The channel impulse response is used to estimate the auto correlation matrix and cross correlation vector of the DFE. The tap coefficients of the DFE are determined by using the Wiener-Hopf equations, such that the MSE at the DFE output is minimized.

In practice, information of the time-varying channel is unknown to the receiver, and hence has to be estimated. The performance of such an ideal receiver only serves as a lower bound for the other DFE receivers. As the channel estimation algorithm improves in terms of accuracy, the system performance will become closer to this

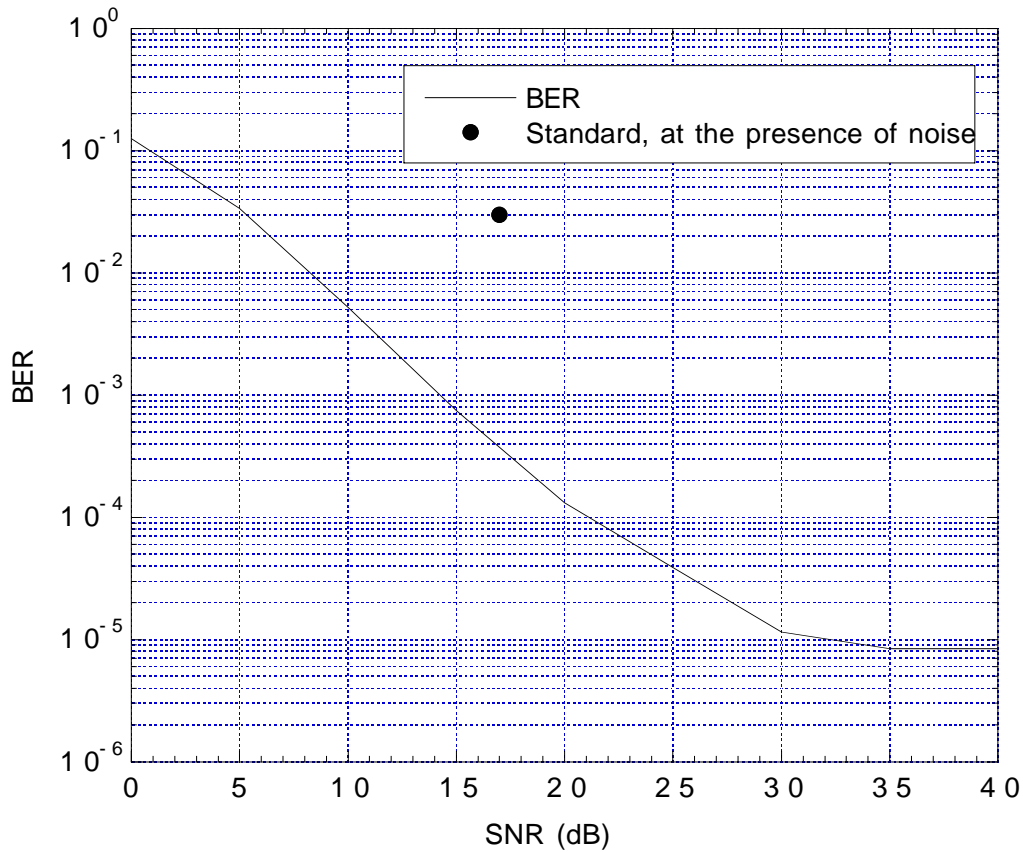
lower bound.

Figure 4.5 and Figure 4.6 illustrate the BER bounds for channels with path delay  $T/2$  between the first ray and the second. The  $\bullet$  in the BER figures denotes the performance requirement specified by the IS-136 standard: 3% BER at an SNR of 17 dB and 5% BER at a CIR of 17 dB. If the  $\bullet$  is above the BER curve of a particular receiver, its BER performance satisfies the standard. Figure 4.5 shows the BER lower bound at various values of SNR. In order to investigate the performance of the DFE on a system subjected to additive white Gaussian noise (AWGN) only, the power of the interfering signal is set to zero. At a vehicle speed of 100 km/hr, the lower bound satisfies the 3% BER requirement, specified in the IS-136 standard for a system under noise conditions, with a gain of 11 dB in SNR. Figure 4.6 shows the BER lower bound for the DFE at various CCI levels. This figure is obtained at a vehicle speed of 100 km/hr and an SNR of 30 dB. The DFE can achieve a 5% BER with a gain of 11 dB in CIR. These figures show that the DFE can give good performance provided that the receiver can estimate and track the time-varying channel accurately.

The performance of the DFE for a channel with various path delays is also studied. A plot of BER versus path delay is given in Figure 4.7. This plot is obtained at an SNR of 30 dB, CIR of 17 dB and vehicle speed of 100 km/hr.

As shown in this figure, the BER reaches minimum at a path delay of  $T/2$ . As the path delay increases, the ISI introduced by the channel is more severe. Therefore, the BER goes up at relative path delay of  $3T/4$  and  $T$ . Note also, that the BER is approximately 0.31% at a path delay of  $T$ . This implies that, with a good channel estimation algorithm, 5% BER is achievable at path delay of  $T$ .

When the relative path delay is zero, the transmitted signal is subjected to flat



**Figure 4.5:** BER lower bound for DFE (800 MHz operation,  $CIR = \infty$ )

fading. It is well known that the optimum receiver for flat fading channel is an optimum diversity combiner [25], and the use of equalization in such a system will degrade the performance. This accounts for the poor performance of the receiver under a flat fading channel. When the path delay increases to  $T/4$ , the performance improves, compared to the flat fading case.

### 4.3.2 Adaptive DFE

In most cases in wireless mobile communication, the time-varying channel is unknown to the receiver. In order to recover the transmitted data at the receive end, an adaptive equalizer, which follows certain adaptation rules, is often deployed

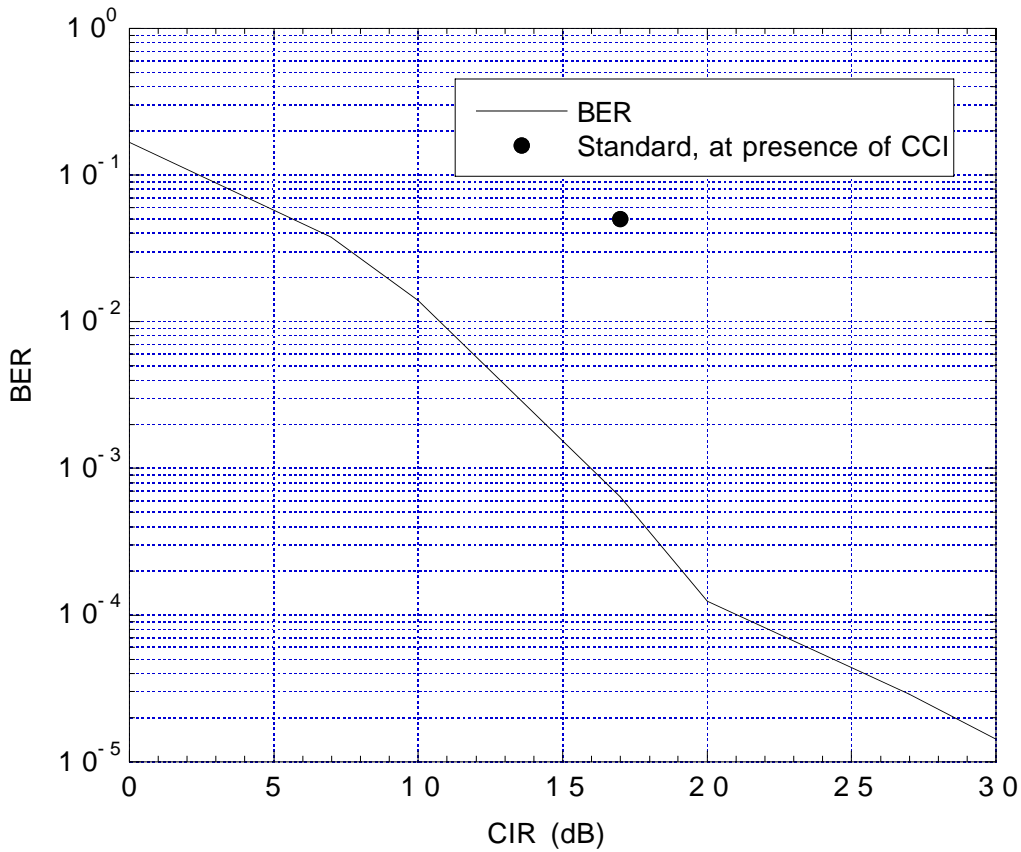


**Figure 4.6:** BER lower bound for DFE (800 MHz operation, SNR = 30 dB)

to adapt to the channel.

For an IS-136 system, there are only 14 training symbols in each time slot. It requires an adaptive algorithm whose convergence can be achieved at the end of the training symbols. The RLS algorithm is chosen for its fast convergence property.

#### 4.3.2.1 RLS-DFE with no Tracking

Here, 14 training symbols in each time slot are used to facilitate the training of the coefficients of the RLS-DFE. Once training is accomplished, the DFE coefficients are fixed until the end of the time slot. There is no tracking or updating of the coefficients in the rest of the time slot. Therefore, this is a fixed DFE.

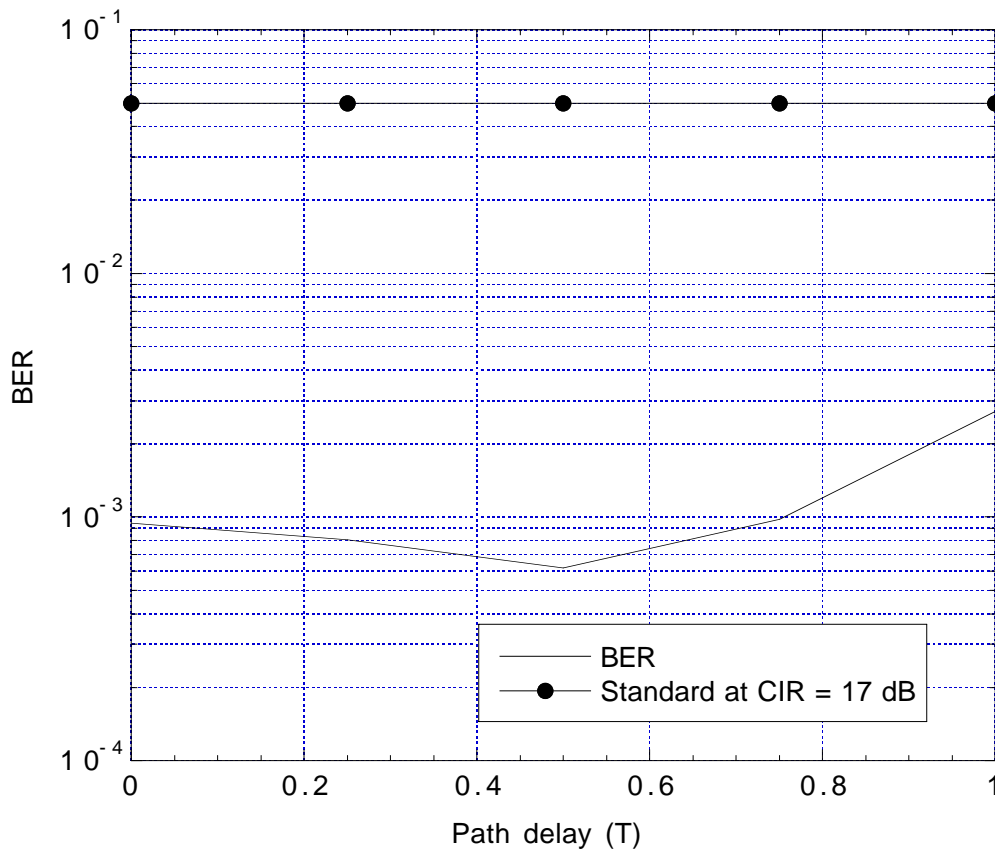


**Figure 4.7:** BER lower bound for DFE at various path delay (800 MHz operation)

Figure 4.8 shows the BER performance of this receiver, at 30 dB SNR for various mobile speeds. At lower mobile speeds, the BER at 17 dB CIR or higher is well below 5% since the time-varying channel changes relatively slowly at these mobile speeds. However, at higher mobile speeds, this receiver scheme is not feasible. Since the channel changes rapidly during the time slot, the DFE with fixed coefficients cannot anticipate these changes. As a result, the transmitted data cannot be retrieved and the BER performance is poor for high mobile speeds.

It is also worth noting the shape of the BER curves for higher mobile speed. In the high CIR region, the curves become flat, which is different from the classic water-fall-shaped BER curves for the AWGN channels. These irreducible BER

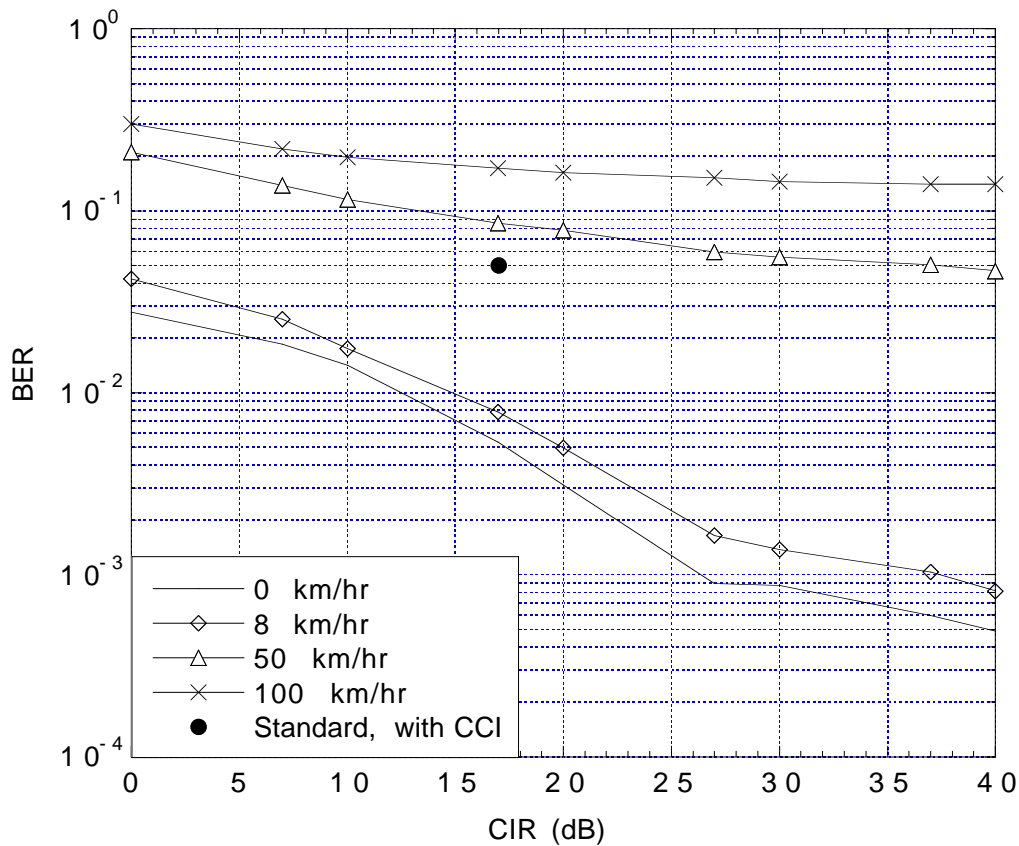


**Figure 4.8:** BER performance of RLS-DFE without tracking

curves demonstrate the presence of error propagation in the receiver resulting from the severe ISI, high Doppler frequency and CCI.

#### 4.3.2.2 RLS-DFE with Tracking

In the case of high mobile speeds, the time-varying channel is changing so fast, that the DFE trained to give good performance at the beginning of the time slot might not be feasible in the middle or at the end of the time slot. Here, a DFE with the ability to update its coefficients, in response to the change in the channel is required in the receiver to maintain the performance.

One typical way to deal with the fast time-varying channel is to incorporate a

tracking ability in the DFE. Both LMS and RLS are the typical adaptive algorithms for updating the DFE coefficients, and their tracking performance is comparable in general [39]. LMS is known for its simplicity; whereas RLS algorithm can provide better and faster tracking of the time-varying channel with spectral nulls [12] [85]. Therefore, RLS algorithm is also used for tracking in the receiver despite its complexity in implementation.

The tracking algorithm used here can be summarized as followed:

Step1: Divide the data sequence into  $M$  blocks.

Step2: Compute  $\underline{w}$  from the training sequence.

Step3: Set  $\underline{w}_t = \underline{w}$

Step4: for  $i = 1$  to  $M$

apply  $\underline{w}$  to block  $i$

update  $\underline{w}_t$

$\underline{w} = \underline{w}_t$

end

Figures 4.9 and 4.10 show the BER curves for the RLS-DFE with tracking capability, with 14 and 7 symbols in each block, respectively. These figures demonstrate improvement in the BER performance, compared to the one with no tracking. However, the error propagation problem still remains, as the BER curve is still relatively flat in the high CIR region. This is inherent with the algorithm. When the above algorithm is applied to the system, the decoded symbols from the previous block are assumed correct and used to facilitate the training of the DFE for the current block. For low vehicle speeds, such as 0 km/hr, 8 km/hr and 50 km/hr, this assumption is valid. In these cases, the performance is good and it meets the requirement specified

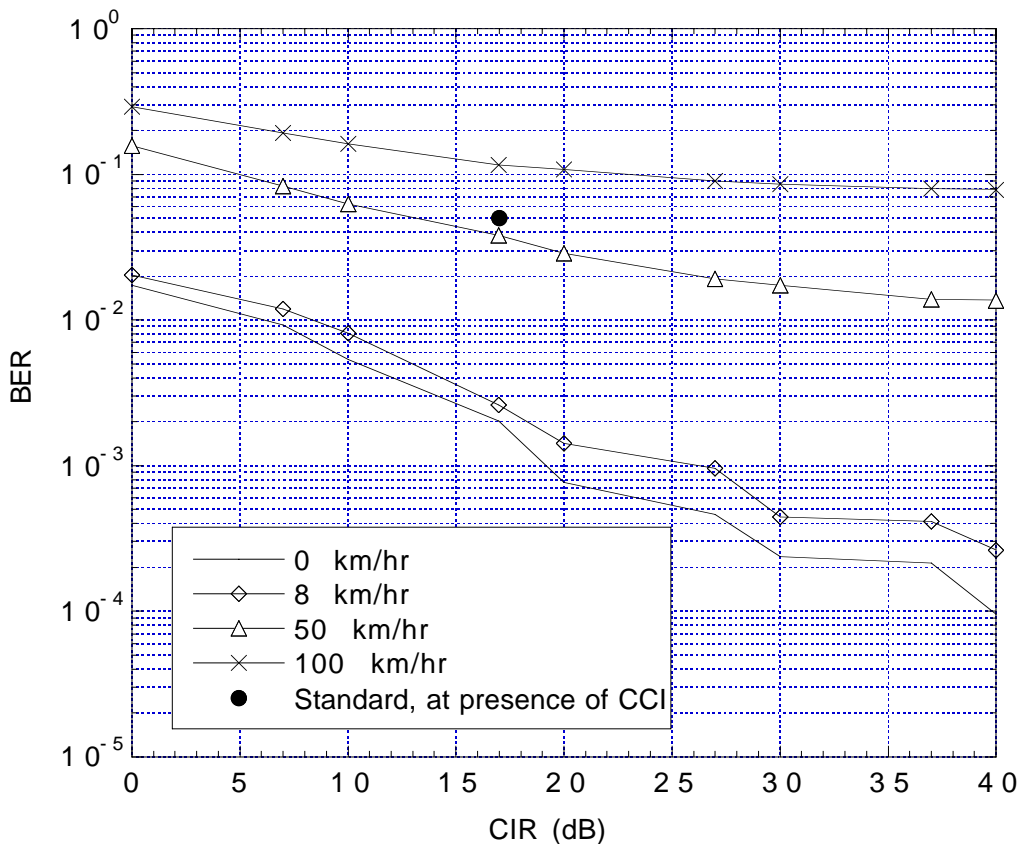


**Figure 4.9:** BER performance of RLS-DFE, 14 symbols per block

in the standard. At high vehicle speeds, such as 100 km/hr, however, due to the fast fading environment, CCI and ISI, this assumption might not be valid. Even though there is improvement, the error generated in the current block will affect the performance of the DFE in the blocks that followed, until the end of the time slot. Therefore, more and more errors are accumulated towards the end of the time slot.

The purpose of tracking is to update the DFE coefficients fast enough so that the DFE can adapt to the fast fading channel. The performance of the receiver also relies on how often the update takes place, compared to the rate of change in the channel. Therefore, the number of symbols in each block plays an important role. If this number is too large, the system is not capable of tracking the fast

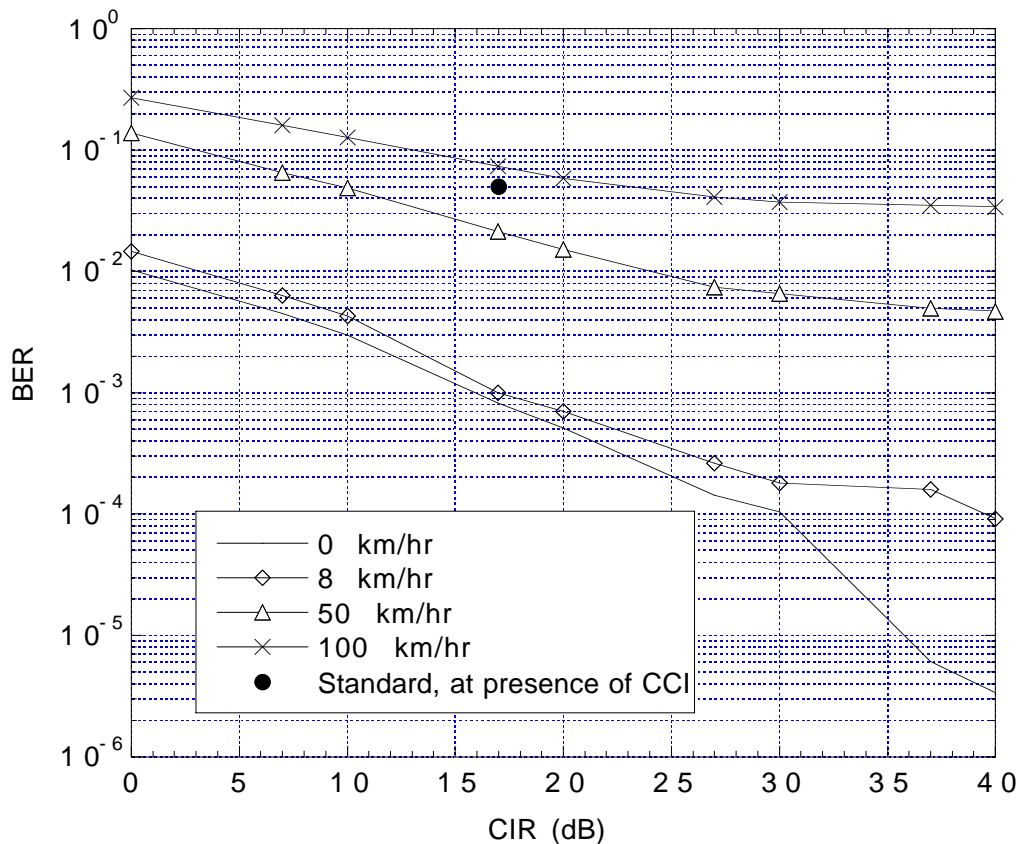


**Figure 4.10:** BER performance of RLS-DFE, 7 symbols per block

fading channel. On the other hand, if the system tracks symbol by symbol, the algorithm might be unstable due to errors and the numerical property of the data sequence. The curves in Figure 4.9 show some improvement over the no tracking case. However, the number of symbols in a block might still be too large. When the number of symbols is reduced to 7, further improvement in BER can be achieved, as shown in Figure 4.10.

As expected, the DFEs with tracking demonstrate better performance, compared to the one with no tracking. However, it cannot satisfy the performance criterion specified in IS-136: 5% BER at 17 dB CIR for higher vehicle speeds.

### 4.3.3 Calculated DFE Using Wiener-Hopf Equations

In this section, a calculated DFE using the Wiener-Hopf equations, based on channel estimation, is tested. In this receiver scheme, the receiver has two stages: the channel estimation stage and the equalization stage.

The motivation for this receiver scheme is the accuracy in the estimation process. Given a training sequence with fixed length, the estimation error is smaller if the number of parameters to be estimated is reduced. With 14 training symbols, or 28 training bits it is more accurate to estimate two parameters in the time-varying channel than the large number of tap coefficients in the DFE. Furthermore, since the number of parameters to be estimated is much less, it is much simpler to estimate the channel than to estimate the taps of the equalizer [39]. For the same reason, channel estimation can also be accomplished with the 12 Coded Digital Verification Color Code (CDVCC) bits, which are in the middle of the time slot and known to the receiver. Therefore, this method should give better BER performance. Since tracking causes error propagation, it is not considered in this case.

#### 4.3.3.1 MSE of Channel Estimation

From the known bits in the time slot, the LSSE algorithm discussed in Section 3.1 is used here to estimate the channel impulse response. It is assumed that the channel is static during the known bits. Since the two sections of known bits are short, compared with the entire time slot, this assumption is valid. In order to ensure that the LSSE channel estimation algorithm gives an accurate channel estimate, the MSE of the channel estimate, in the cases of 28 and 12 training bits, is studied.

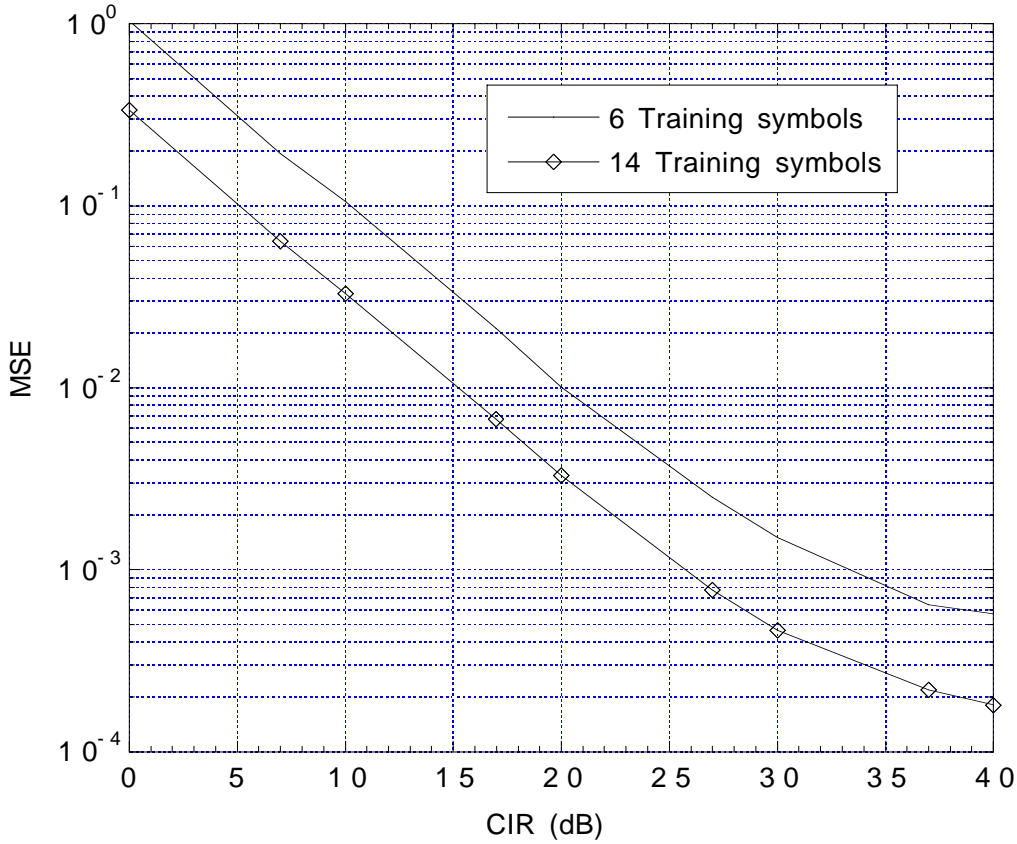


**Figure 4.11:** Channel estimation MSE versus CIR

The MSE of the channel estimate is defined by the following equation:

$$MSE_{\text{ch}} = \frac{1}{N} \sum_{i=0}^{N-1} \left\| \underline{h}_i - \hat{\underline{h}}_i \right\|^2 \quad (4.12)$$

where  $N$  is the number of runs,  $\underline{h}_i$  and  $\hat{\underline{h}}_i$  are the  $i$ th channel and channel estimate.

Figure 4.11 shows the MSE of the channel estimate at different levels of CCI. The quality of channel estimation with 28 training bits is better than that with 12 bits. The curve with 28 training bits exhibits a gain of over 5 dB for a CIR of 25 dB or lower, over that with 12 training bits. This gain increases as the CIR increases. Since there are only two channel parameters to be estimated, the MSE is sufficiently low, even with only 12 bits.

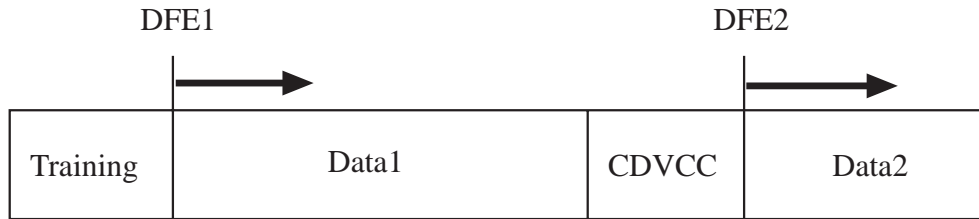


**Figure 4.12:** Calculated DFE used in a time slot

#### 4.3.3.2 Calculation of Optimum DFE Coefficients

After channel estimation is accomplished, the channel estimate is used to compute the estimated auto correlation matrix and cross correlation vector of the DFE, as discussed in Section 3.2.1. The optimum DFE coefficients are given by the Wiener-Hopf equations 3.72.

#### 4.3.3.3 Performance of Calculated DFE Using Wiener-Hopf Equations

Figure 4.12 shows how the calculated DFE works in a time slot. In this case, both channel estimation and calculation of DFE1 is performed at the 28-bit training sequence. DFE1 is applied to the received symbols from the start of the time slot to the 12 CDVCC bits, where the channel estimation and calculation of DFE2 are performed. DFE2 is then applied to the received symbols from this point on until the end of the time slot.

Figure 4.13 shows the error distribution over a time slot for the calculated DFE, at a vehicle speed of 100 km/hr and a CIR of 17 dB. In the regions following the training bits and the CDVCC bits, the average BER is relatively low since changes in the time-varying channel are not significant from regions of known bits. In the regions further away from the training sequences, the BER grows more rapidly due to the more significant changes in the channel and error propagation introduced by

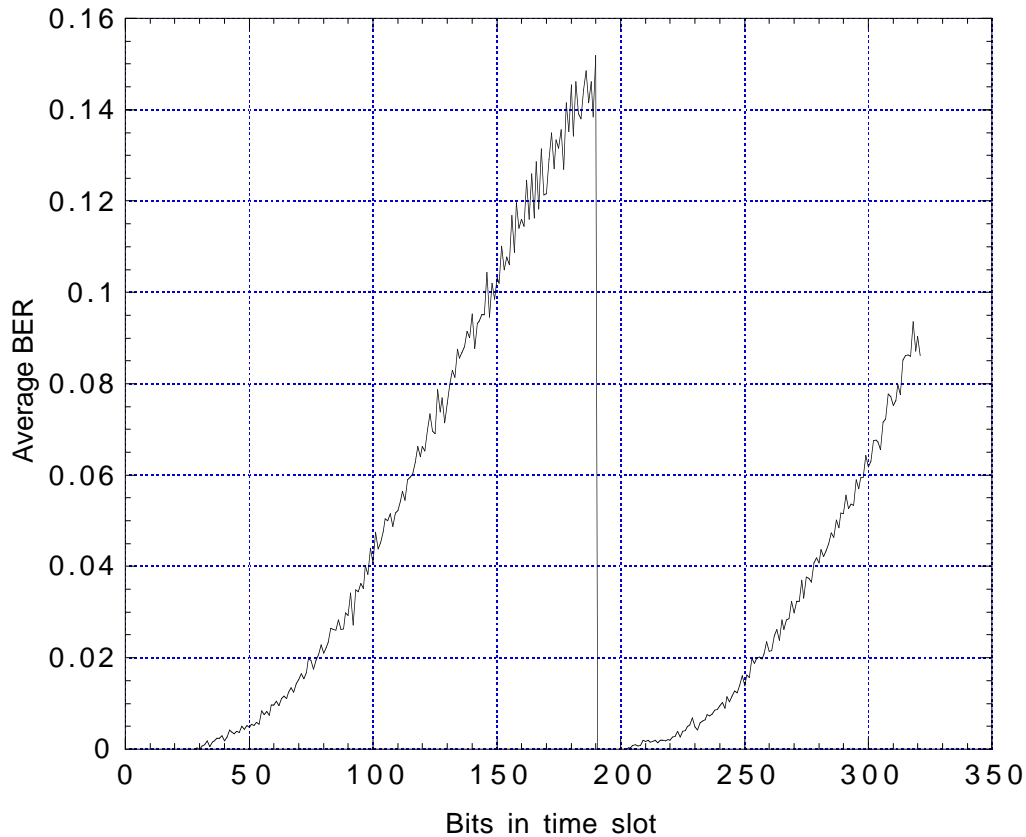


**Figure 4.13:** BER distribution of calculated DFE

the feedback mechanism of the DFE. The average BER here is 4.7%, which satisfies the IS-136 requirement. For higher CIR and lower mobile speed, the BER should also satisfy this requirement.

#### 4.3.4 Displaced DFE

The purpose and advantage of the displaced equalizer technique have been presented and discussed in Section 3.2.3. Here, a DFE receiver using this scheme is applied to the IS-136 received symbols to achieve better BER performance, and such a receiver is called a displaced DFE (DDFE). As in the calculated DFE case, channel estimation and DFE calculation are performed twice in the time slot – once at

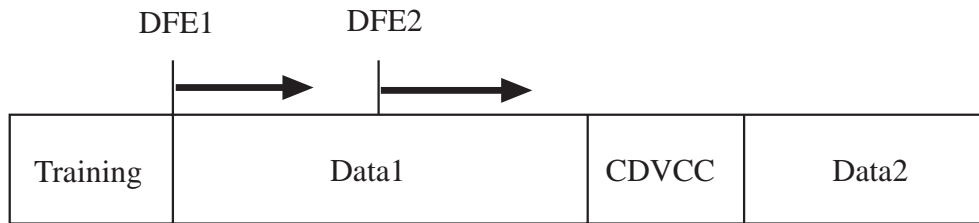


**Figure 4.14:** DDFE used in a time slot

the training bits and the other at the CDVCC bits. The only difference here is that DFE2, instead of DFE1, is applied to the second half of section Data1. Figure 4.14 shows the arrangement of the DDFE applied to a time slot.

The error distribution for the DDFE is presented in Figure 4.15, at a vehicle speed of 100 km/hr, and a CIR of 17 dB. For comparison purpose, the error distribution curve for the standard calculated DFE is also shown in this figure. In the DDFE case, since the second half of section Data1 is filtered by DFE2, the error in this region is significantly reduced, compared to that of the standard calculated DFE. The BER is also reduced to 2.3%. Therefore, by applying a DDFE to the received symbols, the BER performance is improved, without significant increase in system complexity and computational intensity.

## 4.4 Discussion

In this section, comparisons of the receiver schemes detailed in the previous section are presented. Two issues are involved in these comparisons: the BER performance and the computational complexity.

### 4.4.1 Comparison of Performance

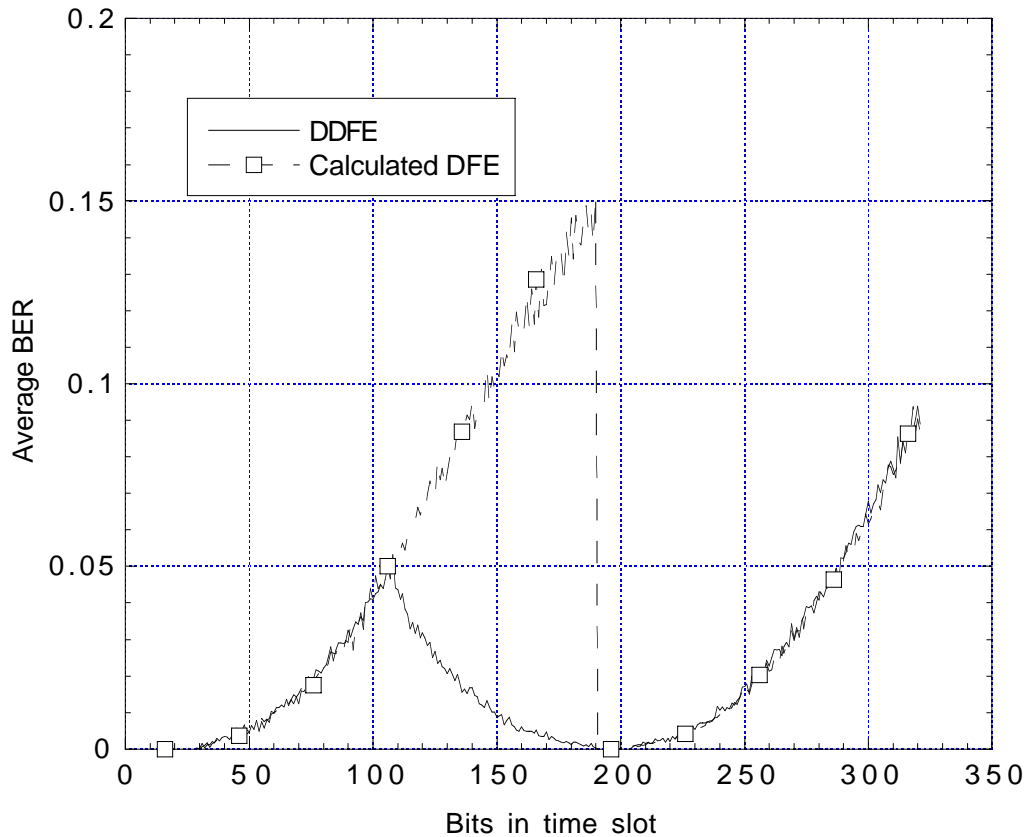


**Figure 4.15:** BER distribution of DDFE and standard calculated DFE

Figure 4.16 shows a comparison of the BER performance of different receiver schemes. Here, only the performance of the worst case vehicle speed of 100 km/hr is considered, at a SNR of 30 dB. The BER performance of the receiver with perfect channel estimate is also presented as the lower bound. With the ideal channel estimator, the maximum gain obtainable for 5% BER at a CIR of 17 dB is 11 dB.

Among all the curves, BER curves of RLS-DFE, for both non-tracking and tracking cases, are the farthest away from the lower bound. Despite the fast convergence property of the RLS algorithm, this class of receivers suffers from several disadvantages in this application. First, the 28 training bits might not be sufficient for the convergence of the algorithm. For channels exhibiting spectral nulls or some other hostile properties, a longer training sequence might be necessary. However, at

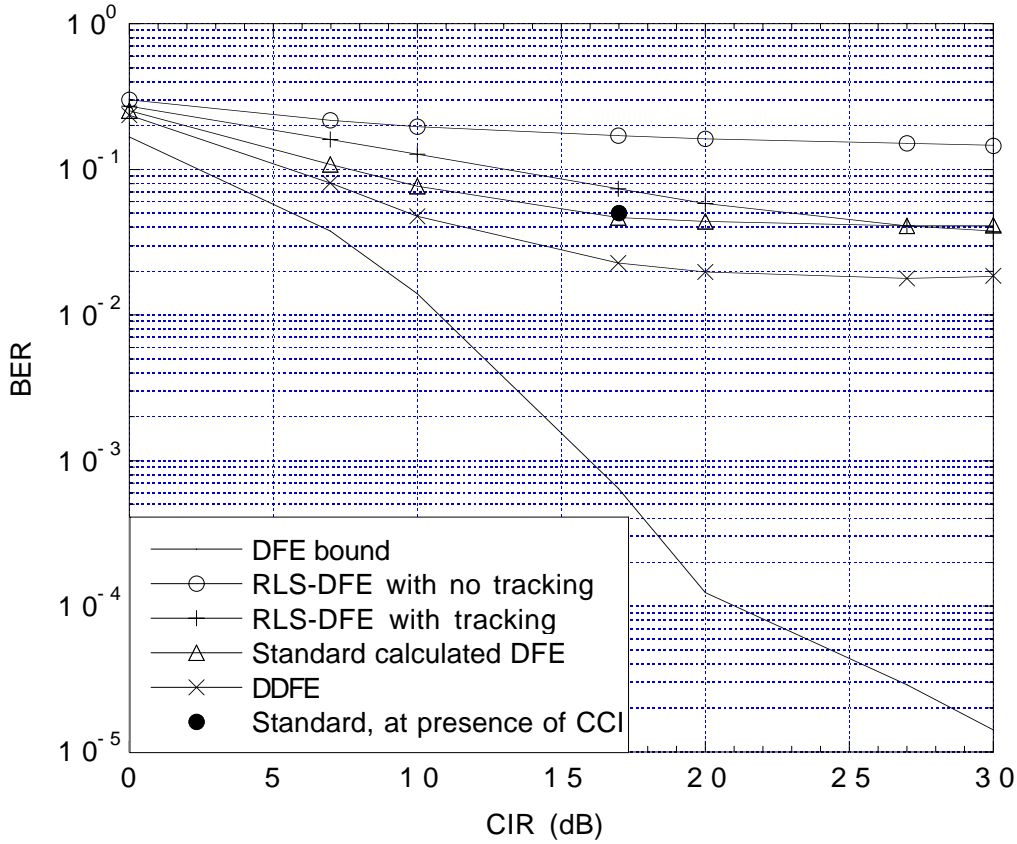


**Figure 4.16:** Comparison of BER performance

higher vehicle speeds, since the channel varies so fast that it changes significantly during the training sequence, a longer training sequence might not provide any improvement. Second, in theory, a large number of taps in the equalizer is required to provide good system performance. However, with only 28 training bits, the large number of parameters estimated will result in higher estimation error, which translate to higher BER. Finally, decision directed tracking, which is one of the solutions to deal with fast time-varying channel, causes error propagation. Therefore, the 5% BER at a CIR of 17 dB is not satisfied by the RLS-DFE.

BER curves for the calculated DFE all satisfy the IS-136 requirement since there are only two channel parameters to be estimated. The standard calculated DFE, with a margin of only 0.5 dB, barely satisfies the BER requirement. On the other

hand, the DDFE meets the BER requirement with margin of 7 dB. With this special DFE technique, the average error is reduced significantly in the time slot for fast time-varying channels.

Comparing the BER curves against the lower bound, there is still much room for improvement, which implies that the potential performance of the DFE is not achieved, with the current channel estimation algorithm. By employing a better channel estimation algorithm, the error floor can be lowered, and more closely approach the lower bound.

#### 4.4.2 Comparison of Complexity

Another comparison of different receiver schemes is its computational complexity. The various algorithms and schemes discussed above involve different numbers of floating point operations and matrix operations. One way to quantify the computational complexity is to use the notion of a flop. A flop is a floating point operation [86]. Each operation, such as a floating point add or floating point multiply, is considered as a flop. Since the number of flops is the same for filtering operations for all the DFE receivers after the DFE coefficients are determined, only the computational load of calculation of the DFE coefficients is considered here.

For the RLS-DFE receivers, the DFE is trained at the beginning of the time slot using 14 training symbols where 14 updates of the DFE coefficients occur. With  $N_w$  coefficients in DFE, each update using the RLS algorithm involves  $5N_w^2 + 6N_w + 2$  flops [87]. In the case of the RLS-DFE with no tracking, the DFE is fixed and no more updates are required. For the RLS-DFE with tracking, there are 147 additional updates of the DFE coefficients, and the total number of updates is 161.

For the calculated DFEs, including the standard calculated DFE and the DDFE,

the operation count consists of two parts: the LSSE channel estimation and the computation of the DFE coefficients using the Wiener-Hopf equations.

For LSSE channel estimation, the numbers of operations required to compute the auto correlation matrix  $\mathbf{S}$  and the cross correlation vector  $\mathbf{z}$  are  $KN_c^2$  and  $KN_c$ , respectively, for a training sequence with length  $N_t$  and a channel with  $N_c$  taps. The operation count for solving Equation 3.5 for  $\hat{\mathbf{c}}_{opt}$  is  $\frac{2}{3}N_c^3 + \frac{3}{2}N_c^2 - \frac{1}{6}N_c$  by using the LU decomposition method, detailed in the work of Press et al. [88].

By applying the LSSE channel estimation algorithm, even though matrix inversion is also involved, the matrix is the auto correlation of the training sequence and it is a function of the training sequence only. For a fixed training sequence, the inverse of the matrix can be pre-computed and stored [39], and no further matrix inversion is required. This can reduce the computational complexity significantly. In this case, only the computation of the cross correlation and a matrix multiplication are involved, and the total number of flops required for LSSE channel estimation can be reduce to  $2N_c^2 + (K - 1)N_c$ . For two antennas in the receiver, this number is doubled.

For computing the optimum DFE coefficients from the channel estimates, the Wiener-Hopf equations are solved. For an overall channel, including the transmit filter and the actual channel, of  $N_h$  taps and a feed forward filter in the DFE with  $N_{ff}$  taps, it takes  $3(2N_h - 1)(2N_{ff} - 1)$  operations for estimating the auto correlation matrix  $\mathbf{R}$ , due to its special structure. It takes no operations for estimating the cross correlation vector  $\mathbf{p}$ . The operation count for solving the Wiener-Hopf equation is  $\frac{2}{3}N_w^3 + \frac{3}{2}N_w^2 - \frac{1}{6}N_w$  flops.

The process of determining the DFE coefficients, including LSSE channel estimation and DFE coefficient computation, takes place twice within a time slot, once

DFE type	Operation count
RLS-DFE, no tracking	$14(5N_w^2 + 6N_w + 2)$
RLS-DFE, tracking	$161(5N_w^2 + 6N_w + 2)$
Calculated DFE	$\frac{4}{3}N_w^3 + 3N_w^2 - \frac{1}{3}N_w + C$

**Table 4.3:** Operation counts for different DFE methods

at the training sequence with 14 symbols and once at the CDVCC with 6 symbols.

In summary, the operation counts for different DFE methods are tabulated in Table 4.3, for  $N_c = 2$ ,  $N_h = 20$  and  $N_{ff} = 5$ .

In Figure 4.17, the number of operations for different DFE methods is plotted against the number of DFE coefficients. Even though the computational complexity of the RLS-DFEs is  $\mathcal{O}(N_w^2)$  and that of the calculated DFEs is  $\mathcal{O}(N_w^3)$ , for small number of taps in the DFE, the number of operations for the RLS-DFEs is much larger, due to the large proportionality constant. This can be observed by comparing the curves in Figure 4.17. Therefore, the calculated DFEs require less computational load than the RLS-DFEs.

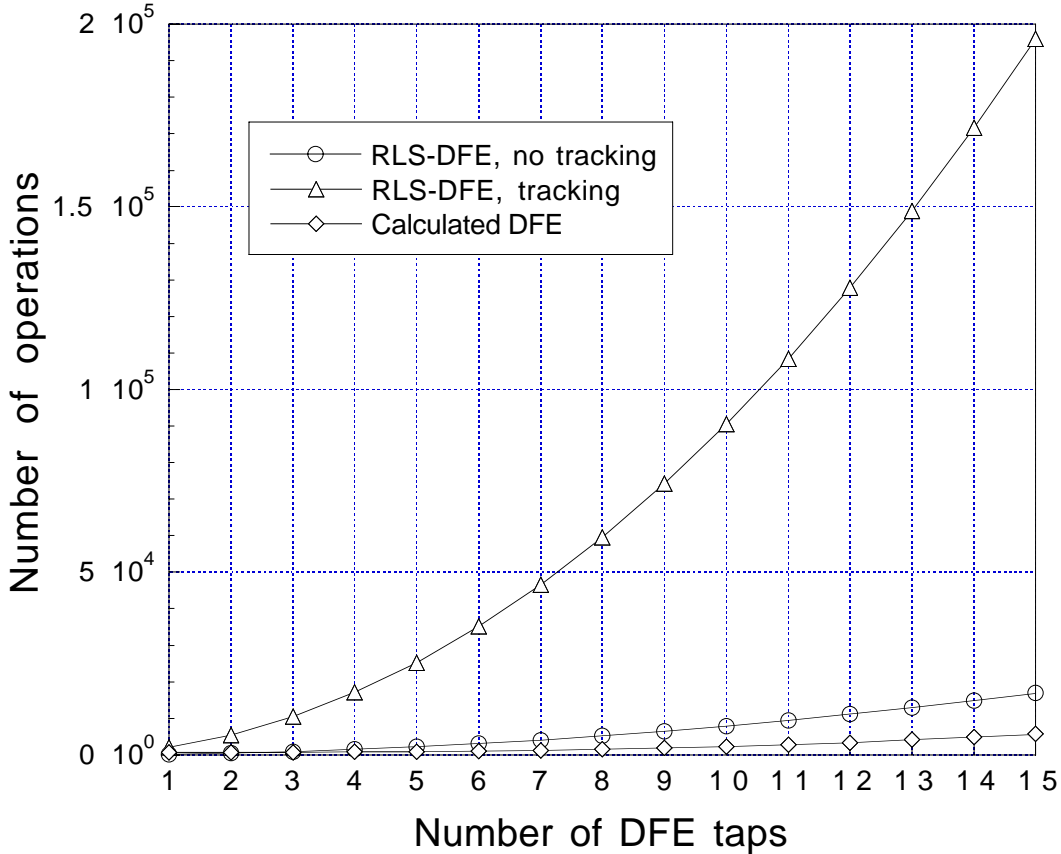


Figure 4.17: Comparison of computational complexity

# Chapter 5

## Application to IS-136 1.9 GHz Operation

### 5.1 Background

The IS-136 TDMA system operates at both 800 MHz and 1.9 GHz. The addition of the 1.9 GHz operation in the IS-136 system is to increase the system capacity so that the increasing demands for wireless mobile communications can be satisfied. Since these are operations of the same system, the specifications on the system set up and the criterion of the system performance for 1.9 GHz operation are identical with those for the 800 MHz operation. The only difference is the center frequency at which the system operates. Since the center frequency is roughly doubled for the 1.9 GHz operation, the Doppler frequency experienced by the system is roughly twice as high. This implies that more channel variations take place within the duration of one TDMA time slot. Higher Doppler frequencies make it more difficult to achieve the specified performance criterion and the equalizer updating techniques employed

in the 800 MHz operations are no longer feasible. Other techniques, usually more complex, have to be found in order to meet the performance requirement under this even more adverse condition [55].

In this chapter, more complex channel estimation techniques discussed in Chapter 3 will be deployed to achieve a 5% BER performance for the 1.9 GHz operation, in the presence of CCI. In particular, blind techniques, such as joint data and channel estimation, and joint data, channel and co-channel estimation, will be used despite their intensive computational complexity. Furthermore, three channel interpolation methods, the displaced LE, the displaced DFE and the curve fitting DFE will be employed, in combination with the various channel estimation methods and their BER performance is tested and compared through simulations. An important issue, the computational complexity of various methods, is also compared at the end of the chapter.

## 5.2 Performance of Receivers

In this section, BER performance of different equalizer schemes with two-antenna diversity will be evaluated with one dominant CCI. For simulation purposes, a two-ray channel with path delay of  $T/2$  is considered. Here, two equalizer structures, the LE and the DFE are used, and they are fractionally spaced equalizers with  $T/2$ -spaced taps. As with those used in the 800 MHz operation, the DFEs used here have five  $T/2$ -spaced taps in the two feed forward filters, and three  $T$ -spaced taps in the feedback filter (5-5-3 DFE). The LEs have eight  $T/2$ -spaced taps (8-8 LE). Since, in general, the receiver scheme will also work in cases of lower velocity, if it can satisfy the performance criterion at high velocity, it is only tested at the

velocity of 100 km/hr.

In the remainder of this section, the lower BER bounds of the system with DFE receivers and LE receivers are evaluated by means of simulations. All the simulation results are obtained by averaging over 1000 simulation runs. The performance of various equalization schemes are evaluated and compared against these lower bounds. In order to verify the theoretical analysis conducted in Chapter 3, the MSE of receivers with DLE and the probability of error in ML data and channel estimation are also simulated to compare against the theoretical results.

### 5.2.1 DFE and LE Bounds

The DFE and LE bounds can be obtained when channel estimation is perfect. In these cases, the receivers are assumed to have perfect knowledge of the time-varying channel, or possibly both channel and co-channel at every symbol period during the time slot. Here, these bounds are obtained by means of simulations, and the results represent the best performance one particular equalizer scheme can achieve. With these simulation results, one can decide if the equalizer scheme can be used to satisfy the performance criterion, by improving the channel estimation quality.

Figure 5.1 shows the BER performance of DFE and LE receivers at the presence of noise, for two antenna diversity. The curves are obtained at a vehicle velocity of 100 km/hr and CCI power of zero. Both lower bounds satisfy the 3% BER performance requirement at SNR of 17 dB, with a margin of 11 dB. Therefore, both receiver schemes are feasible, provided that the channel estimates are accurate enough.

It is worth noting that Chou et al. attempts to use a DFE with two T-spaced

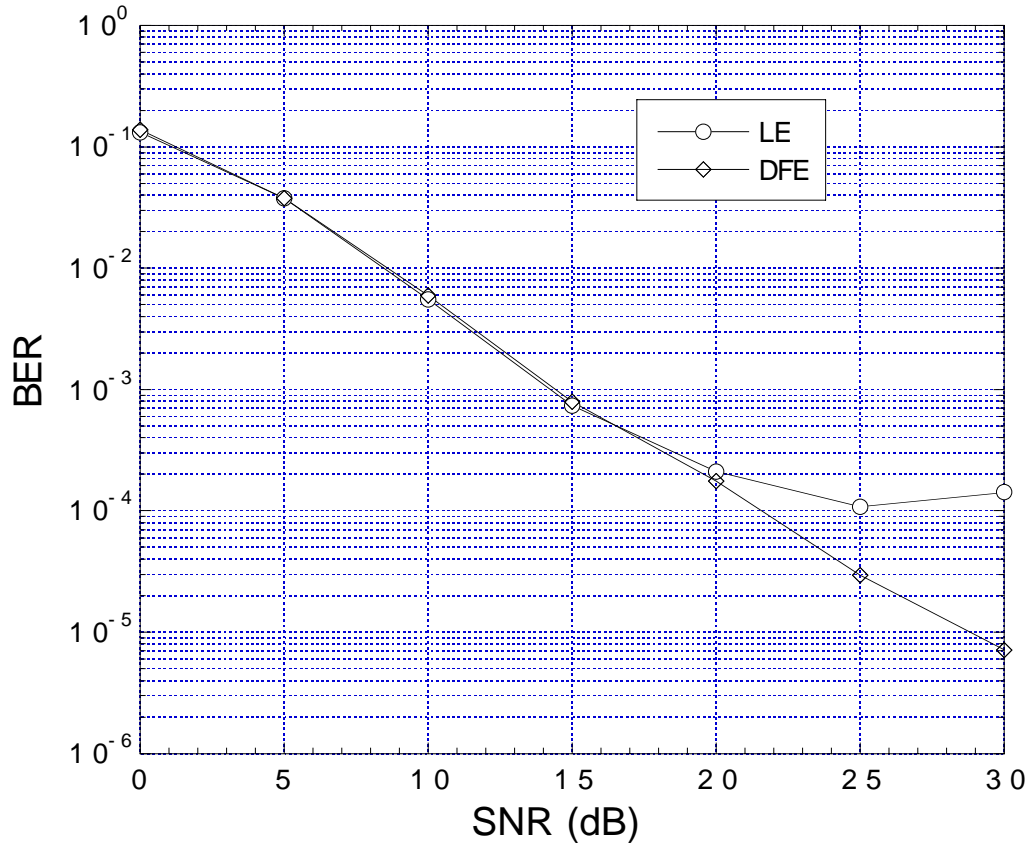


**Figure 5.1:** BER lower bound (1.9 GHz operation,  $CIR = \infty$ )

feedforward filters in the applications of IS-136 800 MHz operation, at vehicle speed of 100 km/hr [89]. It is also assumed that the time-varying channel impulse response is known and a 2-ray channel model with a path delay of  $T/2$  is used [89]. When the 2 rays in the channel model have equal average power, the performance criterion of 3% at 17 dB SNR cannot be satisfied. In this research thesis, a DFE with 2  $T/2$ -spaced feedforward filters are used. As shown in Figure 5.1, superior performance is achieved due to the fact that the fractionally-spaced equalizer approximates the optimal receiver which includes the functions of a matched filter and an equalizer [12, 23, 28].

Also note the changes in these lower bounds as the SNR level increases. At low

SNR, the effect of the noise dominates, and error rate is high for both DFE and LE. As the noise power decreases, the effect of the ISI introduced by the channel dominates, and the performance of DFE surpasses that of LE due to its ability to cancel ISI.

As an alternative to equalization, diversity combining can also be used to mitigate the effect of ISI. In fact, diversity combining is less computationally intensive than equalization. Clark et al. investigated an MMSE diversity combining technique which is designed to combat ISI in wideband digital cellular radio application [90]. It is found that MMSE diversity combining offers significant improvement over selection diversity and maximal ratio combining for slowly time-varying indoor channels with high delay spreads [90]. However, fast fading is not considered in this work.

The curves in Figure 5.2 represent the lower bounds of LE and DFE receivers in the presence of CCI, with and without the information of the co-channel. They are obtained at an SNR level of 30 dB. Unless explicitly specified otherwise, the SNR level will be maintained at 30 dB in the simulations throughout this section. All of these lower bounds satisfy the 5% BER performance requirement at a CIR level of 17 dB. Since these bounds are obtained with perfect channel estimation, by employing a good channel estimation algorithm, these receiver schemes can be used to meet the standard in the presence of CCI.

Without knowledge of the co-channel, the error rate for both DFE and LE receivers is high when CCI is severe. Since the effect of ISI in the system dominates as the level of CCI decreases, the DFE receiver gives better performance than the LE receiver.

Comparing the two DFE lower bounds, it is obvious that the performance of the DFE receiver with the co-channel information is superior to the one without the

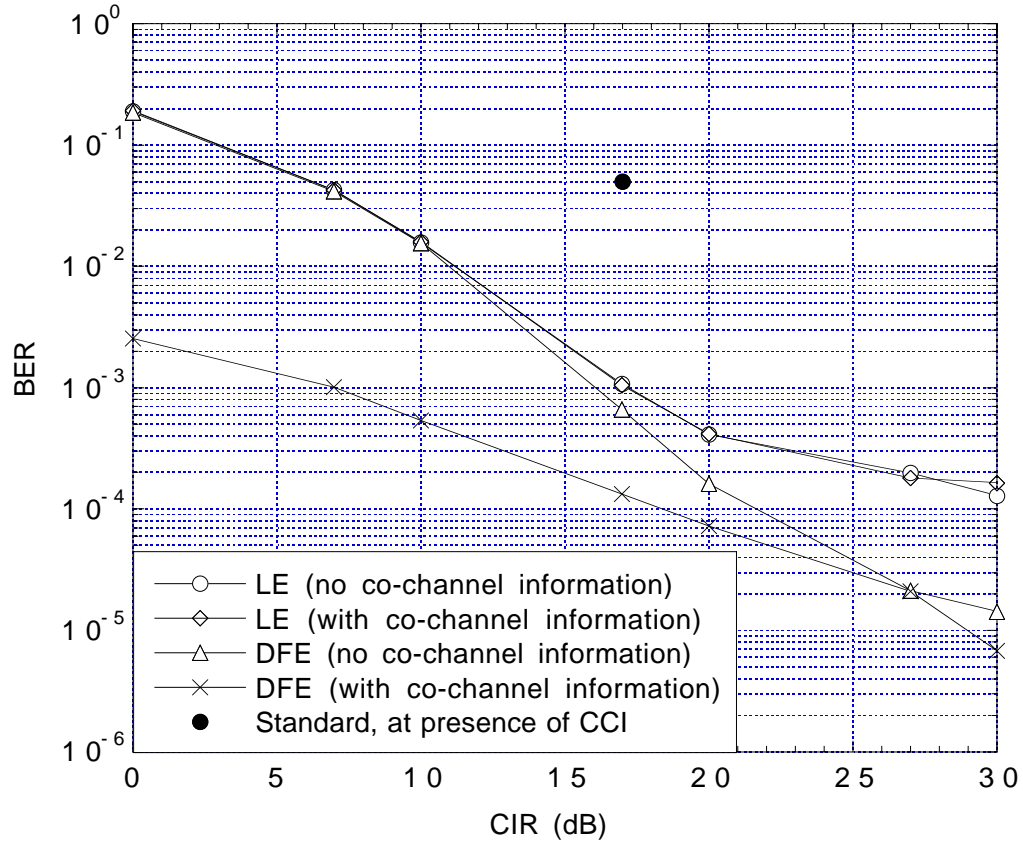


**Figure 5.2:** BER lower bound (1900 MHz operation, SNR = 30 dB)

co-channel information at high level of CCI (low level of CIR). It implies that the DFE receiver with knowledge of both channel and co-channel can suppress both ISI and CCI to achieve outstanding performance. At high CIR, since the level of CCI is low enough, the receiver with knowledge of the co-channel, has similar performance to that of the one without the the co-channel information, and the gap between the bounds for these two types of receivers are closing. Therefore, when the CCI is not so severe, the DFE receiver with no co-channel information, can be used to achieve comparable performance.

On the other hand, the LE receivers, with or without the knowledge of the co-channel, have very similar performance. With the model developed in Chapter 2, the characteristic of the CCI is very similar to that of the ISI. Due to the inherent

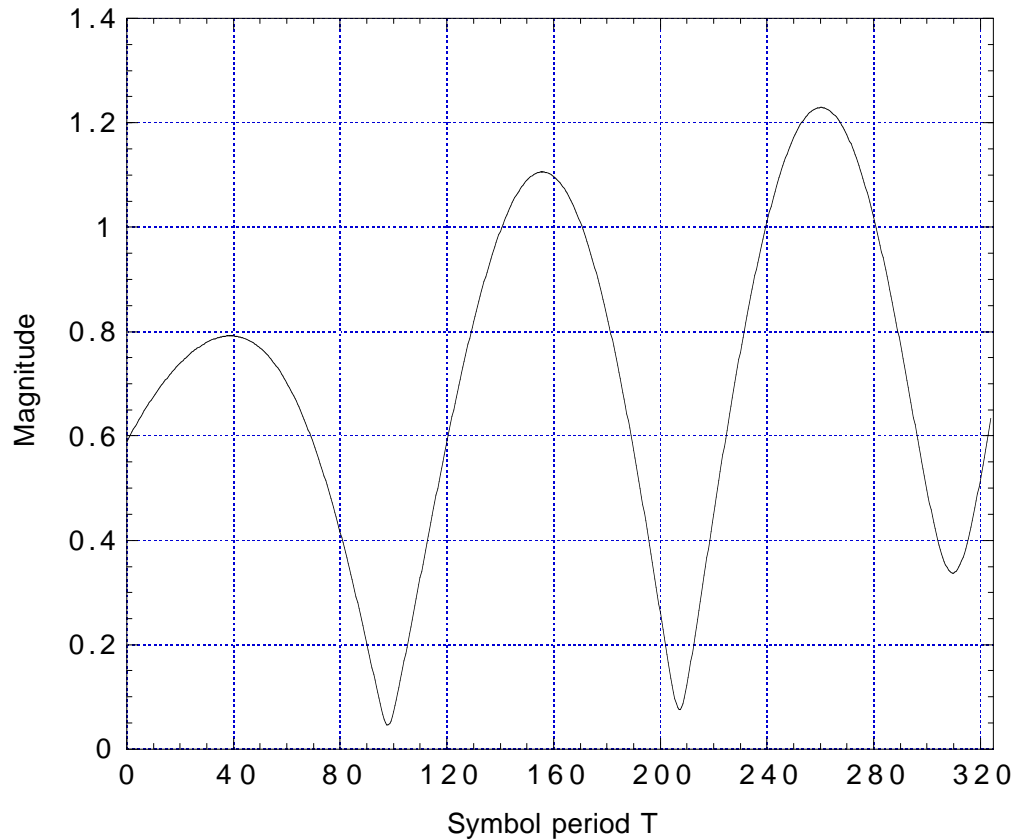


**Figure 5.3:** Variation of one channel tap (1900 MHz operation)

limitation of the LE receivers, they cannot cancel the ISI as well as the CCI, even when provided the co-channel information.

## 5.2.2 DFE and LE Partial Bounds

### 5.2.2.1 Channel Samples at SYNC and CDVCC only

One of the differences between 800 MHz and 1.9 GHz operations is the frequency band where the operation takes place. The center frequencies of the 1.9 GHz operation is more than twice that of the 800 MHz operation. Therefore, more variations in the communication channel during a time slot can be expected. Figure 5.3 shows the magnitude of one channel tap in an interval of two time slots for a mobile speed

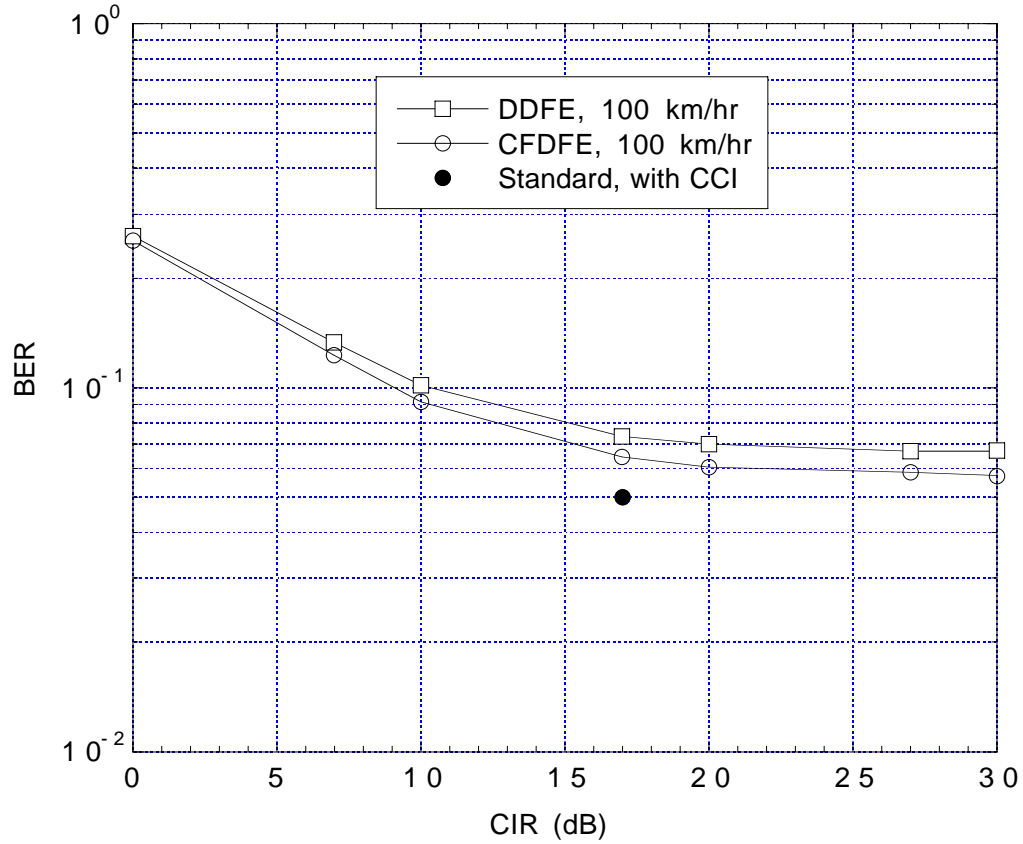


**Figure 5.4:** Performance of DFE receiver, Case A0

of 100 km/hr. On average, there are more than one deep fades in every time slot.

If the LSSE channel estimation method is used on the SYNC and CDVCC sequences in a time slot, two channel samples are available. In this case, there are only two channel samples available in a time slot, and it is called scheme A0. Figure 5.4 shows the BER performance of the DDFE and curve fitting DFE (CFDFE) receivers at vehicle speed of 100 km/hr. It is assumed that the channel estimation at these two known sequences are perfect. The curves in these two figures are referred to as the partial DFE bounds since they are obtained by using perfect channel estimates in only some parts of a time slot, and they represent the best attainable performance these DFE receivers can achieve.

At high vehicle speeds, for example, 100 km/hr, the best performance of these

receivers cannot satisfy the standard. This indicates that with only two channel samples available in a time slot, even with no estimation errors, the channel cannot be accurately interpolated over the entire time slot. In practice, estimation errors associated with the LSSE channel estimation process do occur, and degrade the BER performance. Therefore, two channel samples alone are not adequate to accurately characterize the time-varying channel at high vehicle speed.

Since in the presence of ISI, the performance of a DFE receiver surpasses that of an LE receiver, it can be concluded that the performance of a LE receiver also cannot meet the standard with scheme *A0*.

### 5.2.2.2 Insertion of the Channel Samples

The accuracy of the interpolated channel can be improved by increasing the frequency of the channel samples. However, adding more channel samples in a time slot means an increase in complexity. Therefore, a trade-off must be made between accuracy and complexity. In order to understand how to insert channel samples efficiently so that good BER performance can be achieved with relatively small number of samples inserted, a few insertion schemes are investigated in this section.

These insertion schemes are listed in Figure 5.5. The rectangles in the figure represent the duration of a time slot in the IS-136 mobile cellular system. Inside the rectangles, the symbols  $\times$  denote the channel samples obtained at SYNC and CDVCC by using the LSSE channel estimation method. The symbols  $\circ$  denote the inserted channel samples obtained by some other means, such as ML blind data and channel estimation.

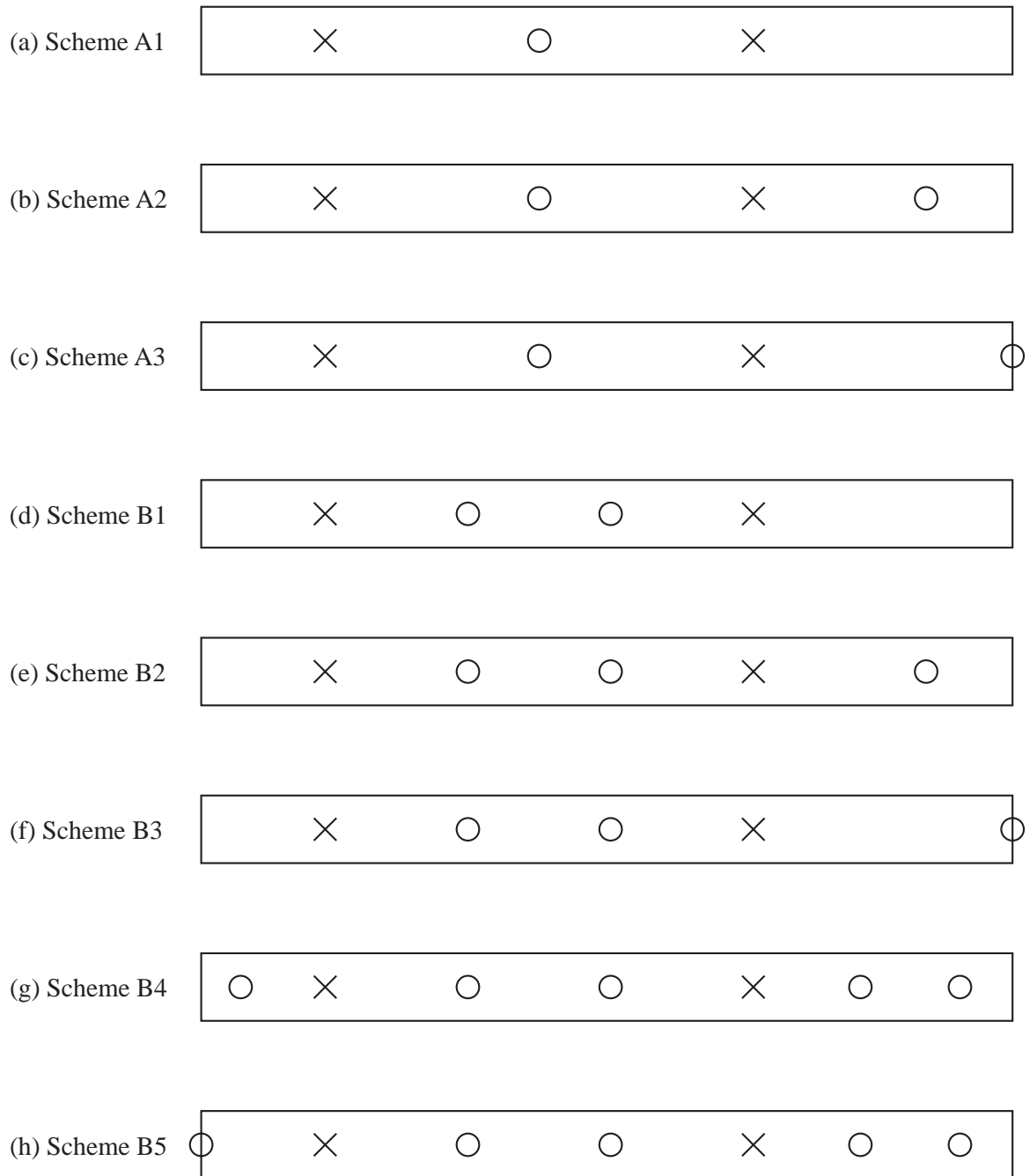


**Figure 5.5:** Channel sample insertion schemes

### 5.2.2.3 Partial Bounds with Channel Information

Figures 5.6 and 5.7 show the BER performance of the DDFE and curve fitting

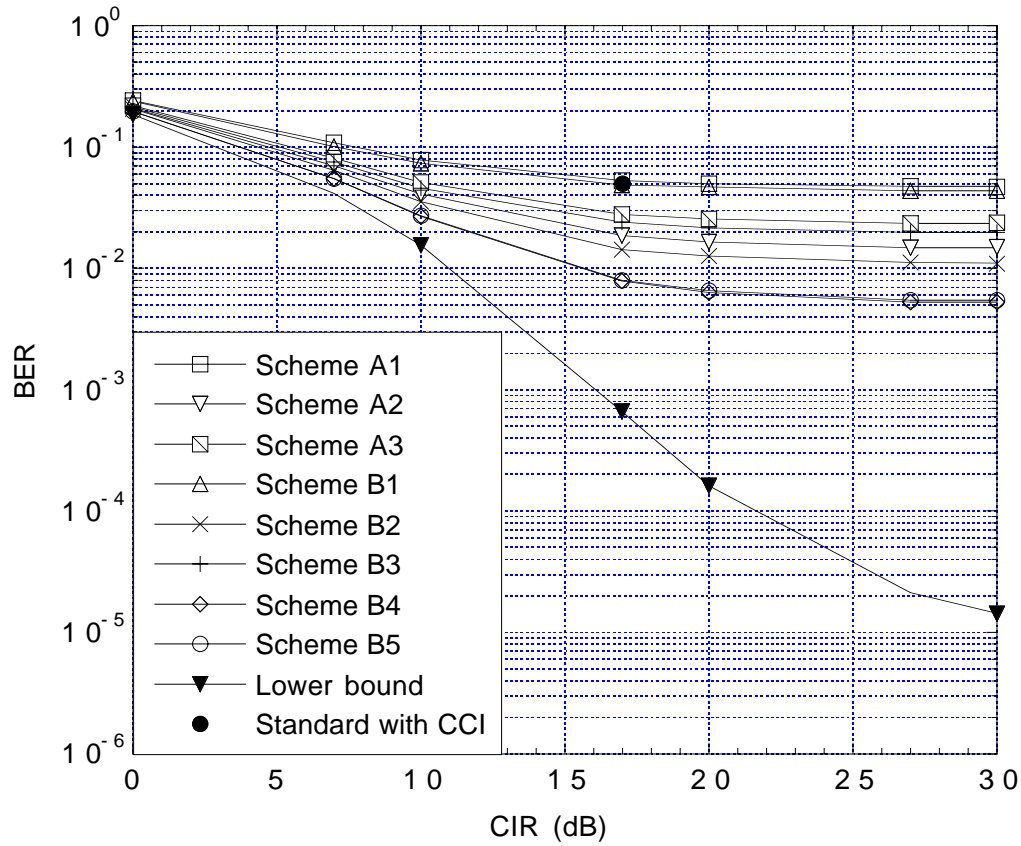
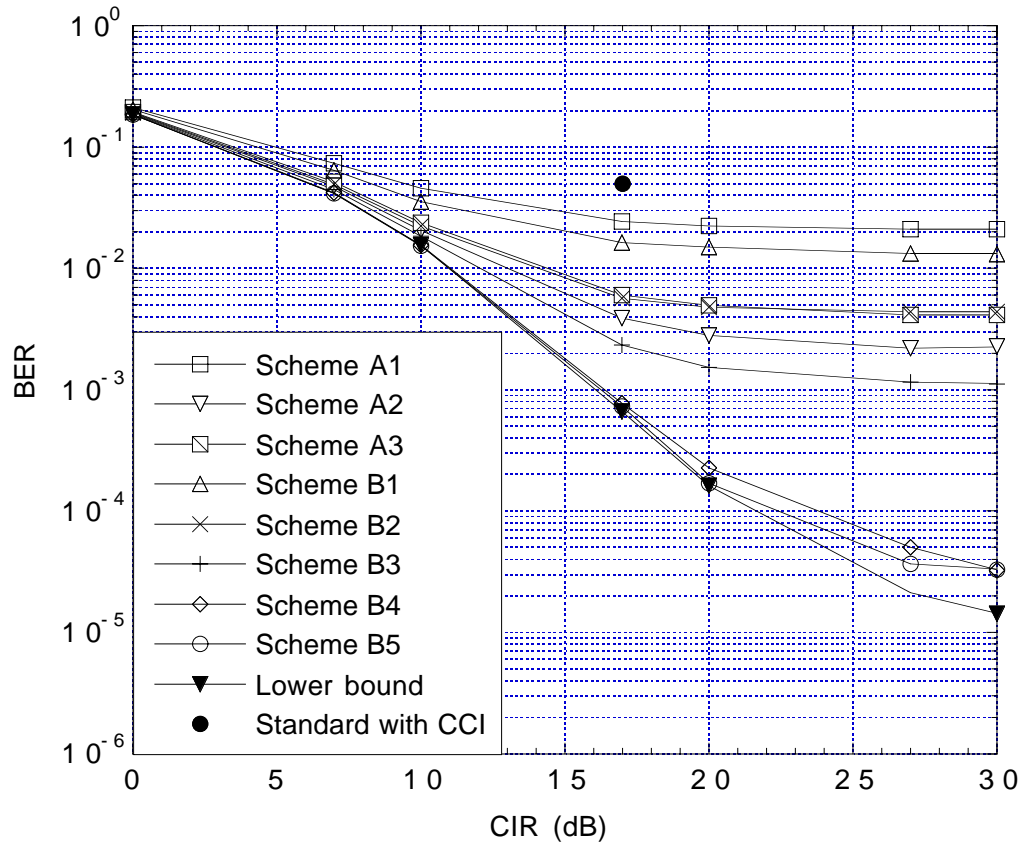


Figure 5.6: DDFE partial bounds

DFE receivers, respectively, by employing the channel sample insertion schemes listed in Figure 5.5 at a vehicle speed of 100 km/hr. These schemes are labeled *A1* through *B5*. For comparison purposes, these channel samples are assumed to be estimated perfectly and they represent the partial DFE bounds.

The partial DDFE bounds satisfy the 5% BER performance criterion at CIR of 17 dB for different insertion schemes, except for scheme *A1*. Among the insertion schemes with 5 channel samples in a time slot, scheme *B2* gives the best BER performance. With 7 channel samples in a time slot, schemes *B4* and *B5* give comparable performance which is the best among all the schemes.

As shown in Figure 5.7, all the partial curve fitting bounds surpass the 5% BER performance criterion. As of the partial DDFE bounds, schemes *B4* and *B5* give



**Figure 5.7:** Curve fitting DFE partial bounds

the best performance among all insertion schemes with a curve fitting DFE receiver. In fact, the gap between these partial bounds and the lower bound is so small that it can be predicted that any additional channel samples to schemes *B4* and *B5* will not improve the BER performance as much as the addition of one of the existing 7 channel samples in these schemes. This implies the marginal improvement in the BER performance associated with the additional channel samples cannot justify the cost of obtaining these channel samples. Therefore, 7 channel samples in a time slot are sufficient to achieve good BER performance.

Since schemes *B2*, *B4* and *B5* give good BER performance for both DDFE and curve fitting DFE receivers, only these three channel sample insertion schemes will be investigated further. The curves in Figure 5.8 represent the partial bounds for

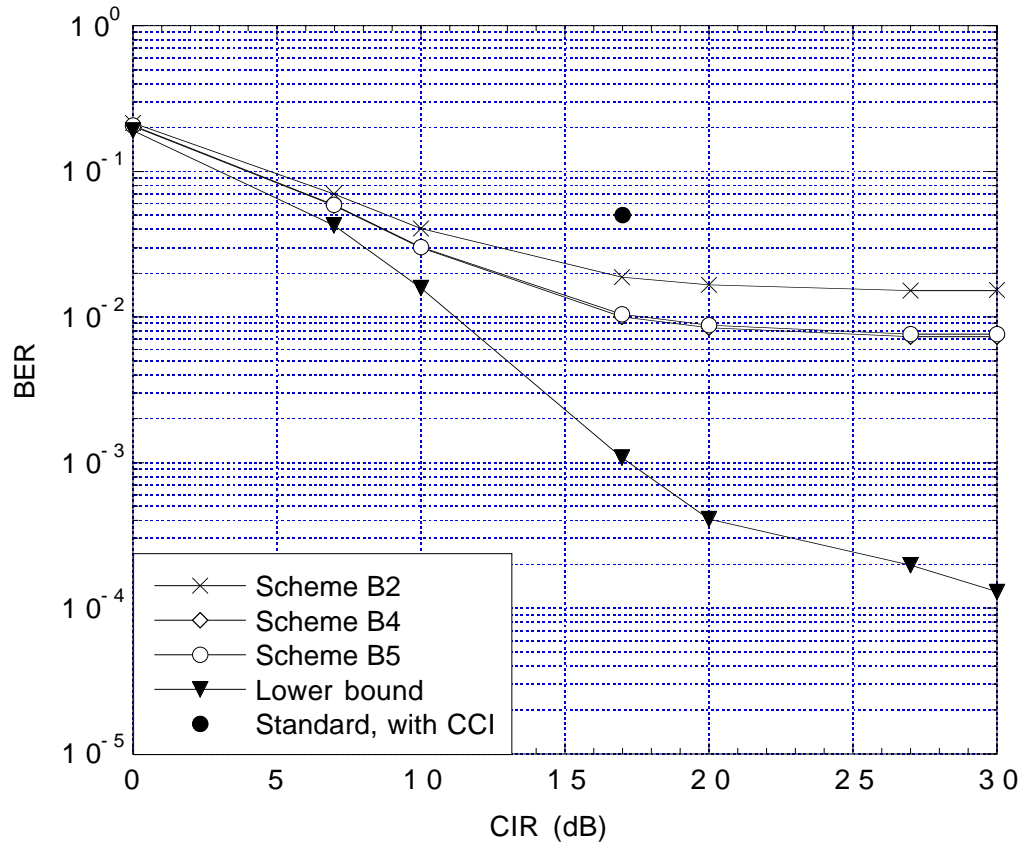
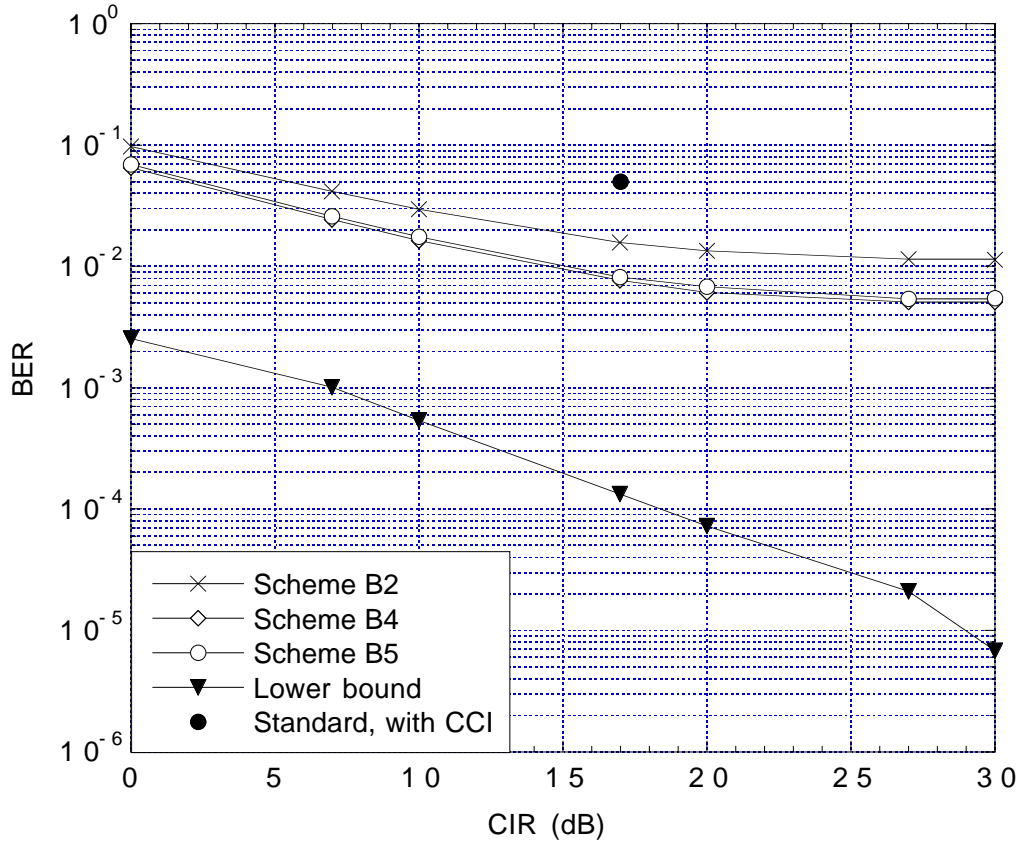


Figure 5.8: DLE partial bounds

a DLE receiver with schemes  $B2$ ,  $B4$  and  $B5$  at a vehicle speed of 100 km/hr. The partial DLE bounds for these three schemes meet the 5% BER performance requirement.

#### 5.2.2.4 Partial Bounds with Channel and Co-channel Information

Partial bound of an equalizer is obtained with the channel estimation is perfect. With the perfect channel estimates at a few points in a time slot, the time-varying channel can be interpolated by the interpolating method associated with a particular equalizer updating technique. Figures 5.9, 5.10 and 5.11 show the partial bounds for the DDFE, curve fitting DFE and DLE receivers with channel and co-channel



**Figure 5.9:** DDFE partial bounds with co-channel information

information, in comparison with the DFE and LE lower bounds. In this case, the channel and co-channel within a time slot are interpolated from the known channel and co-channel samples by using various channel interpolation methods. The equalizer coefficients are calculated using the interpolated channel and co-channel.

With the information about the co-channel, all three receivers give better performance using insertion schemes *B4* and *B5*. With two less channel and co-channel samples in a time slot, the interpolated channel and co-channel in scheme *B2* are not as accurate as those in the two other schemes and the error rate associated with this scheme is larger for all three receiver types.

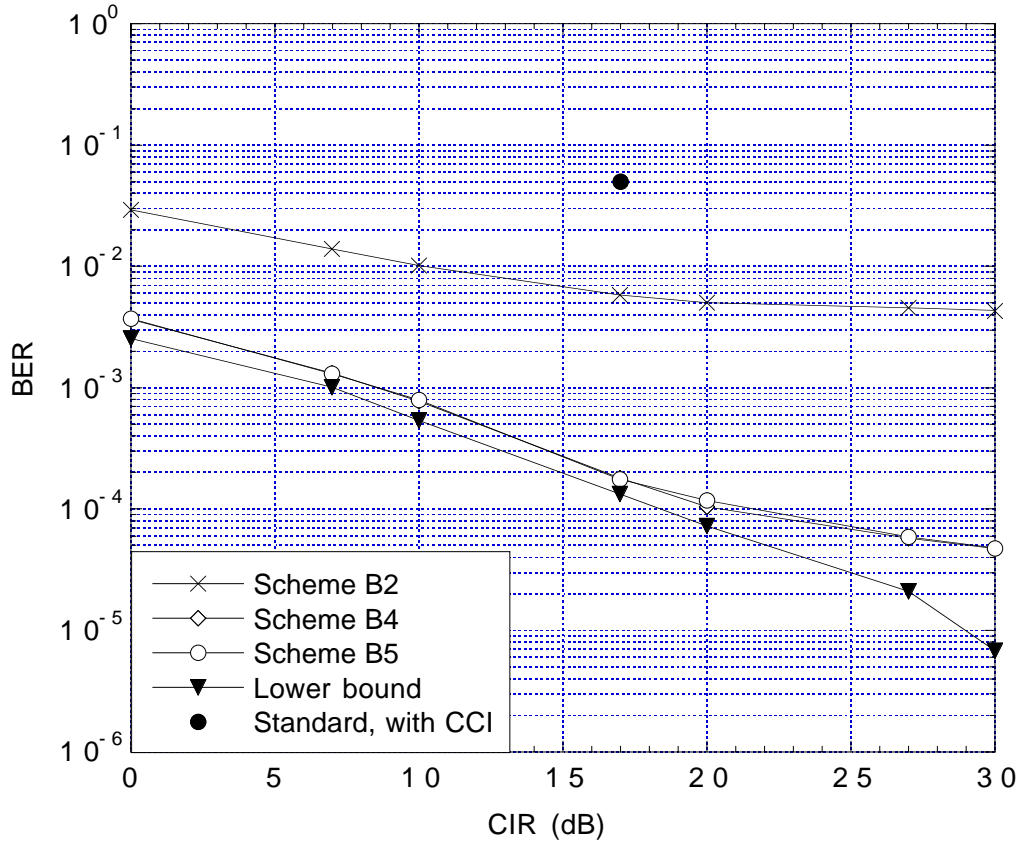
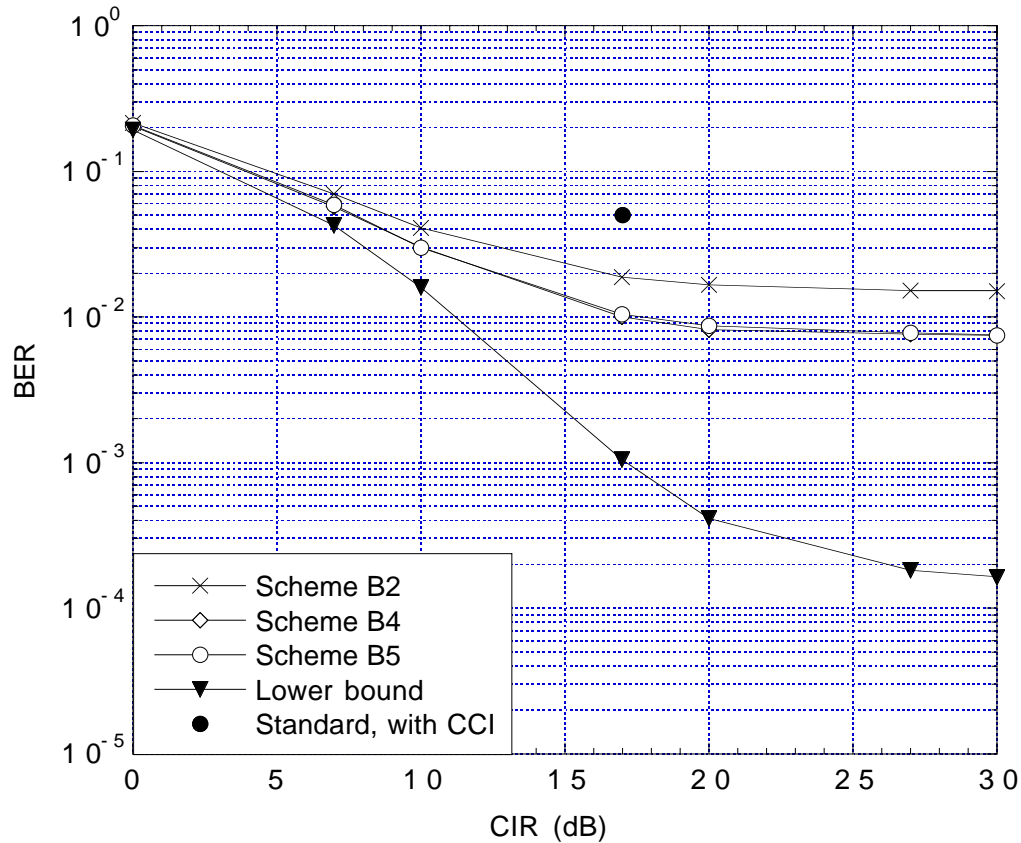


Figure 5.10: Curve fitting DFE partial bounds with co-channel information

### 5.2.2.5 Comparison

This section compares the BER performance of the DDFE, curve fitting DFE and DLE receivers with and without the co-channel information. For this purpose, the partial bounds of scheme *B4* for various receiver schemes are replotted in Figure 5.12.

With co-channel information, the performance of the DDFE receiver and the curve fitting DFE receivers surpasses that of the DFE receivers without co-channel information at the low CIR region. Since the interference power is high in this region, the interference suppression capability of the DFE receivers with co-channel information is obvious. In the high CIR region, since the level of CCI is small,



**Figure 5.11:** DLE partial bounds with co-channel information

the advantage of the DFE receivers with co-channel information disappears and the BER performance is similar with or without co-channel information. On the other hand, the two partial DLE bounds are similar. As with LE lower bounds discussed in Section 5.2.1, the lack of ability of an LE to cancel CCI accounts for the similarity of these two partial bounds.

Among the three types of receivers, with or without information of the co-channel, performance of a DLE is the worst, due to the inherent limitation of an LE. Without the feedback mechanism, an LE can remove neither ISI nor CCI even with perfect channel and co-channel estimates provided. A receiver with a curve fitting DFE gives the best BER performance. The basic difference between the DDFE and the curve fitting DFE methods is the channel model used in the interpolation

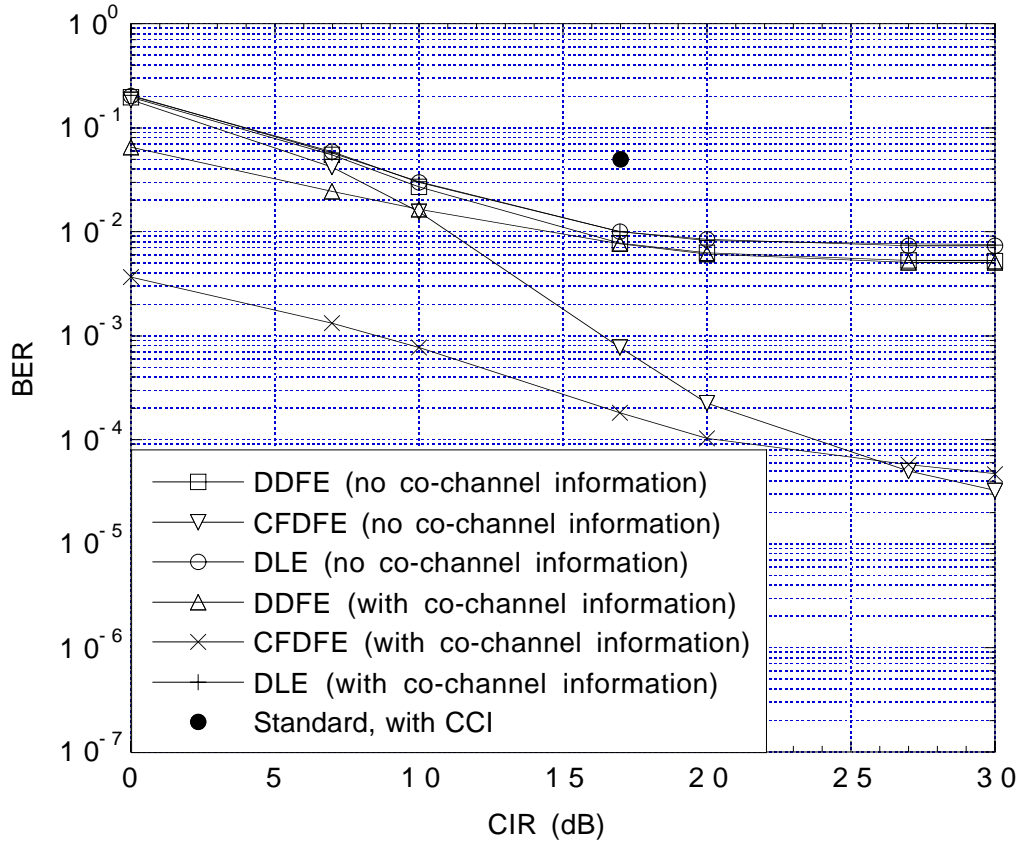


**Figure 5.12:** Partial bounds for scheme *B4*

process. In the case of a curve fitting DFE, a cubic spline interpolation scheme is used to reconstruct the time-varying channel and co-channel during a time slot. Since the interpolated channel and co-channel in a DDFE receiver are only the zero-order (piece-wise) approximation of the physical channels, the interpolated channels in the curve fitting DFE receiver scheme is far more accurate. This accounts for the superior BER performance of the curve fitting DFE receiver. As the number of channel samples increases in a time slot, the difference in BER performance between the DDFE and the curve fitting DFE receiver narrows. Ultimately, if the number of channel samples available is equal to the number of symbols in the time slot, the BER performance of both receivers are the same and these partial bounds will become the DFE lower bound. The fact that the curve fitting DFE method

provides more accurate interpolated channel and co-channel also accounts for the better improvement, in terms of BER, offered by this receiver at low CIR when the co-channel information is available.

### 5.2.3 Performance with Blind ML Data and Channel Estimation

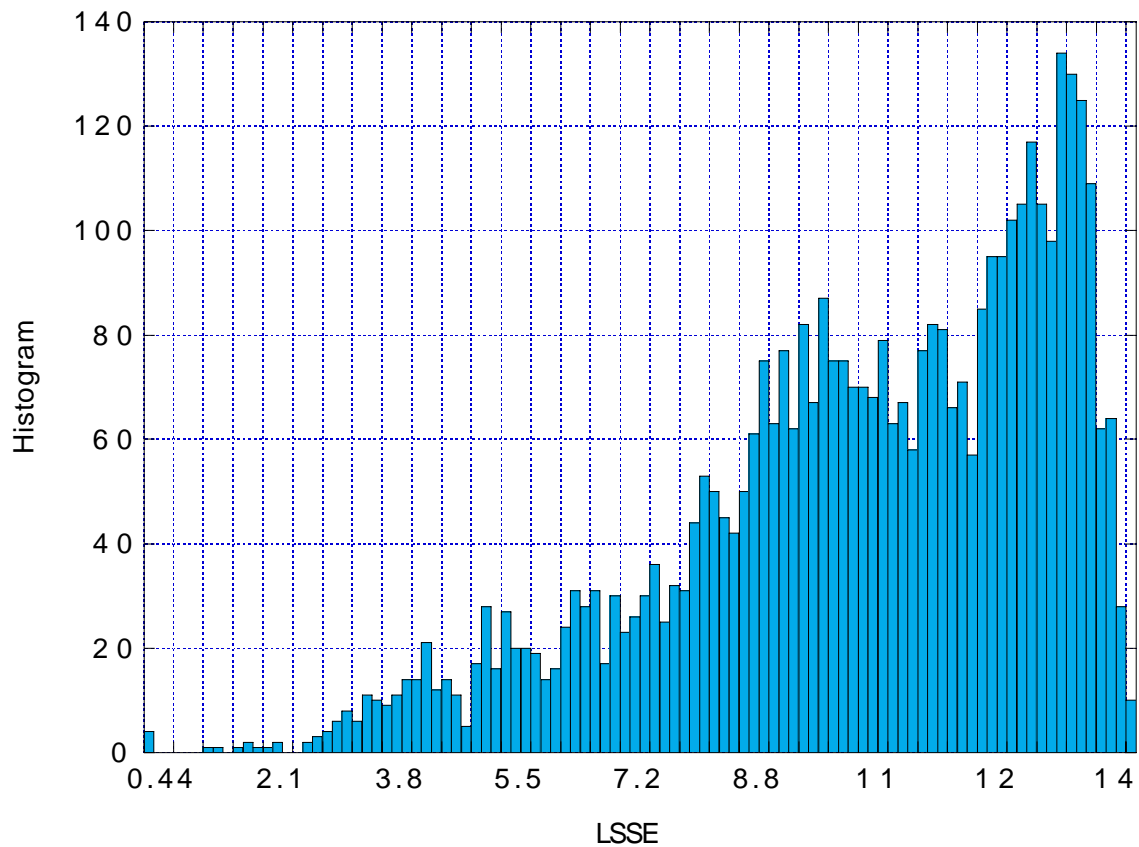


**Figure 5.13:** Histogram of the LSSE

In the case of high vehicle speed, more channel samples are needed in a time slot in order to predict the variations of the time-varying channel. In particular, at a vehicle speed of 100 km/hr, the maximum Doppler frequency is approximately 180 Hz for the 1.9 GHz operation. This implies that the time-varying channel goes

through 1.16 cycles per time slot. As illustrated in the previous sections, with 7 channel samples, insertion schemes  $B4$  and  $B5$  offered superior BER performance. With only two known sequences, SYNC and CDVCC, available in a time slot, more channel samples can only be obtained by means of blind methods. Blind ML data and channel estimation method is one of these blind methods.

Figure 5.13 shows the histogram of the average LSSE over 2000 runs, resulting from the blind data and channel estimation using an estimation sequence of 12 bits. This histogram is obtained at a vehicle speed of 100 km/hr and CIR of 17 dB. It is found that, out of the  $2^{12}$  possible input sequences, the number of input sequences associated with a low LSSE is relatively small. This validates the blind data and channel estimation scheme with an estimation sequence of 12 bits long in the IS-136 application.

The blind data and channel estimation method is tested in the three receiver schemes and the BER performance is shown in Figures 5.14, 5.15 and 5.16 for the DDFE, curve fitting DFE and DLE receivers, respectively. For comparison, the lower bounds for DFE and LE are also plotted in the same figures. Since the IS-136 system uses  $\pi/4$  DQPSK differential encoding scheme, it is assumed that the phase of the symbol prior to the estimation sequence is known in order for the blind data and channel estimation to be applied. With the blind data and channel estimation method, the BER performance of all three receiver schemes satisfy the 5% BER criterion at 17 dB of CIR for various channel sample insertion schemes.

Figure 5.17 shows a comparison of performance of the three receiver schemes with blind data and channel estimation. For comparison purposes, the BER curves of the DDFE, curve fitting DFE and DLE receivers for insertion scheme  $B4$  are regenerated here. Similar to the partial bounds, the DFE receivers give better

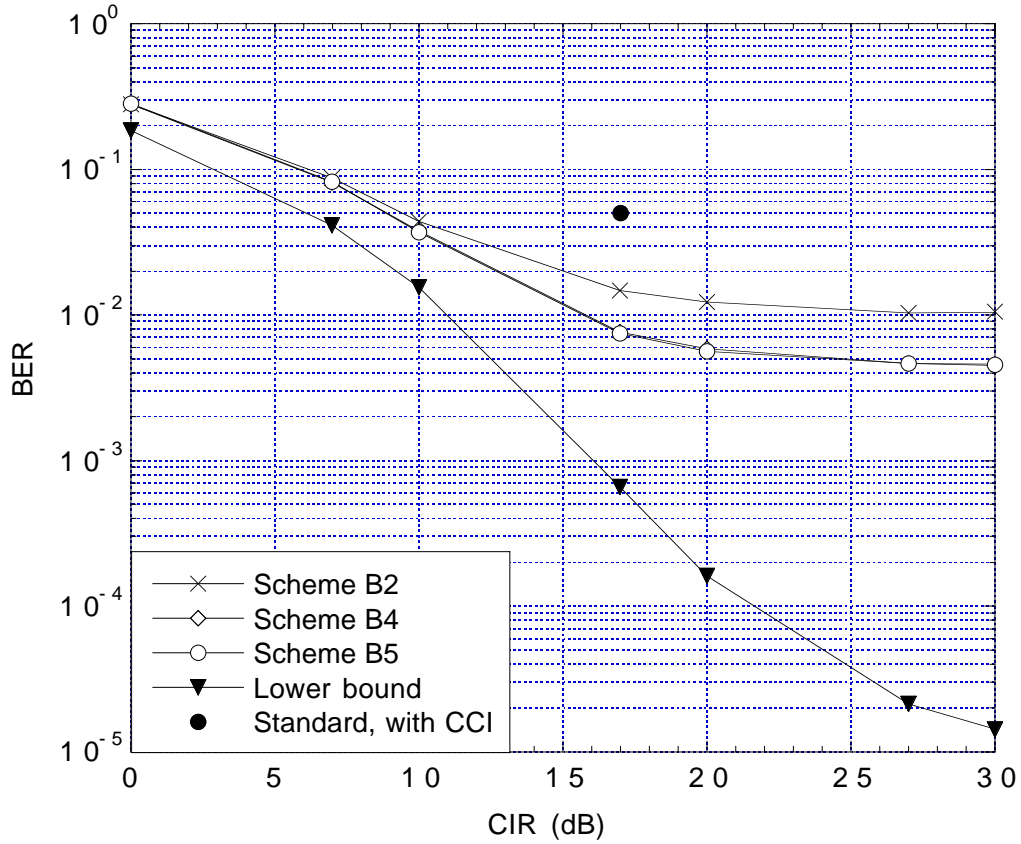


**Figure 5.14:** DDFE receiver with blind channel estimation

performance than the LE receiver in general. Between the two DFE receivers, the BER performance of the curve fitting DFE receiver surpasses that of the DDFE receiver at the high CIR region due to the fact that the curve fitting DFE receiver provides a more accurate interpolated channel than the DDFE receiver.

Comparing the curves in Figures 5.14, 5.15, 5.16 and 5.17, the BER performance is similar at low CIR, in particular, at 0 dB CIR, regardless the type of receiver and the channel sample insertion scheme used. In this region the CCI power is high and the effect of CCI dominates. With only the channel information from blind data and channel estimation, the receivers cannot suppress CCI. This accounts for the similar poor BER performance in the low CIR region for all the receiver types and all insertion schemes.

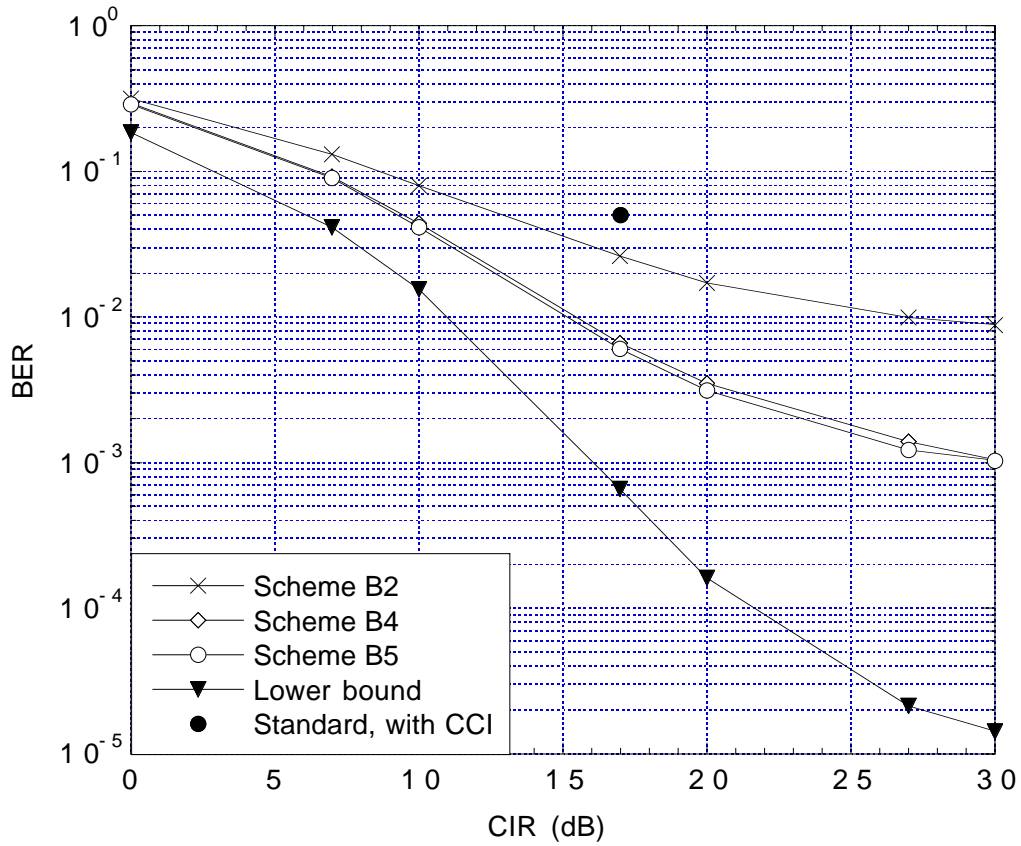


Figure 5.15: Curve fitting DFE receiver with blind channel estimation

#### 5.2.4 MSE of Receivers with DLE

The theoretical MSE analysis of DLE receivers presented in Section 3.4 was intended for the IS-136 application. However, in the course of the mathematical development, some elements in the transmitter, which are different from the IS-136 specification, have been used in order to simplify the analysis and, more importantly, derive an expression for the MSE of the DLE receiver on fading channels. These elements include a BPSK encoder and a rectangular pulse with zero roll-off in the transmit filter. In addition to simplifying the mathematics, adopting a transmit filter with zero roll-off is also critical since the LE can be the optimum receiver only if the channel is band-limited in the interval of  $[-1/2T, 1/2T]$  [72]. Despite

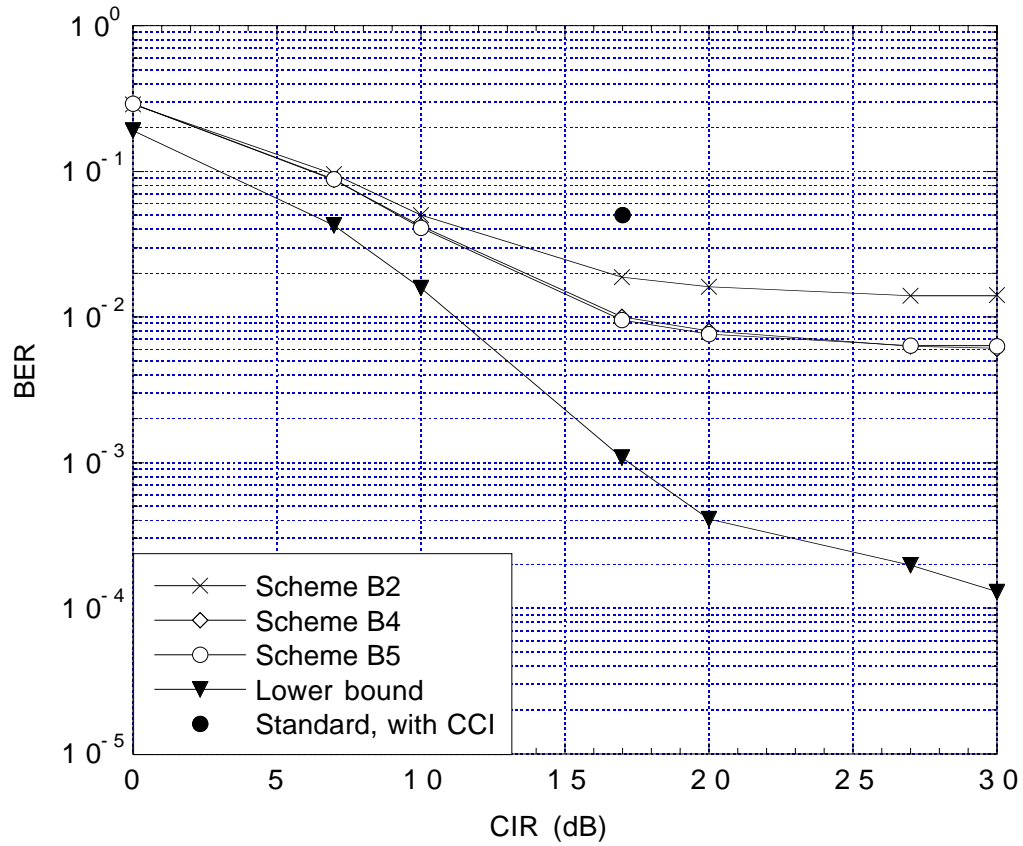
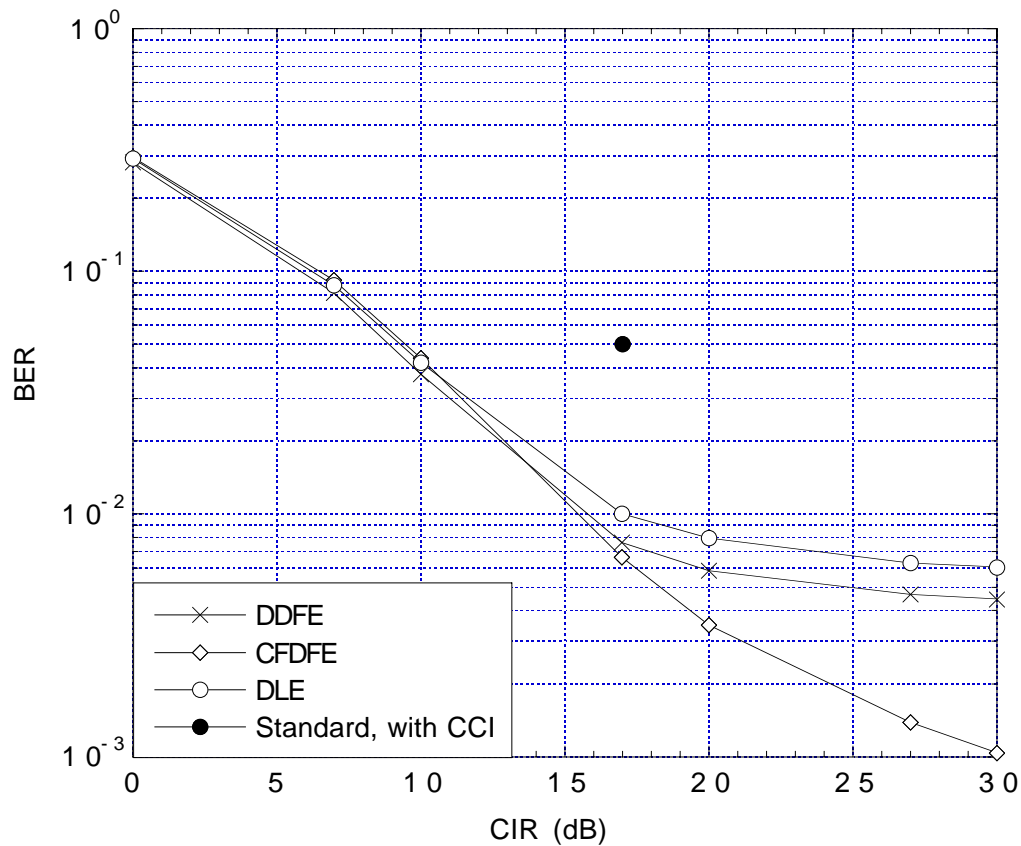


Figure 5.16: DLE receiver with blind channel estimation

these differences, the shape of the MSE curve should remain the same as simulation results, and it can serve as a reference. Therefore, the MSE performance of the DLE receiver of this modified system, obtained by means of theoretical analysis and computer simulations, is presented in this chapter for comparison purposes.

#### 5.2.4.1 Average MMSE

An expression of average MMSE for the infinite LE on time-varying channel was derived in terms of input SNR, and it is given in Equation 3.138. This theoretically derived average MMSE on time-varying channel is plotted in Figure 5.18. For comparison purpose, the average MMSE obtained by means of simulation and the



**Figure 5.17:** Blind channel estimation receivers with scheme *B4*

MMSE of an AWGN channel are also plotted against the input SNR, on the same figure.

The average MMSE of a simulated LE is obtained from the simulation of a baseband communication system with LE receiver, similar to the one described in Figure 3.12, averaging over 4000 channels. In the simulation, the LE receiver has finite length and its optimum coefficients are derived iteratively using the LMS adaptive algorithm. Since both equalizers, the LE with infinite length in the theoretical analysis and the simulated LE with finite length, are optimized in the MSE sense, in the presence of channel noise, they cannot completely eliminate ISI. Therefore, the output of both equalizers contains residual ISI, as well as additive noise. At low SNR, the high noise power results in significant MMSE at the output of both LEs,

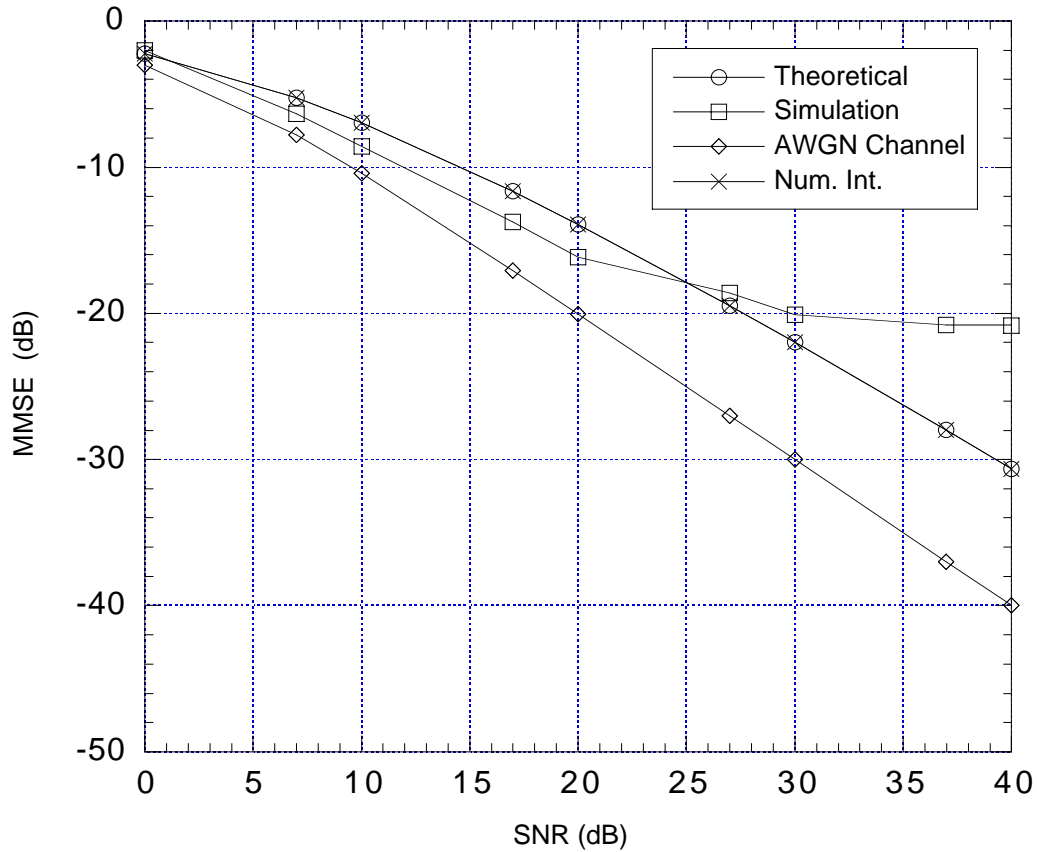


**Figure 5.18:** MMSE for infinite LE

as shown in Figure 5.18. Insufficient averaging of the simulated MMSE accounts for the discrepancy between the two MMSE curves in the low SNR region. Since the theoretical MMSE averages over all possible channels, it represents the mean of the MMSE of an LE with infinite length. As the number of channels used in the computer simulation increases, the simulated average MMSE approaches the theoretical average MMSE asymptotically. At high SNR, the MMSE curve of the finite length LE becomes flat due to the fact that an LE with finite length is inadequate to compensate for the ISI on the channel with spectral nulls. Thus, the ISI at the output remains, even though the noise power is low, and this may lead to serious performance degradation. On the other hand, the MMSE curve for the

LE with infinite length continues to fall as the SNR increases, which indicates that the residual ISI and noise level at the equalizer output decrease. In fact this optimum LE is equivalent to the cascade of a matched filter and a transversal filter. The former reduces the noise effects and provides the principal correction factor when SNR is low. The latter reduces ISI and at high SNR, it attempts to suppress ISI [72]. Furthermore, the finite precision effect of the computer simulation on the simulation result also contributes to the flattening of the simulated average MMSE at high SNR.

The MMSE of an AWGN channel is derived from a special group of channels: the channel consists of an impulse and AWGN. The MMSE of such channels is given by the following equation:

$$\varepsilon_{\text{AWGN},\min} = \frac{1}{1 + \gamma_{\text{in}}}, \quad (5.1)$$

which represents the lowest MMSE attainable by an LE. The derivation of Equation 5.1 is shown in Appendix C. As shown in Figure 5.18, the MMSE of an AWGN channel and the theoretical average MMSE are similar in shape and they both approach zero as  $\text{SNR} \rightarrow \infty$ . Since the channel has only one single tap, there no residual ISI at the output of the LE, and this accounts for the discrepancy between the two MMSE curves: for an MMSE level of 30 dB, the LE requires 9 dB higher in SNR in order to recover the signal from both ISI and noise.

For the purpose of verifying theoretical derivation of the average MMSE of the infinite LE on time-varying channels, a different approach is taken to evaluate the expression in Equation 3.130:  $\varepsilon_{\text{V},\min}(t)$  is first obtained by evaluating the angle bracket analytically, followed by the evaluation of the mathematical expectation using 4-dimensional numerical integration. The angle bracket is an averaging process

over frequency, and its evaluation is given in Appendix A. Since the time-varying channel in the MSE analysis is assumed to have two taps with complex values, there are four variables for the time-varying channel. In order to evaluate the expectation in Equation 3.130, with respect to the time-varying channel, 4-dimensional integration is required, and the details for 4-dimensional numerical integration is given in Appendix B.

The result of the numerical integration approach is also plotted in Figure 5.18. The average MMSE obtained numerically coincides with the theoretical average MMSE, which verifies the theoretical analysis performed in Chapter 3.

#### 5.2.4.2 Average MSE

The MMSE of an LE can be achieved at the symbol period where the perfect channel estimate is available. In the case of a time-varying channel, the MSE will exceed the MMSE at any other point if the LE receiver is fixed. An expression for the average MSE is derived in Chapter 3, and the average MSE in Equation 3.185 is a function of input SNR  $\gamma_{in}$ , the Doppler frequency  $f_m$  and the time difference  $\Delta t$ . In Figure 5.19, the average MSE is plotted against the time difference at various values of SNR for a vehicle speed of 100 km/hr. All these curves are parabolic in shape, and the MSE grows as  $|\Delta t|$  increases. Since, on average, the channel changes more as it moves away from the point where the perfect channel estimate is available, the performance of the receiver which is only optimum with respect to the perfect channel estimate, becomes worse.

It can also be observed that as  $|\Delta t|$  increases, the MSE increases as the noise level reduces. In fact, as  $N_o \rightarrow 0$ , Equation 3.185 yields an infinite MSE. This behavior is unusual, yet can be explained by the fact that an optimum LE in the sense of

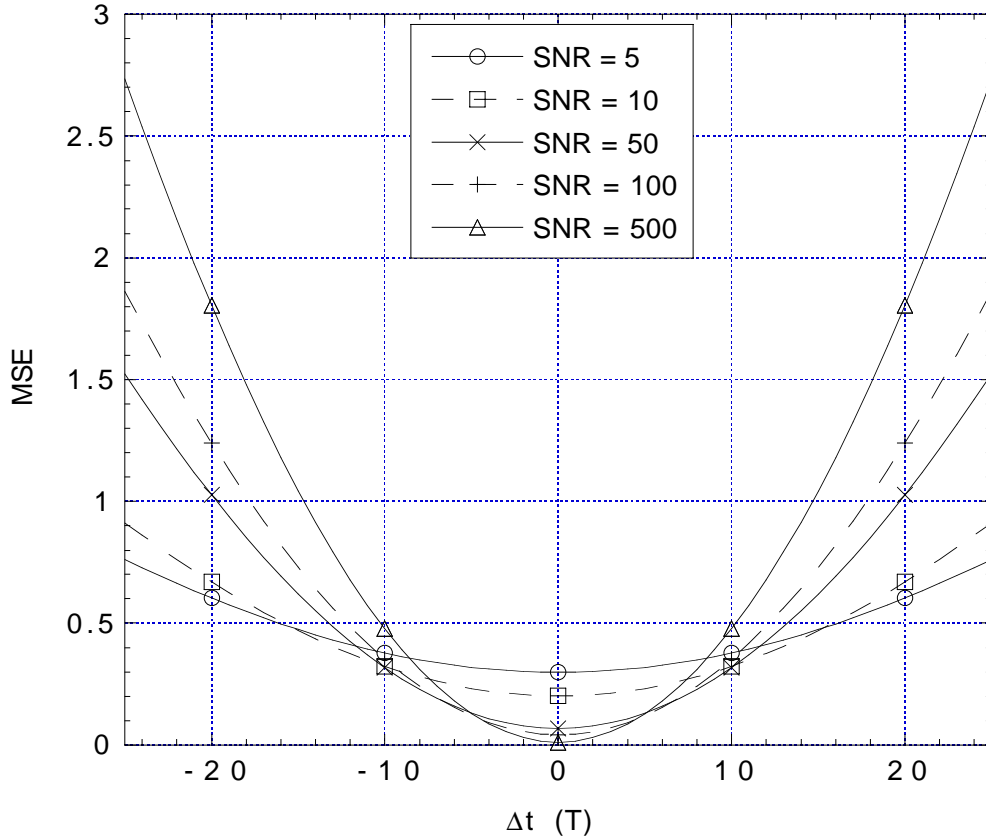


**Figure 5.19:** Average MSE at 100 km/hr, theoretical analysis

minimizing MSE is acting as a zero-forcing filter in the absence of noise in order to suppress ISI. Since the channel consists of two time-varying channel taps, this time-varying channel exhibits spectral nulls, which occur at different frequencies at different time. Figure 5.20 shows four channel and receiver pairs at different values of SNR and  $|\Delta t|$ . The spikes in the frequency response of the LE at an SNR of 30 dB are larger than that at an SNR of 10 dB since the amount of noise at the spectral nulls are much smaller in the case of 30 dB SNR. In the extreme case, the magnitude of this spike approaches infinity as the channel noise disappears. At  $\Delta t = 0$ , this optimum LE strikes a balance between reducing noise and ISI, and the error at the output is low. At  $|\Delta t| \gg 0$ , this LE is no longer optimum and the nulls of the time-varying channel have shifted away from the frequencies where

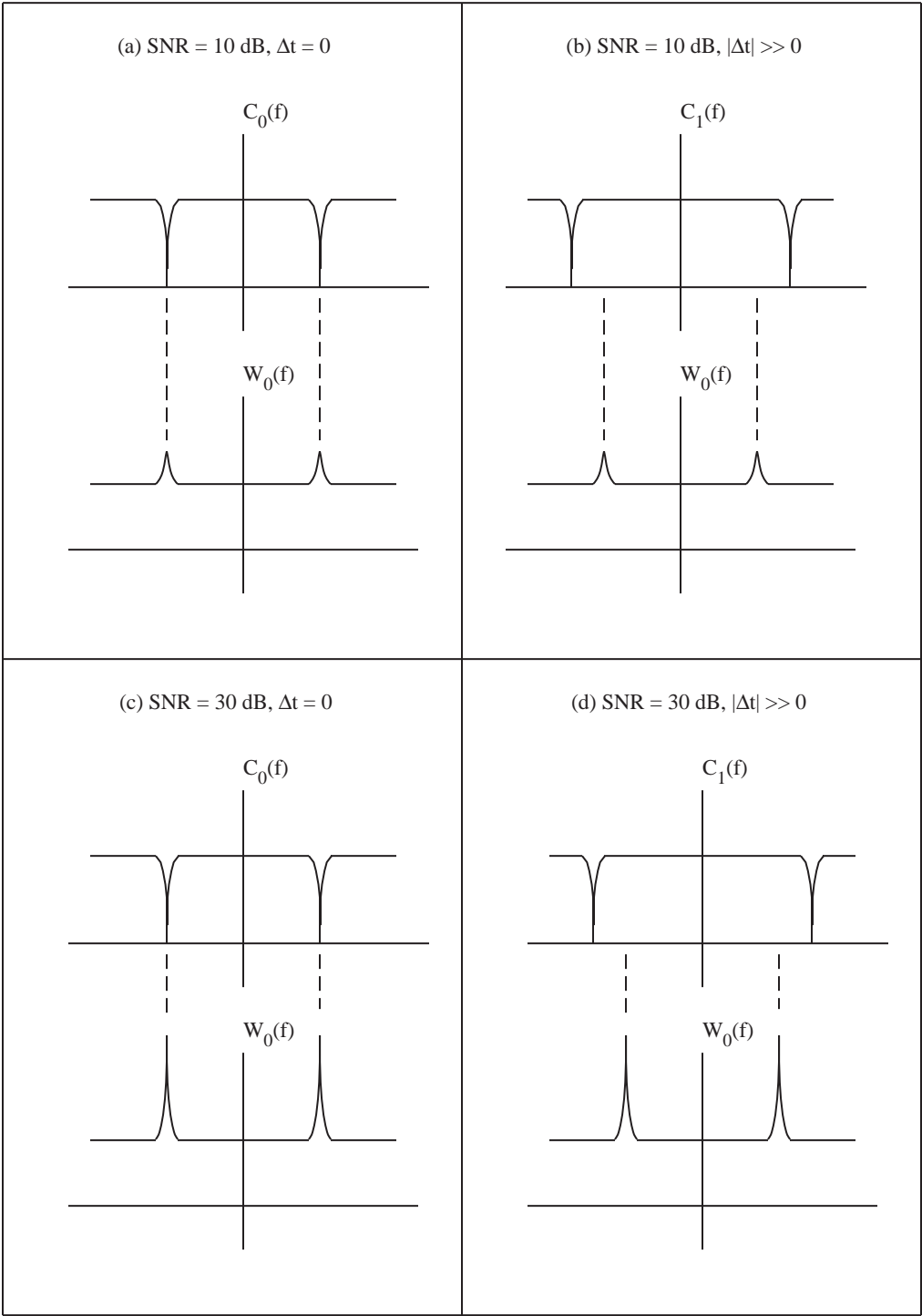
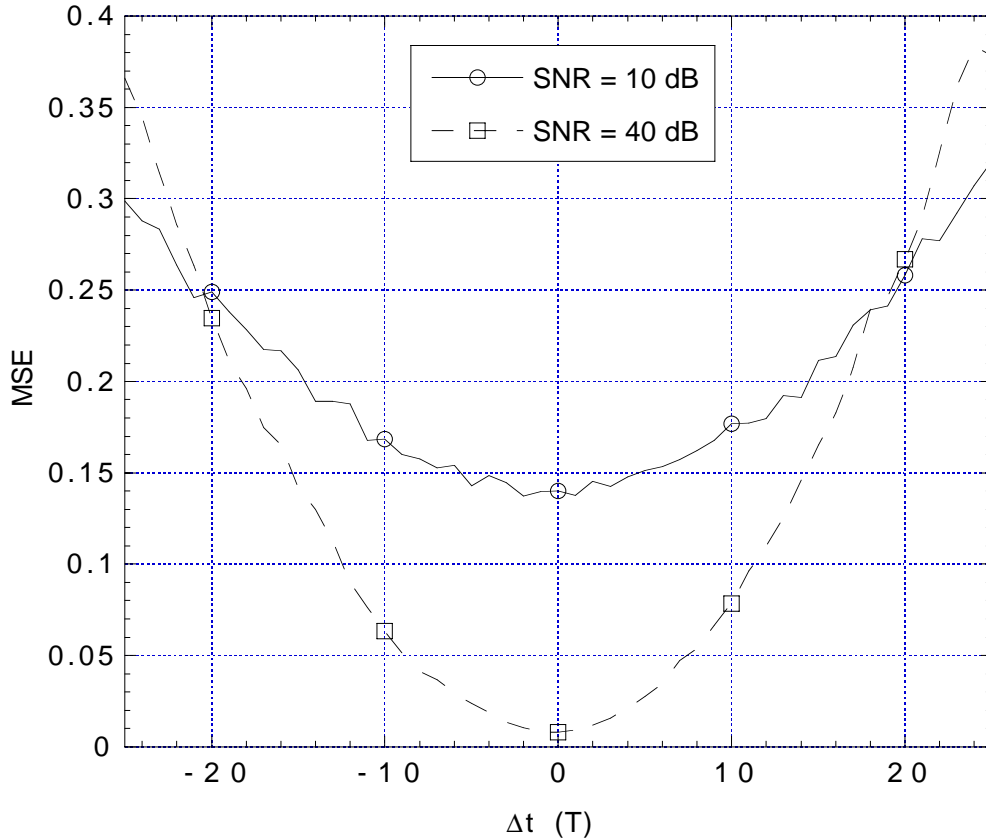


Figure 5.20: Channel and receiver pairs at various SNR and  $|\Delta t|$

the spikes of the LE appear. As a result, at high SNR, the signal at the output of the LE gained a large amount of power, and the error is high compared with the transmitted data with average power of one.



**Figure 5.21:** Average MSE at 100 km/hr, simulation result

Figure 5.21 and Figure 5.22 shows the simulation and theoretical results, respectively, of the average MSE as a function of  $\Delta t$  at two different levels of SNR and a vehicle speed of 100 km/hr. The simulation results are consistent with the theoretical analysis: both average MSE curves are parabolic in shape, and the average MSE at an SNR of 10 dB crosses the one at an SNR of 40 dB. In the case of computer simulation, the two average MSE curves cross at  $\Delta t = 20T$ , whereas the two theoretical average MSE curves at 10 dB and 40 dB input SNR cross at  $\Delta t = 5.5T$ . This can be accounted for by the insufficient averaging of the simulation

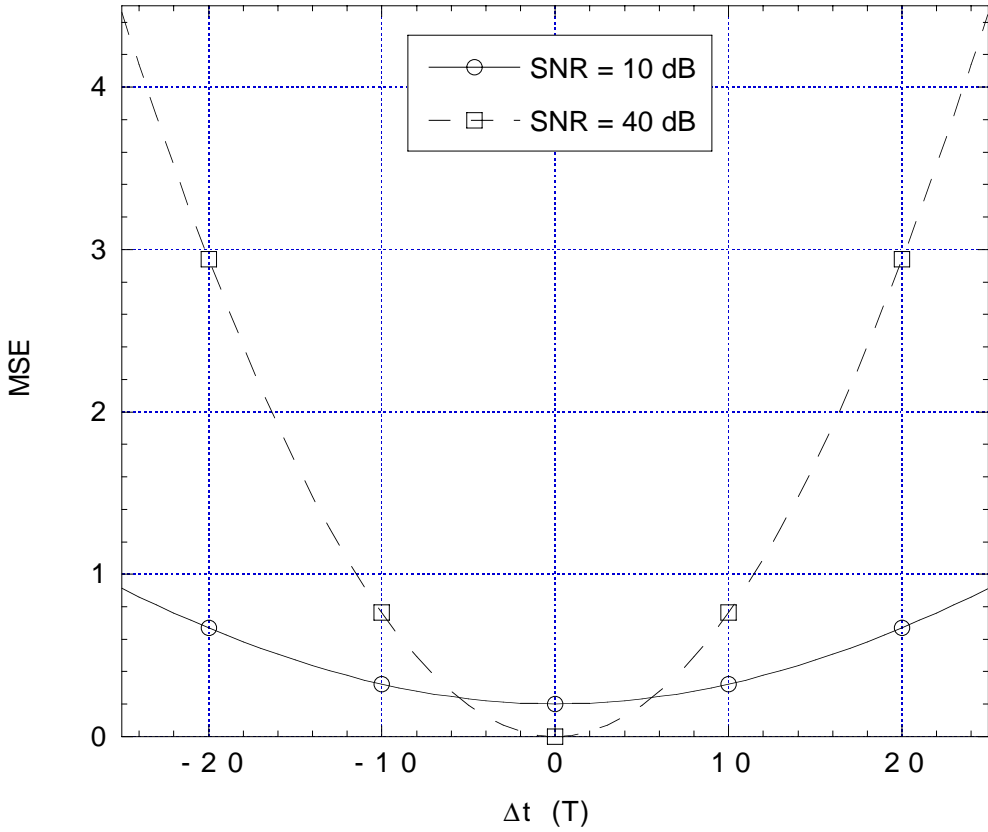
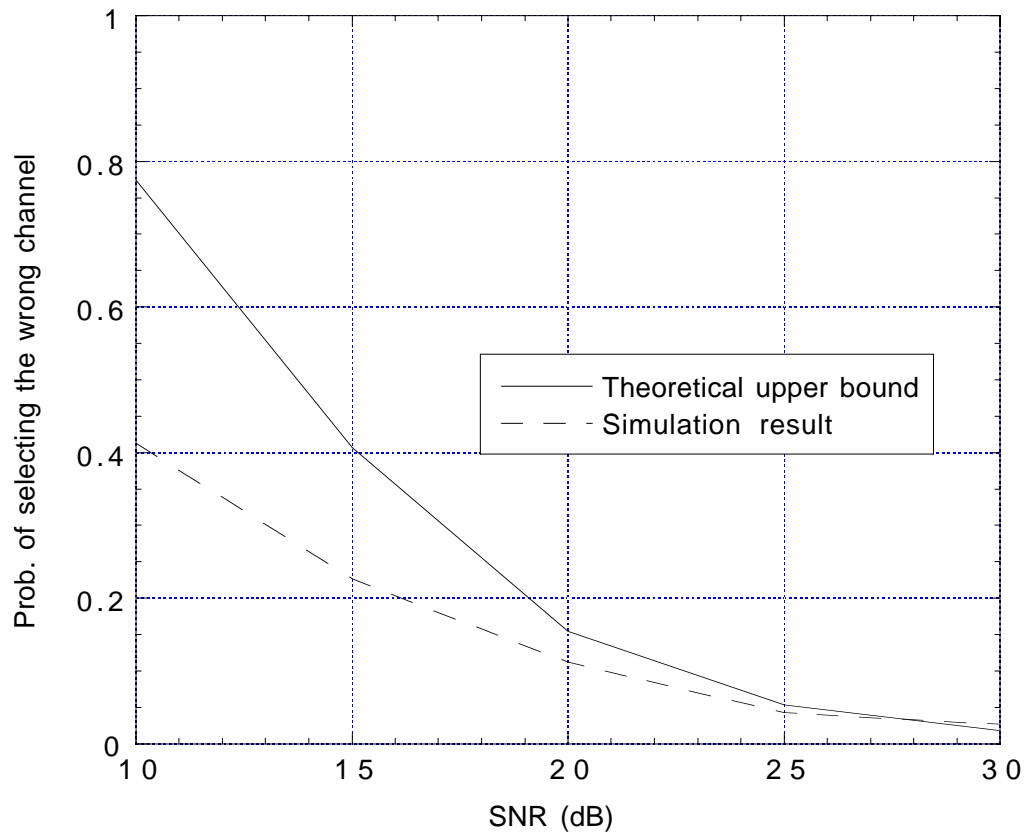


Figure 5.22: Average MSE at 100 km/hr, theoretical result

Results and the finite precision effect of the computer.



**Figure 5.23:** Probability of error in blind channel estimation

### 5.2.5 Probability of Error in ML Blind Data and Channel Estimation

In the process of blind ML data and channel estimation, errors can occur due to the channel noise. In particular, at low SNR, a data and channel pair, which is different from the actual pair, could be selected. The resulting error in channel estimation degrades the system performance.

In Chapter 3, theoretical analysis on the probability of selecting the correct channel estimate using the blind ML data and channel estimation method was performed and an upper bound on the probability of error was derived. This upper bound is plotted in Figure 5.23, and compared with the average probability of error

in blind ML channel estimation obtained by means of simulations.

Note that, in the expression of the upper bound in Equation 3.59,  $d_{\min}$ , which is the distance between the received signal  $r_o$  and the closest possible received signal, is difficult to determine theoretically. Therefore, the value of  $d_{\min}$  used to calculate the upper bound is determined by computer simulations. Since the value of  $d_{\min}$  and, consequently, the upper bound of the probability of error depend on the time-varying channel, the theoretical upper bound plotted in Figure 5.23 is averaged over different values of  $d_{\min}$ , corresponding to different random channels.

It is found that the upper bound for the probability of error is above the simulation result at almost all SNR levels shown, except for 30 dB of SNR, where insufficient averaging might have occurred. It can also be observed that the gap between the curves becomes larger as SNR decreases. This can be explained by the validity of the assumption made in the theoretical analysis: the channel estimation error due to noise and the channel noise are independent. For high SNR, the correlation between the estimation error and the channel noise is insignificant and can be neglected. Therefore, the assumption is valid at high SNR. At low SNR, the correlation becomes more significant as the noise power increases and  $\sigma_{r_o}^2$ , the variance of the sum of the estimation error and the channel noise, given in Equation 3.54 becomes less accurate. Furthermore, the erf function and the power operation in the upper bound expression are highly non-linear. They can magnify any small change in value in the argument, which results in large change in the upper bound. Therefore, this upper bound is not accurate at low SNR.

## 5.3 Discussion

The discussion in this section on the comparison of various receiver types can be divided into two parts. The first deals with the performance issue and the second deals with the complexity issue.

### 5.3.1 Performance Issues

#### 5.3.1.1 DDFE, DLE and Curve Fitting DFE

In general, the performance of a DFE receiver is better than an LE receiver, as shown in Figures 5.2, 5.12 and 5.17. This is true for the lower bounds and the partial bounds for receivers with or without information on the co-channel. It is also true for receivers using channel samples that are estimated perfectly or estimated by using the ML blind data and channel estimation method. This can be explained by the fact that a DFE receiver is capable of cancelling ISI, as well as CCI if co-channel information is provided, with its feedback mechanism, which is not present in an LE receiver.

Between the two DFE receivers, since the curve fitting DFE receiver adopts a cubic spline model to interpolate the channel, its interpolated channel is more accurate than that of the DDFE receiver, which is only a zeroth order approximation of the physical channel. Consequently, at high SNR regions where the channel estimates are relatively more accurate, the BER performance of the curve fitting DFE receiver is better, as shown in Figures 5.12 and 5.17.

#### 5.3.1.2 Lower Bounds, Partial Bounds and Blind Channel Estimation

Figures 5.24 and 5.25 show a comparison of the lower BER bound, the partial bound and BER performance of receiver using blind channel estimation for a DLE

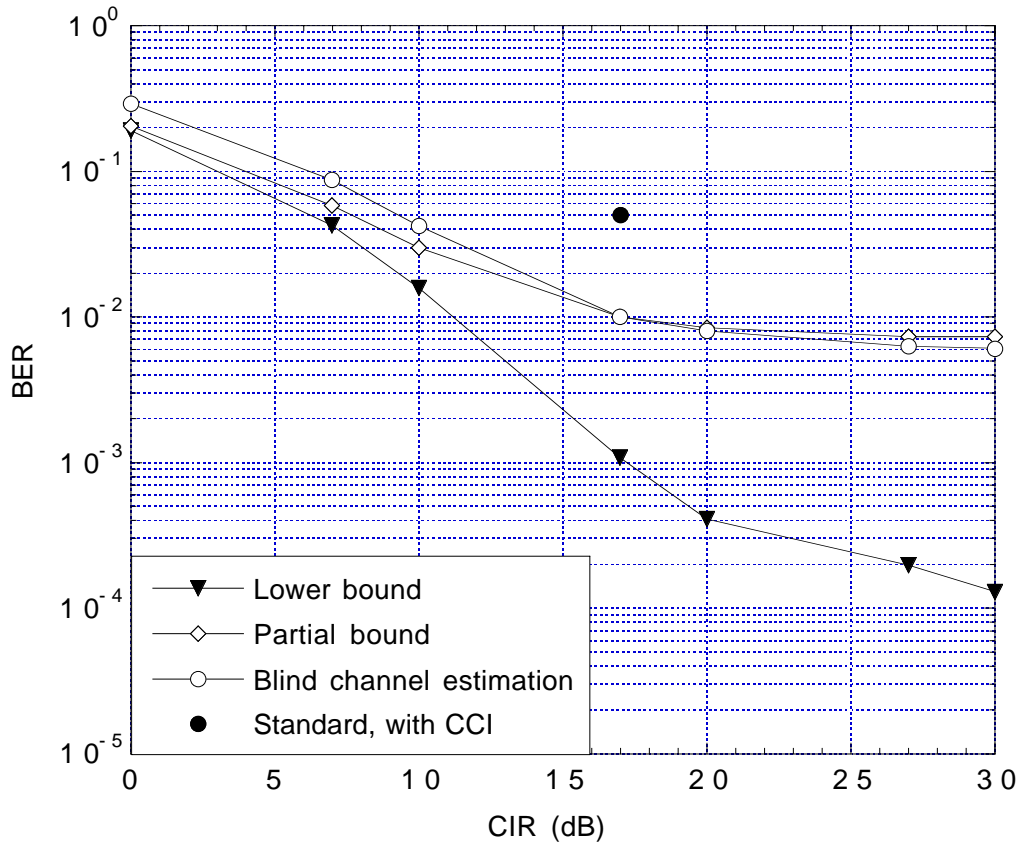


**Figure 5.24:** DLE receiver performance for scheme *B4*

receiver and a DDFE receiver, respectively. In the case of partial bound and receiver using blind channel estimation, channel sample insertion scheme *B4* is used. The gap between the lower bounds and the partial bounds shown in both figures is mainly caused by interpolation errors in the partial bounds. The fact that the displaced equalizers adopt a piece-wise channel interpolation model accounts for the big gap between the lower bounds and the partial bounds.

Note that the partial bounds and the BER curve of a receiver using blind channel estimation cross each other in both figures. This behavior can be explained by the non-linearity in the relationship between the MSE and the BER. In the case of the partial bound, the channel samples in a time slot are estimated without error and, thus, the MSE of the channel samples are minimized. However, it is by no means

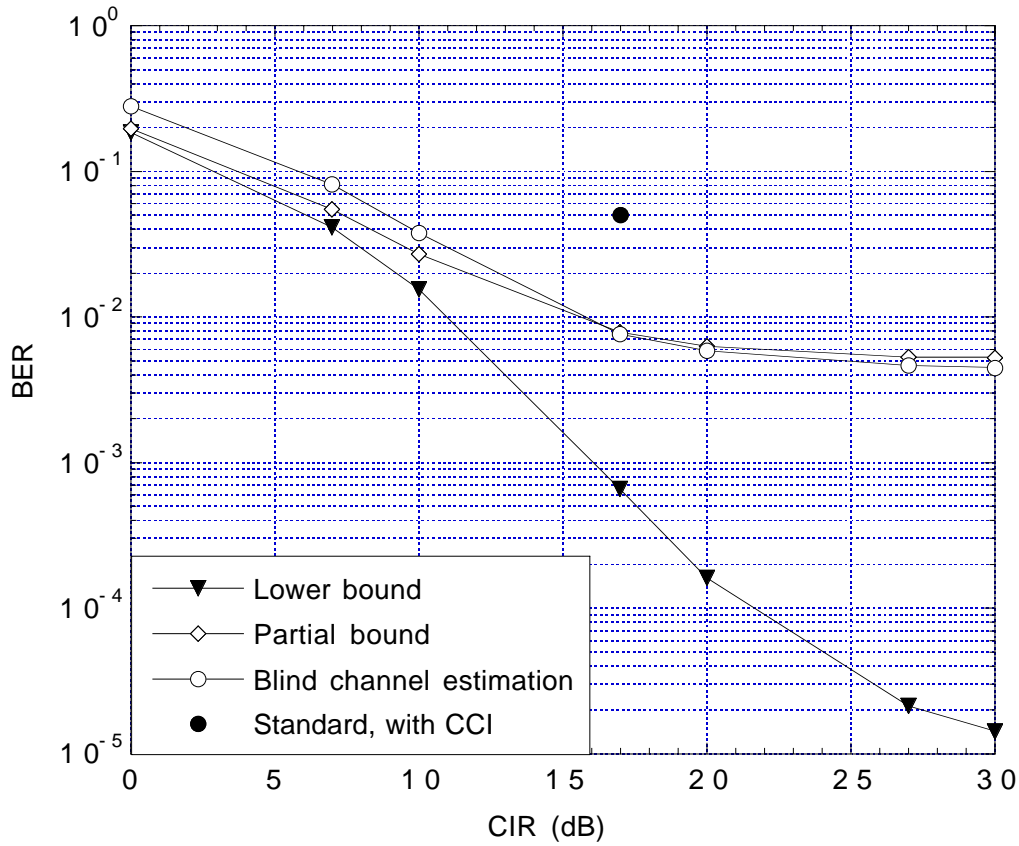


**Figure 5.25:** DDFE receiver performance for scheme *B4*

certain that such a system achieves minimum probability of error. In fact, a channel estimate that gives the lowest probability of error can be found by optimization under the criterion of minimum error probability, which is a rather complex task involving the solution of non-linear equations [11]. Therefore, it is possible for the BER performance of the receiver using blind channel estimation to be better than the partial bounds.

Figure 5.26 shows a comparison of the lower BER bound, the partial bound and BER curve of the curve fitting receiver using blind channel estimation for insertion scheme *B4*. The fact that the lower bound and the partial bound are close to each other indicates that the error in the interpolated channel reconstructed using the cubic spline curve fitting method is minimal. With blind channel estimation, the

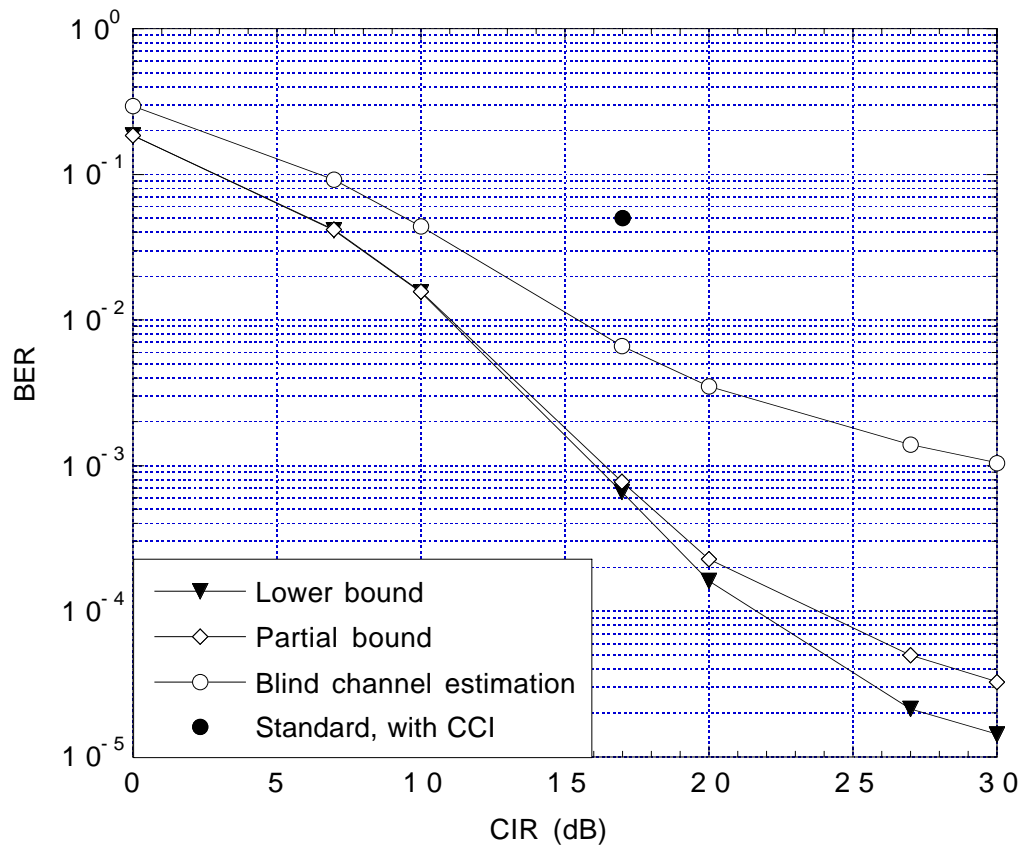


**Figure 5.26:** Curve fitting DFE receiver performance for scheme *B4*

BER curve is much further away from the two bounds. One can observe that with an accurate channel estimate, the channel interpolation error is minimal. However, for a channel estimate with relatively large estimation error, such as the one obtained by using the blind channel estimation method, the estimation error is amplified by the interpolation process, resulting in larger interpolation error. Therefore, the BER performance of the curve fitting DFE is more sensitive to estimation error than the DDFE and DLE.

## 5.3.2 Complexity Issues

### 5.3.2.1 Complexity Measure

The computational complexity of a channel estimation method is usually measured in terms of the number of operations. In the two following sections, Sections 5.3.2.2 and 5.3.2.3, the complexity of the blind channel estimation method and the blind channel and co-channel estimation method will be discussed and compared. The number of operations involved in these two methods is large and it is inconvenient to use such a small unit. Additionally, measuring the complexity of a particular estimation method is mainly for comparison purposes, and it is not necessary to measure the complexity strictly to the exact number of operations. Since both of these two channel estimation methods involve in large number of LSSE channel estimations, in the two following sections, the computational complexity will be measured and compared in terms of the number of LSSE channel estimations.

### 5.3.2.2 Blind Channel Estimation

Channel samples within a time slot can be added by using the blind channel estimation method. As discussed in the earlier sections, the number of channel samples added is dictated by the trade-off between complexity and performance.

Among all the insertion schemes discussed in Section 5.2.2.2, the partial DDFE and curve fitting DFE bounds plotted in Figures 5.6 and 5.7, respectively, show that a minimum of two channel samples need to be inserted, in order to meet the performance criterion. Therefore, the complexity can only be reduced by shortening the estimation sequence with a penalty in performance.

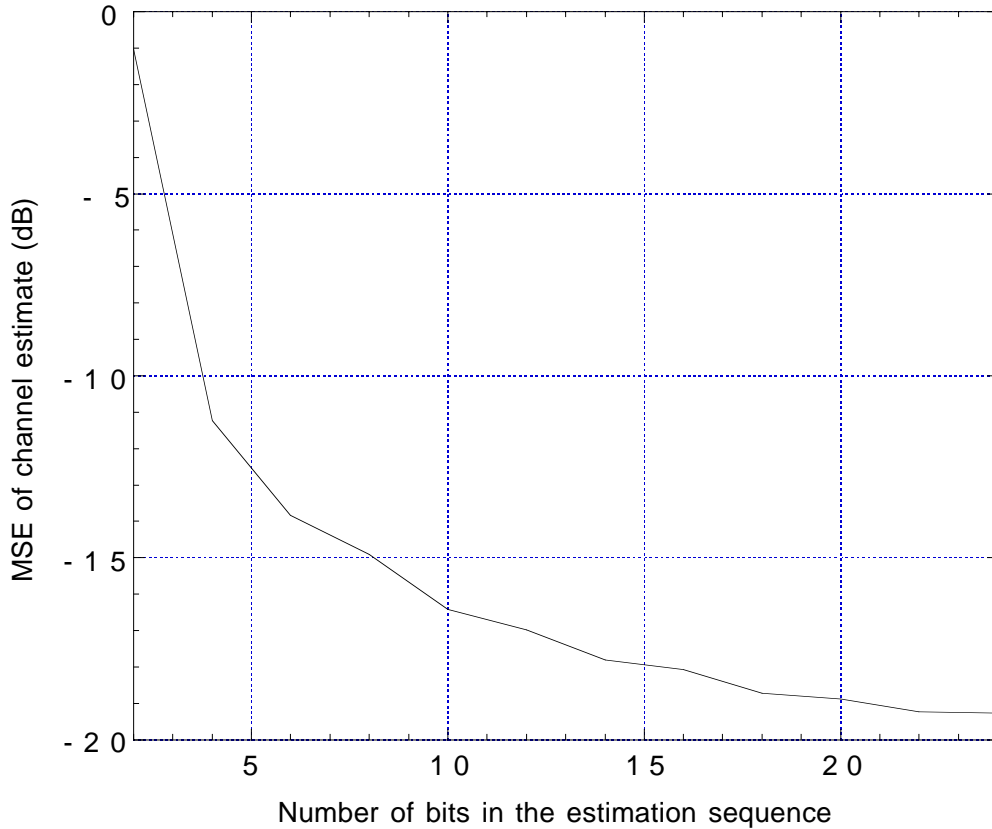


**Figure 5.27:** MSE of channel estimate vs. length of estimation sequence

Figure 5.27 shows the MSE of channel estimate as a function of the number of bits in the estimation sequence at  $\text{SNR} = 30$  dB,  $\text{CIR} = 17$  dB and  $v = 100$  km/hr. The MSE of the channel estimate is given by Equation 4.12 and the MSE curve is obtained by averaging over 10000 channels. As shown in the figure, reducing the number of bits in the estimation sequence from 12 to 10 causes a loss of only 0.5 dB in MSE. This means the number of LSSE channel estimation involved can be reduced by a factor of 4. However, due to the non-linear relationship between MSE and BER, the degradation in terms of BER performance equivalent to the 0.5 dB loss in MSE is not clear. The degradation in BER performance can be determined by means of simulations.

Among the insertion schemes with two channel samples inserted in a time slot,

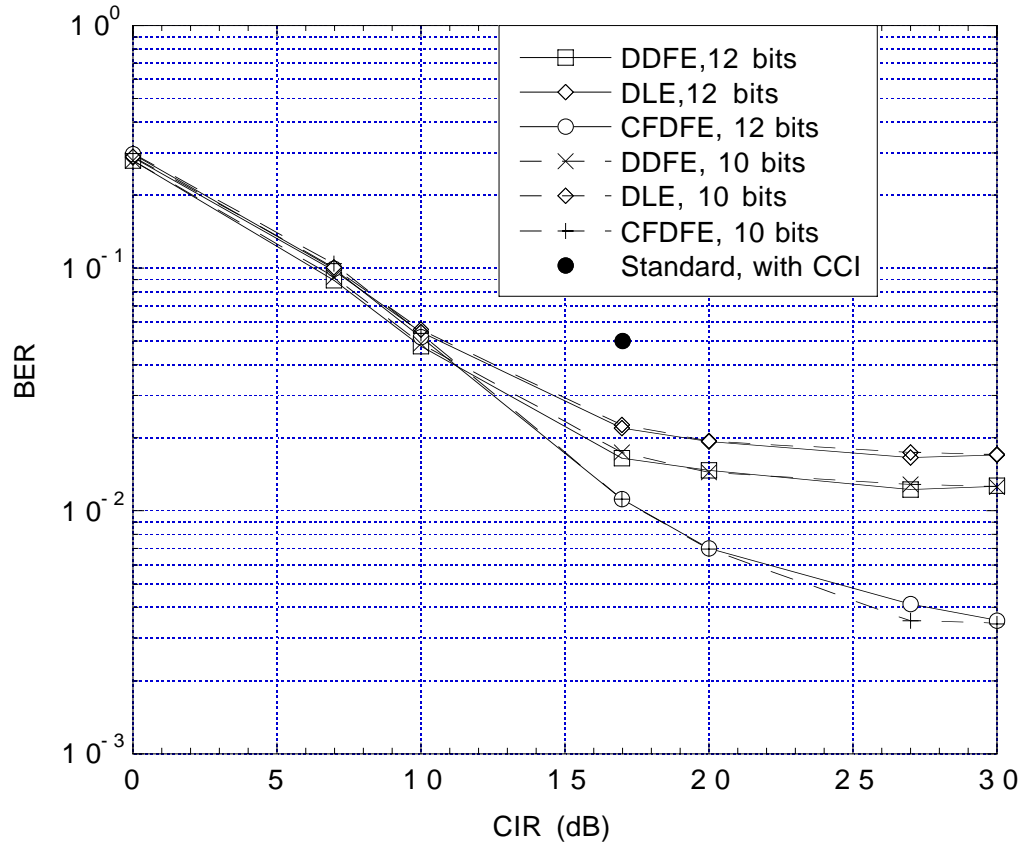


**Figure 5.28:** BER performance for scheme A2

scheme A2 gives the best performance. Therefore, the complexity and BER performance of scheme A2 is used as a reference. Figure 5.28 shows the BER performance of receivers where scheme A2 is adopted, with 12 bits or 10 bits in the estimation sequence. The BER curves are obtained for the DDFE, DLE and curve fitting DFE receiver schemes. For all three types of receivers, the BER performance of a receiver with 10 bits in the estimation sequence is similar to that with 12 bits. Therefore, the complexity of the blind channel estimation process can be reduced significantly from  $2^{12}$  to  $2^{10}$  LSSE channel estimations without severe degradation in the BER performance.

Alternatively, with the same complexity, the number of bits in the estimation sequence can be reduced, so that more channel samples obtained from the blind

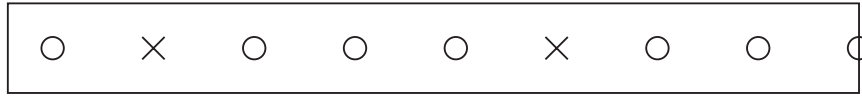


**Figure 5.29:** Insertion scheme *B6*

channel estimation method can be added to the time slot to improve the performance. Suppose the number of bits in the estimation sequence is reduced from 12 bits to 10 bits. Without changing the complexity, the number of channel samples obtained from blind channel estimation can be increased from 2 to 8. These 8 channel samples can be arranged in a time slot as shown in Figure 5.29, and this new insertion scheme is called scheme *B6*.

Figure 5.30 and Figure 5.31 show the BER performance of scheme *B6* with 10 bits in the estimation sequence, in comparison with that of scheme *A2* and scheme *B4* with 12 bits in the sequence, respectively. Scheme *B6* offers far more superior BER performance at higher CIR than scheme *A2*. In fact, the BER performance of scheme *B6* is also better than that of scheme *B4*, despite the fact that scheme *B4* with 12 bits in the estimation sequence requires larger number of LSSE channel estimations. Therefore, with the same or less computational requirement, better BER performance can be achieved by reducing the number of bits in the estimation sequence and adding more channel samples in a time slot.

In summary, Table 5.1 shows a comparison in complexity of the blind channel estimation method, in terms of the number of LSSE channel estimations, and BER performance for different insertion schemes, with different number of bits in the estimation sequence, at a vehicle speed of 100 km/hr and 17 dB CIR. The data in the table suggest that the computational requirement of the blind channel estimation method can be eased by reducing the number of bits in the estimation sequence.

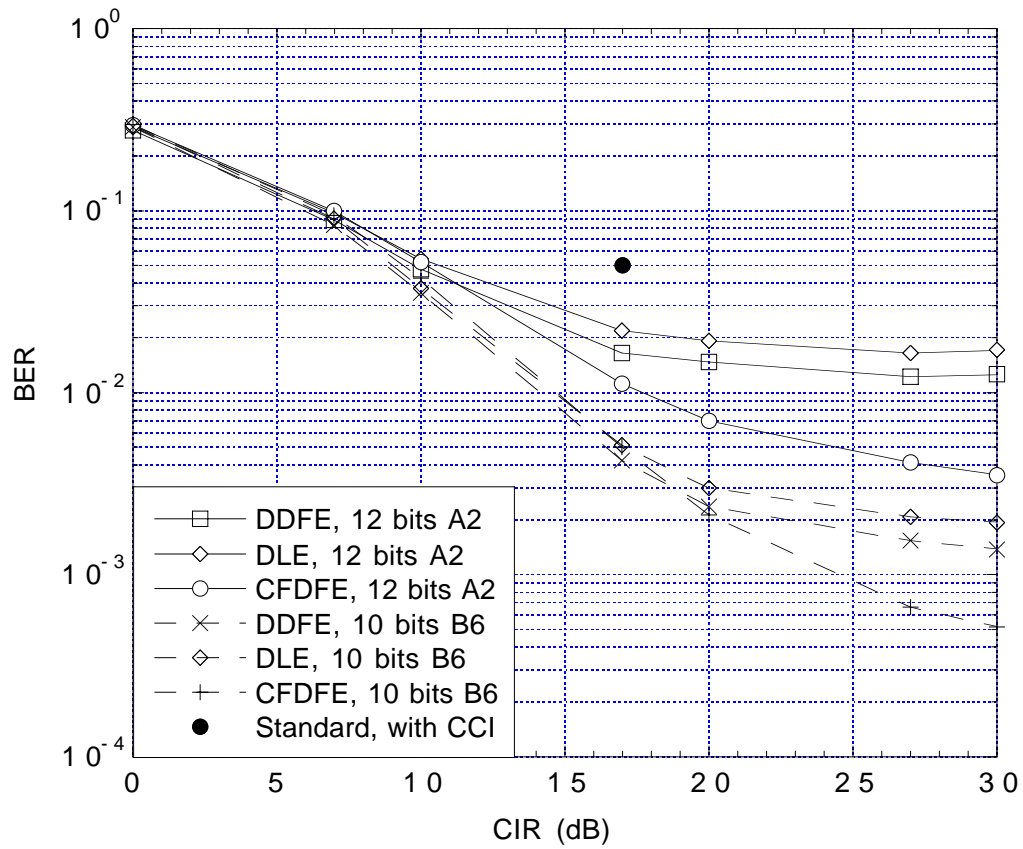
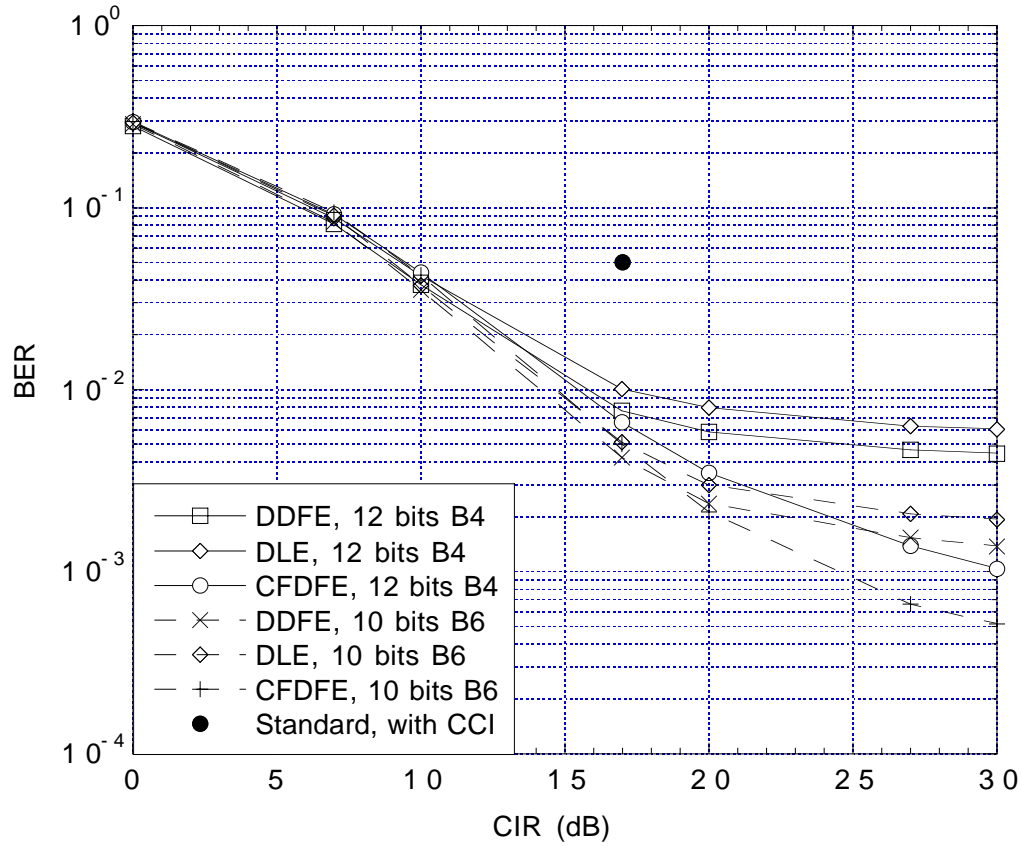


Figure 5.30: BER performance for scheme *A2* and *B6*

### 5.3.2.3 Blind Channel Estimation and Blind Channel and Co-channel Estimation

In this section, the computational requirement of blind channel estimation and blind channel and co-channel estimation methods, in terms of number of LSSE channel estimations is compared. Since the simulation results of the BER performance of a receiver using the blind channel and co-channel estimation method are not available, due to the intensive computational requirements, BER performance discussed in this section is limited to partial bounds only, in which case the channel and co-channel are assumed to be estimated without errors.

If two estimation sequences of 10 bits are used, one for channel and the other



**Figure 5.31:** BER performance for scheme *B4* and *B6*

for co-channel estimation, the number of LSSE channel estimations involved in obtaining a pair of channel and co-channel samples is  $2^{20}$ . This is  $2^{10}$  times more complex than the blind channel estimation with an estimation sequence with the same length. Figure 5.12 shows a comparison of partial bounds of a system using both estimation methods, for all three receiver types and insertion scheme *B4*. With the blind channel and co-channel estimation method, a system gives better BER performance at low level of CIR, especially for the curve fitting DFE receivers. This performance advantage vanishes as the level of CIR at which the system is operating improves. Assuming the difference in estimation errors associated with both channel estimation methods are similar, the performance advantage offered by the blind channel and co-channel estimation method cannot justify its computational cost.

Scheme	BER (%)			Computational Complexity (# of LSSE channel estimations)
	DDFE	DLE	CFDFE	
A2, 12 bits	1.6454	2.1878	1.1226	$2 \times 2^{12} = 8192$
A2, 10 bits	1.7415	2.2607	1.1158	$2 \times 2^{10} = 2048$
B6, 10 bits	0.4222	0.5122	0.5004	$8 \times 2^{10} = 8192$
B4, 12 bits	0.7637	1.0026	0.6617	$5 \times 2^{12} = 20480$

**Table 5.1:** Comparison in complexity and BER performance

Figure 5.32 shows a comparison of BER performance between scheme *B2* with co-channel information and scheme *B4* with no co-channel information for the three receiver types. Here, in scheme *B2* there are three pairs of channel and co-channel samples obtained by the blind channel and co-channel estimation method; whereas there are five channel samples from the blind channel estimation method in the case of scheme *B4*. At low CIR level, the receiver gives better BER performance when the blind channel and co-channel method is adopted. However, the computational cost to achieve this improvement in BER performance is increased from  $5 \times 2^{10} = 5120$  in scheme *B4* to  $3 \times 2^{20} = 3,145,728$  LSSE channel estimations in scheme *B2*. In the high CIR region, the BER performance of scheme *B4* with only channel samples available is much better than that of scheme *B2* with both channel and co-channel samples available. This example shows that, in the high CIR region, by inserting more channel samples in a time slot, instead making an effort to obtain the co-channel information, better BER performance can be achieved with less computational requirement.

Therefore, even though the co-channel estimate can be obtained and CCI can be explicitly suppressed by using blind methods, the cost is too high and the per-

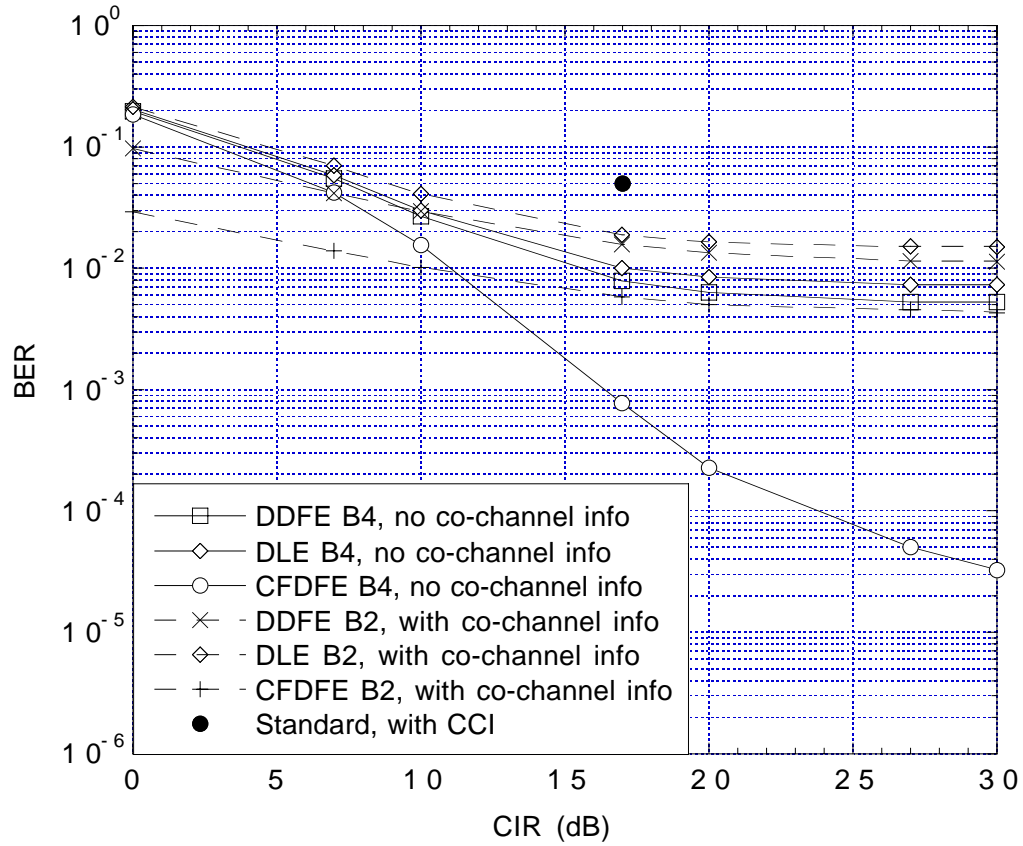


Figure 5.32: BER performance for scheme *B2* and *B4*

formance advantage is not significant enough to justify the cost.

#### 5.3.2.4 DDFE, DLE and Curve Fitting DFE

With the same channel estimation method, the number of operations involved in channel estimation is the same for different receiver schemes. The computational complexity of a receiver scheme mostly depends on the number of operations involved in computing the optimum equalizer tap coefficients. In this section, the “flop” is again used as the complexity measure.

The number of operations required to solve the Wiener-Hopf equations for the optimum equalizer coefficients is  $3(2N_h - 1)(2N_{ff} - 1) + \frac{2}{3}N_w^3 + \frac{3}{2}N_w^2 - \frac{1}{6}N_w$ , as

Receiver type	Operation count
DDFE/DLE	$N_s[3(2N_h - 1)(2N_{ff} - 1) + \frac{2}{3}N_w^3 + \frac{3}{2}N_w^2 - \frac{1}{6}N_w]$
Curve fitting DFE	$(\frac{2}{3}N_s^3 + \frac{3}{2}N_s^2 - \frac{1}{6}N_s) + [14 \times \frac{162}{N_b} + 12(N_s - 1)]$ $+ \frac{162}{N_b}[3(2N_h - 1)(2N_{ff} - 1) + \frac{2}{3}N_w^3 + \frac{3}{2}N_w^2 - \frac{1}{6}N_w]$

**Table 5.2:** Operation counts three receiver types

discussed in Section 4.4. This process is common to all three types of receivers. For the DDFE and DLE receivers, updates of the equalizer take place only when a channel sample is available. With  $N_s$  channel samples available, there are  $N_s$  updates of the equalizer coefficients. For the curve fitting DFE receiver, spline interpolation of the time-varying channel is involved, and this interpolation process is more complex than that in DDFE and DLE receivers. To solve the  $N_s$  equations in Equations 3.91, 3.92 and 3.93 for the  $N_s$  second derivatives  $u_i$ ,  $\frac{2}{3}N_s^3 + \frac{3}{2}N_s^2 - \frac{1}{6}N_s$  operations are involved. These second derivatives can be substituted back into Equation 3.90 to determine the interpolated channel at any time  $t$ . If the Doppler frequency is such that the equalizer coefficients need to be updated every  $N_b$  symbols,  $162/N_b$  interpolated channel samples are to be determined by using Equation 3.90, and the number of flops involved,  $N_f$  is

$$N_f = 14 \times \frac{162}{N_b} + 12(N_s - 1). \quad (5.2)$$

With  $162/N_b$  interpolated channel samples, the equalizer coefficients can be updated  $162/N_b$  times during a time slot.

The number of operations involved in determining and updating the equalizer tap coefficients for the three receiver types is tabulated in Table 5.2. With  $N_h = 20$ ,

$N_s = 7$ ,  $N_b = 6$  and  $N_{ff} = 5$ , number of operations required for a 5-5-3 DDFE is 19383 flops, for a 8-8 DLE is 29155 flops and for a 5-5-3 curve fitting DFE is 75514. From these figures and the BER performance of different receiver types, it can be concluded that the 8-8 DLE is indeed not a desirable solution for this particular application. For updating the equalizer tap coefficients, the curve fitting DFE receiver is almost four times more complex than the DDFE receivers, yet it offers excellent performance at the high CIR region. Furthermore, considering the overall complexity of the entire system, the operation count of the equalizer update is insignificant, compared with that in blind channel estimation. Therefore, the choice of receiver type depends on the specific application.

To reduce the number of matrix inversions involved in the curve fitting DFE method, a second approach to determining the optimum tap coefficients is attempted. In this approach, the optimum equalizer tap coefficients are first determined where the channel samples are available, then the tap coefficients are interpolated with the spline curve fitting method, as opposed to the first approach, where channel interpolation followed by tap coefficients computation takes place. It is found that the second approach is not feasible since the equalizer tap coefficients determined from this approach are different from the first approach. Interpolation and computation of the tap coefficients, are involved in both approaches. The only difference is the order in which these two processes take place. If both processes were linear, interchanging the order of these processes would result in the same tap coefficients at any time in the time slot. Matrix inversion involved in the optimum tap coefficient computation is a non-linear process. Therefore, the resulting equalizer tap coefficients from this approach are not accurate.

# Chapter 6

## Conclusions and Future Work

### 6.1 Summary and Conclusions

The work in this thesis has investigated a variety of channel estimation and equalization techniques for TDMA cellular radio transmission over the fast time-varying selective fading channel. In this section, a summary of the work accomplished in this research thesis is presented and the conclusions about the channel estimation and equalization methods in different applications are also highlighted.

The issues that cause the degradations in TDMA cellular radio transmission include ISI, CCI and the fast time-varying nature of the radio channel. To fully characterize the time-varying channel within a TDMA time slot, channel estimation is first performed at some points during a time slot, then the time-varying channel is reconstructed by interpolation. In Chapter 3, new channel and co-channel estimation technique, together with the channel estimation techniques were discussed. It was proven that the sign ambiguity problem associated with the blind data and channel estimation method can be avoided by using differential encoding scheme.

In order to improve the system performance in a fast time-varying environment, a novel block adaptation with blind channel estimation strategy was developed, which involves in combinations of channel estimation and interpolation methods. Analysis was also performed on the probability of error in the ML blind data and channel estimation method and an upper bound for the probability of error was derived. To reduce the impact of ISI and CCI on the system performance, equalization is required. Two new equalizer updating techniques based on channel interpolation methods, displaced equalizer and curve fitting equalizer, were also presented. With the estimated channel and possibly the estimated co-channel, equalizer coefficients can be computed by using the Wiener-Hopf equations. In this thesis, two types of equalizers, LE and DFE, were considered. An expression for average MSE for a displaced LE on time-varying channel was also derived in this chapter.

Chapters 4 and 5 show two applications of these channel estimation and equalization techniques. The first application deals with the IS-136 800 MHz operation. In this application, the adaptive DFE methods are not feasible due to insufficient training of the equalizer and error propagation caused by decision-directed tracking. Since the carrier frequency, and hence the Doppler frequency are relatively low, with the two existing known sequences in a time slot, both fixed DFE and DDFE calculated based on channel estimation satisfy the IS-136 system performance criteria.

This is not true in the IS-136 1.9 GHz application. Since the carrier frequency is roughly doubled, the Doppler effect is twice as severe as that in the case of 800 MHz operation and more variations in the time-varying channel can be expected. With channel information at the two points, SYNC and CDVCC, it is insufficient to characterize the time-varying channel during the entire time slot; more channel samples were obtained by means of blind ML channel estimation. With these

additional channel samples in a time slot, the time-varying channel was interpolated by using one of the two new channel interpolation methods. Among the three types of receivers, the DDFE, DLE and curve fitting DFE receivers, the curve fitting DFE gives the best BER performance at high CIR. However, it is the most complex receiver scheme. The DDFE receiver requires the least number of operations and it gives good BER performance. A DLE receiver is not recommended in this application since its BER performance is worse than the DDFE receiver, but it requires more operations. In the low CIR region, the performance of all three types of receivers suffers due to the fact that without the information about the co-channel, these receivers cannot explicitly suppress CCI. This gives rise to the need for co-channel estimation.

The partial bounds of the DFE receiver types show that, with information about both channel and co-channel, these receivers can suppress CCI and achieve excellent performance at low CIR. Without the feedback filter, the LE receiver can suppress neither CCI nor ISI, even when provided with accurate channel and co-channel information, and the performance of the LE receivers with or without co-channel information are the same. At high CIR, since the power of CCI is so low, it makes little difference in performance whether or not co-channel information is used for all receiver types. For system operating in high CIR region, better BER performance can be achieved by putting more effort in obtaining more channel samples in a time slot, instead of estimating the co-channel.

Whether or not the co-channel information is needed depends not only on the CIR level, but also the system cost as well. If a 10-bit estimation sequence is used, estimating both channel and co-channel requires  $2^{10}$  times more operations than estimating the channel only. Therefore, even though receiver with co-channel

information offers better performance at low CIR, one should make sure that the cost can be justified.

## 6.2 Future Work

Many issues and research topics related to this research thesis were not addressed and accomplished in this thesis, due to limitations in time and resources. In this section, some of these issues are suggested for possible future study.

The simulation results for BER performance of a system with both channel and co-channel information available presented in this thesis are obtained with the assumption that the channel and co-channel can be estimated perfectly. This assumption was made to avoid the intensive computational demand of the blind channel and co-channel estimation method. How the estimation error in this method affects the BER performance would be a good topic to investigate. This can be accomplished, using the optimum but exhaustive method described in this thesis, when the availability of computer time and memory is not a concern. Another approach is to search for a sub-optimum algorithm for the blind channel and co-channel estimation. A sub-optimal blind trellis search technique was proposed by Seshadri [17] to estimate data and channel jointly. How to extend this algorithm to estimate co-channel as well, is itself a useful topic.

Suppression of CCI can also be achieved by performing constrained optimization on the output signal of the receiver. The output signal power of the receiver consists of residual ISI, CCI and noise, and it is also a function of the equalizer tap coefficients. The constrained optimization is to ensure that the worst case interference level at the receiver output does not exceed a prescribed level. One approach

to solve this problem is to maximize the output power of the receiver subject to the constraint that the power of the interference and noise is less than a certain level. Equivalently, one can also find the equalizer tap coefficients so that the power of the receiver output is minimized while setting the power of the desired signal at the output to a constant. Due to the second order dependence of the power at the receiver output on the equalizer tap coefficients, which defines in a multi-dimensional parabolic power surface with a distinct maximum or minimum point, the optimum equalizer resulting from the constrained optimization is guaranteed to be the unique global solution. Therefore, suppression of CCI by constrained optimization is a useful research topic to explore.

Since performance of a communication system is often evaluated in terms of BER, intuition suggests the equalizer is optimized when the probability of error is minimized. However, the probability of error is a highly non-linear function of the equalizer tap coefficients [11], and the solution to this problem is mathematically intractable. Finding an analytical solution or its approximation is a challenging yet interesting research topic.

Finally, an analysis was performed on the average MSE of a infinite DLE on fading channels and an expression for it was presented in this research thesis. Finding the average MSE of a DDFE on fading channels is a good topic for theoretical analysis and it is meaningful to compare the average MSE of these two equalizer types on fading channels.

# References

- [1] T. S. Rappaport, *Wireless Communications, Principles and Practice*, Prentice Hall Inc., Upper Saddle River, NJ, 1996.
- [2] B. Miller, “Satellites free the mobile phone,” *IEEE Spectrum*, vol. 35, no. 3, pp. 26–35, March 1998.
- [3] AT&T Wireless Services, “AT&T wireless services facts,” <http://www.attws.com>, downloaded in Aug. 2000.
- [4] S. Nanda, K. Balachandran, and S. Kumar, “Adaptation techniques in wireless packet data services,” *IEEE Communications Magazine*, vol. 38, no. 1, pp. 54–64, January 2000.
- [5] S. Dehghan, D. Lister, R. Owen, and P. Jones, “W-CDMA capacity and planning issues,” *IEE Electronics & Communication Engineering Journal*, vol. 12, no. 3, pp. 101–118, June 2000.
- [6] W. Honcharenko, J. P. Kruys, D. Y. Lee, and N. J. Shah, “Broadband wireless access,” *IEEE Communications Magazine*, vol. 35, no. 1, pp. 20–26, January 1997.
- [7] M. Srivastava, “Mobile multimedia computing systems,” in *Conf. Rec. Wireless '99*, Calgary, AB, July 1999, TR Labs, vol. Tutorial, p. T1.

- 
- [8] M. Madfors, K. Wallstedt, S. Magnusson, H. Olofsson, P.-O. Backman, and S. Engström, “High capacity with limited spectrum in cellular systems,” *IEEE Communications Magazine*, vol. 35, no. 8, pp. 38–45, August 1997.
- [9] J. Zander, “Radio resource management in future wireless networks: requirements and limitations,” *IEEE Communications Magazine*, vol. 35, no. 8, pp. 30–36, August 1997.
- [10] X. Lagrange, “Multitier cell design,” *IEEE Communications Magazine*, vol. 35, no. 8, pp. 60–64, August 1997.
- [11] J. G. Proakis, *Digital Communications*, McGraw-Hill Inc., New York, NY, 1995.
- [12] J. G. Proakis, “Adaptive equalization for TDMA digital mobile radio,” *IEEE Transactions on Vehicular Technology*, vol. 40, no. 2, pp. 333–341, May 1991.
- [13] G. Castellini, F. Conti, E. Del Re, and L. Pierucci, “A continuously adaptive MLSE receiver for mobile communications: algorithm and performance,” *IEEE Transactions on Communications*, vol. 45, no. 1, pp. 80–89, January 1997.
- [14] J. Lin, F. Ling, and J. G. Proakis, “Joint data and channel estimation for TDMA mobile channels,” in *Indoor and Mobile Radio Communications*, Boston, MA, October 1991, pp. 235–238.
- [15] E. Baccarelli and R. Cusani, “Combined channel estimation and data detection using soft statistics for frequency-selective fast-fading digital links,” *IEEE Transactions on Communications*, vol. 46, no. 4, pp. 424–427, April 1998.
- [16] K. Fukawa and H. Suzuki, “Adaptive equalization with RLS-MLSE for fre-

- quency selective fast fading mobile radio channels,” in *Conf. Rec. IEEE Globecom 91*, Phoenix, AZ, December 1991, IEEE, vol. 1, pp. 548–552.
- [17] N. Seshadri, “Joint data and channel estimation using blind trellis search techniques,” *IEEE Transactions on Communications*, vol. 42, no. 2/3/4, pp. 1000–1011, February/March/April 1994.
- [18] H. Kubo, K. Murakami, and T. Fujino, “An adaptive maximum likelihood sequence estimator for fast time-varying intersymbol interference channels,” *IEEE Transactions on Communications*, vol. 42, no. 2/3/4, pp. 1872–1880, February/March/April 1994.
- [19] R. Raheli, A. Polydoros, and C. K. Tzou, “Per-survivor processing: a general approach to MLSE in uncertain environments,” *IEEE Transactions on Communications*, vol. 43, no. 2/3/4, pp. 354–364, February/March/April 1995.
- [20] C. A. Belfiore and J. H. Park, Jr., “Decision feedback equalization,” *Proceedings of the IEEE*, vol. 67, no. 8, pp. 1143–1156, August 1979.
- [21] Y.-J. Liu, “Bi-directional equalization technique for TDMA communication systems over land mobile radio channels,” in *Conf. Rec. IEEE Globecom 91*, Phoenix, AZ, December 1991, IEEE, vol. 2, pp. 1458–1462.
- [22] S. Haykin, *Adaptive Filter Theory*, Prentice Hall Inc., Englewood Cliffs, NJ, 1991.
- [23] S. U. H. Qureshi, “Adaptive equalization,” *Proceedings of the IEEE*, vol. 73, no. 9, pp. 1349–1387, September 1985.
- [24] S. Haykin, A. H. Sayed, J. R. Zeidler, P. Yee, and P. C. Wei, “Adaptive

- tracking of linear time-variant systems by extended RLS algorithms,” *IEEE Transactions on Signal Processing*, vol. 45, no. 5, pp. 1118–1128, May 1997.
- [25] J. H. Winters, “Signal acquisition and tracking with adaptive arrays in the digital mobile radio system IS-54 with flat fading,” *IEEE Transactions on Vehicular Technology*, vol. 42, no. 4, pp. 377–384, November 1993.
- [26] J. H. Winters, “Optimum combining in digital mobile radio with cochannel interference,” *IEEE Journal on Selected Areas in Communications*, vol. SAC-2, no. 4, pp. 528–539, July 1984.
- [27] K. E. Scott, *Adaptive Equalization and Antenna Diversity in Digital Radio*, PhD thesis, University of Calgary, August 1991.
- [28] R. D. Gitlin and S. B. Weinstein, “Fractionally-spaced equalization: A improved digital transversal equalizer,” *The Bell System Technical Journal*, vol. 60, no. 2, pp. 275–296, February 1981.
- [29] A. R. Calderbank, G. Pottie, and N. Seshadri, “Co-channel interference suppression through time/space diversity,” *IEEE Transactions on Information Theory*, vol. 46, no. 3, pp. 922–932, May 2000.
- [30] J. H. Winters, “Optimum combining for indoor radio systems with multiple users,” *IEEE Transactions on Communications*, vol. COM-35, no. 11, pp. 1222–1230, November 1987.
- [31] J. H. Winters, J. Salz, and R. D. Gitlin, “The impact of antenna diversity on the capacity of wireless communication systems,” *IEEE Transactions on Communications*, vol. 42, no. 2/3/4, pp. 1740–1751, February/March/April 1994.

- 
- [32] T. A. Thomas and M. D. Zoltowski, "Novel receiver space-time processing for interference cancellation and equalization in narrowband TDMA communication," in *Conf. Rec. IEEE VTC 97*, Phoenix, AZ, May 1997, IEEE, vol. 1, pp. 160–164.
- [33] S. Verdú, "Minimum probability of error for asynchronous Gaussian multiple-access channels," *IEEE Transactions on Information Theory*, vol. IT-32, no. 1, pp. 85–96, January 1986.
- [34] S. Verdú, "Linear multiuser detectors for synchronous code-division multiple-access channels," *IEEE Transactions on Information Theory*, vol. IT-35, no. 1, pp. 123–136, January 1989.
- [35] K. Anand, G. Mathew, and V. U. Reddy, "Blind separation of multiple co-channel BPSK signals arriving at an antenna array," *IEEE Signal Processing Letters*, vol. 2, no. 9, pp. 176–178, September 1995.
- [36] J. Joung and G. L. Stüber, "Performance of truncated co-channel interference canceling MLSE for TDMA systems," in *Conf. Rec. IEEE VTC 98*, Ottawa, ON, May 1998, IEEE, vol. 3, pp. 1710–1714.
- [37] P. A. Ranta, A. Hottinen, and Z-C Honkasalo, "Co-channel interference cancelling receiver for TDMA mobile systems," in *Conf. Rec. IEEE ICC 95*, Seattle, WA, June 1995, IEEE, vol. 1, pp. 17–21.
- [38] G. E. Bottomley and K. J. Molnar, "Interference cancellation for improved channel estimation in array processing MLSE receivers," in *Conf. Rec. IEEE VTC 97*, Phoenix, AZ, May 1997, IEEE, vol. 1, pp. 140–144.

- 
- [39] S. N. Crozier, D. D. Falconer, and S. A. Mahmoud, "Least sum of squared errors (LSSE) channel estimation," *IEE Proceedings-E*, vol. 138, no. 4, pp. 371–378, August 1991.
- [40] R. A. Ziegler and J. M. Cioffi, "Estimation of time-varying digital mobile radio channels," in *Conf. Rec. IEEE Globecom 91*, Phoenix, AZ, December 1991, IEEE, vol. 2, pp. 1130–1134.
- [41] H.-N. Lee and G. J. Pottie, "Channel estimation based adaptive equalization/diversity combining for time-varying dispersive channels," in *Conf. Rec. IEEE VTC 97*, Phoenix, AZ, May 1997, IEEE, vol. 2, pp. 884–888.
- [42] H.-N. Lee and G. J. Pottie, "Fast adaptive equalization/diversity combining for time-varying dispersive channels," *IEEE Transactions on Communications*, vol. 46, no. 9, pp. 1146–1162, September 1998.
- [43] P. K. Shukla and L. F. Turner, "Channel-estimation-based adaptive dfe for fading multipath radio channels," *IEE Proceedings-I, Communications, Speech and Vision*, vol. 138, no. 6, pp. 525–543, December 1991.
- [44] L. M. Davis, I. B. Collings, and R. J. Evans, "Coupled estimators for equalization of fast-fading mobile channels," *IEEE Transactions on Communications*, vol. 46, no. 10, pp. 1262–1265, October 1998.
- [45] L. Tong, G. Xu, and T. Kailath, "Blind identification and equalization based on second-order statistics: a time domain approach," *IEEE Transactions on Information Theory*, vol. 40, no. 2, pp. 340–349, March 1994.
- [46] E. Moulines, P. Duhamel, J. F. Cardoso, and S. Mayrargue, "Subspace methods

- for blind identification of multichannel FIR filters,” *IEEE Transactions on Signal Processing*, vol. 43, no. 2, pp. 516–525, February 1995.
- [47] G. B. Giannakis and J. M. Mendel, “Identification of nonminimum phase systems using higher order statistics,” *IEEE Trans. Acoust., Speech, Signal Processing*, vol. 37, no. 3, pp. 360–377, March 1989.
- [48] D. Boss and K.-D. Kammeyer, “Blind GSM channel estimation based on higher order statistics,” in *Conf. Rec. IEEE ICC 97*, Montreal, QC, June 1997, IEEE, vol. 1, pp. 46–50.
- [49] S. Haykin, *Blind Deconvolution*, Prentice Hall Inc., Englewood Cliffs, NJ, 1994.
- [50] S. Chen and Y. Wu, “Maximum likelihood joint data and channel estimation using genetic algorithms,” *IEEE Transactions on Signal Processing*, vol. 46, no. 5, pp. 1469–1473, May 1998.
- [51] E. Zervas, J. Proakis, and V. Eyuboğlu, “A “quantized” channel approach to blind equalization,” in *Conf. Rec. IEEE ICC 92*, Chicago, IL, June 1992, IEEE, vol. 3, pp. 1539–1543.
- [52] E. Eweda, “Comparison of RLS, LMS, and sign algorithms for tracking randomly time-varying channels,” *IEEE Transactions on Signal Processing*, vol. 42, no. 11, pp. 2937–2944, November 1994.
- [53] Y.-J. Liu, M. Wallace, and J. W. Ketchum, “A soft-output bidirectional decision feedback equalization techniques for TDMA cellular radio,” *IEEE Journal on Selected Areas in Communications*, vol. 11, no. 7, pp. 1034–1045, September 1993.

- [54] M.-J. Chen and B. C. Shung, "Multiple-training bi-directional adaptive equalizers for TDMA digital cellular systems," *International Journal of Communication Systems*, vol. 9, no. 4, pp. 175–184, July-August 1996.
- [55] N. W. K. Lo, D. D. Falconer, and A. U. H. Sheikh, "Adaptive equalization and diversity combining for mobile radio using interpolated channel estimates," *IEEE Transactions on Vehicular Technology*, vol. 40, no. 3, pp. 636–645, August 1991.
- [56] T. Eyceöz and A. Duel-Hallen, "Reduced complexity diversity combining and adaptive equalization using interpolated channel estimates with applications to cellular mobile radio channels," in *Conf. Rec. IEEE ICUPC 96*, New York, NY, 1996, IEEE, vol. 1, pp. 51–55.
- [57] M. K. Tsatsanis and G. B. Giannakis, "Modeling and equalization of rapidly fading channels," *International Journal of Adaptive Control and Signal Processing*, vol. 10, no. 2/3, pp. 159–176, March 1996.
- [58] H. A. Cirpan and M. K. Tsatsanis, "Maximum likelihood blind channel estimation in the presence of Doppler shifts," *IEEE Transactions on Signal Processing*, vol. 47, no. 6, pp. 1559–1569, June 1999.
- [59] J. M. Wozencraft and I. M. Jacobs, *Principles of Communication Engineering*, John Wiley & Sons, Inc., New York, NY, 1965.
- [60] S. Haykin, *An Introduction to Analog and Digital Communications*, John Wiley & Sons, Inc., Toronto, ON, 1989.
- [61] V. H. MacDonald, "The cellular concept," *The Bell System Technical Journal*, vol. 58, no. 1, pp. 15–43, January 1979.

- 
- [62] B. R. Petersen and D. D. Falconer, "Suppression of adjacent-channel, cochannel, and intersymbol interference by equalizers and linear combiners," *IEEE Transactions on Communications*, vol. 42, no. 12, pp. 3109–3118, December 1994.
- [63] P. A. Bello, "Characterization of randomly time-variant linear channels," *IEEE Transactions on Communications Systems*, vol. CS-11, no. 4, pp. 360–393, December 1963.
- [64] W. C. Jakes, *Microwave Mobile Communications*, IEEE Press, Piscataway, NJ, 1974.
- [65] M. Slack, "The probability distributions of sinusoidal oscillations combined in random phase," *Journal of the IEE*, vol. 93, pp. 76–86, 1946.
- [66] R. D. Koilpillai, S. Chennakeshu, and R. L. Toy, "Low complexity equalizers for U.S. digital cellular system," in *Conf. Rec. IEEE VTC 92*, Denver, CO, May 1992, IEEE, vol. 2, pp. 744–747.
- [67] B. R. Petersen, "Wireless communications," Course Notes of ENEL 673, the University of Calgary, 1996.
- [68] G. E. Bottomley and S. Chennakeshu, "Unification of MLSE receivers and extension to time-varying channels," *IEEE Transactions on Communications*, vol. 46, no. 4, pp. 464–472, April 1998.
- [69] Q. Liu, K. E. Scott, Y. Wan, and A. M. Sendyk, "Performance of decision-feedback equalizers with dual antenna diversity," in *Conf. Rec. IEEE VTC 93*, Secaucus, NJ, May 1993, IEEE, vol. 2, pp. 637–640.

- 
- [70] L. Marple, “Resolution of conventional Fourier, autoregressive, and special arma methods of spectrum analysis,” in *Conf. Rec. 1977 IEEE Int. Conf. on Acoust., Speech, Signal Process.* IEEE, May 1977, pp. 74–77.
- [71] W. Cheney and D. Kincaid, *Numerical Mathematics and Computing*, Brook/Cole Publishing Company, Pacific Grove, CA, 1999.
- [72] S. Benedetto, E. Biglieri, and V. Castellani, *Digital Transmission Theory*, Prentice Hall Inc., Englewood Cliffs, NJ, 1987.
- [73] B. R. Petersen, *Equalization in Cyclostationary Interference*, PhD thesis, Carleton University, January 1992.
- [74] B. R. Saltzberg, “Intersymbol interference error bounds with application to ideal bandlimited signaling,” *IEEE Transactions on Information Theory*, vol. IT-14, no. 8, pp. 563–568, July 1968.
- [75] P. Balaban and J. Salz, “Dual diversity combining and equalization in digital cellular mobile radio,” *IEEE Transactions on Vehicular Technology*, vol. 40, no. 2, pp. 342–354, May 1991.
- [76] R. D. Gitlin, J. F. Hayes, and S. B. Weinstein, *Data Communications Principles*, Plenum Press, New York, NY, 1992.
- [77] G. L. Turin, “The characteristic function of hermitian quadratic forms in complex normal variables,” *Biometrika*, vol. 47, pp. 199–201, 1960.
- [78] A. Papoulis, *Probability, Random Variables, and Stochastic Processes*, McGraw-Hill, Inc., New York, NY, 1991.
- [79] I. S. Gradshteyn and I. M. Ryzhik, *Table of Integrals, Series and Products*, Academic Press, Boston, MA, 1994.

- 
- [80] Telecommunications Industry Association, "TDMA cellular/PCS - radio interface - minimum performance standards for base stations: TIA/EIA/IS-138-A," July 1996.
- [81] J. Cochenec, "Activities on next-generation networks under global information infrastructure in ITU-T," *IEEE Communications Magazine*, vol. 40, no. 7, pp. 98–101, July 2002.
- [82] S. Dixit, Y. Guo, and Z. Antoniou, "Resource management and quality of service in third generation wireless networks," *IEEE Communications Magazine*, vol. 39, no. 2, pp. 125–133, February 2001.
- [83] S. Chennakeshu and G. J. Saulnier, "Differential detection of  $\pi/4$ -shifted-DQPSK for digital cellular radio," *IEEE Transactions on Vehicular Technology*, vol. 42, no. 1, pp. 46–57, February 1993.
- [84] A. V. Oppenheim and R. W. Schaffer, *Discrete-Time Signal Processing*, Prentice Hall Inc., Englewood Cliffs, NJ, 1989.
- [85] E. Eleftheriou and D. D. Falconer, "Adaptive equalization techniques for HF channels," *IEEE Journal on Selected Areas in Communications*, vol. SAC-5, no. 2, pp. 238–247, February 1987.
- [86] G. H. Golub and C. F. Van Loan, *Matrix Computations*, The Johns Hopkins Press Ltd., London, UK, 1989.
- [87] B. R. Petersen, "Adaptive signal processing," Course Notes of ENEL 671, the University of Calgary, 1995.
- [88] W. H. Press, S. A. Teukolsky, W. T. Vetterling, and B. P. Flannery, *Numerical Recipes in C*, Cambridge University Press, New York, NY, 1992.

- 
- [89] W. P. Chou and P. J. McLane, "16-States non-linear equalizer for IS-54 digital cellular channels," *IEEE Transactions on Vehicular Technology*, vol. 45, no. 1, pp. 12–25, February 1996.
- [90] M. V. Clark, L. J. Greenstein, W. K. Kennedy, and M. Shafi, "MMSE diversity combining for wideband digital cellular radio," in *Conf. Rec. IEEE Globecom 90*, San Diego, CA, December 1990, pp. 495–499.
- [91] M. G. Salvadori and M. L. Baron, *Numerical Methods in Engineering*, Prentice Hall Inc., Englewood Cliffs, NJ, 1961.

# Appendix A

## Evaluation of Instantaneous MMSE

The instantaneous MMSE of an infinite LE on time-varying channels is given by Equation 3.128. The key to the evaluation of the instantaneous MMSE is the evaluation the angle bracket, or integration over frequency. With some algebraic manipulations, the integral is in the form in which the integration result is provided by Gradshteĭn and Ryzhik [79]. Due to an incompleteness associated with the integration result given by Gradshteĭn and Ryzhik, a modification to the expression is made, and the correct integration result is also presented in this appendix.

The two channel taps  $c_0(t)$  and  $c_1(t)$  can be written in polar form:

$$c_0(t) = r_0 e^{j\theta_0(t)}, \quad (\text{A.1})$$

and

$$c_1(t) = r_1 e^{j\theta_1(t)}, \quad (\text{A.2})$$

where  $r_0(t)$  and  $\theta_0(t)$  are the magnitude and the phase of  $c_0(t)$ , and  $r_1(t)$  and  $\theta_1(t)$  are the magnitude and the phase of  $c_1(t)$ . The magnitude and the phase of the two channel taps are random processes and they change with time. For simplicity in equation writing, they will be represented as  $r_0$ ,  $\theta_0$ ,  $r_1$  and  $\theta_1$  in the remainder of this appendix. Therefore, the discrete-time continuous-frequency Fourier transform of the auto correlation of the time-varying channel,  $\Xi_{\frac{1}{T}}(f; t)$ , can be expressed in terms of  $r_0$ ,  $\theta_0$ ,  $r_1$  and  $\theta_1$ , by substituting Equations A.1 and A.2 into Equation 3.118:

$$\Xi_{\frac{1}{T}}(f; t) = r_0^2 + r_1^2 + 2r_0r_1 \cos\left(2\pi\frac{T}{2}f + \theta_0 - \theta_1\right). \quad (\text{A.3})$$

Substituting the above equation into Equation 3.128 and re-arranging, the instantaneous MMSE of an infinite LE on time-varying channel is given by the following equation:

$$\begin{aligned} \varepsilon_{V,\min}(t) &= \varepsilon_{V,\min}(r_0, r_1, \theta_0, \theta_1) \\ &= \frac{1}{\pi} \int_{-\frac{\pi}{2}+\Delta\theta}^{\frac{\pi}{2}+\Delta\theta} h(y) dy, \end{aligned} \quad (\text{A.4})$$

where

$$h(y) = \frac{1}{A + B \cos y}, \quad (\text{A.5})$$

$$A = 1 + \frac{1}{N_o} (r_0^2 + r_1^2), \quad (\text{A.6})$$

$$B = \frac{2}{N_o} r_0 r_1, \quad (\text{A.7})$$

$$\Delta\theta = \theta_0 - \theta_1, \quad (\text{A.8})$$

and

$$y = 2\pi \frac{T}{2} f + \Delta\theta. \quad (\text{A.9})$$

The integral on the right hand side of Equation A.4, is now in the form in which the integration result is provided by Gradshtĕin and Ryzhik in the *Table of Integrals* [79]. Evaluation of the limits of integration in Equation A.4 gives:

$$\varepsilon_{\text{V,min}}(r_0, r_1, \theta_0, \theta_1) = \frac{2}{\sqrt{A^2 - B^2}} \frac{1}{\pi} \arctan \left( \frac{\sqrt{A^2 - B^2} \tan \left( \frac{y}{2} \right)}{A + B} \right) \Bigg|_{-\frac{\pi}{2} + \Delta\theta}^{\frac{\pi}{2} + \Delta\theta}, \quad (\text{A.10})$$

$$= \frac{2}{\sqrt{A^2 - B^2}} \frac{1}{\pi} \arctan \left( \frac{\sqrt{A^2 - B^2}}{B \cos(\Delta\theta)} \right). \quad (\text{A.11})$$

Figure A.1 shows the function to be integrated,  $h(y)$ , between the integration limits, for a given channel with  $A = 3.655 \times 10^4$  and  $B = 3.5896 \times 10^4$ . The function to be integrated is continuous over the integration interval, as should be the area under it. However, since the function  $\tan \left( \frac{y}{2} \right)$  is discontinuous at  $y = \pm\pi$ , the area under the curve in Figure A.1 cannot be smooth, if  $\pm\pi \in \left[ -\frac{\pi}{2} + \Delta\theta, \frac{\pi}{2} + \Delta\theta \right]$ . Figure A.2 shows the expression on the right hand side of Equation A.10 between the integration limits, which displays a discontinuity at  $\pi$ .

In order to remove the discontinuity in the curve for the area under  $h(y)$ , a modified step function is added to the expression on the left hand side of Equation A.10:

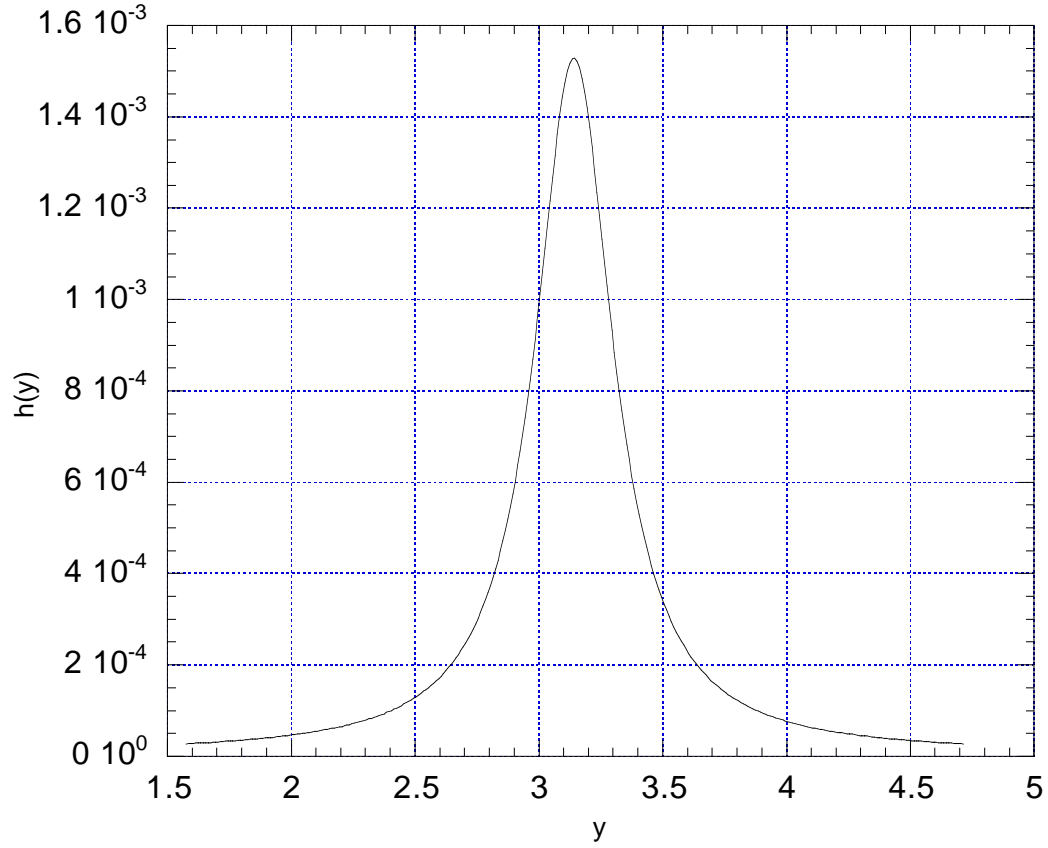


**Figure A.1:** Function to be integrated,  $h(y)$

$$\varepsilon_{V,\min}(r_0, r_1, \theta_0, \theta_1) = \frac{2}{\sqrt{A^2 - B^2}} \left[ \frac{1}{\pi} \arctan \left( \frac{\sqrt{A^2 - B^2} \tan \left( \frac{y}{2} \right)}{A + B} \right) + u_m(\Delta\theta) \right] \Bigg|_{-\frac{\pi}{2} + \Delta\theta}^{\frac{\pi}{2} + \Delta\theta}, \quad (\text{A.12})$$

$$= \frac{2}{\sqrt{A^2 - B^2}} \left[ \frac{1}{\pi} \arctan \left( \frac{\sqrt{A^2 - B^2}}{B \cos(\Delta\theta)} \right) + u_m(\Delta\theta) \right]. \quad (\text{A.13})$$

The modified step function  $u_m(\Delta\theta)$  is defined as

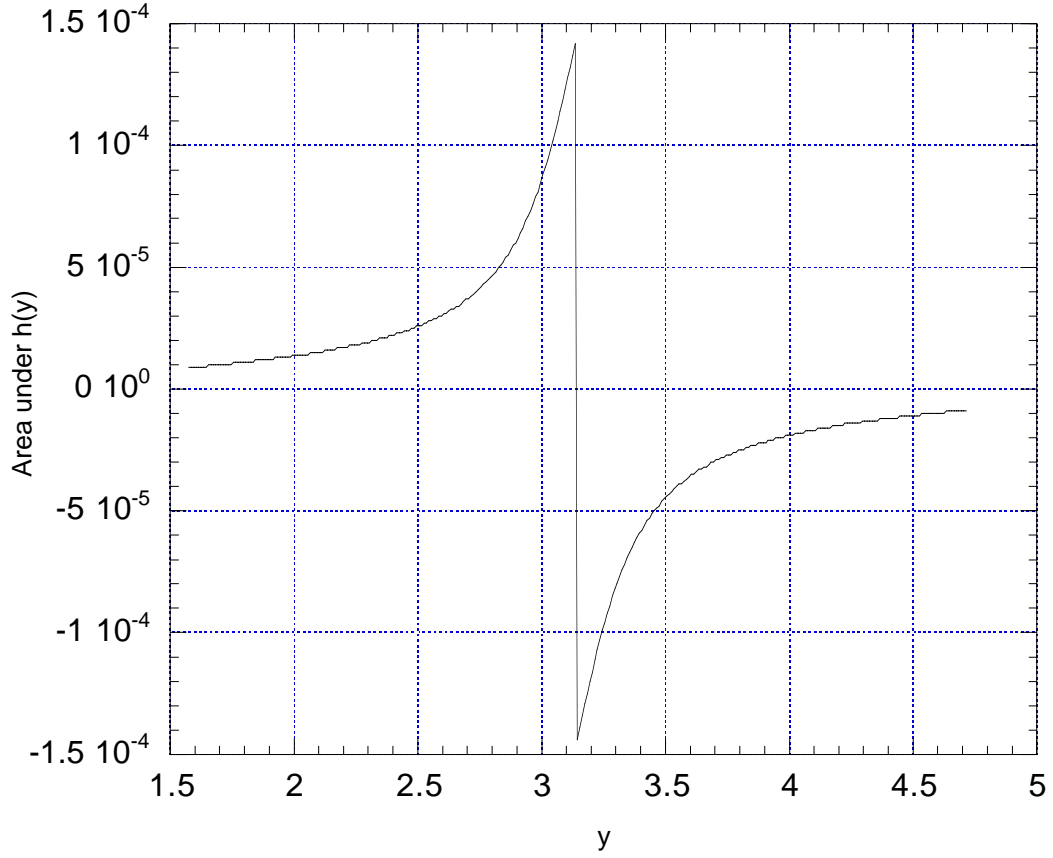


**Figure A.2:** Area under the curve  $h(y)$ , using *Table of Integrals*

$$u_m(\Delta\theta) = u^- \left( \Delta\theta + \frac{3\pi}{2} \right) - u^- \left( \Delta\theta + \frac{\pi}{2} \right) + u^- \left( \Delta\theta - \frac{\pi}{2} \right) - u^- \left( \Delta\theta - \frac{3\pi}{2} \right), \quad (\text{A.14})$$

where

$$u^-(x) = \begin{cases} 1, & x > 0 \\ 0, & x \leq 0. \end{cases} \quad (\text{A.15})$$

Figure A.3 shows the area under the curve in Figure A.1, using the expression

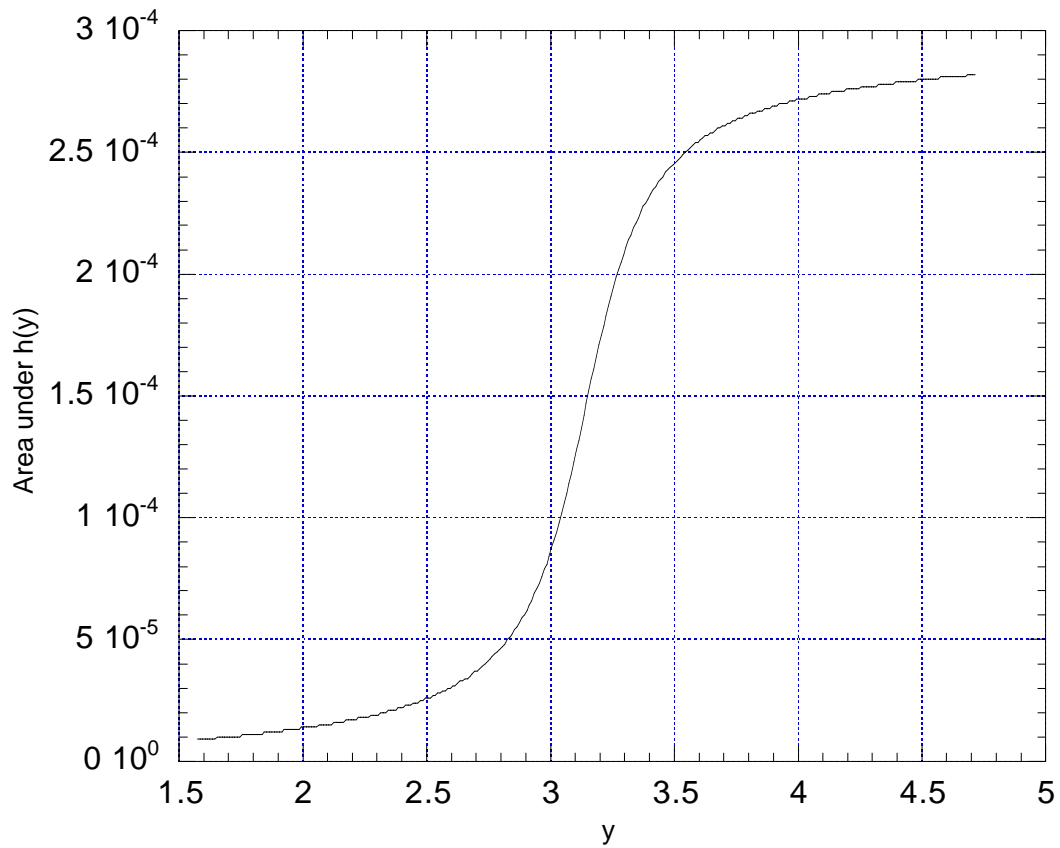


**Figure A.3:** Correct area under the curve  $h(y)$

given in Equation A.12. By adding the modified step function, the discontinuity disappeared. It can be concluded that the expression in Equation A.13 correctly represents the instantaneous MMSE.

# Appendix B

## Evaluation of Expectation by Four-Dimensional Numerical Integration

In this section, the method of evaluating the expectation in Equation 3.130, with respect to the time-varying channel, by using four-dimensional numerical integration is presented. The four-dimensional Simpson's rule for numerical integration is first derived, and the evaluation of the four-dimensional integral in Equation 3.130 by Simpson's rule and its result are discussed.

### B.1 Four-dimensional Simpson's Rule

Let  $f(w)$  be continuous on the interval  $[w_l, w_u]$ , the area under which is divided into  $M_w$  strips with equal width, for an even integer  $M_w$ . The width of the strips

$h_w$  is given by the following equation:

$$h_w = \frac{w_u - w_l}{M_w}, \quad (\text{B.1})$$

and the area of two consecutive strips, a one-dimensional element, can then be approximated by the one-dimensional Simpson's rule [91]:

$$\begin{aligned} V_{1D}(i) &= \int_{w_{i-1}}^{w_{i+1}} f(w) dw \\ &= \frac{h_w}{3} [f(w_{i-1}) + 4f(w_i) + f(w_{i+1})]. \end{aligned} \quad (\text{B.2})$$

In the four-dimensional case, the surface  $f(w, x, y, z)$  is continuous for  $w \in [w_l, w_u]$ ,  $x \in [x_l, x_u]$ ,  $y \in [y_l, y_u]$ , and  $z \in [z_l, z_u]$ . By means of four successive applications of the one-dimensional Simpson's rule, in the  $w$ ,  $x$ ,  $y$  and  $z$  directions, the volume of one four-dimensional element is approximated by

$$\begin{aligned} V_{4D}(i, j, m, n) &= \int_{z_{n-1}}^{z_{n+1}} \int_{y_{m-1}}^{y_{m+1}} \int_{x_{j-1}}^{x_{j+1}} \int_{w_{i-1}}^{w_{i+1}} f(w, x, y, z) dw dx dy dz \\ &= \frac{h_z h_y h_x h_w}{81} [(S_1 + S_2) + 4(S_3 + S_4 + S_5 + S_6) \\ &\quad + 16(S_7 + S_8 + S_9) + 64S_{10} + 256S_{11}], \end{aligned} \quad (\text{B.3})$$

where  $h_w$  is defined in Equation B.1,

$$h_x = \frac{x_u - x_l}{M_x}, \quad (\text{B.4})$$

$$h_y = \frac{y_u - y_l}{M_y}, \quad (\text{B.5})$$

$$h_z = \frac{z_u - z_l}{M_z}. \quad (\text{B.6})$$

The variables  $S_k$ , for  $k = 1, \dots, 11$  are the sums of the 4D function  $f(w, x, y, z)$  evaluated at different sets of  $w, x, y$ , and  $z$ :

$$\begin{aligned} S_1 = & f(w_{i-1}, x_{j-1}, y_{m-1}, z_{n-1}) + f(w_{i-1}, x_{j-1}, y_{m-1}, z_{n+1}) \\ & + f(w_{i-1}, x_{j-1}, y_{m+1}, z_{n-1}) + f(w_{i-1}, x_{j-1}, y_{m+1}, z_{n+1}) \\ & + f(w_{i-1}, x_{j+1}, y_{m-1}, z_{n-1}) + f(w_{i-1}, x_{j+1}, y_{m-1}, z_{n+1}) \\ & + f(w_{i-1}, x_{j+1}, y_{m+1}, z_{n-1}) + f(w_{i-1}, x_{j+1}, y_{m+1}, z_{n+1}), \end{aligned} \quad (\text{B.7})$$

$$\begin{aligned} S_2 = & f(w_{i+1}, x_{j-1}, y_{m-1}, z_{n-1}) + f(w_{i+1}, x_{j-1}, y_{m-1}, z_{n+1}) \\ & + f(w_{i+1}, x_{j-1}, y_{m+1}, z_{n-1}) + f(w_{i+1}, x_{j-1}, y_{m+1}, z_{n+1}) \\ & + f(w_{i+1}, x_{j+1}, y_{m-1}, z_{n-1}) + f(w_{i+1}, x_{j+1}, y_{m-1}, z_{n+1}) \\ & + f(w_{i+1}, x_{j+1}, y_{m+1}, z_{n-1}) + f(w_{i+1}, x_{j+1}, y_{m+1}, z_{n+1}), \end{aligned} \quad (\text{B.8})$$

$$\begin{aligned} S_3 = & f(w_{i-1}, x_{j-1}, y_{m-1}, z_n) + f(w_{i-1}, x_{j-1}, y_m, z_{n-1}) \\ & + f(w_{i-1}, x_{j-1}, y_m, z_{n+1}) + f(w_{i-1}, x_{j-1}, y_{m+1}, z_n) \\ & + f(w_{i-1}, x_{j+1}, y_{m-1}, z_n) + f(w_{i-1}, x_{j+1}, y_m, z_{n-1}) \\ & + f(w_{i-1}, x_{j+1}, y_m, z_{n+1}) + f(w_{i-1}, x_{j+1}, y_{m+1}, z_n), \end{aligned} \quad (\text{B.9})$$

$$\begin{aligned}
S_4 &= f(w_{i+1}, x_{j-1}, y_{m-1}, z_n) + f(w_{i+1}, x_{j-1}, y_m, z_{n-1}) \\
&\quad + f(w_{i+1}, x_{j-1}, y_m, z_{n+1}) + f(w_{i+1}, x_{j-1}, y_{m+1}, z_n) \\
&\quad + f(w_{i+1}, x_{j+1}, y_{m-1}, z_n) + f(w_{i+1}, x_{j+1}, y_m, z_{n-1}) \\
&\quad + f(w_{i+1}, x_{j+1}, y_m, z_{n+1}) + f(w_{i+1}, x_{j+1}, y_{m+1}, z_n), \tag{B.10}
\end{aligned}$$

$$\begin{aligned}
S_5 &= f(w_{i-1}, x_j, y_{m-1}, z_{n-1}) + f(w_{i-1}, x_j, y_{m-1}, z_{n+1}) \\
&\quad + f(w_{i-1}, x_j, y_{m+1}, z_{n-1}) + f(w_{i-1}, x_j, y_{m+1}, z_{n+1}) \\
&\quad + f(w_i, x_{j-1}, y_{m-1}, z_{n-1}) + f(w_i, x_{j-1}, y_{m-1}, z_{n+1}) \\
&\quad + f(w_i, x_{j-1}, y_{m+1}, z_{n-1}) + f(w_i, x_{j-1}, y_{m+1}, z_{n+1}), \tag{B.11}
\end{aligned}$$

$$\begin{aligned}
S_6 &= f(w_i, x_{j+1}, y_{m-1}, z_{n-1}) + f(w_i, x_{j+1}, y_{m-1}, z_{n+1}) \\
&\quad + f(w_i, x_{j+1}, y_{m+1}, z_{n-1}) + f(w_i, x_{j+1}, y_{m+1}, z_{n+1}) \\
&\quad + f(w_{i+1}, x_j, y_{m-1}, z_{n-1}) + f(w_{i+1}, x_j, y_{m-1}, z_{n+1}) \\
&\quad + f(w_{i+1}, x_j, y_{m+1}, z_{n-1}) + f(w_{i+1}, x_j, y_{m+1}, z_{n+1}), \tag{B.12}
\end{aligned}$$

$$\begin{aligned}
S_7 &= f(w_{i-1}, x_{j-1}, y_m, z_n) + f(w_{i-1}, x_{j+1}, y_m, z_n) \\
&\quad + f(w_{i+1}, x_{j-1}, y_m, z_n) + f(w_{i+1}, x_{j+1}, y_m, z_n) \\
&\quad + f(w_{i-1}, x_j, y_{m-1}, z_n) + f(w_{i-1}, x_j, y_m, z_{n-1}) \\
&\quad + f(w_{i-1}, x_j, y_m, z_{n+1}) + f(w_{i-1}, x_j, y_{m+1}, z_n), \tag{B.13}
\end{aligned}$$

$$\begin{aligned}
S_8 &= f(w_i, x_{j-1}, y_{m-1}, z_n) + f(w_i, x_{j-1}, y_m, z_{n-1}) \\
&+ f(w_i, x_{j-1}, y_m, z_{n+1}) + f(w_i, x_{j-1}, y_{m+1}, z_n) \\
&+ f(w_i, x_{j+1}, y_{m-1}, z_n) + f(w_i, x_{j+1}, y_m, z_{n-1}) \\
&+ f(w_i, x_{j+1}, y_m, z_{n+1}) + f(w_i, x_{j+1}, y_{m+1}, z_n),
\end{aligned} \tag{B.14}$$

$$\begin{aligned}
S_9 &= f(w_{i+1}, x_j, y_{m-1}, z_n) + f(w_{i+1}, x_j, y_m, z_{n-1}) \\
&+ f(w_{i+1}, x_j, y_m, z_{n+1}) + f(w_{i+1}, x_j, y_{m+1}, z_n) \\
&+ f(w_i, x_j, y_{m-1}, z_{n-1}) + f(w_i, x_j, y_{m-1}, z_{n+1}) \\
&+ f(w_i, x_j, y_{m+1}, z_{n-1}) + f(w_i, x_j, y_{m+1}, z_{n+1}),
\end{aligned} \tag{B.15}$$

$$\begin{aligned}
S_{10} &= f(w_{i-1}, x_j, y_m, z_n) + f(w_i, x_{j-1}, y_m, z_n) \\
&+ f(w_i, x_{j+1}, y_m, z_n) + f(w_{i+1}, x_j, y_m, z_n) \\
&+ f(w_i, x_j, y_{m-1}, z_n) + f(w_i, x_j, y_m, z_{n-1}) \\
&+ f(w_i, x_j, y_m, z_{n+1}) + f(w_i, x_j, y_{m+1}, z_n),
\end{aligned} \tag{B.16}$$

and

$$S_{11} = f(w_i, x_i, y_i, z_i). \tag{B.17}$$

The total volume under the four-dimensional surface is the sum of all the elements:

$$V = \sum_{n=1}^{M_z-1} \sum_{m=1}^{M_y-1} \sum_{j=1}^{M_x-1} \sum_{i=1}^{M_w-1} V_{4D}(i, j, m, n), \quad i, j, m, n \text{ odd integers.} \tag{B.18}$$

## B.2 Evaluation of the Expectation

In this section, the four-dimensional Simpson's rule is applied to evaluation the mathematical expectation in Equation 3.130. From Equations 3.130 and 3.128, the average MMSE of a time-varying channel  $\bar{\varepsilon}_{V,\min}$  is given by

$$\begin{aligned}
 \bar{\varepsilon}_{V,\min} &= \iiint \int \varepsilon_{V,\min}(r_0, r_1, \theta_0, \theta_1) P_{\Theta_0}(\theta_0) P_{\Theta_1}(\theta_1) P_{R_0}(r_0) P_{R_1}(r_1), d\theta_0 d\theta_1 dr_0 dr_1 \\
 &= \frac{1}{4\pi^2 \sigma_r^4} \int_0^\infty \int_0^\infty \int_{-\pi}^\pi \int_{-\pi}^\pi \varepsilon_{V,\min}(r_0, r_1, \theta_0, \theta_1) r_0 r_1 e^{-\frac{r_0^2 + r_1^2}{2\sigma_r^2}} d\theta_0 d\theta_1 dr_0 dr_1 \\
 &= \frac{1}{4\pi^2 \sigma_r^4} \int_0^\infty \int_0^\infty \int_{-\pi}^\pi \int_{-\pi}^\pi f(r_0, r_1, \theta_0, \theta_1) d\theta_0 d\theta_1 dr_0 dr_1, \tag{B.19}
 \end{aligned}$$

where  $P_{\Theta_0}(\theta_0)$ ,  $P_{\Theta_1}(\theta_1)$ ,  $P_{R_0}(r_0)$  and  $P_{R_1}(r_1)$  are the PDFs of  $\theta_0$ ,  $\theta_1$ ,  $r_0$  and  $r_1$ , respectively and  $\sigma_r^2$  is the variance of  $r_0$  and  $r_1$ .

Figure B.1 shows the results of the numerical integration. For comparison purpose, the theoretical average MMSE is also plotted in the same figure. In approximation 1, the number of intervals for  $\theta_0$  and  $\theta_1$  is 45 and that for  $r_0$  and  $r_1$  is 210. The upper limit for  $r_0$  and  $r_1$  is 60. In approximation 2, the number of intervals for  $\theta_0$  and  $\theta_1$  is 45 and that for  $r_0$  and  $r_1$  is 1024. The upper limit for  $r_0$  and  $r_1$  is 5. It can be observed that approximation 2 gives a more accurate result. This suggests that the function  $f(r_0, r_1, \theta_0, \theta_1)$  decays rapidly as  $r_0$  and  $r_1$  increase. Due to the discontinuities in the arctan function in the equation for  $g(r_0, r_1, \theta_0, \theta_1)$ , a large number of intervals is required in order to accurately approximate the four-dimensional function  $f(r_0, r_1, \theta_0, \theta_1)$  at the discontinuity.

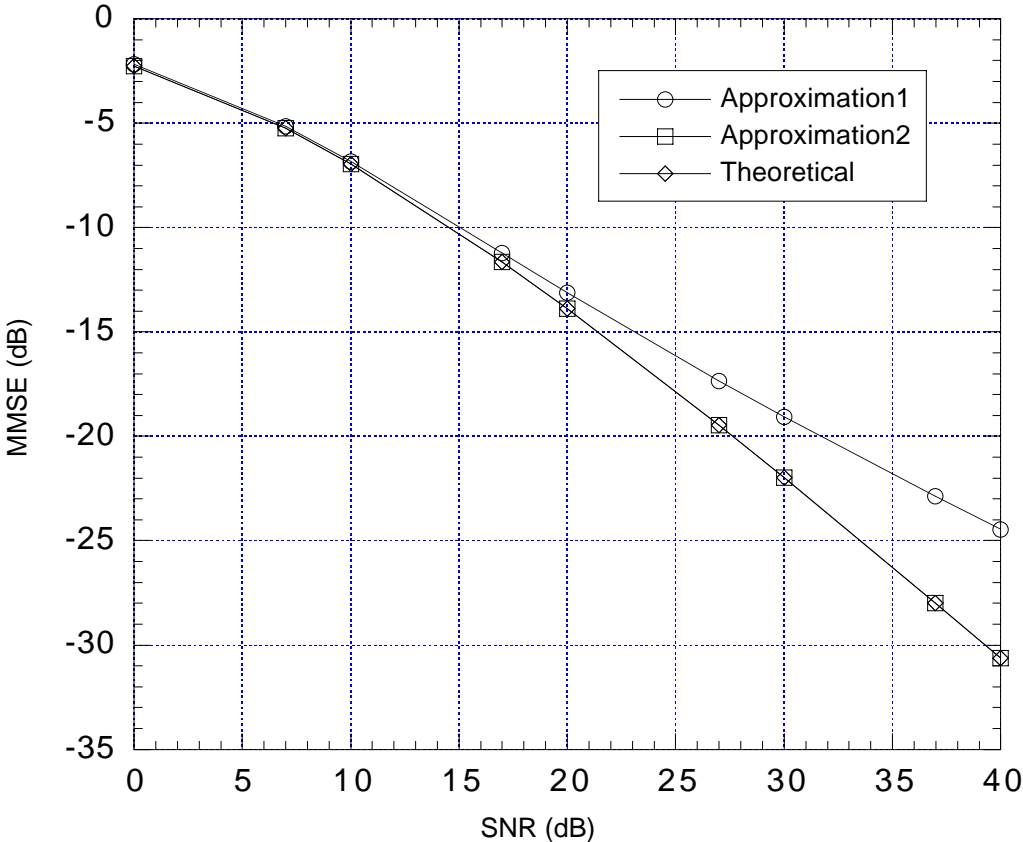


Figure B.1: Comparison of numerical integration results

# Appendix C

## MMSE of an AWGN Channel

In this appendix, an expression for the MMSE of an AWGN channel, in terms of the input SNR, is derived.

Figure C.1 shows a simple data communication in an AWGN channel.  $d_n$  is the uncorrelated transmitted data with zero mean and unit variance:

$$E[d_n] = 0 \tag{C.1}$$

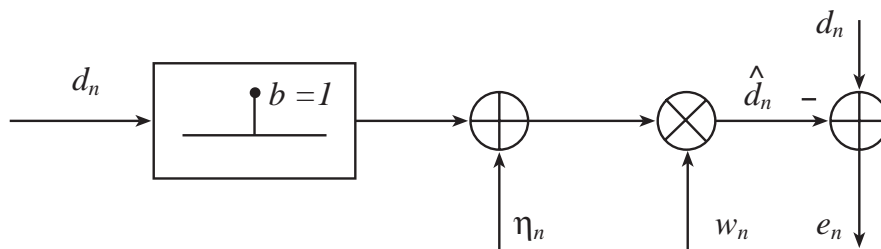


**Figure C.1:** Data communication in an AWGN channel

and

$$E[d_n d_m] = \begin{cases} 1, & n = m \\ 0, & n \neq m \end{cases}. \quad (\text{C.2})$$

The AWGN channel is modeled as a unit impulse, followed by the AWGN. The AWGN, denoted by  $\eta_n$ , is a random process, with the following statistical properties

$$E[\eta_n] = 0, \quad (\text{C.3})$$

$$E[\eta_n \eta_m] = \begin{cases} \sigma_n^2, & n = m \\ 0, & n \neq m \end{cases}, \quad (\text{C.4})$$

and it is uncorrelated with the transmitted data:

$$E[d_n \eta_m] = 0. \quad (\text{C.5})$$

$\hat{d}_n$  is the estimate of the desired signal, at the output of the receiver  $w_n$ , that is,

$$\hat{d}_n = w_n b d_n + w_n \eta_n. \quad (\text{C.6})$$

$e_n$  is the error in the estimate  $\hat{d}_n$ , and it is given by the following equation:

$$e_n = d_n - \hat{d}_n. \quad (\text{C.7})$$

The MSE of the estimate,  $\varepsilon_{\text{AWGN}}(w_n)$ , is given by

$$\begin{aligned}\varepsilon_{\text{AWGN}}(w_n) &= E[|e_n|^2], \\ &= E[|d_n - \hat{d}_n|^2],\end{aligned}\tag{C.8}$$

where the expectation is taken over the ensemble of the data  $d_n$  and the noise,  $\eta_n$ . By substituting Equation C.6 into the above equation, and simplifying, the MSE of an AWGN channel can be rewritten:

$$\varepsilon_{\text{AWGN}}(w_n) = (b^2 + \sigma_n^2)w_n^2 - 2bw_n + 1.\tag{C.9}$$

In order to determine the minimum MSE, derivative of both sides in Equation C.9 is taken with respect to  $w_n$ , and set to zero. Then the optimum receiver,  $w_{\text{MMSE}}$ , at which the MMSE occurs, is given by

$$w_{\text{MMSE}} = \frac{b}{b^2 + \sigma_n^2},\tag{C.10}$$

and the MMSE of an AWGN channel can be obtained by substituting Equation C.10 into Equation C.9:

$$\varepsilon_{\text{AWGN},\min} = \frac{\sigma_n^2}{b^2 + \sigma_n^2}.\tag{C.11}$$

Since the SNR at the input of the receiver,  $\gamma_{\text{in}}$  is defined as

$$\gamma_{\text{in}} = \frac{P_s}{P_n} = \frac{1}{\sigma_n^2},\tag{C.12}$$

for  $b = 1$ , the MMSE of an AWGN can be written in terms of  $\gamma_{\text{in}}$ :

$$\varepsilon_{\text{AWGN},\text{min}} = \frac{1}{1 + \gamma_{\text{in}}}. \quad (\text{C.13})$$